DOCTOR OF PHILOSOPHY

Thermodynamically Consistent Phase-Field Models and Their Energy Law Preserving Finite Element Schemes for Two-Phase Flows and Their Interaction with Boundaries

Shen, Lingyue

Award date:
2022

Thermodynamically Consistent Phase-Field Models and Their Energy Law Preserving Finite Element Schemes for Two-Phase Flows and Their Interaction with Boundaries

Lingyue Shen

Doctor of Philosophy

UNIVERSITY OF DUNDEE

2022

Abstract

Phase-field theory is a powerful method which is widely used in dealing with multiphase problem in fluid dynamics in recent years. In this thesis, models of moving contact lines and vesicle motion, deformation and interaction would be established with phase-field method. Energy variational approach is used to derive the governing equations from some basic energy assumption. C^0 finite element scheme is given to perform numerical test. Continuous and discrete energy decaying law are also given to prove the feasibility of the model. Finally, numerical simulation is applied. A number of results in different conditions are shown. By comparing with experimental data from previous research, the models are proven to be with good accuracy.

Acknowledgements

I'd like to thank my supervisor Professor Ping Lin for his help in my research works and support during the pandemic. It is him who instructs me step inside the field of applied mathematics and show great patience on my questions.

I am greatly thankful to my grandma, grandpa and other family members. Their love always supports and protects me during my growing up. That is the biggest support of my PhD study.

Many thanks to Professor Shixin Xu who keeps collaborating with me since I started my research. The help and support from such a peer researcher really helps me to get along with my work smoothly.

Thanks to all the people who have ever helped me. It is the very help that motivates me to overcome the difficulties in my life.

Declaration

I declare that this thesis was composed by myself, that the work contained herein is my own except where explicitly stated otherwise in the text, and that this work has not been submitted for any other degree or professional qualification except as specified.

Lingyue Shen

Contents

Figures and Tables

Figures

Tables

Chapter 1

Introduction

1.1 Modelling Methods of Multiphase Flow

Multiphase flow refers to the coexistence of substances in fluid flow with an exact interface between two (or more) phases or different components. The study of multiphase flow mainly focus on its dynamics [114, 78, 151, 150], thermodynamics [62, 39, 43], heat and mass transfer [144, 61] at the interface. The research covers a wide range of subjects like mantle melting [151, 150] in geophysics, printing [84] and spray cooling of surfaces [15] in industrial application, blood clot growth [162] and red blood cell property [148, 18, 112] in biomedical research. Thus, establishing accurate mathematical models of multiphase flow has became a point of interest in recent years.

Compared with single phase fluid flow, there are more features and difficulties in modelling of multiphase flow problem. Firstly, multiphase flow contains several different immersible components, each of them has its unique physical features (density, viscosity, specific heat...). Thus, more parameters are required to describe the flow which makes the mathematical model more difficult. Secondly, There are complex interactions at the interface of two phases like fraction, displacement, energy exchange, chemical reaction and deformation. Those interactions would affect the flow greatly. Finally, in some cases such as large density ratio between two phases and non-constant temperature, the problem becomes highly nonlinear, which brings difficulties to calculation.

Aiming at modelling of multiphase flow, a number of methods and approximations are developed. Molecular dynamics simulations [82, 83, 145], microscopic–macroscopic hybrid model [58, 124] and dissipative particle dynamics model [89] are introduced in microscopic scale. In macro-scale, the modelling can be generally divided into two types: sharp interface model and diffuse interface model. Sharp interface model consider the interface of different phases as a sudden cut. The interface works as a boundary of the phases. In mathematical treatment, the feature of the interface would be expressed as boundary condition of the governing equations. There have been various methods under sharp interface frame such as front tracking model [86, 122, 123, 175], boundary integral model [65] and immersed boundary model [106]. Some scientific research has been applied based on sharp interface models like multi-phased fluid

flow [176, 69] and Marangoni effect [149, 113]. However, in numerical calculation, sharp interface models require the mesh of the domain renewed frequently in order to track the interface. The boundary condition at the interface need to be handled properly at the same time. These factors make it hard to solve the discrete partial differential equations with general calculation software which decrease the universality of the models.

Compared with sharp interface model, diffuse interface model could adapt numerical calculation better and show better continuity in mathematics. In the model, the material interface is treated as a diffuse layer instead of a sharp discontinuity. The position of the interface is no more defined explicitly as a variable in the governing equations (the position of the boundary) but captured by a solution of the equation of an implicit function defined in the whole domain. Thus the boundaries between different phases do not exist anymore which makes the derivation of the governing equations much easier. Also, the position of the interface is now received by solving the equations directly, remeshing of the domain is not necessary, which simplifies the numerical calculation greatly. So far, a lot of typical interface capturing methods have been reported such as volume-of-fluid methods [130], level set method [109, 159, 158, 127] and phase-field method.

Among those models, phase-field method [6, 57, 73] is one of the most popular and powerful methodologies. This regularization can be rigorously formulated through a variational process. The main advantages of the phase-field method are twofolds. First, the phase-field order parameter identifying the diffuse interface is treated as an additional primary unknown variable of the problem to be solved on the whole domain. The governing equations can be derived by energy-based variational approach [38, 172, 94]. As a result, the obtained system is compatible with the law of energy dissipation, which makes it possible to design efficient and energetically stable numerical schemes. Second, interface transformations are predicted without the necessity of a remeshing algorithm to treat the evolution of the interface, thus it becomes easy to track the interface and numerically implement even if there are large topological changes [28]. In this thesis, we focus on phase field method. Based on proper assumption in Navier-Stokes equations, energy variational approach [95, 126, 119] is used to establish thermodynamically consistent models.

With so many models in multiphase flow, a variety of numerical methods are developed. Lattice Boltzmann method is reported in [173], layer-by-layer decomposition methods is used in [167]. The most common methods are finite difference and finite element method which are widely used in calculation of various methods such as immersed boundary model [79, 131, 108, 153, 156], immersed interface model, [67, 81], spectral model [97], fictitious domain model [60] and phase-field model [53, 52, 54]. Also, the energy law of discrete scheme is considered by some of the researches. In [51, 53] energy law is presented based on finite element scheme. In [54] a mass conservative and energy stable finite difference methods is introduced. In this thesis, works are done referring to the idea of [53, 52] to establish

phase-field models and the corresponded C^0 finite element schemes are given as well. The corresponding discrete energy decaying law is then derived and tested numerically to prove the thermodynamic consistency of the discrete scheme. In recent years, the invariant energy quadratic (IEQ) approach is proposed in [166, 169]. The basic idea is to convert the volume potential in the model into a quadratic form by using a new set of variables. Also semi-explicit treatment is applied on all non-linear terms, making the governing equations discretized into linear elliptic equations. The method is successfully applied to various gradient flow models. However, this approach has some shortcomings as indicated in [134, 133] and see also [88]. Firstly, the method requires solving a complex variable coefficient linear equation. Secondly, a lower bound of the energy density function is needed which decrease its scope of application. Finally, the method would result in a coupled system for gradient flows with multiple components. To improve the IEQ approach, a new method called scalar assisted variable (SAV) method is developed in [134, 133]. The SAV enjoys all advantages of the IEQ approach but overcomes the disadvantages mentioned above. The SAV method only needs to solve the decoupled equation with constant coefficients at each time step. Thus, an unconditionally energy stable numerical scheme could be obtained. The scheme is not limited to the special form of the nonlinear part of free energy, so it is suitable for a large class of large gradient flows. Though the discrete energy in IEQ or SAV is usually a numerical approximation of the energy in the continuous model. Or in other word, the discrete energy law in IEQ or SAV is a numerical approximation of the continuous energy law. In this thesis our numerical method will be based on mid-point type of schemes where the discrete energy law usually has the same form of the continuous energy law.

In this thesis, phase-field modeling of two specific cases are studied: moving contact lines problem and vesicle motion and interaction problem. In the following part of the chapter, a brief introduction of the problems is given together with the related works published recently.

1.2 Application of Multiphase Flow Modelling

1.2.1 Moving contact lines

The modeling and simulation of moving contact lines (MCLs), where the interface of two or more immersible fluids intersects with a solid wall [23, 33], have attracted much attention in fluid mechanics study in recent years. Applications of MCLs in industries and medical fields (for example, printing [84], spray cooling of surfaces [15], blood clot [162], microfluidics [152], surfactant[158, 175]) have motivated scientific interests and mathematical challenges on associated issues such as the stress singularity and contact angle hysteresis. In order to model the dynamics around the contact lines, various types of models and approximations

have been developed, such as direct molecular dynamics simulations [82, 83, 145], microscopic–macroscopic hybrid model [58, 124], front tracking model [86, 122, 123, 175], phase-field model [8, 77, 116, 128, 139] and Lattice Boltzmann model[71]. For reviews of the current status of the MCLs problem, we refer to the articles [13] and [146].

Among the modelling methods, phase-field modelling shows great efficiency and accuracy on dealing with moving contact line problem of multi-phased flow. However, one of the main challenges in phase-field method is to model the immersible two-phase flow with different densities. When the density ratio between the two phases is small, it could be handled by the Boussinesq approximation [93]. However, it could not be extended to the case with a large density ratio due to its underlying assumption [94]. One key problem arises from the inconsistency between the mass conservation and the incompressibility especially near the diffusive interface region. It was first pointed out by Lowengrub [99] and later by Shen et al. [94, 138]. Two main approaches are proposed to overcome this difficulty: one is based on volume averaged velocity; the other is based on the mass averaged velocity. For the volume averaged velocity model, the incompressiblity is assumed everywhere including the interfacial region [1, 14, 25, 136, 135]. A thermodynamically consistent and frame invariant model was developed by Abels et al. [2], where the mass conservation equation is modified with a mass correction term. On the other hand, for the mass averaged velocity method, the mass conservation is assured instead of incompressibility. This naturally yields the quasi-incompressible Navier-Stoker-Cahn-Hilliard (q-NSCH) model [54, 99], which in fact leads to a slightly compressible mixture only inside the interfacial region.

Besides, the boundary condition of the contact point is also relatively hard to handle. The velocity of the fluid on the wall is treated as 0 in many researches on single-phased fluid flow. However, this non-slip boundary condition is incompatible with moving contact lines problem since it leads to a non-integrable singularity [116]. Navier boundary condition arose to describe the slip of the fluid at the wall [104, 5]. In the past decade, a number of studies on moving contact lines have applied generalized Navier boundary condition (GNBC) [115, 116] in which the slipping is proportional to the sum of tangential viscous stress and the uncompensated Young stress.

In chapter 3 of the thesis, a quasi-incompressible phase field model of moving contact lines is established through energy variational method and general Navier boundary condition (GNBC) is adapted and applied to our model. A thermodynamically consistent C^0 finite element scheme is derived with an discrete energy law. Numerical simulations are shown to prove the feasibility of our model.

1.2.2 Vesicle motion and deformation

Studying dynamic motion and shape transformation of biological cells (vesicles) has recently become a point of interest in biological fluid dynamics, because the shapes of the cells usually relate to their function. For example, many blood-related diseases are known to be associated with alterations in the geometry and membrane properties of red blood cells [148]. Red blood cells in diabetes or sepsis patients exhibit impaired cell deformability [18, 112]. During blood clot formation, an indicator of platelet activation is its shape change by forming filopodia and lamellipodia. Notably, platelets shape changes facilitate their adhesion to the site of vascular injury and cohesion with other platelets or erythrocytes [143, 7].

In simulation studies, it is vitally important to establish a proper model of cell membranes for analyzing the dynamical shape transformation of cells, in addition to modeling intracellular and extracellular fluids. Various mathematical models were introduced for predicting cell morphology and function. Dissipative particle dynamics [89] models of red blood cell were developed in [111, 89, 110] and were used to study effects of red blood cells on platelet aggregation [111]. Models based on interface tracking or capturing such as level set method [159, 158, 127] were also developed [12, 75, 66, 60] to take into consideration the fluid-cell-structure interaction. In numerical treatment, various methods such as immersed boundary method [79, 131, 108, 153, 156], immersed interface method, [67, 81], spectral method [97] and fictitious domain method [60] using finite difference or finite element formulation have been introduced to solve governing equations of these models.

Lots of phase-field type vesicle models have been introduced lately [70, 170, 100, 30]. Mechanical properties of the vesicle membrane such as bending stiffness and inextensibility can be incorporated rigorously by the phase-field theory [30, 27, 29, 32] to establish a realistic mechanistic model. For instance, the bending energy of bending resistance of the lipid bilayer membrane in the isotropic case (neglecting the proteins and channels on the membrane) given in the form of the Helfrich bending energy can be approximated by a modified elastic energy defined on the whole domain in the phase-field formulation [21, 31, 27, 29]. Constraints conserving cell mass and ensuring global inextensibility of cell membrane are frequently introduced into vesicle models to keep the mass and surface area of the vesicle constant [32, 3].

In chapter 4 of the thesis, a vesicle model is established using Allan-Chan type interface through eneregy variational method. A GNBC is applied to deal with the wetting phenomenon when the vesicle contact the wall. A second ordered convergent C^0 finite element scheme is derived later. Finally, bench mark test and and simulation results compared with lab data are posted to show that our model fits the experiment well.

1.2.3 Interaction of multiple vesicles

In the study of hemodynamics, the interaction between various structures (cell-cell and cell-vessel) is a very important part since it is related to a wild range of problem like red blood cell distribution [80] in blood vessel, the growth of blood clot [42], blood cell aggregation [87], sickle cell disease [4], tumor cell dynamics [22] and diabetes study [24].

So far, under the frame of sharp interface condition, there are a number of studies focusing on the modeling of this interaction effect in blood flow. Cell-wall interaction models have been arise in [22] to simulate the adhesion and deformation of tumor cells at the vessel wall. Local and non-local models are introduced in [46] to explain the invasion and growth of tumor cells. Cell-cell interaction modeling at micro-scale is performed in [178, 98, 177, 173] to study red blood cell aggregation problem. Multi-scale models are introduced in [37, 165] where dissipative particle dynamics is used in [37] to establish a blood cell model in blood flow and a stochastic Cellular Potts Model (CPM) is introduced in [165] for blood clot growing simulation. In [41, 118] Lennard-Jones type potential arises in cell-cell interaction to study cell deformation and doublet suspension.

By regarding the membrane as a diffused interface, some vesicle interaction model based on phase-field method has been reported recently. Fusion of cellular aggregates in biofabrication is modelled with a single phase field function in [167]. Vesicle-substrate adhesion model is established in [48] where two phase feild function is used to indicate wall and vesicle. Vesicle-vesicle adhesion model is introduced in [49] where different phase field function represents different vesicles. Further, a multiple cell aggregation model and corresponding simulation is reported in [76].

In the thesis, an energy stable C^0 finite element scheme is established based on a Chan-Hilliard type interface model of multiple vesicle. Energy variational method is used for continuous model derivation. Simulation results indicates that the model fits the experiment well.

Chapter 2

Mathematical Background and Notations

2.1 Material Derivative

Consider a physical variable $v(\boldsymbol{x},t)$ of the fluid defined in a fixed domain, such as temperature and density where $\boldsymbol{x}$ is space coordinate and t is time. It is obvious that the velocity of such a physical quantity is same as the velocity of the fluid $\mathbf{u}(\boldsymbol{x},t)$ which means the physical quantity is moving with the substance of the fluid. Taking the time derivative of the variable and applying the chain rule, we have:

$$\frac{d}{dt}v(\boldsymbol{x},t) = \frac{\partial v}{\partial t} + \frac{d\boldsymbol{x}}{dt}\cdot\nabla v \tag{2.1}$$

As mentioned before, the velocity of v is equal to the fluid, thus we have:

$$\frac{d\boldsymbol{x}}{dt} = \mathbf{u} \tag{2.2}$$

Substitute Eq.(2.2) back into Eq.(2.1) and use the new notation $\frac{D}{Dt}$ to represent such a material. We finally have the formula:

$$\frac{D}{Dt}v(\boldsymbol{x},t) = \frac{\partial v}{\partial t} + \mathbf{u}\cdot\nabla v \tag{2.3}$$

Equation (2.3) is celled the material derivative of quantity v.

For a scalar field, the calculation is trivial as shown in Equation (2.3). While for a vector field $\vec{v} = (v_x, v_y, v_z)$, the calculation result is:

$$\frac{D\vec{v}}{Dt} = \begin{pmatrix} \frac{\partial v_x}{\partial t} + u_x\frac{\partial v_x}{\partial x} + u_y\frac{\partial v_x}{\partial y} + u_z\frac{\partial v_x}{\partial z} \\ \frac{\partial v_y}{\partial t} + u_x\frac{\partial v_y}{\partial x} + u_y\frac{\partial v_y}{\partial y} + u_z\frac{\partial v_y}{\partial z} \\ \frac{\partial v_z}{\partial t} + u_x\frac{\partial v_z}{\partial x} + u_y\frac{\partial v_z}{\partial y} + u_z\frac{\partial v_z}{\partial z} \end{pmatrix} \tag{2.4}$$

according to tensor analysis.

2.2 Conservation Law of Mass

In this thesis, conservation law of mass is always discussed in the model derivation. We start from the integral form. Consider an arbitrary volume $V(t)$ whose shape and size changes with time. The conservation law of mass ρ states [56]:

$$\frac{d}{dt}\int_{V(t)} \rho d\boldsymbol{x} = 0 \tag{2.5}$$

The physical meaning of the equation is that the mass of a control volume doesn't change with time as the volume deforms and moves.

By applying Reynolds' transport relation, the deviation form of the conservation law can be written as [56]:

$$\frac{\partial \rho}{\partial t} + \nabla \cdot (\mathbf{u}\rho) = 0 \tag{2.6}$$

For other conservation laws, the detail would be discussed in the following sections.

2.3 Sobolev Space

C^0 finite element scheme would be used for discrete analysis and this requires the discrete variable functions defined properly. In this thesis, the functions are all defined in Sobolev space with notation goes: $W^{l,p}$. Where l means the order of the derivatives of the functions that are integrable and p means the order of the L^p-norm that the space equipped with. The definition of L^p-norm is shown below:

$$||f||_p = (\int_\Omega |f|^p)^{\frac{1}{p}} \tag{2.7}$$

More detail of the property and definition of Soblev space could be found in [17]. In this thesis, L^2-norm are used to measure the convergence rate of the numerical scheme.

2.4 Energy Variational Method

Derivation of the model in this thesis is based on the energy dissipation law which holds ubiquitously in physical systems involving irreversible processes [160, 35, 72, 161, 55]. This law states that for an isothermal and closed system, the rate of change of the energy balances with the energy dissipation [160]:

$$\frac{d}{dt}E^{\text{total}} = -\Delta \leq 0\ , \tag{2.8}$$

where E^{total} is the total energy of the system and Δ is the rate of energy dissipation or entropy production, which is usually represented as a quadratic function of certain rates such as the fluid velocity [160]. Eq. (2.8) can be easily derived via the combination of the First and Second Laws of Thermodynamics [161]:

From the first law of thermodynamics we can get

$$\frac{d(K+U)}{dt} = \frac{dw}{dt} + \frac{dQ}{dt} \tag{2.9}$$

From the second law of thermodynamics we have

$$\frac{TdS}{dt} = \frac{dQ}{dt} + \Delta \tag{2.10}$$

Where K is the kinetic energy, U is the internal energy, w is the work done from outside of the system, Q is the heat generated, S is the entropy, T is the temperature and Δ is the entropy production [161]. Combine the two equations and assume the system is thermostatic, we have:

$$\frac{d}{dt}(K+U-TS) = \frac{dw}{dt} - \Delta \tag{2.11}$$

Where $K+U-TS$ is the total energy E^{total}. If the system is enclosed, which means $\frac{dw}{dt} = 0$, then we have the energy dissipation law:

$$\frac{dE^{total}}{dt} = -\Delta \tag{2.12}$$

The choices of the total energy functional and the dissipation functional, together with the kinematic (transport) relations of the variables employed in the system, determine all the physical and mechanical considerations and assumptions for the problem [47]. A general technique to determine these relations of variables may be found in [52, 55].

2.5 Finite Element Method

Finite element method (FEM) has been introduced into computational fluid dynamics for a long time [20]. FEM is suitable to solve problems that requires different space accuracy in different part of the domain or requires a smooth solution in the whole domain. This property makes FEM a very good choice when dealing with phase-field method.

The first step of FEM is to discretise the domain into a mesh which is consist of small triangles as shown in Figure 2.1. The specific grouping of the triangles are called the element. Different kinds of elements are used in different problem depending on its behaviour. By doing this, the

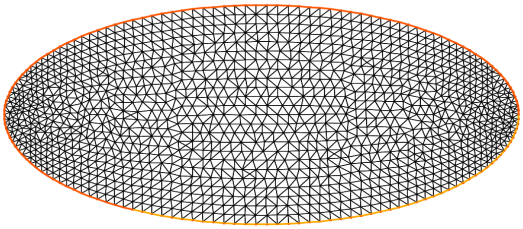

Figure 2.1: Mesh generated in an ellipse.

initial problem could be divided into a combination of problems in each small elements. By solving the equation set of all the elements, we are finally able to get an approximation of the solution on the domain. More details of the theoretical support of FEM could be found in [121].

Chapter 3

Moving Contact Lines Problem

3.1 Introduction

In this chapter, the phase field function is firstly defined using volume averaged density and mass fraction of a control volume. Then, we rederive and generalize the thermodynamically consistent q-NSCH moving contact lines model in [99] from a variational point of view by combining with the Energy Variational Approach (EnVarA) [35, 96, 172] and Onsager's Variation Principle [2, 122, 123, 175]. It starts from two functionals for the total energy and dissipation, together with the kinematic equations based on physical laws of conservation. The specific forms of the fluxes and stresses in the kinematic equations is obtained by taking the time derivative of the total energetic functional and comparing with the predefined dissipation functional. More details could be found in [163]. In addition to bulk energy and dissipation, the energy and dissipation on the boundary are introduced to model the dynamics of contact lines. Our energy variational approach consistently yields both the correct bulk equations (the q-NSCH sytem) and a modified General Navier Boundary Condition (GNBC) for the case of mass averaged velocity. The density effect on the contact line is explicitly modelled compared with the traditional GNBC [44, 45, 116, 160, 171] in the case of volume averaged velocity, where the effect is modelled implicitly by the bulk and boundary interactions.

The second goal is to design an efficient energy stable scheme for the obtained q-NSCH system with large density ratio. There are not many such schemes developed for the MCLs. For the incompressible NSCH system, the development of such schemes may be found in [128, 44, 45, 101, 174, 26, 137, 168, 171] and only a few of them [45, 171] are for variable density MCL models using the volume-averaged velocity (satisfying the incompressible condition in the whole domain). We shall develop an energy stable scheme for our thermodynamically consistent variable density q-NSCH system using the mass-averaged velocity. Based on the author's previous works [53, 54, 77], we design a mass conservative C^0 finite element method for the q-NSCH system with a consistent discrete energy law. Thanks to a Δp term in the quasi-incompressible condition, which is similar to the pressure stabilization of pseudo-compressibility methods [16, 120, 132], q-NSCH system does not need to satisfy the Babuska-Brezzi inf-sup condition [90, 91, 92, 132]. This may be considered as another benefit of the developed quasi-incompressible NSCH system.

The rest of this chapter is organized as follows. In Section 3.2, we present the thermodynamically consistent derivation of the q-NSCH system and its non-dimensionlization. The C^0 finite element algorithm for the q-NSCH system and the energy stable analysis are shown in Section 3.3. Section 3.4 presents the numerical results, including the convergence case study and the example of rising bubbles.

3.2 Mathematical Model

3.2.1 Phase field function and laws of conservation

We consider a complex mixture consisting of two phase fluids with different density. The interface of two fluids intersects with the wall $\partial\Omega_w$ at the contact line Γ_w (see Fig. 3.1 (a)). Around the interface, we choose a control volume $V(t)$, where there are two phases labeled by $i = 1,2$, with volume V_i and mass M_i (see Fig. 3.1 (b)). If local average density of each phase is denoted by $\bar{\rho}_i = M_i/V$ and pure phase density is denoted by $\rho_i = M_i/V_i$, then we define the density of mixture as:

$$\rho = \frac{M}{V} = \frac{M_1}{V} + \frac{M_2}{V} = \bar{\rho}_1 + \bar{\rho}_2. \tag{3.1}$$

Let $c_i = \frac{M_i}{M}$ be the mass fraction of each phase. Then we have [52]

$$\frac{1}{\rho} = \frac{V}{M} = \frac{V_1}{M} + \frac{V_2}{M} = \frac{c_1}{\rho_1} + \frac{c_2}{\rho_2} = \frac{c}{\rho_1} + \frac{1-c}{\rho_2}, \tag{3.2}$$

where $c = c_1$ is adopted in last equality. By its definition we can easily find that $c = 1$ indicates that the domain is purely consist of phase 1, with $c = 0$ for pure phase 2, and $0 < c < 1$ for mixture of phase 1 and 2. Thus c actually works as a measurement of the composition of substance at every space point in the domain. In the rest of the chapter, c is called the phase field function or phase order which works as a variable that describes the distribution of different phases.

Remark 3.2.1. *In this thesis, ρ_1 and ρ_2 are given as constants. Thus, according to the definition* (3.2)*, the mixture density ρ is constant almost everywhere except the interfacial region.*

If we assume those two fluids move with velocities $\mathbf{u}_i$ ($i = 1,2$), then the mass conservation of each phase inside the control volume is

$$\frac{\partial \bar{\rho}_i}{\partial t} + \nabla \cdot (\mathbf{u}_i \bar{\rho}_i) = 0, \quad i = 1,2. \tag{3.3}$$

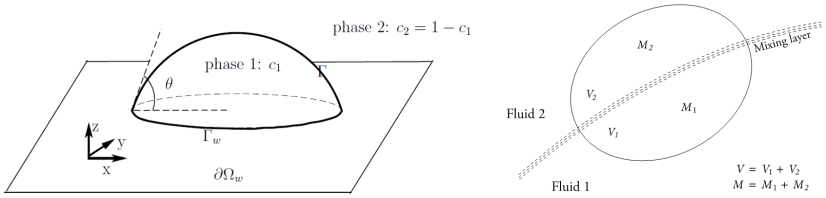

(a) (b)

Figure 3.1: Schematic of moving contact line problems (a) and interface (b).

Introducing the mass averaged velocity as

$$\rho\mathbf{u} = \bar{\rho}_1\mathbf{u}_1 + \bar{\rho}_2\mathbf{u}_2, \tag{3.4}$$

and combining with Eq.(3.1) yields the conservation of mass for the mixture

$$\frac{\partial\rho}{\partial t} + \nabla\cdot(\mathbf{u}\rho) = 0. \tag{3.5}$$

Next, with an arbitrary volume $V(t) \in \Omega$, laws of conservation state [52]

$$\frac{d}{dt}\int_{V(t)}\rho c dx = -\int_{\partial V(t)}\boldsymbol{j}_c\cdot\mathbf{n}dS, \tag{3.6}$$

$$\frac{d}{dt}\int_{V(t)}\rho\mathbf{u}dx = \int_{\partial V(t)}(\boldsymbol{\sigma}_\eta + \boldsymbol{\sigma}_c)\cdot\mathbf{n}dS. \tag{3.7}$$

Here, the first equation is the conservation of phase-field function (phase 1) and $\boldsymbol{j}_c$ is the flux of phase-field function. The second equation is the conservation of momentum, where $\boldsymbol{\sigma}_\eta$ is the viscous stress and $\boldsymbol{\sigma}_c$ is the extra stress induced by two-phase interface due to nonzero ∇c.

Thanks to the Reynold transport theory, Eqs.(3.5)-(3.7) yield the following kinematic equations in the domain Ω [54, 163]

$$\begin{cases} \rho\frac{Dc}{Dt} = -\nabla\cdot\boldsymbol{j}_c, \\ \frac{D\rho}{Dt} + \rho\nabla\cdot\mathbf{u} = \frac{\partial\rho}{\partial t} + \nabla\cdot(\mathbf{u}\rho) = 0, \\ \rho(\frac{\partial\mathbf{u}}{\partial t} + \mathbf{u}\cdot\nabla\mathbf{u}) = \nabla\cdot\boldsymbol{\sigma}_\eta + \nabla\cdot\boldsymbol{\sigma}_c. \end{cases} \tag{3.8}$$

By definition of $\rho = \rho(c(\mathbf{x},t))$ in Eq. (3.2), above equations yield the quasi-incompressibility condition [54, 99]

$$\nabla\cdot\mathbf{u} = \frac{1}{\rho^2}\frac{d\rho}{dc}(\nabla\cdot\boldsymbol{j}_c). \tag{3.9}$$

In the present case, we denote

$$\alpha = -\frac{1}{\rho^2}\frac{d\rho}{dc} = \frac{\rho_2 - \rho_1}{\rho_1 \rho_2}, \tag{3.10}$$

then the quasi-incompressibility condition is written as

$$\nabla \cdot \mathbf{u} = -\alpha \nabla \cdot \boldsymbol{j}_c. \tag{3.11}$$

Remark 3.2.2. *Equations* (3.10)-(3.11) *show that the quasi-incompressibilty condition depends on the density difference of two fluids. When the two phases have the same density, i.e.* $\rho_1 = \rho_2$*, it will consistently degenerate to the incompressibility condition. It makes a difference when two fluids have large density ratio and near the interfacial region [52, 54, 99].*

On the boundary of domain $\partial\Omega$, the following boundary conditions are used

$$\begin{cases} \mathbf{u}\cdot\mathbf{n} = 0, \;\; \mathbf{u}^s \cdot \boldsymbol{\tau}_i = u^s_{\tau_i} = f_{\tau_i} \\ \frac{\partial c}{\partial t} + \mathbf{u}\cdot\nabla_\Gamma c = J_\Gamma, \\ \boldsymbol{j}_c \cdot \mathbf{n} = 0, \end{cases} \tag{3.12}$$

where $\mathbf{u}^s = \mathbf{u}_\tau - \mathbf{u}_w$ with $\mathbf{u}_\tau = \mathbf{u} - (\mathbf{u}\cdot\mathbf{n})\mathbf{n}$ is the fluid slip velocity with respect to the wall, $\frac{D_\Gamma c}{Dt} = \frac{\partial c}{\partial t} + \mathbf{u}\cdot\nabla_\Gamma c$ is the surface material derivative, the Allen-Cahn type boundary condition is used for c and $\nabla_\Gamma = \nabla - \mathbf{n}(\mathbf{n}\cdot\nabla)$ is surface gradient on the boundary $\partial\Omega$. The quantities f_{τ_i} and J_Γ are to be determined. During the derivation, we assume the solid wall is fixed, i.e. $\mathbf{u}^s = \mathbf{u}_\tau$.

3.2.2 Model derivation

Now we start to derive the exact forms of $\boldsymbol{j}_c$, $\boldsymbol{\sigma}_\eta$, $\boldsymbol{\sigma}_c$ in Eq. (3.8), f_{τ_i} and J_Γ in Eq. (3.12) by using energy variation method.

The total energy consists of the kinetic energy, the phase mixing energy and the energy on solid wall boundary $\partial\Omega_w$

$$\begin{aligned} E^{tot} &= E_{kin} + E_{mix} + E_w \\ &= \int_\Omega \frac{\rho(c)|\mathbf{u}|^2}{2} d\boldsymbol{x} + \int_\Omega \lambda_c \rho(c) \left(G(c) + \frac{\gamma^2}{2}|\nabla c|^2 \right) d\boldsymbol{x} + \int_{\partial\Omega_w} f_w(c) dS, \end{aligned} \tag{3.13}$$

together with

$$G(c) = \frac{1}{4}c^2(1-c)^2, \quad f_w(c) = -\frac{\sigma}{2}\cos(\theta_s)\sin(\frac{(2c-1)\pi}{2}), \tag{3.14}$$

where λ_c is the mixing energy density, γ is the capillary width of the interface, θ_s is static contact angle and σ is surface tension. The mixing energy E_{mix} represents the competition between a homogeneous bulk mixing energy density term $G(c)$ ('hydrophobic' part) that enforces total separation of the two phases into pure components, and a gradient distortional term $\frac{|\nabla c|^2}{2}$ ('hydrophilic' part) that represents the nonlocal interactions between two phases and penalizes spatial heterogeneity.

The dissipation functional is composed of the dissipations due to fluid friction and irreversible mixing of two phases in bulk and the dissipation on the boundary

$$\Delta = \int_\Omega 2\eta(c)|\boldsymbol{D}_\eta|^2 d\boldsymbol{x} + \int_\Omega \lambda(c)|\nabla\cdot\mathbf{u}|^2 d\boldsymbol{x} + \int_\Omega M^{-1}|\boldsymbol{j}_c|^2 d\boldsymbol{x} + \int_{\partial\Omega_w} \left(M_\Gamma^{-1} J_\Gamma^2 + \beta_\Gamma|\mathbf{u}_\tau|^2\right) dS \tag{3.15}$$

where $\lambda(c)$ and $\eta(c)$ are the two Lamé coefficients, $\boldsymbol{D}_\eta = (\nabla\mathbf{u} + (\nabla\mathbf{u})^T)/2$ is the strain rate, M is mobility coefficient in bulk, M_Γ is mobility coefficient on the wall, in this thesis M and M_Γ are treated as constant for convenience. $\beta_\Gamma(c)$ is wall friction coefficient. In the present chapter, $\eta(c)$ and β_Γ are linearly approximated by

$$\frac{1}{\eta(c)} = \frac{c}{\eta_1} + \frac{(1-c)}{\eta_2}, \quad \frac{1}{\beta_\Gamma(c)} = \frac{c}{\beta_{\Gamma_1}} + \frac{(1-c)}{\beta_{\Gamma_2}},$$

where η_i and $\beta_{\Gamma,i}$ with $i = 1,2$ are coefficients of each phase.

Remark 3.2.3. *A recent paper has pointed out that the mobility of the multiphase flow M should take a degenerate form $M(c)$ where $M(c) = 0$ when $c = 1$ and 0 in order to make the system consistent in single fluid [34]. In this thesis, we take M a constant in consideration of the simplicity of numerical calculation. However, it should be mentioned that in our model, we can let the mobility depend on c so as to satisfy the requirements in [34].*

During the derivation, the following lemma is frequently used.

Lemma 3.2.1. *For a continuous function $f(\boldsymbol{x},t)$, if the density ρ satisfies the conservation law* (3.5) *in the domain Ω and $\mathbf{u}\cdot\mathbf{n} = 0$ on the boundary $\partial\Omega$, then we have*

$$\frac{d}{dt}\int_\Omega \rho(\boldsymbol{x},t) f(\boldsymbol{x},t) d\boldsymbol{x} = \int_\Omega \rho \frac{df}{dt} d\boldsymbol{x}.$$

By taking the time derivative of the total energetic functional, we have

$$\frac{dE^{tot}}{dt} = \frac{d}{dt}E_{kin} + \frac{d}{dt}E_{mix} + \frac{d}{dt}E_w = I_1 + I_2 + I_3. \tag{3.16}$$

For the first term in (3.16), using the last two equations in Eq.(3.8) yields

$$\begin{aligned} I_1 &= \frac{d}{dt}\int_\Omega \frac{\rho|\mathbf{u}|^2}{2}d\boldsymbol{x} \\ &= -\int_\Omega(\boldsymbol{\sigma}_\eta : \nabla\mathbf{u} + \boldsymbol{\sigma}_c : \nabla\mathbf{u})d\boldsymbol{x} + \int_\Omega \alpha\nabla p\cdot \boldsymbol{j}_c d\boldsymbol{x} - \int_\Omega p\nabla\cdot\mathbf{u}d\boldsymbol{x} \\ &\quad + \int_{\partial\Omega_w}((\boldsymbol{\sigma}_\eta+\boldsymbol{\sigma}_c)\cdot\mathbf{n})\cdot\mathbf{u}_\tau dS, \end{aligned} \tag{3.17}$$

where we have introduced a Lagrangian multiplier p with respect to the quasi-compressibility condition (3.9) and have used the boundary conditions $\mathbf{u}\cdot\mathbf{n}=0$ and $\boldsymbol{j}_c\cdot\mathbf{n}=0$. For the second term in (3.16), using the first equation in Eq.(3.8) and last two boundary conditions in Eq. (3.12) yields

$$\begin{aligned} I_2 &= \frac{d}{dt}\int_\Omega \rho\lambda_c\left(G(c)+\frac{\gamma^2}{2}|\nabla c|^2\right)d\boldsymbol{x} \\ &= \int_\Omega \nabla\mu\cdot\boldsymbol{j}_c d\boldsymbol{x} - \int_\Omega \lambda_c\gamma^2(\rho\nabla c\otimes\nabla c):\nabla\mathbf{u}d\boldsymbol{x} + \int_{\partial\Omega_w}\rho\lambda_c\gamma^2\partial_n c\frac{D_\Gamma c}{Dt}dS, \end{aligned} \tag{3.18}$$

where $\mu = \lambda_c\left(\frac{dG}{dc} - \frac{1}{\rho}\gamma^2\nabla\cdot(\rho\nabla c)\right)$.

where we have used the definition $\frac{D_\Gamma c}{Dt} = \frac{\partial c}{\partial t} + \mathbf{u}_\tau\cdot\nabla_\Gamma c$ and $\mathbf{u}_\tau = \mathbf{u}^s$. Also we have used the boundary conditions in (3.26). The detailed derivations of Eqs.(3.17) -(3.18) are given in Appendix A.1.1. The last term I_3 in (3.16) yields

$$I_3 = \frac{d}{dt}\int_{\partial\Omega_w} f_w dS = \int_{\partial\Omega_w}\frac{df_w}{dc}\frac{\partial c}{\partial t}dS \tag{3.19}$$

Combining Eqs.(3.17) -(3.19), we obtain the derivative of the energy functional

$$\begin{aligned} \frac{dE^{tot}}{dt} &= -\int_\Omega \boldsymbol{\sigma}_\eta : \nabla\mathbf{u}d\boldsymbol{x} - \int_\Omega\left(\boldsymbol{\sigma}_c + \lambda_c\gamma^2\rho\nabla c\otimes\nabla c\right):\nabla\mathbf{u}d\boldsymbol{x} \\ &\quad + \int_\Omega \nabla\mu\cdot\boldsymbol{j}_c d\boldsymbol{x} + \int_\Omega\nabla(\alpha p)\cdot\boldsymbol{j}_c d\boldsymbol{x} - \int_\Omega p\nabla\cdot\mathbf{u}d\boldsymbol{x} \\ &\quad + \int_{\partial\Omega_w}((\boldsymbol{\sigma}_\eta+\boldsymbol{\sigma}_c)\cdot\mathbf{n})\cdot\mathbf{u}_\tau dS + \int_{\partial\Omega_w}\rho\lambda_c\gamma^2\partial_n c\frac{dc}{dt}dS + \int_{\partial\Omega_w}\frac{df_w}{dc}\frac{\partial c}{\partial t}dS \\ &= -\int_\Omega \boldsymbol{\sigma}_\eta : \nabla\mathbf{u}d\boldsymbol{x} - \int_\Omega\left(\boldsymbol{\sigma}_c + \lambda_c\gamma^2\rho\nabla c\otimes\nabla c\right):\nabla\mathbf{u}d\boldsymbol{x} \\ &\quad + \int_\Omega \nabla\tilde{\mu}\cdot\boldsymbol{j}_c d\boldsymbol{x} - \int_\Omega p\nabla\cdot\mathbf{u}d\boldsymbol{x} \\ &\quad + \int_{\partial\Omega_w}\left((\boldsymbol{\sigma}_\eta+\boldsymbol{\sigma}_c)\cdot\mathbf{n} - \frac{df_w}{dc}\nabla_\Gamma c\right)\cdot\mathbf{u}_\tau dS + \int_{\partial\Omega_w}L(c)\frac{dc}{dt}dS \\ &= -\int_\Omega \boldsymbol{\sigma}_\eta : \nabla\mathbf{u}d\boldsymbol{x} - \int_\Omega\left(\boldsymbol{\sigma}_c + \lambda_c\gamma^2\rho\nabla c\otimes\nabla c\right):\nabla\mathbf{u}d\boldsymbol{x} \\ &\quad + \int_\Omega \nabla\tilde{\mu}\cdot\boldsymbol{j}_c d\boldsymbol{x} - \int_\Omega p\nabla\cdot\mathbf{u}d\boldsymbol{x} \end{aligned}$$

$$+\int_{\partial\Omega_w}\left((\boldsymbol{\sigma}_\eta+\boldsymbol{\sigma}_c)\cdot\mathbf{n}-\frac{df_w}{dc}\nabla_\Gamma c\right)\cdot\mathbf{u}_\tau dS+\int_{\partial\Omega_w}L(c)J_\Gamma dS, \tag{3.20}$$

where we have defined

$$\tilde{\mu} = \mu+\alpha p=\lambda_c\frac{dG}{dc}-\frac{\lambda_c\gamma^2}{\rho}\nabla\cdot(\rho\nabla c)+\alpha p, \tag{3.21}$$

$$L(c) = \rho\lambda_c\gamma^2\partial_n c+\frac{df_w}{dc}. \tag{3.22}$$

Using energy dissipation law $dE^{tot}/dt=-\Delta$ [35, 161] and comparing (3.20) with the pre-defined dissipation functional in Eq.(3.15) yields

$$\begin{cases} \boldsymbol{j}_c=-M\nabla\tilde{\mu},\\ \boldsymbol{\sigma}_\eta=2\eta\boldsymbol{D}_\eta+\lambda\nabla\cdot\mathbf{u}I-pI=\eta(\nabla\mathbf{u}+(\nabla\mathbf{u})^T)+\lambda\nabla\cdot\mathbf{u}I-pI,\\ \boldsymbol{\sigma}_c=-\lambda_c\gamma^2\rho\,(\nabla c\otimes\nabla c),\\ J_\Gamma=-M_\Gamma L(c),\\ u_{\tau_i}=\beta_\Gamma^{-1}\boldsymbol{\tau}_i\cdot(-(\boldsymbol{\sigma}_\eta+\boldsymbol{\sigma}_c)\cdot\mathbf{n}+\frac{df_w}{dc}\nabla_\Gamma c). \end{cases} \tag{3.23}$$

By the definition of $\boldsymbol{\sigma}_\eta$ and $\boldsymbol{\sigma}_c$, the slip boundary condition (last equation in (3.23)) could be further written in the GNBC format

$$u^s_{\tau_i}=\beta_\Gamma^{-1}\boldsymbol{\tau}_i\cdot(-\boldsymbol{\sigma}_\eta\cdot\mathbf{n}+L(c)\nabla_\Gamma c). \tag{3.24}$$

To summarize, we have the following model for the two-phase flow with variable density for three unknowns $c,\mathbf{u},p$, in domain Ω,

$$\rho\frac{Dc}{Dt}=\nabla\cdot(M\nabla\tilde{\mu}), \tag{3.25a}$$

$$\tilde{\mu}=\lambda_c\frac{dG}{dc}-\frac{\lambda_c\gamma^2}{\rho}\nabla\cdot(\rho\nabla c)+\alpha p, \tag{3.25b}$$

$$\frac{D\rho}{Dt}+\rho\nabla\cdot\mathbf{u}=0, \tag{3.25c}$$

$$\rho\frac{D\mathbf{u}}{Dt}=\nabla\cdot(2\eta\boldsymbol{D}_\eta)+\nabla(\lambda\nabla\cdot\mathbf{u})-\nabla p-\nabla\cdot(\lambda_c\gamma^2\rho\nabla c\otimes\nabla c), \tag{3.25d}$$

with boundary conditions on $\partial\Omega$

$$\begin{cases} \frac{D_\Gamma c}{Dt}=-M_\Gamma L(c),\\ \nabla\tilde{\mu}\cdot\mathbf{n}=0,\\ \mathbf{u}\cdot\mathbf{n}=0,\\ u^s_{\tau_i}=\beta_\Gamma^{-1}(-(\mathbf{n}\cdot\boldsymbol{\sigma}_\eta\cdot\boldsymbol{\tau}_i)+L(c)\partial_{\tau_i}c), i=1,2. \end{cases}, \tag{3.26}$$

where $L(c)$ and $\boldsymbol{\sigma}_\eta$ are defined in (3.22) and (3.23).

Remark 3.2.4. *Note that in the above boundary conditions* (3.26)*, the density effect on the contact line dynamics is explicitly modelled both in the boundary dynamics of phase-field and in velocity slip boundary condition through $L(c)$ term.*

It is worth noting that the above system satisfies the following energy dissipation law.

Theorem 3.2.2. *If $c, \mathbf{u}, p$ are smooth solutions of above system* (3.25)-(3.26)*, then the following energy law is satisfied:*

$$\begin{aligned}\frac{dE^{tot}}{dt} &= \frac{d}{dt}\left\{\int_\Omega \frac{\rho|\mathbf{u}|^2}{2}d\boldsymbol{x} + \int_\Omega \lambda_c\rho\left(G(c)+\frac{\gamma^2}{2}|\nabla c|^2\right)d\boldsymbol{x} + \int_{\partial\Omega_w} f_w(c)dS\right\}\\ &= -\int_\Omega 2\eta|\boldsymbol{D}_\eta|^2 d\boldsymbol{x} - \int_\Omega \lambda|\nabla\cdot\mathbf{u}|^2 d\boldsymbol{x} - \int_\Omega M|\nabla\tilde{\mu}|^2 d\boldsymbol{x}\\ &\quad - \int_{\partial\Omega_w}\left(M_\Gamma|L(c)|^2 + \beta_\Gamma|\mathbf{u}_\tau^s|^2\right)dS. \end{aligned} \tag{3.27}$$

Proof: The main idea of the proof is obtained by multiplying the phase-field equation (3.25a) by $\tilde{\mu}$, multiplying the chemical potential equation (3.25b) by $\frac{dc}{dt}$, multiplying the mass conservation equation (3.25c) by p, multiplying the Navier-Stokes equation (3.25d) by $\mathbf{u}$, and then summing them up.

Taking the inner product of the phase-field equation (3.25a) with $\tilde{\mu}$ results in the following equation

$$\int_\Omega \rho\frac{Dc}{Dt}\tilde{\mu}d\boldsymbol{x} = -\int_\Omega M|\nabla\tilde{\mu}|^2 d\boldsymbol{x}, \tag{3.28}$$

where we used the boundary condition $\partial_n\tilde{\mu} = 0$ in (3.26).

Multiplying the chemical potential (3.25b) by $\rho\frac{Dc}{Dt}$ yields

$$\int_\Omega \tilde{\mu}\rho\frac{Dc}{Dt} = \int_\Omega \lambda_c\rho\frac{DG}{Dt}d\boldsymbol{x} + \int_\Omega \lambda\gamma^2\nabla c\nabla\left(\frac{Dc}{Dt}\right)d\boldsymbol{x} - \int_\Omega \frac{p}{\rho}\frac{d\rho}{dc}\frac{Dc}{Dt}d\boldsymbol{x} - \int_{\partial\Omega_w}\lambda\gamma^2\rho\partial_n c\frac{D_\Gamma c}{Dt}dS. \tag{3.29}$$

Summing up the above two equations, we have

$$\begin{aligned}&\int_\Omega \lambda_c\rho\frac{DG}{Dt}d\boldsymbol{x} + \int_\Omega \lambda\gamma^2\nabla c\nabla\left(\frac{Dc}{Dt}\right)d\boldsymbol{x}\\ &= -\int_\Omega M|\nabla\tilde{\mu}|^2 d\boldsymbol{x} + \int_\Omega \frac{p}{\rho}\frac{d\rho}{dc}\frac{Dc}{Dt}d\boldsymbol{x} + \int_{\partial\Omega_w}\lambda\gamma^2\rho\partial_n c\frac{D_\Gamma c}{Dt}dS. \end{aligned} \tag{3.30}$$

where the boundary condition $\mathbf{u}\cdot\mathbf{n} = 0$ is used.

Multiplying the Navier-stokes equation (3.25d) by $\mathbf{u}$ followed by integration by parts, the rate of change of kinetic energy is calculated as

$$\frac{d}{dt}\int_\Omega \rho\frac{|\mathbf{u}|^2}{2}d\boldsymbol{x}$$

$$
\begin{aligned}
&= -\int_\Omega 2\eta|\boldsymbol{D}_\eta|^2 d\boldsymbol{x} - \int_\Omega \lambda|\nabla\cdot\mathbf{u}|^2 d\boldsymbol{x} + \int_\Omega p\nabla\cdot\mathbf{u} d\boldsymbol{x} + \int_\Omega \lambda\gamma^2\rho(\nabla c\otimes\nabla c):\nabla\mathbf{u} d\boldsymbol{x} \\
&\quad - \int_{\partial\Omega_w} \beta_\Gamma|\mathbf{u}_\tau|^2 + \int_{\partial\Omega_w} \frac{df_w}{dc}\nabla_\Gamma c\cdot\mathbf{u}_\tau dS \\
&= -\int_\Omega 2\eta|\boldsymbol{D}_\eta|^2 d\boldsymbol{x} - \int_\Omega \lambda|\nabla\cdot\mathbf{u}|^2 d\boldsymbol{x} + \int_\Omega p\nabla\cdot\mathbf{u} d\boldsymbol{x} + \int_\Omega \lambda\gamma^2\rho(\nabla c\otimes\nabla c):\nabla\mathbf{u} d\boldsymbol{x} \\
&\quad - \int_{\partial\Omega_w} \beta_\Gamma|\mathbf{u}_\tau|^2 - \frac{d}{dt}\int_{\partial\Omega_w} f_w dS - \int_{\partial\Omega_w} \frac{df_w}{dc} M_\Gamma L(c) dS, \qquad (3.31)
\end{aligned}
$$

From the derivation of I_2 in Appendix A, we get

$$
\begin{aligned}
&\frac{d}{dt}\int_\Omega \rho\lambda_c\left(G(c)+\frac{\gamma^2}{2}|\nabla c|^2\right)d\boldsymbol{x} \\
&= \int_\Omega \rho\lambda_c\frac{DG}{Dt}d\boldsymbol{x} + \int_\Omega \rho\lambda_c\gamma^2\nabla c\cdot\nabla\left(\frac{Dc}{Dt}\right)d\boldsymbol{x} - \int_\Omega \rho\lambda_c\gamma^2(\nabla c\otimes\nabla c):\nabla\mathbf{u} d\boldsymbol{x}. \qquad (3.32)
\end{aligned}
$$

Combining the equations (3.30)-(3.32) leads to the final energy dissipation law. □

Remark 3.2.5. *In the above derivation, we have neglected the external body force, for example the gravity. If the effect of gravity needs to be taken into consideration, an extra gravitational potential should be added to the total energy*

$$
E^{tot} = \int_\Omega \frac{\rho|\mathbf{u}|^2}{2}d\boldsymbol{x} + \int_\Omega \lambda_c\rho\left(G(c)+\frac{\gamma^2}{2}|\nabla c|^2\right)d\boldsymbol{x} + \int_{\partial\Omega_w} f_w(c)dS + \int_\Omega \rho g z d\boldsymbol{x}, \qquad (3.33)
$$

where g is the gravitational constant and z is the vertical position. Using the fact that [52]

$$
\frac{d}{dt}\int_\Omega \rho g z dv = \int_\Omega \rho g\mathbf{u}\cdot\boldsymbol{e}_z d\boldsymbol{x}, \quad \boldsymbol{e}_z = (0,0,1)^T, \qquad (3.34)
$$

the conservation of momentum equation (3.25d) *is changed to*

$$
\rho\frac{D\mathbf{u}}{Dt} = \nabla\cdot(2\eta\boldsymbol{D}_\eta) + \nabla(\lambda\nabla\cdot\mathbf{u}) - \nabla p - \nabla\cdot(\lambda_c\gamma^2\rho\nabla c\otimes\nabla c) - \rho g\boldsymbol{e}_z. \qquad (3.35)
$$

3.2.3 Non-dimensionalization and reformulation

In the following parts of the chapter, we assume that $\lambda = -\frac{2\eta}{3}$ for simplicity. Now we introduce the dimensionless variables

$$
\begin{aligned}
&\hat{x} = \tfrac{x}{L^*}, \quad \hat{\mathbf{u}} = \tfrac{\mathbf{u}}{U^*}, \quad \hat{\rho} = \tfrac{\rho}{\rho_*}, \quad \hat{t} = \tfrac{t}{t^*}, \quad \hat{\tilde{\mu}} = \tfrac{\tilde{\mu}}{\mu^*}, \quad \hat{p} = \tfrac{p}{P_*}, \\
&\hat{\eta} = \tfrac{\eta}{\eta^*}, \quad \hat{\mathscr{M}} = \tfrac{M}{M^*}, \quad \hat{\mathscr{M}}_\Gamma = \tfrac{M_\Gamma}{M_\Gamma^*}, \quad l_s^{-1} = \tfrac{\beta_\Gamma}{\beta_\Gamma^*}, \quad \varepsilon = \tfrac{\gamma}{L^*}, \qquad (3.36)
\end{aligned}
$$

where L^*, U^*, ρ^*, η^* and M^* are the characteristic scales of length, velocity, density, viscosity, and mobility coefficient,

$$t^* = \frac{L^*}{U^*}, \quad \mu^* = \lambda_c \varepsilon, \quad P^* = \rho^* \mu^*, \quad M^* = \frac{\rho^* U^* L^*}{\mu^*}, \quad M_\Gamma^* = \frac{1}{t^* \rho^* \lambda_c \gamma}, \quad \beta_\Gamma^* = \frac{\eta^*}{L^*}. \tag{3.37}$$

For convenience, the hat symbol will be removed in the dimensionless quantities, and the dimensionless system of (3.25,3.26) is given by

$$\rho \frac{Dc}{Dt} = \nabla \cdot (\mathscr{M} \nabla \tilde{\mu}), \tag{3.38a}$$

$$\tilde{\mu} = \frac{1}{\varepsilon} \frac{dG}{dc} - \frac{\varepsilon}{\rho} \nabla \cdot (\rho \nabla c) + \alpha p, \tag{3.38b}$$

$$Re \rho \frac{D\mathbf{u}}{Dt} = \nabla \cdot (\eta (\nabla \mathbf{u} + (\nabla \mathbf{u})^T)) - \nabla (\frac{2\eta}{3} \nabla \cdot \mathbf{u}) - \frac{Re}{\beta} \nabla p - \frac{Re}{\beta} \varepsilon \nabla \cdot (\rho \nabla c \otimes \nabla c), \tag{3.38c}$$

$$\nabla \cdot \mathbf{u} = \alpha \nabla \cdot (\mathscr{M} \nabla \tilde{\mu}), \tag{3.38d}$$

with boundary conditions

$$\frac{D_\Gamma c}{Dt} = -\mathscr{M}_\Gamma L(c), \tag{3.39a}$$

$$\partial_n \tilde{\mu} = 0, \tag{3.39b}$$

$$\mathbf{u} \cdot \mathbf{n} = 0, \tag{3.39c}$$

$$l_s^{-1} u_{\tau_i}^s = -\mathbf{n} \cdot \boldsymbol{\sigma}_\eta \cdot \boldsymbol{\tau}_i + \frac{Re}{\beta} L \partial_{\tau_i} c, \tag{3.39d}$$

where

$$L(c) = \varepsilon \rho \partial_n c + \alpha_w \frac{df_w}{dc}, \quad f_w(c) = -\frac{1}{2} \cos(\theta_s) \sin(\frac{(2c-1)\pi}{2}). \tag{3.40}$$

and with dimensionless parameters

$$Re = \frac{\rho^* U^* L^*}{\eta^*}, \quad \beta = \frac{(U^*)^2}{\mu^*}, \quad \alpha_w = \frac{\sigma}{\rho^* \lambda_c \gamma}. \tag{3.41}$$

If we redefine

$$\bar{p} = p + \rho (\frac{1}{\varepsilon} G(c) + \frac{\varepsilon}{2} |\nabla c|^2), \tag{3.42a}$$

$$\bar{\mu} = \tilde{\mu} - \alpha \bar{p}, \tag{3.42b}$$

then the system (3.38) could be rewritten as

$$\rho\frac{Dc}{Dt} = \nabla\cdot(\mathscr{M}\nabla\bar{\mu}) + \alpha\nabla\cdot(\mathscr{M}\nabla\bar{p}), \tag{3.43a}$$

$$\bar{\mu} = \frac{1}{\varepsilon}\frac{dG}{dc} - \frac{\varepsilon}{\rho}\nabla\cdot(\rho\nabla c) - \alpha\rho(\frac{1}{\varepsilon}G(c) + \frac{\varepsilon}{2}|\nabla c|^2), \tag{3.43b}$$

$$Re\rho\frac{D\mathbf{u}}{Dt} = \nabla\cdot(\eta(\nabla\mathbf{u} + (\nabla\mathbf{u})^T)) - \nabla(\frac{2\eta}{3}\nabla\cdot\mathbf{u}) - \frac{Re}{\beta}\nabla\bar{p} + \frac{Re}{\beta}\rho\bar{\mu}\nabla c \tag{3.43c}$$

$$\nabla\cdot\mathbf{u} = \alpha\nabla\cdot(\mathscr{M}\nabla\bar{\mu}) + \alpha^2\nabla\cdot(\mathscr{M}\nabla\bar{p}), \tag{3.43d}$$

For the purpose of obtaining a meaningful weak form, we define the Sobolev spaces as follows [53]

$$\boldsymbol{W}^{1,3}(\Omega) = (W^{1,3}(\Omega))^2, \tag{3.44}$$

$$\boldsymbol{W}_b^{1,3}(\Omega) = \{\mathbf{u} = (u_x, u_y)^T \in \boldsymbol{W}^{1,3} | u_y = b, \text{on } \partial\Omega_w\}, \tag{3.45}$$

$$\boldsymbol{W}_b = W^{1,3}(\Omega)\times W^{1,3}(\Omega)\times \boldsymbol{W}_b^{1,3}(\Omega)\times W^{1,3/2}(\Omega), \tag{3.46}$$

where Ω is the domain that considered. Then,the system satisfies the following energy dissipation law.

Theorem 3.2.3. *If $(c,\mu,\mathbf{u},\bar{p}) \in \boldsymbol{W}_b$, be smooth solutions of above system* (3.43) *with boundary conditions* (3.39)*, then the following energy law is satisfied:*

$$\begin{aligned}\frac{d\mathscr{E}^{tot}}{dt} &= \frac{d}{dt}\left\{\int_\Omega \frac{\rho|\mathbf{u}|^2}{2}d\boldsymbol{x} + \frac{1}{\beta}\int_\Omega \rho\left(\frac{1}{\varepsilon}G(c) + \frac{\varepsilon}{2}|\nabla c|^2\right)d\boldsymbol{x} + \frac{\alpha_w}{\beta}\int_{\partial\Omega_w} f_w dS\right\}\\ &= -\frac{1}{Re}\int_\Omega \eta\sum_{i<j}|\partial_i u_j + \partial_j u_i|^2 d\boldsymbol{x} - \frac{2}{3Re}\int_\Omega \eta\sum_{i<j}|\partial_i u_i - \partial_j u_j|^2 d\boldsymbol{x} - \frac{1}{\beta}\int_\Omega \mathscr{M}|\nabla\tilde{\mu}|^2 d\boldsymbol{x}\\ &\quad - \int_{\partial\Omega_w}\left(\frac{1}{\beta}\mathscr{M}_\Gamma|L(c)|^2 + \frac{1}{l_s Re}|\mathbf{u}^s|^2\right)dS.\end{aligned} \tag{3.47}$$

The proof is similar as Theorem 3.2.2. Here we omit the details.

Remark 3.2.6. *When the walls move, i.e. $\mathbf{u}_w \neq 0$, the above energy dissipation law has an extra term induced by external energy input*

$$\begin{aligned}\frac{d\mathscr{E}^{tot}}{dt} &= -\frac{1}{Re}\int_\Omega \eta\sum_{i<j}|\partial_i u_j + \partial_j u_i|^2 d\boldsymbol{x} - \frac{2}{3Re}\int_\Omega \eta\sum_{i<j}|\partial_i u_i - \partial_j u_j|^2 d\boldsymbol{x} - \frac{1}{\beta}\int_\Omega \mathscr{M}|\nabla\tilde{\mu}|^2 d\boldsymbol{x}\\ &\quad - \int_{\partial\Omega_w}\left(\frac{1}{\beta}\mathscr{M}_\Gamma|L(c)|^2 + \frac{1}{l_s Re}|\mathbf{u}^s|^2\right)dS - \int_{\partial\Omega_w}\frac{1}{l_s Re}\mathbf{u}^s\cdot\mathbf{u}_w dS.\end{aligned} \tag{3.48}$$

3.3 Numerical Scheme and Analysis

3.3.1 Time-discrete primitive method

In this section, we present the numerical method of system (3.43) with boundary conditions (3.39) in the primitive variable formulation. Let $\Delta t > 0$ denote the time step, and assume $(\mathbf{u}^n, \bar{p}^n, c^n, \bar{\mu}^n)$ are the solutions at the time $t = n\Delta t$. We then find the solutions at time $t = (n+1)\Delta t$ are $\left(\mathbf{u}^{n+1}, \bar{p}^{n+1}, c^{n+1}, \bar{\mu}^{n+1}\right)$ that satisfy

$$\rho^n \frac{c^{n+1}-c^n}{\Delta t} + \rho^{n+1}(\mathbf{u}^{n+1}\cdot\nabla)c^{n+1} = \nabla\cdot(\mathscr{M}\nabla\bar{\mu}^{n+1}) + \alpha\nabla\cdot(\mathscr{M}\nabla\bar{p}^{n+1}), \tag{3.49a}$$

$$\rho^n\bar{\mu}^{n+1} = \frac{\rho^{n+1/2}}{\varepsilon}g(c^{n+1},c^n) - \varepsilon\nabla\cdot(\rho^{n+1/2}\nabla c^{n+1/2}) - \alpha\rho^n\rho^{n+1}\left(\frac{G^{n+1/2}}{\varepsilon} + \frac{\varepsilon}{2}(|\nabla c|^2)^{n+1/2}\right), \tag{3.49b}$$

$$\rho^n\frac{\mathbf{u}^{n+1}-\mathbf{u}^n}{\Delta t} + \rho^n(\mathbf{u}^n\cdot\nabla)\mathbf{u}^{n+1} + \frac{1}{2}\left(\frac{\rho^{n+1}-\rho^n}{\Delta t} + \nabla\cdot(\rho^n\mathbf{u}^n)\right)\mathbf{u}^{n+1} + \frac{1}{\beta}\nabla\bar{p}^{n+1} = \frac{1}{\beta}\rho^{n+1}\bar{\mu}^{n+1}\nabla c^{n+1} + \frac{1}{Re}\nabla\cdot(\eta^n(\nabla\mathbf{u}^{n+1} + (\nabla\mathbf{u}^{n+1})^T)) - \frac{2}{3Re}\nabla(\eta^n\nabla\cdot\mathbf{u}^{n+1}), \tag{3.49c}$$

$$\nabla\cdot\mathbf{u}^{n+1} = \alpha\nabla\cdot(\mathscr{M}\nabla\bar{\mu}^{n+1}) + \alpha^2\nabla\cdot(\mathscr{M}\nabla\bar{p}^{n+1}), \tag{3.49d}$$

with boundary conditions

$$\frac{c^{n+1}-c^n}{\Delta t} + \mathbf{u}_{\boldsymbol{\tau}}^{n+1}\cdot\nabla_\Gamma c^{n+1/2} = -\mathscr{M}_\Gamma L^{n+1/2}(c), \tag{3.50a}$$

$$\partial_n\tilde{\mu}^{n+1} = 0, \tag{3.50b}$$

$$L^{n+1/2}(c) = \varepsilon\rho^{n+1/2}\partial_n c^{n+1/2} + \alpha_w\frac{f_w(c^{n+1})-f_w(c^n)}{c^{n+1}-c^n}, \tag{3.50c}$$

$$\mathbf{u}^{n+1}\cdot\mathbf{n} = 0, \tag{3.50d}$$

$$l_s^{-1}u_{\tau_i}^{n+1} = -\mathbf{n}\cdot(\eta^n(\nabla\mathbf{u}^{n+1} + (\nabla\mathbf{u}^{n+1})^T))\cdot\boldsymbol{\tau}_i + \frac{Re}{\beta}L^{n+1/2}\partial_{\tau_i}c^{n+1/2}, \tag{3.50e}$$

Note that Eq.(3.50a) and Eq.(3.50c) would give out the description of $\partial_n c$ on the boundary, together with Eq.(3.50b), making Eq.(3.49b) uniquely solvable. $\tilde{\mu}$ is defined in (3.42b) and we have used the notations

$$(\cdot)^{n+1/2} = \tfrac{1}{2}[(\cdot)^{n+1} + (\cdot)^n], \quad \rho^{n+1} = \rho(c^{n+1}), \tag{3.51}$$

$$g(c^{n+1},c^n) = \tfrac{1}{4}(c^{n+1}(c^{n+1}-1) + c^n(c^n-1))(c^{n+1}+c^n-1). \tag{3.52}$$

For above discretization, it satisfies the following properties.

Lemma 3.3.1. *([54]) If c^{n+1} is the solution of above system* (3.49)-(3.50)*, then we have*

$$G(c^{n+1}) - G(c^n) = g(c^{n+1}, c^n)(c^{n+1} - c^n), \tag{3.53a}$$

$$\rho(c^{n+1}) - \rho(c^n) = -\alpha\rho^{n+1}\rho^n(c^{n+1} - c^n). \tag{3.53b}$$

And the system (3.49)-(3.50) *yields mass conservation for each component of binary fluid*

$$\int_\Omega \rho^{n+1} d\boldsymbol{x} = \int_\Omega \rho^n d\boldsymbol{x}, \tag{3.54a}$$

$$\int_\Omega \rho^{n+1} c^{n+1} d\boldsymbol{x} = \int_\Omega \rho^n c^n d\boldsymbol{x}. \tag{3.54b}$$

Theorem 3.3.2. *If $\left(c^{n+1}, \mu^{n+1}, \mathbf{u}^{n+1}, \bar{p}^{n+1}\right) \in \boldsymbol{W}_b$ are solutions of above system* (3.49) *with boundary conditions* (3.50)*, then the following energy law is satisfied:*

$$\begin{aligned} & \mathscr{E}^{n+1,tot} - \mathscr{E}^{n,tot} \\ = \; & -\frac{\Delta t}{Re}\int_\Omega \eta^n \sum_{i<j} |\partial_i u_j^{n+1} + \partial_j u_i^{n+1}|^2 d\boldsymbol{x} - \frac{2\Delta t}{3Re}\int_\Omega \eta^n \sum_{i<j} |\partial_i u_i^{n+1} - \partial_j u_j^{n+1}|^2 d\boldsymbol{x} \\ & -\frac{\Delta t}{\beta}\int_\Omega \mathscr{M} |\nabla \tilde{\mu}^{n+1}|^2 d\boldsymbol{x} - \int_{\partial\Omega_w} \left(\frac{\Delta t}{\beta} \mathscr{M}_\Gamma \left| L^{n+1/2}(c) \right|^2 + \frac{1}{l_s Re} |\mathbf{u}_\tau^{n+1}|^2 \right) dS, \end{aligned} \tag{3.55}$$

where

$$\mathscr{E}^{n+1,tot} = \int_\Omega \frac{\rho^{n+1}}{2} |\mathbf{u}^{n+1}|^2 d\boldsymbol{x} + \frac{1}{\beta}\int_\Omega \rho^{n+1} \left(\frac{1}{\varepsilon} G(c^{n+1}) + \frac{\varepsilon}{2} |\nabla c^{n+1}|^2 \right) d\boldsymbol{x} + \frac{\alpha_w}{\beta}\int_{\partial\Omega_w} f_w(c^{n+1}) dS$$

is the discretized total energy.

Proof: Taking inner product of the first equation (3.49a) with $\frac{\Delta t}{\beta}\bar{\mu}^{n+1}$ results in the following equation

$$\begin{aligned} & \frac{1}{\beta}\int_\Omega \rho^n (c^{n+1} - c^n)\bar{\mu}^{n+1} d\boldsymbol{x} + \frac{\Delta t}{\beta}\int_\Omega \rho^{n+1}\mathbf{u}^{n+1} \cdot \nabla c^{n+1} \bar{\mu}^{n+1} d\boldsymbol{x} \\ = \; & -\frac{\Delta t}{\beta}\int_\Omega \mathscr{M} \nabla \bar{\mu}^{n+1} \cdot \nabla \tilde{\mu}^{n+1} d\boldsymbol{x}, \end{aligned} \tag{3.56}$$

where we used the boundary condition (3.50b) and the definition of $\bar{\mu}$ in (3.42b).

Multiplying the second equation (3.49b) with $\frac{c^{n+1}-c^n}{\beta}$ yields [54]

$$\begin{aligned} & \frac{1}{\beta}\int_\Omega \rho^n (c^{n+1} - c^n)\bar{\mu}^{n+1} d\boldsymbol{x} \\ = \; & \frac{1}{\beta}\int_\Omega \rho^{n+1} \left(\frac{1}{\varepsilon} G(c^{n+1}) + \frac{\varepsilon}{2} |\nabla c^{n+1}|^2 \right) d\boldsymbol{x} - \frac{1}{\beta}\int_\Omega \rho^n \left(\frac{1}{\varepsilon} G(c^n) + \frac{\varepsilon}{2} |\nabla c^n|^2 \right) d\boldsymbol{x} \\ & -\frac{1}{\beta}\int_{\partial\Omega_w} \varepsilon \rho^{n+1/2} \partial_n c^{n+1/2} (c^{n+1} - c^n) dS, \end{aligned} \tag{3.57}$$

where we use the results in above Lemma and the boundary condition (3.50a).

Multiplying the Navier-Stokes equation (3.49c) with $\Delta t \mathbf{u}^{n+1}$, we have

$$\begin{aligned}
&\frac{1}{2}\int_\Omega(\rho^{n+1}|\mathbf{u}^{n+1}|^2)d\boldsymbol{x}-\frac{1}{2}\int_\Omega(\rho^n|\mathbf{u}^n|^2)d\boldsymbol{x}\\
=\;&-\frac{\Delta t}{Re}\int_\Omega\eta^n\sum_{i<j}|\partial_i u_j^{n+1}+\partial_j u_i^{n+1}|^2d\boldsymbol{x}-\frac{2\Delta t}{3Re}\int_\Omega\eta^n\sum_{i<j}|\partial_i u_i^{n+1}-\partial_j u_j^{n+1}|^2d\boldsymbol{x}\\
&+\frac{\Delta t}{\beta}\int_\Omega\bar{p}^{n+1}\nabla\cdot\mathbf{u}^{n+1}d\boldsymbol{x}+\frac{\Delta t}{\beta}\int_\Omega\rho^{n+1}\bar{\mu}^{n+1}\nabla c^{n+1}\cdot\mathbf{u}^{n+1}d\boldsymbol{x}\\
&-\frac{\Delta t}{Re}\int_{\partial\Omega_w}l_s^{-1}|\mathbf{u}^{s,n+1}|^2dS+\frac{\Delta t}{\beta}\int_{\partial\Omega_w}L^{n+1/2}\nabla_\Gamma c^{n+1/2}\cdot\mathbf{u}_{\boldsymbol{\tau}}^{n+1}dS,\\
&-\frac{\Delta t}{Re}\int_{\partial\Omega_w}l_s^{-1}\mathbf{u}^{s,n+1}\cdot\mathbf{u}_w dS,
\end{aligned}\tag{3.58}$$

where we used the slip boundary condition (3.50e) and the tensor calculation in Appendix A.1.3.

For the last term in above equation, combining the definition of $L^{n+1/2}$ (3.50c) and equation (3.50a) yields

$$\begin{aligned}
&\frac{\Delta t}{\beta}\int_{\partial\Omega_w}L^{n+1/2}\nabla_\Gamma c^{n+1/2}\cdot\mathbf{u}_{\boldsymbol{\tau}}^{n+1}dS\\
=\;&\frac{\Delta t}{\beta}\left(\int_{\partial\Omega_w}\alpha_w\frac{f_w(c^{n+1})-f_w(c^n)}{c^{n+1}-c^n}\nabla_\Gamma c^{n+1/2}\cdot\mathbf{u}_{\boldsymbol{\tau}}^{n+1}dS\right.\\
&\left.+\int_{\partial_\Omega}\varepsilon\rho^{n+1/2}\partial_n c^{n+1/2}\nabla_\Gamma c^{n+1/2}\cdot\mathbf{u}_{\boldsymbol{\tau}}^{n+1}dS\right)\\
=\;&-\frac{1}{\beta}\int_{\partial\Omega_w}\alpha_w(f_w(c^{n+1})-f_w(c^n))dS-\frac{\Delta t}{\beta}\int_{\partial\Omega_w}\alpha_w\frac{f_w(c^{n+1})-f_w(c^n)}{c^{n+1}-c^n}\mathscr{M}_\Gamma L^{n+1/2}dS\\
&+\frac{\Delta t}{\beta}\int_{\partial_\Omega}\varepsilon\rho^{n+1/2}\partial_n c^{n+1/2}\nabla_\Gamma c^{n+1/2}\cdot\mathbf{u}_{\boldsymbol{\tau}}^{n+1}dS.
\end{aligned}\tag{3.59}$$

Then equation (3.58) could be rewritten as

$$\begin{aligned}
&\frac{1}{2}\int_\Omega(\rho^{n+1}|\mathbf{u}^{n+1}|^2)d\boldsymbol{x}-\frac{1}{2}\int_\Omega(\rho^n|\mathbf{u}^n|^2)d\boldsymbol{x}+\frac{1}{\beta}\int_{\partial\Omega_w}\alpha_w(f_w(c^{n+1})-f_w(c^n))dS\\
=\;&-\frac{\Delta t}{Re}\int_\Omega\eta^n\sum_{i<j}|\partial_i u_j^{n+1}+\partial_j u_i^{n+1}|^2d\boldsymbol{x}-\frac{2\Delta t}{3Re}\int_\Omega\eta^n\sum_{i<j}|\partial_i u_i^{n+1}-\partial_j u_j^{n+1}|^2d\boldsymbol{x}\\
&+\frac{\Delta t}{\beta}\int_\Omega\bar{p}^{n+1}\nabla\cdot\mathbf{u}^{n+1}d\boldsymbol{x}+\frac{\Delta t}{\beta}\int_\Omega\rho^{n+1}\bar{\mu}^{n+1}\nabla c^{n+1}\cdot\mathbf{u}^{n+1}d\boldsymbol{x}\\
&-\frac{\Delta t}{Re}\int_{\partial\Omega_w}l_s^{-1}|\mathbf{u}^{s,n+1}|^2dS-\frac{\Delta t}{\beta}\int_{\partial\Omega_w}\alpha_w\frac{f_w(c^{n+1})-f_w(c^n)}{c^{n+1}-c^n}\mathscr{M}_\Gamma L^{n+1/2}dS\\
&+\frac{\Delta t}{\beta}\int_{\partial_\Omega}\varepsilon\rho^{n+1/2}\partial_n c^{n+1/2}\nabla_\Gamma c^{n+1/2}\cdot\mathbf{u}_{\boldsymbol{\tau}}^{n+1}dS-\frac{\Delta t}{Re}\int_{\partial\Omega_w}l_s^{-1}\mathbf{u}^{s,n+1}\cdot\mathbf{u}_w dS.
\end{aligned}\tag{3.60}$$

Multiplying the last equation (3.49d) with $\frac{\Delta t}{\beta}\bar{p}^{n+1}$ yields

$$0 = -\int_\Omega \frac{\Delta t}{\beta}\bar{p}^{n+1}\nabla\cdot\mathbf{u}^{n+1}d\boldsymbol{x} - \frac{\Delta t}{\beta}\int_\Omega \mathscr{M}\nabla\tilde{\mu}^{n+1}\cdot\nabla\bar{p}^{n+1}d\boldsymbol{x}. \tag{3.61}$$

Summing up equations (3.56), (3.57), (3.60) and (3.61) results

$$\begin{aligned}
&\mathscr{E}^{n+1,tot} - \mathscr{E}^{n,tot}\\
=\ & -\frac{\Delta t}{Re}\int_\Omega \eta^n \sum_{i<j}|\partial_i u_j^{n+1} + \partial_j u_i^{n+1}|^2 d\boldsymbol{x} - \frac{2\Delta t}{3Re}\int_\Omega \eta^n \sum_{i<j}|\partial_i u_i^{n+1} - \partial_j u_j^{n+1}|^2 d\boldsymbol{x}\\
& -\frac{\Delta t}{\beta}\int_\Omega \mathscr{M}|\nabla\tilde{\mu}^{n+1}|^2 d\boldsymbol{x} - \int_{\partial\Omega_w}\frac{\Delta t}{l_s Re}|\mathbf{u}^{s,n+1}|^2 dS - \int_{\partial\Omega_w}\frac{\Delta t}{l_s Re}\mathbf{u}^{s,n+1}\cdot\mathbf{u}_w dS\\
& -\frac{\Delta t}{\beta}\int_{\partial\Omega_w}\alpha_w\frac{f_w(c^{n+1}) - f_w(c^n)}{c^{n+1}-c^n}\mathscr{M}_\Gamma L^{n+1/2} dS\\
& +\frac{1}{\beta}\int_{\partial\Omega_w}\varepsilon\rho^{n+1/2}\partial_n c^{n+1/2}(c^{n+1}-c^n)dS + \frac{\Delta t}{\beta}\int_{\partial_\Omega}\varepsilon\rho^{n+1/2}\partial_n c^{n+1/2}\nabla_\Gamma c^{n+1/2}\cdot\mathbf{u}_\tau^{n+1} dS\\
=\ & -\frac{\Delta t}{Re}\int_\Omega \eta^n \sum_{i<j}|\partial_i u_j^{n+1} + \partial_j u_i^{n+1}|^2 d\boldsymbol{x} - \frac{2\Delta t}{3Re}\int_\Omega \eta^n \sum_{i<j}|\partial_i u_i^{n+1} - \partial_j u_j^{n+1}|^2 d\boldsymbol{x}\\
& -\frac{\Delta t}{\beta}\int_\Omega \mathscr{M}|\nabla\tilde{\mu}^{n+1}|^2 d\boldsymbol{x} - \int_{\partial\Omega_w}\frac{\Delta t}{l_s Re}|\mathbf{u}^{s,n+1}|^2 dS - \int_{\partial\Omega_w}\frac{\Delta t}{l_s Re}\mathbf{u}^{s,n+1}\cdot\mathbf{u}_w dS\\
& -\frac{\Delta t}{\beta}\int_{\partial\Omega_w}\alpha_w\frac{f_w(c^{n+1}) - f_w(c^n)}{c^{n+1}-c^n}\mathscr{M}_\Gamma L^{n+1/2} dS - \frac{\Delta t}{\beta}\int_{\partial\Omega_w}\varepsilon\rho^{n+1/2}\partial_n c^{n+1/2}\mathscr{M}_\Gamma L^{n+1/2} dS\\
=\ & -\frac{\Delta t}{Re}\int_\Omega \eta^n \sum_{i<j}|\partial_i u_j^{n+1} + \partial_j u_i^{n+1}|^2 d\boldsymbol{x} - \frac{2\Delta t}{3Re}\int_\Omega \eta^n \sum_{i<j}|\partial_i u_i^{n+1} - \partial_j u_j^{n+1}|^2 d\boldsymbol{x}\\
& -\frac{\Delta t}{\beta}\int_\Omega \mathscr{M}|\nabla\tilde{\mu}^{n+1}|^2 d\boldsymbol{x} - \int_{\partial\Omega_w}\frac{\Delta t}{l_s Re}|\mathbf{u}^{s,n+1}|^2 dS - \frac{\Delta t}{\beta}\int_{\partial\Omega_w}\mathscr{M}_\Gamma|L^{n+1/2}|^2 dS\\
& -\int_{\partial\Omega_w}\frac{\Delta t}{l_s Re}\mathbf{u}^{s,n+1}\cdot\mathbf{u}_w dS,
\end{aligned} \tag{3.62}$$

where we used the definition of $\bar{\mu}$ (3.42b) and slip boundary condition (3.50e). □

Remark 3.3.1. *The scheme is highly nonlinear and coupled since we would like to ensure that the discretise energy decays in the same manner as the continous version, i.e. the equality. However, it brings difficulties on analysis of convergence study. The proof of the unique solvability could be as hard as the original PDE. Most of existing studies on the solvability of Cahn-Hilliard system [36, 154, 68], are done by using the linearization (convex splitting) treatments which highly decrease the nonlinearity.*

Newton's method [54, 53] is utilized to solve the nonlinear system and the solvability of Newton iteration is given in the following Theorem.

Theorem 3.3.3. *If time-step Δt is small enough, Newton method of system* (3.49) *with boundary condition* (3.50) *is uniquely solvable.*

Proof: Combining Eqs.(3.49) (b)(d) with boundary conditions (3.50) yields:

$$\bar{p}^{n+1} = \bar{p}(\mathbf{u}^{n+1}, c^{n+1}) \tag{3.63}$$

$$\bar{\mu}^{n+1} = \bar{\mu}(c^{n+1}) \tag{3.64}$$

Substitute $\bar{p}^{n+1}$ and $\bar{\mu}^{n+1}$ into Eqs. (3.49) (a) and (c), then apply Newton method to the equations. Let $()^{n+1,k}$ be the value of the variable at kth iteration loop at time step $(n+1)\Delta t$. Let $()^n$ be the value of the variable at time step $n\Delta t$. Assume that $\mathbf{u}^{n+1,k}$, $c^{n+1,k}$, $\bar{p}^{n+1,k}$, and $\bar{\mu}^{n+1,k}$ are the original guess of solution of the equations, we have:

$$\mathscr{F}(\mathbf{u}^{n+1,k}, c^{n+1,k}) + \nabla_{\mathbf{u}^{n+1,k}, c^{n+1,k}} \mathscr{F} \begin{pmatrix} \mathbf{u}^{n+1,k+1} - \mathbf{u}^{n+1,k} \\ c^{n+1,k+1} - c^{n+1,k} \end{pmatrix} + \mathscr{C}(\mathbf{u}^n, c^n) = 0 \tag{3.65}$$

Where $\mathscr{F}(\mathbf{u}^{n+1,k}, c^{n+1,k})$ and $\mathscr{C}(\mathbf{u}^n, c^n)$ are known. $\nabla_{\mathbf{u}^{n+1,k}, c^{n+1,k}} \mathscr{F}$ is Jacobian of $\mathscr{F}$. Multiplying $\frac{\Delta t)}{\rho^n}$ to the equation and merge the known terms we have:

$$\begin{pmatrix} I - \Delta t A_1 & A_2 \\ A_3 & I - \Delta t A_4 \end{pmatrix} \begin{pmatrix} \mathbf{u}^{n+1,k+1} \\ c^{n+1,k+1} \end{pmatrix} = \mathscr{C}' \left(\mathbf{u}^{n+1,k}, c^{n+1,k}, \mathbf{u}^n, c^n \right) \tag{3.66}$$

where

$$A_1 = -\mathbf{u}_n \cdot \nabla - \frac{1}{\rho^n \beta} \nabla \frac{\partial \bar{p^{n+1,k}}}{\partial \mathbf{u}^{n+1,k}} + \frac{\eta^n}{\rho^n Re} \nabla \cdot (\nabla + (\nabla)^T) - \frac{2\eta^n}{3\rho^n Re} \nabla^2 \tag{3.67}$$

$$\begin{aligned} A_2 = -\frac{1}{\rho^n \beta} (& \rho^{n+1,k} \bar{\mu}^{n+1,k} \nabla + \frac{\partial \bar{\rho^{n+1,k}}}{\partial c^{n+1,k}} \bar{\mu}^{n+1,k} \nabla c^{n+1,k} \\ & + \rho^{n+1,k} \frac{\partial \bar{\mu}^{n+1,k}}{\partial c^{n+1,k}} \nabla c^{n+1,k}) \end{aligned} \tag{3.68}$$

$$A_3 = \frac{1}{\rho^n} (\rho^{n+1,k} \nabla c^{n+1,k} - \alpha \mathscr{M} \nabla^2 \frac{\partial \bar{p}^{n+1,k}}{c^{n+1,k}}) \tag{3.69}$$

$$\begin{aligned} A_4 = -\frac{1}{\rho^n} (& \frac{\partial \rho^{n+1,k}}{\partial c^{n+1,k}} (\mathbf{u}^{n+1,k} \cdot \nabla) c^{n+1,k} + \rho^{n+1,k} \mathbf{u}^{n+1,k} \cdot \nabla \\ & - \mathscr{M} \nabla^2 \frac{\partial \bar{\mu}^{n+1,k}}{c^{n+1,k}} - \alpha \mathscr{M} \nabla^2 \frac{\partial \bar{p}^{n+1,k}}{c^{n+1,k}}) \end{aligned} \tag{3.70}$$

$$\bar{\mu}^{n+1,k} = \bar{\mu}(c^{n+1,k}), \bar{p}^{n+1,k} = \bar{p}(c^{n+1,k}, \mathbf{u}^{n+1,k}), \rho^{n+1,k} = \rho(c^{n+1,k}) \tag{3.71}$$

With Gauss' elimination, we have:

$$\begin{pmatrix} I - \Delta t A_1 & A_2 \\ 0 & I - \Delta t A_4 - (I - \Delta t A_1)^{-1} \Delta t A_3 \end{pmatrix} \begin{pmatrix} \mathbf{u}^{n+1,k+1} \\ c^{n+1,k+1} \end{pmatrix} = \mathscr{C}''(\mathbf{u}^{n+1,k}, c^{n+1,k}, \mathbf{u}^n, c^n).$$

When Δt is small enough, $I-\Delta t A_i$, $i=1,2$ is invertible.

$$(I-\Delta t A_i)^{-1} = I+\Delta t A_i+\Delta t^2 A_i^2+... \tag{3.72}$$

Thus the coefficient matrix is invertible. So the Newton iteration of system (3.49) is uniquely solvable.

3.3.2 Fully-discrete C^0 finite element scheme

The fully-discrete C^0 finite element scheme for this time-discrete primitive scheme (3.49)-(3.50) is presented in this section. For simplicity, we only consider a two-dimensional case here. It is straightforward to extend the results to three-dimensional case. The domain Ω is a bounded domain with Lipschitz-continuous boundary $\partial\Omega$. Specifically, we denote $\partial\Omega_w$ as the solid wall where the slip boundary condition is used. Let $\boldsymbol{W}_b^h = H^h \times H^h \times \boldsymbol{U}_b^h \times P^h$ be the finite dimensional space of $\boldsymbol{W}_b$ based on a given finite element discretization of Ω. If we assume that $\rho^n \in L^\infty(\Omega)$ and positive [53], then the weak form of semi-discrete system (3.49) with boundary conditions (3.50) is the following: finding $(c_h^{n+1}, \bar{\mu}_h^{n+1}, \mathbf{u}_h^{n+1}, \bar{p}_h^{n+1}) \in \boldsymbol{W}_b^h$, such that

$$\begin{aligned}
&\int_\Omega \left(\rho_h^n \frac{c_h^{n+1}-c_h^n}{\Delta t} + \rho_h^{n+1}(\mathbf{u}_h^{n+1}\cdot\nabla)c_h^{n+1}\right)\psi_h d\boldsymbol{x} \\
&= -\int_\Omega \mathscr{M}\left(\nabla\bar{\mu}_h^{n+1} + \alpha\nabla\bar{p}_h^{n+1}\right)\cdot\nabla\psi_h d\boldsymbol{x}, \qquad (3.73a)\\
&\int_\Omega \rho_h^n \bar{\mu}_h^{n+1}\chi_h d\boldsymbol{x} = \int_\Omega \frac{\rho_h^{n+1/2}}{\varepsilon} g(c_h^{n+1}, c_h^n)\chi_h d\boldsymbol{x} + \int_\Omega \varepsilon\rho_h^{n+1/2}\nabla c_h^{n+1/2}\cdot\nabla\chi_h d\boldsymbol{x} \\
&- \int_\Omega \alpha\rho_h^n\rho_h^{n+1}\left(\frac{G_h^{n+1/2}}{\varepsilon} + \frac{\varepsilon}{2}(|\nabla c_h|^2)^{n+1/2}\right)\chi_h d\boldsymbol{x} \\
&+ \int_{\partial\Omega_w} (\mathscr{M}_\Gamma^{-1}(\frac{c_h^{n+1}-c_h^n}{\Delta t} + \mathbf{u}_{h,\tau}^{n+1}\cdot\nabla_\Gamma c_h^{n+1/2}) + \alpha_w\frac{f_w(c_h^{n+1})-f_w(c_h^n)}{c_h^{n+1}-c_h^n})\chi_h dS, \qquad (3.73b)\\
&\int_\Omega \left\{\rho_h^n\frac{\mathbf{u}_h^{n+1}-\mathbf{u}_h^n}{\Delta t} + \rho_h^n(\mathbf{u}_h^n\cdot\nabla)\mathbf{u}_h^{n+1} + \frac{1}{2}\left(\frac{\rho_h^{n+1}-\rho_h^n}{\Delta t} + \nabla\cdot(\rho_h^n\mathbf{u}_h^n)\right)\right\}\cdot\mathbf{v}_h d\boldsymbol{x} \\
&= -\frac{1}{\beta}\int_\Omega \nabla\bar{p}_h^{n+1}\cdot\mathbf{v}_h d\boldsymbol{x} \int_\Omega \frac{1}{\beta}\rho_h^{n+1}\bar{\mu}_h^{n+1}\nabla c^{n+1}\cdot\mathbf{v}_h d\boldsymbol{x} \\
&- \frac{1}{Re}\int_\Omega (\eta^n(\nabla\mathbf{u}_h^{n+1} - (\nabla\mathbf{u}_h^{n+1})^T)) : \nabla\mathbf{v}_h d\boldsymbol{x} + \frac{2}{3Re}\int_\Omega \eta^n\nabla\cdot\mathbf{u}_h^{n+1}\nabla\cdot\mathbf{v}_h d\boldsymbol{x} \\
&- \int_{\partial\Omega_w}\frac{1}{Rel_s}\mathbf{u}_{h,\tau}\cdot\mathbf{v}_h dS + \int_{\partial_\Omega}\frac{1}{\beta}L_h^{n+1/2}\nabla_\Gamma c_h^{n+1/2}\cdot\mathbf{v}_h d\boldsymbol{x}, \qquad (3.73c)\\
&- \int_\Omega \nabla q_h\cdot\mathbf{u}_h^{n+1} = -\alpha\int_\Omega \mathscr{M}\left(\nabla\bar{\mu}_h^{n+1} + \alpha\nabla\bar{p}_h^{n+1}\right)\cdot\nabla q_h d\boldsymbol{x}, \qquad (3.73d)
\end{aligned}$$

for any $(\psi_h, \chi_h, \mathbf{v}_h, q_h) \in \boldsymbol{W}_0^h$. Here we use boundary condition (3.50a) and (3.50c) in Eq.(3.73b) to get the final term.

Lemma 3.3.4. *The fully discretized system* (3.73) *satisfies mass conservation for each component of binary fluid*

$$\int_\Omega \rho_h^{n+1} d\boldsymbol{x} = \int_\Omega \rho_h^n d\boldsymbol{x}, \tag{3.74a}$$

$$\int_\Omega \rho_h^{n+1} c_h^{n+1} d\boldsymbol{x} = \int_\Omega \rho_h^n c_h^n d\boldsymbol{x}. \tag{3.74b}$$

Proof: Setting $\psi_h = q_h = \rho_h^{n+1}$ in Eqs.(3.73a) and (3.73d), we have

$$\begin{aligned}
&\int_\Omega \left(\rho_h^n \rho_h^{n+1} \frac{c_h^{n+1} - c_h^n}{\Delta t} + (\rho_h^{n+1})^2 (\mathbf{u}_h^{n+1} \cdot \nabla) c_h^{n+1} \right) d\boldsymbol{x} \\
&= -\int_\Omega \mathscr{M} \left(\nabla \bar{\mu}_h^{n+1} + \alpha \nabla \bar{p}_h^{n+1} \right) \cdot \nabla \rho_h^{n+1} d\boldsymbol{x}, \\
&-\frac{1}{\alpha} \int_\Omega \nabla \rho_h^{n+1} \cdot \mathbf{u}_h^{n+1} d\boldsymbol{x} = \int_\Omega \mathscr{M} \left(\nabla \bar{\mu}_h^{n+1} + \alpha \nabla \bar{p}_h^{n+1} \right) \cdot \nabla \rho_h^{n+1} d\boldsymbol{x}.
\end{aligned}$$

Adding the above two equations and using Eqs. (3.10) and (3.53b) yields

$$\int_\Omega \left(\frac{\rho_h^{n+1} - \rho_h^n}{\Delta t} + \nabla \cdot (\rho^{n+1} \mathbf{u}_h^{n+1}) \right) d\boldsymbol{x} = 0. \tag{3.75}$$

Using the boundary condition $\mathbf{u}_h^{n+1} \cdot \mathbf{n} = 0$, we have the conservation of total mass

$$\int_\Omega (\rho_h^{n+1} - \rho_h^n) d\boldsymbol{x} = 0. \tag{3.76}$$

Choosing $\psi_h = q_h = \hat{\rho}_h^{n+1} c_h^{n+1}$ in Eqs.(3.73a) and (3.73d), similarly we have

$$\int_\Omega \left(\frac{\rho_h^{n+1} - \rho_h^n}{\Delta t} c_h^{n+1} + \nabla \cdot (\rho^{n+1} \mathbf{u}_h^{n+1}) \right) c_h^{n+1} d\boldsymbol{x} = 0. \tag{3.77}$$

Choosing $\psi_h = 1$ in Eq.(3.73a) yields

$$\int_\Omega \left(\rho_h^n \frac{c_h^{n+1} - c_h^n}{\Delta t} + \rho_h^{n+1} (\mathbf{u}_h^{n+1} \cdot \nabla) c_h^{n+1} \right) d\boldsymbol{x} = 0. \tag{3.78}$$

Adding the above two equations and using the velocity boundary condition $\mathbf{u}_h^{n+1} \cdot \mathbf{n} = 0$, we have

$$\int_\Omega (\rho_h^{n+1} c_h^{n+1} - \rho_h^n c_h^n) d\boldsymbol{x} = 0. \qquad \square$$

Theorem 3.3.5. *If* $(c_h^{n+1}, \bar{\mu}_h^{n+1}, \mathbf{u}_h^{n+1}, \bar{p}_h^{n+1})$ *are solutions of above system* (3.73)*, then the following energy law is satisfied:*

$$\mathscr{E}_h^{n+1,tot} - \mathscr{E}_h^{n,tot}$$

$$
\begin{aligned}
= & -\frac{\Delta t}{Re}\int_\Omega \eta_h^n \sum_{i<j} |\partial_i u_{h,j}^{n+1} + \partial_j u_{h,i}^{n+1}|^2 d\boldsymbol{x} - \frac{2\Delta t}{3Re}\int_\Omega \eta^n \sum_{i<j} |\partial_i u_{h,i}^{n+1} - \partial_j u_{h,j}^{n+1}|^2 d\boldsymbol{x} \\
& -\frac{\Delta t}{\beta}\int_\Omega \mathscr{M} |\nabla \tilde{\mu}_h^{n+1}|^2 d\boldsymbol{x} - \Delta t \int_{\partial\Omega_w} \left(\frac{1}{\beta}\mathscr{M}_\Gamma \left| L_h^{n+1/2}(c_h) \right|^2 + \frac{1}{l_s Re} |\mathbf{u}_h^{s,n+1}|^2 \right) dS \\
& -\Delta t \int_{\partial\Omega_w} \frac{1}{l_s Re} \mathbf{u}_h^{s,n+1} \cdot \mathbf{u}_w dS
\end{aligned} \tag{3.79}
$$

where

$$
\mathscr{E}_h^{n+1} = \int_\Omega \frac{\rho_h^{n+1} |\mathbf{u}_h^{n+1}|^2}{2} d\boldsymbol{x} + \frac{1}{\beta}\int_\Omega \rho_h^{n+1} \left(\frac{1}{\varepsilon} G(c_h^{n+1}) + \frac{\varepsilon}{2} |\nabla c_h^{n+1}|^2 \right) d\boldsymbol{x} + \frac{\alpha_w}{\beta}\int_{\partial\Omega_w} f_w(c_h^{n+1}) dS
$$

is the discretized total energy.

It can be proved by choosing

$$
\psi_h = \frac{\Delta t}{\beta}\bar{\mu}_h^{n+1}, \;\; \chi_h = \frac{c_h^{n+1} - c_h^n}{\beta}, \;\; \mathbf{v}_h = \Delta t \mathbf{u}_h^{n+1}, \;\; q_h = \frac{\Delta t}{\beta}\bar{p}_h^{n+1} \tag{3.80}
$$

in Eq. (3.73) and following the proof of Theorem 3.3.2. The proof of sovability of the fully discrete scheme could be referred to Theorem 4.4.5 in Chapter 3. We don't show the detail here.

3.4 Simulation Results

In this section, we present some numerical simulations using the aforementioned algorithm. Three cases are considered: Couette flow, moving oil-water mix in shear flow and rising bubbles to illustrate the convergence rate, the effect of contact angle and the quasi-incompressibility of two-phase flow with large density ratio. All of the numerical simulations in this part are based on above debeloped finite element scheme and implemented with the software FreeFem++ [63].

3.4.1 Convergence study: Couette flow

We first present the convergence test by using Couette flow with different density and viscosity [45, 171] (see Fig. 3.2). The domain size is $[0, 0.6] \times [0, 0.1]$ The top and bottom walls move oppositely with $\mathbf{u}_w = (1, 0)^T$. We do the convergence state for two-phase fluids with both low and high density ratios.

For the case of low density ratio, the parameters are listed as follows:

$$
Re = 200, \beta = 10, \mathscr{M} = 2.5 \times 10^{-8}, \varepsilon = 0.01, \alpha_w = 4.17 \times 10^{-3}, \rho_1 = 0.8, \rho_2 = 1,
$$

$$
\eta_1 = \eta_2 = 1, \theta_s = 120^\circ, \mathscr{M}_\Gamma = 5 \times 10^5,
$$

$$l_{s1} = l_{s2} = 0.01, \Delta t = 1 \times 10^{-3}.$$

We first present the convergence study for P1 element with $h = 1/160, 1/226, 1/320, 1/640$ and P2 element with $h = 1/80, 1/113, 1/160, 1/320$. The results with $h = 1/640$ and $1/320$ are used as the reference solutions for P1 and P2 elements, respectively.

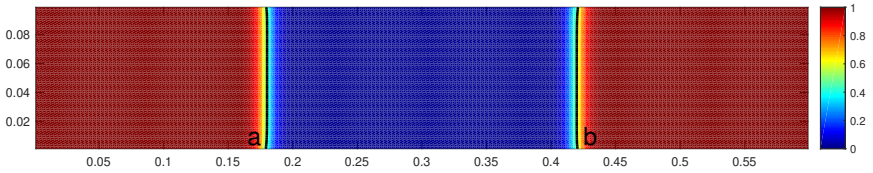

Figure 3.2: Initial condition of phase 1 concentration c for the two phase Couette flow. Positions a and b are two contact points on the bottom walls.

Space step h	P1 Element					
	Err(u_x)	Rate	Err(u_y)	Rate	Err(c)	Rate
1/160	4.9e-2		2.6e-2		8.5e-2	
1/226	1.9e-2	2.57	1.8e-2	1.46	5.3e-2	1.59
1/320	7.2e-3	2.64	6.4e-3	2.78	2.2e-2	2.38
Space step h	P2 Element					
	Err(u_x)	Rate	Err(u_y)	Rate	Err(c)	Rate
1/80	2.9e-2		2.5e-2		7.4e-2	
1/113	9.9e-3	2.93	7.5e-3	3.32	2.8e-2	2.63
1/160	3.0e-3	3.34	2.5e-3	2.97	1.0e-2	2.80

Table 3.1: L^2 norm of the error and convergence rate for velocity $\mathbf{u} = (u_x, u_y)$, phase function c, at time $t = 0.4$ with density ratio $\rho_1 : \rho_2 = 0.8 : 1$ viscosity ratio $\eta_1 : \eta_2 = 1 : 1$.

For the case of high density ratio, the parameters are listed as follows:

$$Re = 20, \beta = 1.67 \times 10^{-2}, \mathscr{M} = 3 \times 10^{-9}, \rho_1 = 0.01, \rho_2 = 1,$$

$$\eta_1 = 0.01, \eta_2 = 1, \varepsilon = 1.5 \times 10^{-3}, \alpha_w = 8.33 \times 10^{-8}, \theta_s = 120^\circ, \mathscr{M}_\Gamma = 5 \times 10^5,$$

$$l_{s1} = 1.33, l_{s2} = 0.1, \Delta t = 0.25 \times 10^{-3}.$$

The convergence rate for both P1 element and P2 element are shown in Table 3.2. It illustrates the 2nd-order for P1 element and 3rd-order for P2 element convergence rate in the sense of L^2 norm.

The profile of interface and velocity fields around steady state are shown in Fig. 3.5.

The fluid velocities on the wall are shown in Fig.3.6. It shows that for both low and high density ratio case, P1 element could yield consistent contact velocity with P2 element.

In Fig.3.7, we check the L^2 norm of $\nabla \cdot \mathbf{u}$ with different ε. The results confirm that as ε decreases, the solution converges to the sharp interface incompressible fluids.

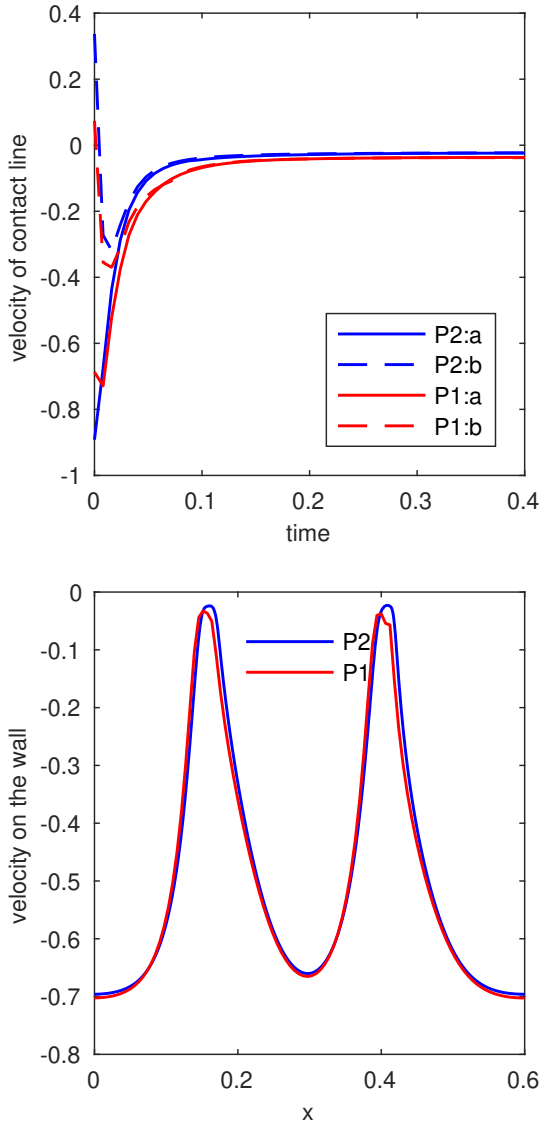

Figure 3.3: The velocity on wall for low density ratio. Left: Dynamics of two contact points a and b.; Right:velocity u_x along lower boundary at T=0.4.

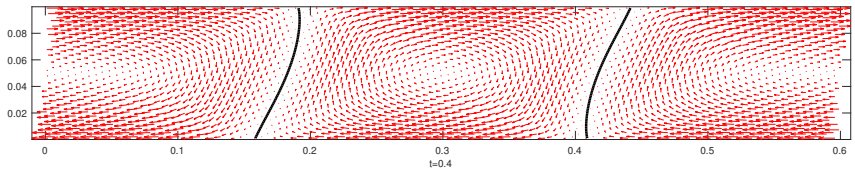

Figure 3.4: The interface and velocity profile at steady state $T = 0.4$ with density $\rho_1 = 0.8,\ \rho_2 = 1$.

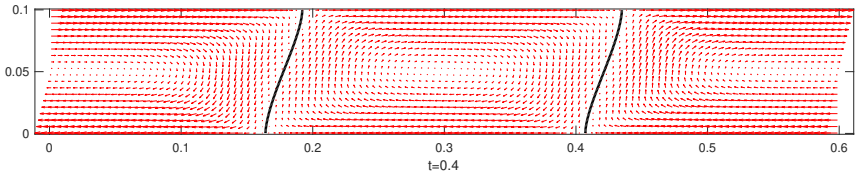

Figure 3.5: The interface and velocity profile at $T = 0.4$ with large density ratio $\rho_1 = 0.1,\ \rho_2 = 10$.

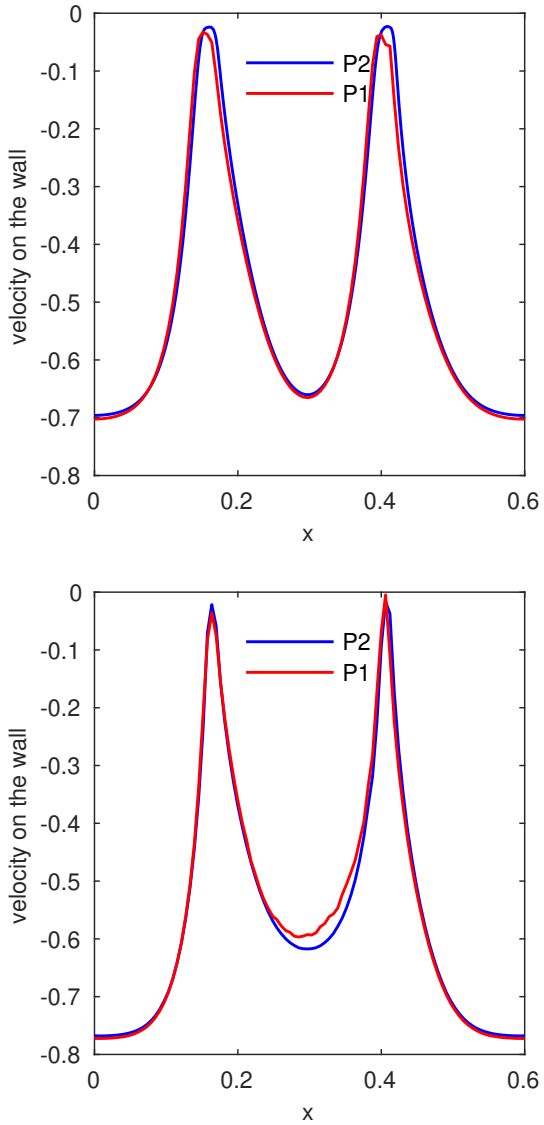

Figure 3.6: Velocity on wall around equilibrium state.Left: low density ratio $\rho_1 = 0.8$, $\rho_2 = 1$; Right: large density ratio $\rho_1 = 0.01,\ \rho_2 = 1$.

Space step h	P1 Element					
	Err(u_x)	Rate	Err(u_y)	Rate	Err(c)	Rate
1/160	8.8e-3		4.9e-3		2.2e-2	
1/226	6.9e-3	1.27	3.8e-3	1.27	2.0e-2	1.12
1/320	2.2e-3	3.17	1.5e-3	2.59	7.8e-3	2.52
Space step h	P2 Element					
	Err(u_x)	Rate	Err(u_y)	Rate	Err(c)	Rate
1/80	5.8e-3		3.6e-3		2.5e-2	
1/113	4.0e-3	1.46	1.9e-3	1.86	1.1e-2	2.20
1/160	1.1e-3	3.83	6.3e-4	3.08	3.5e-3	3.27

Table 3.2: L^2 norm of the error and convergence rate for velocity $\mathbf{u} = (u_x, u_y)$, phase function c, at time $T = 0.2$ with density ratio $\rho_1 : \rho_2 = 0.1 : 10$ viscosity ratio $\eta_1 : \eta_2 = 0.1 : 10$.

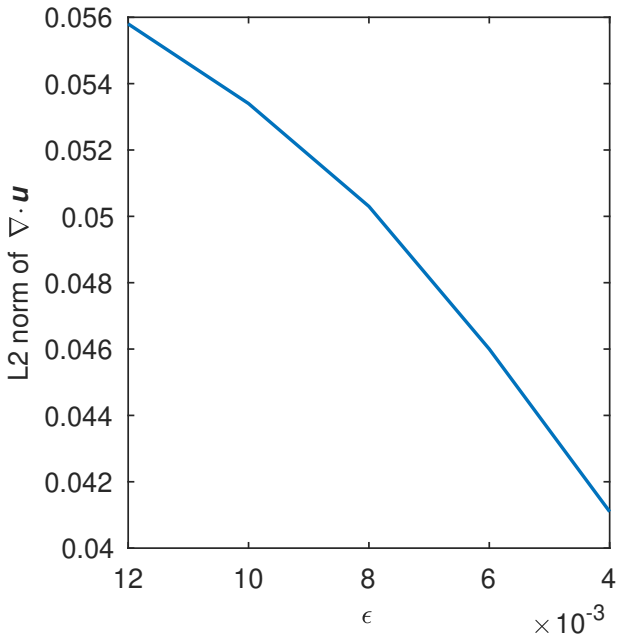

Figure 3.7: L^2 norm of $\nabla \cdot \mathbf{u}$ with different ε.

In Fig. 3.8, we check the total mass convergence of each phase in Lemma 3.3.4 for both low and high density ratios. It confirms that P1 and P2 elements could preserve the mass very well in both cases.

Then we set the wall velocity $\mathbf{u}_w = (0,0)^T$ to check the evolution of the total free energy when there is no input energy from outside. It is shown in Fig.3.9 that the free energy decreases over time for both methods and two density ratios, indicating that our schemes are energy stable.

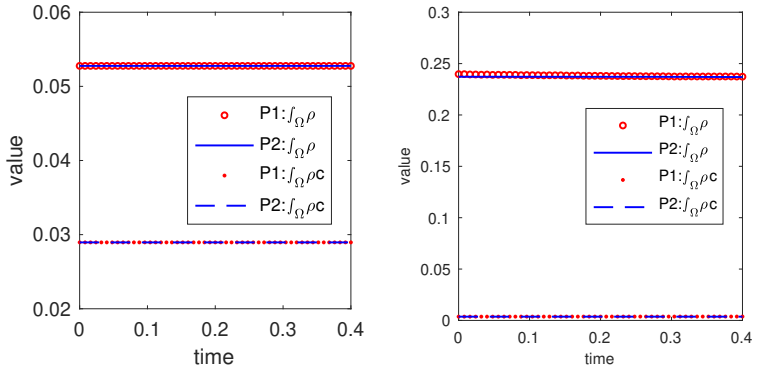

Figure 3.8: Mass conservation for each component. Left: low density ratio; Right: high density ratio.

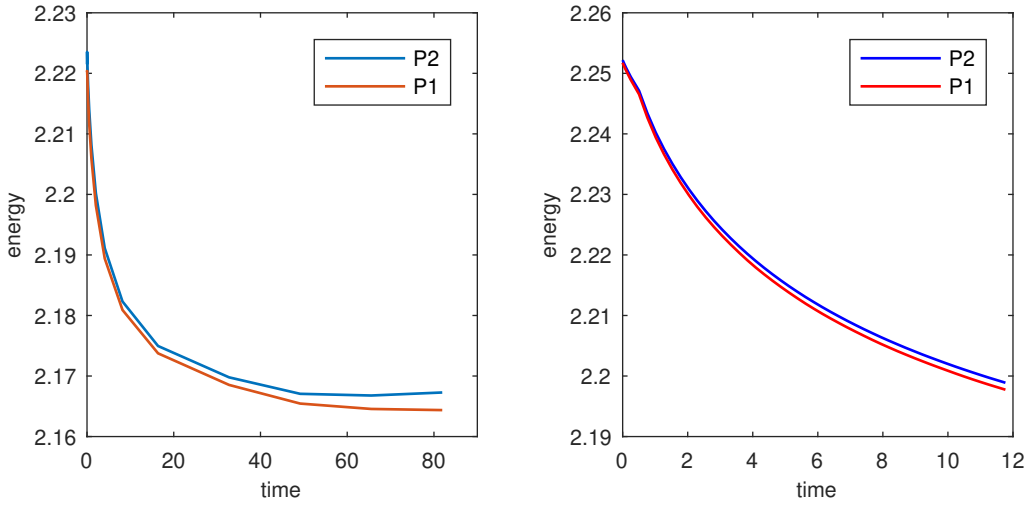

Figure 3.9: Total energy as a function of time. Left: lower density ratio; Right: high density ratio.

3.4.2 Contact angle effect: moving droplet

In this example, we show the dynamics of an oil droplet in water with shear flow. The density ratio is $\rho_1 : \rho_2 = 0.8 : 1$ and viscosity ratio is $\eta_1 : \eta_2 = 1 : 1$. The other parameters are as follows

$$Re = 5, \beta = 7.14 \times 10^{-3}, \mathscr{M} = 2.8 \times 10^{-4}, \varepsilon = 0.005, \alpha_w = 0.129,$$

$$\mathscr{M}_\Gamma = 5 \times 10^8, l_s = 6.667 \times 10^{-5}.$$

The domain size is $[0,4] \times [0,0.5]$ with adaptive mesh and $\Delta t = 4 \times 10^{-4}$. The initial profile is set to be a half circle

$$c_0 = 0.5 - 0.5 \tanh\left(\frac{\sqrt{(x-1)^2 + y^2} - 0.2}{\sqrt{2}\varepsilon}\right).$$

In Figs. 3.10 and 3.12, the profiles of droplets under shear flow at different time are presented. For the acute contact angle cae (Fig. 3.10), the droplet is elongated by the shear flow force and hydrophilic force on the wall. The distance between two contact points increases over time (see Fig. 3.13 black curve) as a spreading droplet. While for the obtuse case (see Fig. 3.12), the hydrophobic force induced the shrink of contact lines on the wall. The distance between two contact points keeps decreasing (see Fig.3.13 blue curve). With the help of shear force, the droplet eventually detaches from the wall around $t = 0.1$ and get stabilized at the center of the flow. When the contact angle is 90° (Fig. 3.11), the competition between wall attraction force and bulk shear force first elongates the droplet and finally breaks the bubble around time $t = 0.15$.

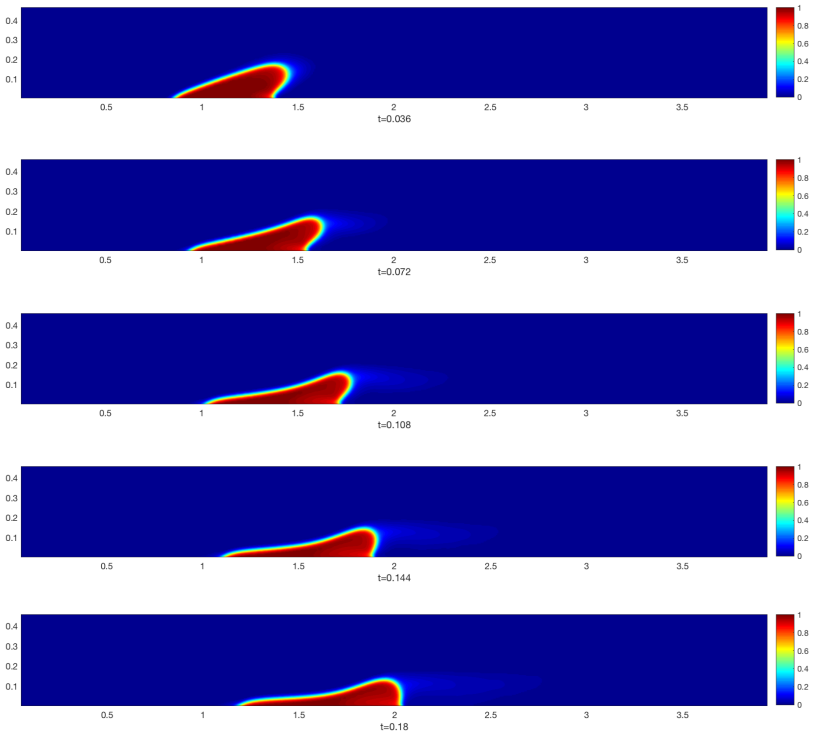

Figure 3.10: Moving droplet in shear flow with acute static contact angle $\theta_s = 60^\circ$.

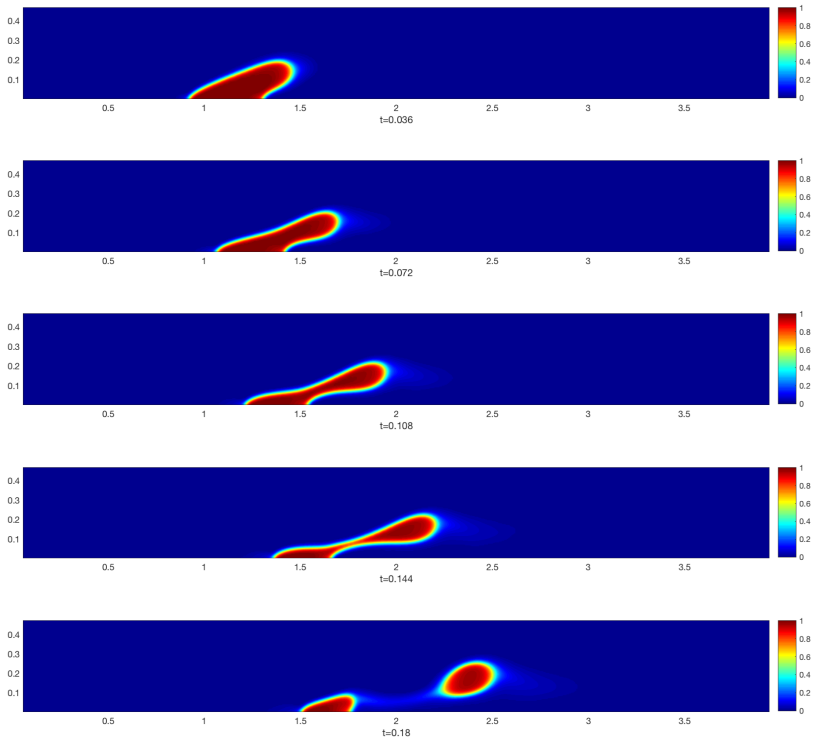

Figure 3.11: Moving droplet in shear flow with acute static contact angle $\theta_s = 90^\circ$.

3.4.3 Large density ratio: rising bubble

As the last test, we simulate the air bubble rising in water. The density ratio is set to be $\rho_1 : \rho_2 = 0.001 : 1$ and viscosity ratio is $\eta_1 : \eta_2 = 0.01 : 1$. The domain size is $(x, y) \in [0, 0.15] \times [0, 0.15]$ with mesh size $h = 1/540$ and timestep $\Delta t = 2 \times 10^{-4}$. Parameters are listed as follows

$$Re = 300, \beta = 0.09, \mathscr{M} = 6.67 \times 10^{-17}, \varepsilon = 0.01, \alpha_w = 100,$$

$$\mathscr{M}_\Gamma = 5 \times 10^8, l_s = 0.04.$$

The initial profile is set to be a half circle with radius 0.05 and center at $(0.075, 0)$:

$$c_0 = 0.5 + 0.5(-tanh((\sqrt{(x-0.075)^2 + y^2} - 0.05)/0.007))$$

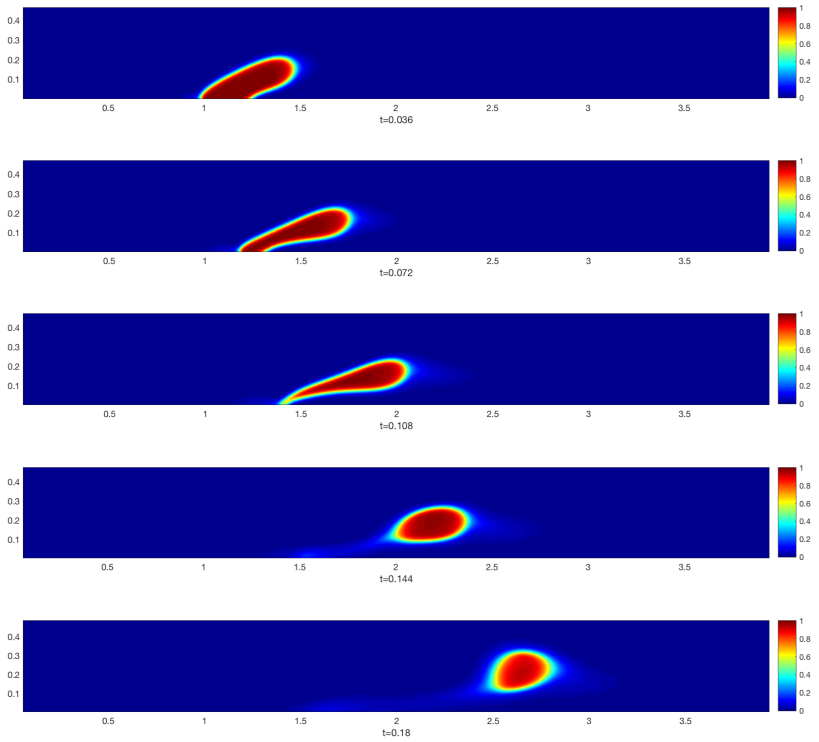

Figure 3.12: Moving droplet in shear flow with obtuse static contact angle $\theta_s = 120^\circ$.

The snapshots of interfaces with velocity fields and $\nabla \cdot \mathbf{u}$ profiles for droplets with acute contact angle $\theta_s = 60^\circ$ and obtuse angle $\theta_s = 120^\circ$ are presented in Figs. 3.14 and 3.15, respectively. When the angle is acute, the attractive (hydrophilic) force from the wall competes with the buoyancy force and break the bubble. While for the obtuse case, the wall repulsive (hydrophobic) fore enhances the bubble rising under buoyancy force. The $\nabla \cdot \mathbf{u}$ profiles confirm that the quasi-impressible property of two-phase fluid with different density only happens around the interface due to the slightly mixing [54].

In Fig. 3.16, we show the dynamics of rising velocity $V_c = \frac{\int_\Omega u_y c d\boldsymbol{x}}{\int_\Omega c d\boldsymbol{x}}$ of bubble with different static contact angles. The vertical dash lines are the time when bubbles break ($\theta_s = 60^\circ, 90^\circ$) or fully detach ($\theta_s = 120^\circ$) from wall. It shows that the hydrophobic bubble (Blue line $\theta_s = 120^\circ$) has a larger acceleration to form a sealing bubble. At $t = 0.0384$, the bubble fully detaches from the wall. For the hydrophilic bubbles, in the beginning, the velocity increases slowly due to

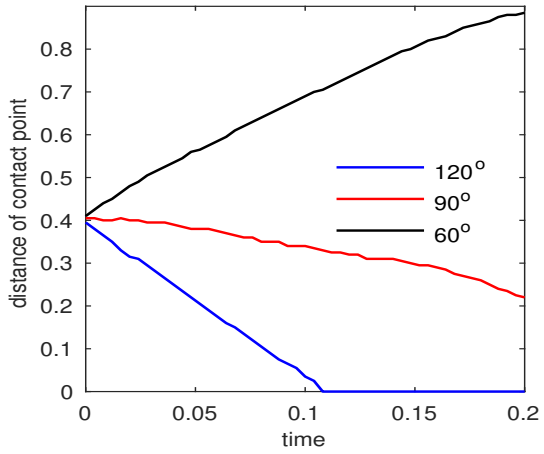

Figure 3.13: Moving droplet in shear flow: dynamics of the distance between two contact points.

the competition between hydrophilic force, surface tension and buoyancy force. The bubble is stretched into a tear shape which induces a larger velocity around the narrow neck region (see Fig. 3.14). The maximum velocity is achieved around the break time because of the instantaneous response of the surface tension to the large surface deformation.

3.5 Conclusion of The Chapter

In this chapter, we first derived the quasi-incompressible NSCH system for MCLs with variable density by using energy variational method consistently. GNBC for mass-averaged velocity is obtained during the variation due to the boundary dissipation.

Then we designed an energy stable C^0 finite element scheme to solve the obtained system. We also proved that the fully discrete scheme is mass conservative for each phase. Thanks to the quasi-incompressible and Δp term, the finite element space for Navier-Stokes equations do not need to satisfy the Babuska-Brezzi inf-sup condition (as in the case of the pressure stabilization method for the standard Navier-Stokes equations).

Three numerical examples were investigated numerically. The Couette flow test illustrates the 2nd-order for P1 element and 3-order for P2 element convergence rate and the energy decay of the scheme. The contact angle effect on the droplet is illustrated by oil-water droplet in shear flow. Finally, the rising bubble is applied to confirm the ability of our scheme to handle large density ratio and the quasi-incompresiblity only happens around the interface.

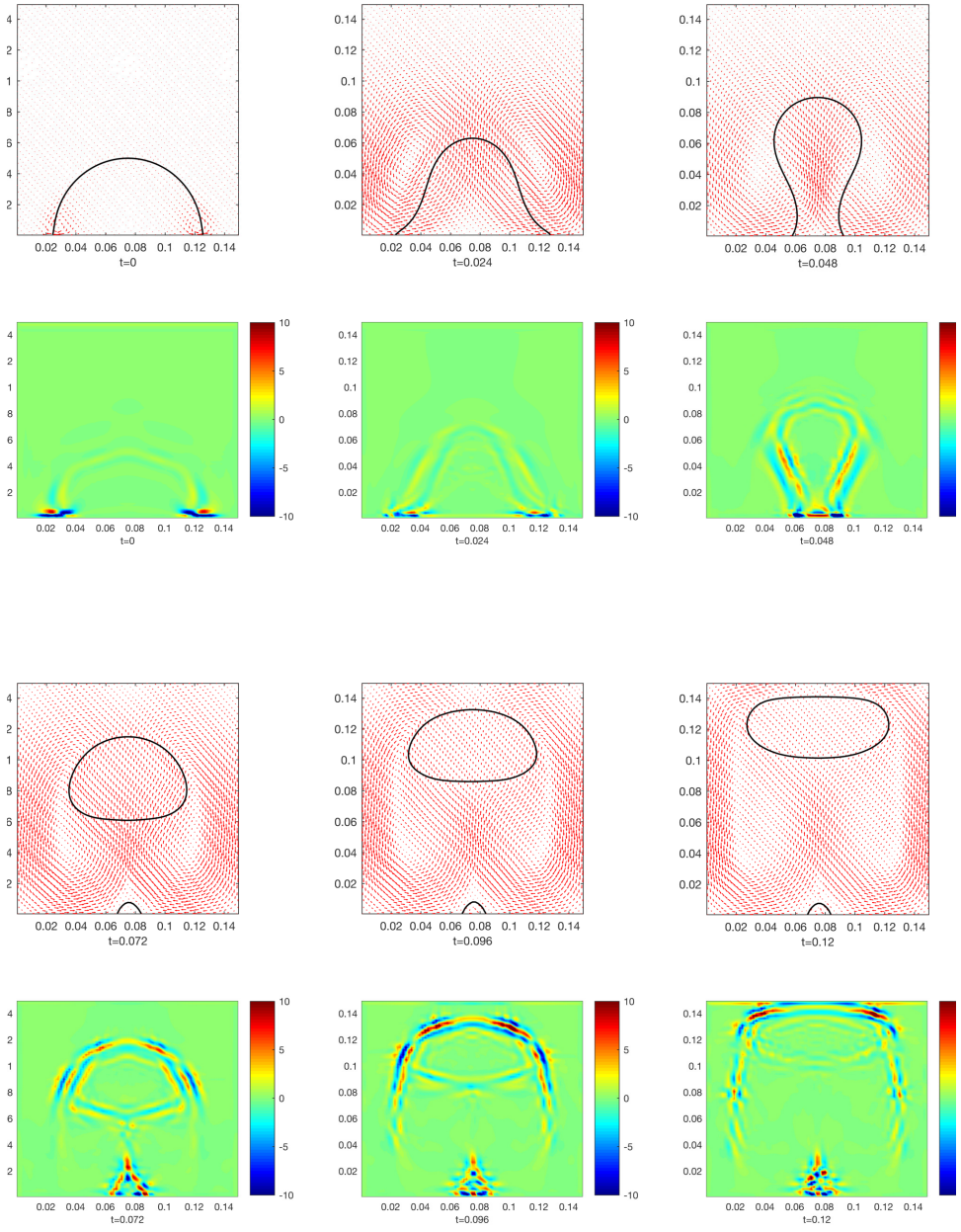

Figure 3.14: Rising Bubble interface with velocity filed (first and third rows) and $\nabla \cdot \mathbf{u}$ (second and fourth rows) at different time when $\theta_s = 60^\circ$.

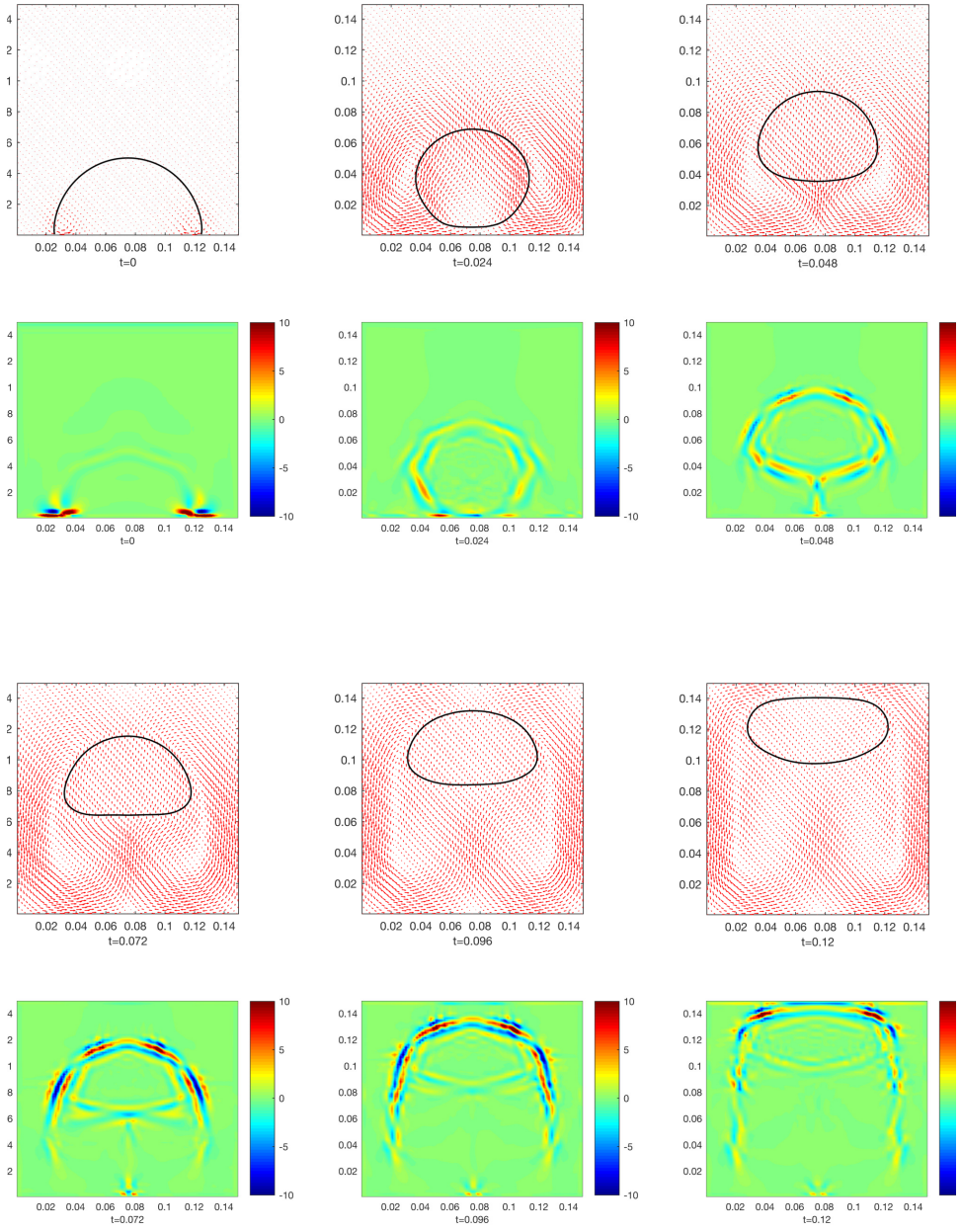

Figure 3.15: Rising Bubble interface with velocity filed (first and third rows) and $\nabla \cdot \mathbf{u}$ (second and fourth rows) at different time when $\theta_s = 120^\circ$.

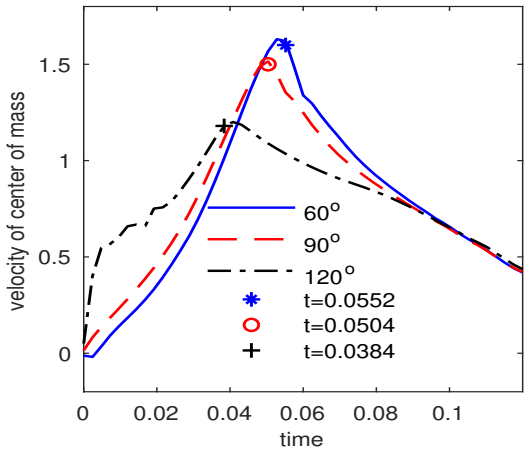

Figure 3.16: Rising velocity. Solid lines are rising velocity and vertical dash lines are time when bubble break or full removed from wall. Black: $\theta = 60^\circ$ with break time $t = 0.0552$; Red: $\theta = 90^\circ$ with break time $t = 0.0504$; Blue: $\theta = 120^\circ$ with removed time $t = 0.0384$.

Chapter 4

Single Vesicle Motion Model with Allan-Cahn Type Interface

4.1 Introduction

With the works done in chapter 1 it is likely to find out that the interface model can be applied to modelling of biological membrane by taking the corresponding energy into account in energy variational approach. The focus of this chapter is to model flowing vesicles interacting with the domain boundaries which mimics scenarios such as red blood cells passing a narrowed blood vessel in the absence of the cell-wall adhesion introduced by ligand-receptor binding or when the impact of this cell-wall adhesion can be neglected. This involves considering a moving contact lines problem since three different phases meet to form a triple point [116].

The first goal of this chapter thus is to derive a thermodynamically consistent phase-field model for vesicles' motion and shape transformation in a closed spatial domain by using an energy variational method [140, 52]. All the physics taken into consideration are introduced through definitions of energy functionals and dissipation functional, together with the kinematic assumptions of laws of conservation. Besides the energy and dissipation terms defined on bulk region of the domain, terms accounting for boundary effects are also added to the functionals. Then performing variation of these functionals yields an Allen-Cahn-Navier-Stokes (ACNS) system [155] with Allen-Cahn general Navier boundary conditions (GNBC) [116]. This is in contrast to most previous works [27, 29, 19] in which dynamic boundary condition was rarely derived during the course of model derivation. Dirichlet or Neumann type conditions were simply added to these models at the end to close the governing equations [3, 32, 31]. Moreover, in model derivation, the incompressibility of the fluid, the local and global inextensibility of the vesicle membrane and the conservation of vesicle mass are taken into account by introducing two Lagrangian multipliers, hydrostatic pressure and surface pressure [108] and penalty terms, respectively.

The second goal is to propose an efficient and accurate numerical scheme for solving the obtained fourth-order nonlinear coupled partial differential equation (PDE) system. Over the past decades, a lot of schemes have been developed for Allen-Cahn- or Cahn-Hilliard-Navier-Stokes systems. As for systems such as vesicle models introduced in the current and other works which are more sophisticated than the Allen-Cahn- or Cahn-Hilliard-Navier-Stokes systems, backward Euler time discretization method is frequently used [3, 27, 49, 48] leading to a first-order accurate scheme. Later on, decoupled energy stable schemes were proposal in [19] and [51] by introducing explicit, convective velocities. Liu et al. [97] introduce a variational framework for inextensible membrane with immerse boundary formula and propose a spectral method for solving the obtained problem. In the current work, an efficient, energy-law preserving (thus energy stable) and second-order accurate C^0 finite element scheme is proposed to solve the obtained vesicle system using ideas introduced in [53]. The key idea of this scheme is to utilize the mid-point method in time discretizaiton to ensure the accuracy in time, and that the form of the discrete energy dissipation law is same as that of the continuous model. In order to properly treat the term related to inextensibility of the membrane, a relaxation term of local inextensibility as in [3] is introduced. The numerical study of convergence confirms the proposed scheme is second-order convergence in both time and space. Furthermore vesicle deformation simulations illustrate it is energy stable, and numerically conserves mass and surface area of vesicles.

The introduction of the GNBC in this work makes it possible to study a broad class of complicated fluid-structure interaction problems. In this chapter, the developed model is applied to studying vesicles passing narrow channels. The results confirm that the more rounded the vesicles (smaller surface-volume ratio) are, the more likely the vesicles form lockage when they pass through narrow channels.It is also worth noting that it is critical to include the local inextensibility of the vesicle membrane in the model when studying this type of problems. Without the local inextensibility, the vesicle membrane can be falsely stretched or compressed. Lastly, although membrane structures of vesicles and blood cells are quite different, a blood cell in many studies can be treated as an elastic capsule with bending rigidity, in which the membrane is impenetrable to both interior and exterior fluids. Therefore our model developed for vesicles can be readily applied for studying a vast body of blood cells related problems [103].

The rest of chapter is organized as follows. Section 4.2 begins with introducing basic dynamical assumptions that have been used in many papers [32, 116], and is devoted to model derivation. Dimensionless model governing equations and the energy decaying law of the model are presented in Section 4.3. In Section 4.4, the numerical scheme solving the proposed

model is developed, and its energy law is given. Numerical simulation results are described in Section 4.5 to confirm the energy law of the numerical scheme and the feasibility of our model. A case study of vesicle passing through a narrow channel is shown, which is to simulate the motion of red blood cells in small blood vessel. Conclusions are drawn in Section 4.6.

4.2 Model Derivation

Derivation of the model for simulating a flowing vesicle deforming in a channel filled with extracellular fluid is presented in this section. A new phase-field label function ϕ is introduced to track the motion of the vesicle where $\phi(\boldsymbol{x}) = \pm 1$ denotes the intracellular and extracellular space, and $\phi = 0$ is the vesicle membrane or interface. Note that different from c in the previous chapter, ϕ is a more abstract concept that is directly given without definition.

The model is derived using an energy variational method [140]. It begins with defining two functionals for the total energy and dissipation of the system, and introducing the kinematic equations based on physical laws of conservation. The specific forms of the flux and stress functions in the kinematic equations are obtained by taking the time derivative of the total energy functional and comparing with the defined dissipation functional. More details of this method can be found in [140].

In what follows, we detail steps of using this method to derive the model. We first make the following assumptions about mass and momentum conservation of the mixture of extracellular fluid and vesicle and interface inextensibility, and assume that the dynamics of the phase-field function ϕ is an L^2 gradient flow:

$$\begin{cases} \frac{\partial \phi}{\partial t} + \nabla \cdot (\mathbf{u}\phi) = q_\phi \ , \\ \rho(\frac{\partial \mathbf{u}}{\partial t} + (\mathbf{u}\cdot\nabla)\mathbf{u}) = \nabla \cdot \boldsymbol{\sigma}_\eta + \mathbf{F}_{inter} \ , \\ \nabla \cdot \mathbf{u} = 0 \ , \\ \delta_\gamma(\mathscr{P} : \nabla \mathbf{u}) + \ \xi\gamma^2 \nabla \cdot (\phi^2 \nabla \lambda) = 0 \ . \end{cases} \tag{4.1}$$

with specific forms of flux q_ϕ, stress $\boldsymbol{\sigma}_\eta$ and interfacial forces $\mathbf{F}_{inter}$ induced by the physics of the interface such as bending energy and local inextensibility constrain, which is to be determined. ρ and $\mathbf{u}$ are the density and velocity of the mixture, respectively. In this paper, we assume that the density is a constant. The first equation is the Allen-Cahn type equation to track the interface. The second equation is the conservation of momentum. The third equation accounts for the fluid incompressibility (or mass conservation).

The last equation is related to the local inextensibility of the vesicle membrane. This local inextensibility prevents from stretching on any point of the vesicle membrane surface [11]. In the sharp interface model, the local inextensibility (or mass conservation on the interface) is represented by $\nabla_\Gamma \cdot \mathbf{u} = 0$ defined on the interface Γ [100, 103]. This equation is equivalent

to $\mathscr{P} : \nabla \mathbf{u} = 0$ where the projection operator $\mathscr{P} = \mathscr{P}_\phi$ is defined to be $(I - \mathbf{n}_m \otimes \mathbf{n}_m)$, and $\mathbf{n}_m = \frac{\nabla \phi}{|\nabla \phi|}$ is the unit outward normal vector of the interface when it is defined as an implicit surface by the level function. In the phase-field formulation, the interface is modelled as a diffuse layer. This is different from the sharp interface concept. For computational convenience using phase-field formulation, this local inextensibility constraint on the interface Γ is extended to the domain Ω by multiplying with a scalar function

$$\delta_\gamma = \frac{1}{2}\gamma^2 |\nabla \phi|^2 \,, \tag{4.2}$$

where $\nabla \phi$ is nonzero only in the diffuse interface layer, and γ is the thickness of the diffuse interface layer. Here a relaxation term $\xi \gamma^2 \nabla \cdot (\phi^2 \nabla \lambda)$ for the local inextensibility near the membrane is introduced as shown in [3]. ξ is a parameter independent of γ, and λ is the a function that measures the interface "pressure" induced by the inextensibility of the membrane.

On the wall boundary $\partial \Omega_w$ of the domain, without considering wall movement, the following boundary conditions are assumed

$$\begin{cases} \mathbf{u} \cdot \mathbf{n} = 0 \,, \\ \mathbf{u}_\tau \cdot \boldsymbol{\tau}_i = f_{\tau_i} \,, \\ \dot{\phi} = \frac{\partial \phi}{\partial t} + \mathbf{u} \cdot \nabla_\Gamma \phi = J_\Gamma \,, \\ f = 0 \,, \\ \partial_n \lambda = 0 \,, \end{cases} \tag{4.3}$$

where an Allen-Cahn type boundary condition is employed for ϕ, $\mathbf{u}_\tau = \mathbf{u} - (\mathbf{u} \cdot \mathbf{n})\mathbf{n}$ is the fluid slip velocity with respect to the wall, $\boldsymbol{\tau}_i, i = 1, 2$ are the tangential directions of the wall surface (2D), and $\nabla_\Gamma = \nabla - \mathbf{n}(\mathbf{n} \cdot \nabla)$ is the surface gradient operator on the boundary $\partial \Omega_w$. f_{τ_i} is the slip velocity of the fluid on the wall along the τ_i direction. And J_Γ represents the Allan-Cahn type of relaxation on the wall by using the phase-field method. Here we abuse the notation when there is no confusion, and the subscript Γ refers to $\partial \Omega_w$, and $\mathbf{n}$ is its unit outward normal. The meaning of equation $f = 0$ will be made explicit after definition of the interface curvature (see Eq. (4.8)).

The rest part of this section is devoted to deriving the exact forms of q_ϕ, $\boldsymbol{\sigma}_\eta$, $\mathbf{F}$, f_{τ_i} and J_Γ using the energy variational method. By following the works in [155, 30], the total energy functional E_{total} of a cell- (or vesicle-) fluid system is defined to be the sum of the kinetic energy E_{kin}, the cell membrane energy E_{cell} and the specific wall energy E_w due to the cell-wall interaction

$$E_{total} = \underbrace{E_{kin}}_{Macroscale} + \underbrace{E_{cell} + E_w}_{Microscale} \,. \tag{4.4}$$

The kinetic energy accounts for the transport of the cell-fluid mixture, and is defined as:

$$E_{kin} = \int_{\Omega} \left(\frac{1}{2} \rho |\mathbf{u}|^2 \right) d\boldsymbol{x} \ , \tag{4.5}$$

where ρ is the macroscale density of the mixture, and is assumed to be equal to a constant ρ_0 in this work (matched density case).

The cell energy E_{cell} is defined to be the sum of the bending energy E_{bend} and two penalty terms in order to preserve the total volume and surface area of the cell:

$$E_{cell} \quad = \quad E_{bend} + \frac{M_v}{2} \frac{\left(V(\phi) - V(\phi_0)\right)^2}{V(\phi_0)} + \frac{M_s}{2} \frac{\left(S(\phi) - S(\phi_0)\right)^2}{S(\phi_0)} \ , \tag{4.6}$$

where $V(\phi) = \int_{\Omega} \phi d\boldsymbol{x}$ is the volume difference of the cell-fluid system and the value of $S(\phi) = \int_{\Omega} \frac{G(\phi)}{\gamma} d\boldsymbol{x}$ is used to measure the surface area of the cell with $G(\phi) = \int_{\Omega} \frac{\gamma^2 |\nabla \phi|^2}{2} + \frac{(1-\phi^2)^2}{4} d\boldsymbol{x}$. M_v and M_s are cell volume and surface area constraint coefficients, respectively.

If the cell membrane is assumed to be isotropic and only composed of lipid bilayer, the bending energy of the bending resistance of the cell membrane can be modeled by an approximation of the Helfrich bending energy [30] as follows

$$E_{bend} = \int_{\Omega} \frac{\hat{\kappa}_B}{2\gamma} \left| \frac{f(\phi)}{\gamma} \right|^2 d\boldsymbol{x} \ , \tag{4.7}$$

where $\hat{\kappa}_B$ is the bending modulus and

$$f(\phi) := \frac{\delta G}{\delta \phi} = -\gamma^2 \Delta \phi + (\phi^2 - 1)\phi \ . \tag{4.8}$$

In order to take into account the interaction at the interface between vesicle, fluid and vessel wall on $\partial\Omega_w$, the wall free energy E_w is introduced

$$E_w = \int_{\partial\Omega_w} f_w(\phi) ds \ , \tag{4.9}$$

where f_w is the vesicle-wall interaction energy density.

Remark 4.2.1. *Here we borrow the idea introduced in moving contact lines models [116] :*

$$f_w(\phi) = -\frac{\sigma}{2} \sin\left(\frac{\phi\pi}{2}\right) \cos(\theta_s) \ , \tag{4.10}$$

with a static contact angle θ_s [122, 124] when the cell-wall adhesion is absent or negligible. This is justified by the fact that a triple point is formed when cell contacts the wall, cell and extracellular fluid meet, and its dynamics can be modeled through a contact line model. We also note that the choice of contact angle can be subtle and affects the simulation outcome.

Low contact angle values show a tendency of the cell to spread and "adhere" to the surface (hydrophilic) due to the existence of a wetting force, whereas high contact angle values represent the surface's tendency to repel the cell or an absence of the wetting force (hydrophobic) (See Figure 4.4 in Section 5.2 later). In fact, the wall energy f_w can be made more sophisticated in order to faithfully represent the complicated vesicle-wall interaction in case that the cell-wall adhesion by ligand-receptor binding is involved, for example by introducing a new phase to represent the wall [48].

The chemical potential μ is obtained by taking the variation of $E_{bulk} = E_{kin} + E_{cell}$ with respect to ϕ,

$$\mu = \frac{\delta E_{bulk}}{\delta \phi} = \frac{\hat{\kappa}_B}{\gamma^3} g(\phi) + M_v \frac{V(\phi) - V(\phi_0)}{V(\phi_0)} + \frac{M_s}{\gamma} \frac{S(\phi) - S(\phi_0)}{S(\phi_0)} f(\phi) \ , \tag{4.11}$$

where $g(\phi) = -\gamma^2 \Delta f + (3\phi^2 - 1) f$.

It is assumed in the present work that dissipation of the system energy is due to fluid viscosity, friction on the wall, and interfacial mixing due to diffuse interface representation. Accordingly, the total dissipation functional Δ is defined as follows

$$\begin{aligned} \Delta \ = \ & \int_\Omega 2\eta |\boldsymbol{D}_\eta|^2 d\boldsymbol{x} + \int_\Omega M_\phi^{-1} |q_\phi|^2 d\boldsymbol{x} + \int_\Omega \xi |\gamma \phi \nabla \lambda|^2 d\boldsymbol{x} + \int_{\partial \Omega_w} \beta_s |\mathbf{u}_{\boldsymbol{\tau}}|^2 ds \\ & + \int_{\partial \Omega_w} \kappa_\Gamma |J_\Gamma|^2 ds \ . \end{aligned} \tag{4.12}$$

Here the first term is the macroscopic dissipation induced by the fluid viscosity with $\boldsymbol{D}_\eta = \frac{1}{2}[\nabla \mathbf{u} + (\nabla \mathbf{u})^T]$, the second term is the microscopic dissipation induced by the diffuse interface, the third term is the dissipation induced by diffuse interface method for imposing local inextensibilty of the interface, the fourth term is the boundary friction dissipation, where β_s is related to the roughness of the vessel wall, and the last term is the dissipation induced by the diffuse interface contacting the wall.

By taking the time derivative of the total energy functional (4.4), it is obtained that (detailed derivation is given in the Appendix of this paper)

$$\begin{aligned} & \frac{dE_{total}}{dt} = \frac{d}{dt} E_{kin} + \frac{d}{dt} E_{cell} + \frac{d}{dt} E_w \\ = \ & -\int_\Omega ((\boldsymbol{\sigma}_\eta + pI) : \nabla \mathbf{u}) d\boldsymbol{x} + \int_\Omega (\mathbf{F}_{inter} - \mu \nabla \phi - \nabla \cdot (\lambda \delta_\gamma \mathscr{P})) \cdot \mathbf{u} d\boldsymbol{x} + \int_\Omega \mu q_\phi d\boldsymbol{x} \\ & + \int_\Omega \xi (\gamma \phi \nabla \lambda)^2 d\boldsymbol{x} + \int_{\partial \Omega_w} ((\boldsymbol{\sigma}_\eta + \lambda \delta_\gamma \mathscr{P}) \cdot \mathbf{n}) \cdot \mathbf{u}_\tau ds + \int_{\partial \Omega_s} \hat{L}(\phi) \frac{\partial \phi}{\partial t} ds \\ = \ & -\int_\Omega ((\boldsymbol{\sigma}_\eta + pI) : \nabla \mathbf{u}) d\boldsymbol{x} + \int_\Omega (\mathbf{F}_{inter} - \mu \nabla \phi - \nabla \cdot (\lambda \delta_\gamma \mathscr{P})) \cdot \mathbf{u} d\boldsymbol{x} + \int_\Omega \mu q_\phi d\boldsymbol{x} \\ & + \int_\Omega \xi (\gamma \phi \nabla \lambda)^2 d\boldsymbol{x} + \int_{\partial \Omega_w} ((\boldsymbol{\sigma}_\eta + \lambda \delta_\gamma \mathscr{P}) \cdot \mathbf{n}) \cdot \mathbf{u}_\tau ds + \int_{\partial \Omega_s} \hat{L}(\phi)(-\mathbf{u} \cdot \nabla_\Gamma \phi + J_\Gamma) ds \\ = \ & -\int_\Omega ((\boldsymbol{\sigma}_\eta + pI) : \nabla \mathbf{u}) d\boldsymbol{x} + \int_\Omega (\mathbf{F}_{inter} - \mu \nabla \phi - \nabla \cdot (\lambda \delta_\gamma \mathscr{P})) \cdot \mathbf{u} d\boldsymbol{x} + \int_\Omega \mu q_\phi d\boldsymbol{x} \end{aligned}$$

$$+\int_{\Omega}\xi(\gamma\phi\nabla\lambda)^2 d\boldsymbol{x}+\int_{\partial\Omega_w}((\boldsymbol{\sigma}_\eta+\lambda\delta_\gamma\mathscr{P})\cdot\mathbf{n}-\hat{L}(\phi)\nabla_\Gamma\phi)\cdot\mathbf{u}_\tau ds$$
$$+\int_{\partial\Omega_w}\hat{L}(\phi)J_\Gamma ds\ , \tag{4.13}$$

where p and λ are introduced as Lagrange multipliers accounting for fluid incompressiblity and local inextensibility of the cell membrane, respectively. Further, δ_γ is defined in Eq. (4.2) and $\hat{L}(\phi)=\dfrac{\hat{\kappa}_B}{\gamma}\partial_n f+M_s\dfrac{S(\phi)-S(\phi_0)}{S(\phi_0)}\gamma\partial_n\phi+\dfrac{\partial f_w}{\partial\phi}$.

Using the energy dissipation law $\frac{dE_{total}}{dt}=-\Delta$ [161, 35], and the definition of the dissipation functional (4.12), it is obtained that

$$\begin{cases}\boldsymbol{\sigma}_\eta=2\eta\boldsymbol{D}_\eta-pI\ , & \text{in } \Omega\ ,\\ q_\phi=-M_\phi\mu\ , & \text{in } \Omega\ ,\\ \mathbf{F}_{inter}=\mu\nabla\phi+\nabla\cdot(\lambda\delta_\gamma\mathscr{P})\ , & \text{in } \Omega\ ,\\ J_\Gamma=-\kappa_\Gamma^{-1}\hat{L}(\phi)\ , & \text{on } \partial\Omega_w\ ,\\ u_{\tau_i}=\beta_s^{-1}(-(\mathbf{n}\cdot(\boldsymbol{\sigma}_\eta+\lambda\delta_\gamma\mathscr{P})\cdot\boldsymbol{\tau}_i)+\hat{L}(\phi)\partial_{\tau_i}\phi)\ ,\ i=1,2, & \text{on } \partial\Omega_w\ .\end{cases} \tag{4.14}$$

Here constant M_ϕ is called the mobility (a phenomenological parameter), κ_γ is the boundary mobility (a phenomenological parameter) and β_s is the wall friction coefficient.

To this end, the proposed phase-field model is composed of the following equations

$$\begin{cases}\frac{\partial\phi}{\partial t}+\nabla\cdot(\mathbf{u}\phi)=-M_\phi\mu\ ,\\ \mu=\frac{\hat{\kappa}_B}{\gamma^3}g(\phi)+M_v\frac{V(\phi)-V(\phi_0)}{V(\phi_0)}+\frac{M_s}{\gamma}\frac{S(\phi)-S(\phi_0)}{S(\phi_0)}f(\phi)\ ,\\ g(\phi)=-\gamma^2\Delta f+(3\phi^2-1)f(\phi),\\ f(\phi)=-\gamma^2\Delta\phi+(\phi^2-1)\phi\ ,\\ \rho(\frac{\partial\mathbf{u}}{\partial t}+(\mathbf{u}\cdot\nabla)\mathbf{u})+\nabla p=\nabla\cdot(2\eta\boldsymbol{D}_\eta)+\mu\nabla\phi+\nabla\cdot(\lambda\delta_\gamma\mathscr{P})\ ,\\ \nabla\cdot\mathbf{u}=0\ ,\\ \delta_\gamma(\mathscr{P}:\nabla\mathbf{u})+\xi\gamma^2\nabla\cdot(\phi^2\nabla\lambda)=0\ ,\end{cases} \tag{4.15}$$

with the boundary conditions

$$\begin{cases}\mathbf{u}\cdot\mathbf{n}=0\ ,\\ -\beta_s u_{\tau_i}=(\mathbf{n}\cdot(\boldsymbol{\sigma}_\eta+\lambda\delta_\gamma\mathscr{P})\cdot\boldsymbol{\tau}_i)-\hat{L}(\phi)\partial_{\tau_i}\phi\ ,\ i=1,2,\\ f=0\ ,\\ \kappa_\Gamma\left(\frac{\partial\phi}{\partial t}+\mathbf{u}\cdot\nabla_\Gamma\phi\right)=-\hat{L}(\phi)\ ,\\ \hat{L}(\phi)=\frac{\hat{\kappa}_B}{\gamma}\partial_n f+M_s\frac{S(\phi)-S(\phi_0)}{S(\phi_0)}\gamma\partial_n\phi+\frac{\partial f_w}{\partial\phi}\ ,\\ \partial_n\lambda=0\ .\end{cases} \tag{4.16}$$

4.3 Dimensionless Model Governing Equations and Energy Dissipation Law

If the viscosity, length, velocity, time, bulk and boundary chemical potentials in Eqs. (4.15)-(4.16) are scaled by their corresponding characteristic values η_0, L, U, $\frac{L}{U}$ $\frac{\eta_0 U}{L}$ and $\eta_0 U$, respectively, and let $\varepsilon = \frac{\gamma}{L}$ be the non-dimensionalised thickness of the interface. Eqs. (4.15)-(4.16) can be rewritten as

$$\begin{cases} Re(\frac{\partial \mathbf{u}}{\partial t} + (\mathbf{u}\cdot\nabla)\mathbf{u}) + \nabla P = \nabla\cdot(2\eta \boldsymbol{D}) + \mu\nabla\phi + \nabla\cdot(\lambda\delta_\varepsilon\mathscr{P}) \ , & \text{in } \Omega \ , \\ \nabla\cdot\mathbf{u} = 0 \ , & \text{in } \Omega \ , \\ \frac{\partial\phi}{\partial t} + \mathbf{u}\cdot\nabla\phi = -\mathscr{M}\mu \ , & \text{in } \Omega \ , \\ \mu = \kappa_B g(\phi) + \mathscr{M}_v\frac{(V(\phi)-V(\phi_0))}{V(\phi_0)} + \mathscr{M}_s\frac{(S(\phi)-S(\phi_0))}{S(\phi_0)}f(\phi) \ , & \text{in } \Omega \ , \\ f(\phi) = -\varepsilon\Delta\phi + \frac{(\phi^2-1)}{\varepsilon}\phi, \ g(\phi) = -\Delta f + \frac{1}{\varepsilon^2}(3\phi^2-1)f(\phi) \ , & \text{in } \Omega \ , \\ \delta_\varepsilon(\mathscr{P}:\nabla\mathbf{u}) + \xi\varepsilon^2\nabla\cdot(\phi^2\nabla\lambda) = 0 \ , & \text{in } \Omega \ , \end{cases} \tag{4.17}$$

with the boundary conditions

$$\begin{cases} \kappa\dot{\phi} + L(\phi) = 0 \ , & \text{on } \partial\Omega_w \ , \\ L(\phi) = \kappa_B\partial_n f + \varepsilon\mathscr{M}_s\frac{S(\phi)-S(\phi_0)}{S(\phi_0)}\partial_n\phi + \alpha_w\frac{df_w}{d\phi} \ , & \text{on } \partial\Omega_w \ , \\ -l_s^{-1}u_{\tau_i} = \boldsymbol{\tau_i}\cdot(2\eta\mathbf{D}_\eta + \lambda\delta_\varepsilon\mathscr{P})\cdot\boldsymbol{n} - L(\phi)\partial_{\tau_i}\phi \ , \ i=1,2, & \text{on } \partial\Omega_w \ , \\ f = 0 \ , & \text{on } \partial\Omega_w \ , \\ \partial_n\lambda = 0 \ , & \text{on } \partial\Omega_w \ , \end{cases} \tag{4.18}$$

where $V(\phi) = \int_\Omega \phi d\boldsymbol{x}$, $S(\phi) = \int_\Omega \frac{\varepsilon}{2}|\nabla\phi|^2 + \frac{1}{4\varepsilon}(\phi^2-1)^2 d\boldsymbol{x}$ and $\delta_\varepsilon = \frac{1}{2}\varepsilon^2|\nabla\phi|^2$. The dimensionless constants appeared in Eqs. (4.17)-(4.18) are given by $\varepsilon = \frac{\gamma}{L}$, $Re = \frac{\rho_0 UL}{\eta_0}$, $\mathscr{M} = M_\phi\eta_0$, $\kappa_B = \frac{\hat{\kappa}_B}{L^2\eta_0 U}$, $k = \frac{\hat{\kappa}_B}{\eta_0 L}$, $l_s = \frac{\eta_0}{\beta_s L}$, $\alpha_w = \frac{\sigma}{\eta_0 U}$, $\mathscr{M}_s = \frac{M_s}{\eta_0 U}$, and $\mathscr{M}_v = \frac{M_v L}{\eta_0 U}$.

If we define the Sobolev spaces as follows [53, 140]

$$\boldsymbol{W}^{1,3} = (W^{1,3})^2 \ , \tag{4.19}$$

$$\boldsymbol{W}^{1,3}(\Omega) = \left\{\mathbf{u} = (u_x,u_y)^T \in \boldsymbol{W}^{1,3} | \mathbf{u}\cdot\boldsymbol{n} = 0, \text{ on } \partial\Omega_w\right\} \ , \tag{4.20}$$

$$\boldsymbol{W}_b = W^{1,3}(\Omega)\times W^{1,3}(\Omega)\times W^{1,3}(\Omega)\times W^{1,3/2}(\Omega)\times W^{1,3/2}(\Omega)\times \boldsymbol{W}^{1,3}(\Omega) \ , \tag{4.21}$$

and let $\|\cdot\| = \left(\int_\Omega|\cdot|^2 d\boldsymbol{x}\right)^{\frac{1}{2}}$ and $\|\cdot\|_w = \left(\int_{\partial\Omega_w}|\cdot|^2 ds\right)^{\frac{1}{2}}$ denote the L^2 norm defined in the domain and on the domain boundary respectively, then the system (4.17)-(4.18) satisfies the following energy law.

Theorem 4.3.1. *If* $(\phi,\ f,\ \mu,\ \lambda,\ P,\ \mathbf{u}) \in \boldsymbol{W}_b$ *are smooth solutions of the above system* (4.17)-(4.18)*, then the following energy law is satisfied:*

$$\begin{aligned}\frac{d}{dt}\mathscr{E}_{total} &= \frac{d}{dt}(\mathscr{E}_{kin}+\mathscr{E}_{cell}+\mathscr{E}_w)\\ &= \frac{1}{Re}\left(-2\|\eta^{1/2}\mathbf{D}_\eta\|^2-\mathscr{M}\|\mu\|^2-\xi\|\varepsilon\phi\nabla\lambda\|^2-\kappa\|\dot{\phi}\|_w^2-\|l_s^{-1/2}\mathbf{u}_\tau\|_w^2\right), \quad (4.22)\end{aligned}$$

where $\mathscr{E}_{total}=\mathscr{E}_{kin}+\mathscr{E}_{cell}+\mathscr{E}_w$, $\mathscr{E}_{kin}=\frac{1}{2}\int_\Omega|\mathbf{u}|^2d\boldsymbol{x}$, $\mathscr{E}_{cell}=\frac{\kappa_B}{2Re\varepsilon}\int_\Omega|f|^2d\boldsymbol{x}+\mathscr{M}_v\frac{(V(\phi)-V(\phi_0))^2}{2ReV(\phi_0)}+\mathscr{M}_s\frac{(S(\phi)-S(\phi_0))^2}{2ReS(\phi_0)}$ *and* $\mathscr{E}_w=\frac{\alpha_w}{Re}\int_{\partial\Omega_w}f_w ds$.

Proof: Multiplying the first equation in Eq. (4.17) with $\mathbf{u}$ and integration by parts yield

$$\begin{aligned}\frac{d}{dt}\mathscr{E}_{kin} &= \frac{1}{Re}\left\{-\int_\Omega 2\eta|\boldsymbol{D}_\eta|^2d\boldsymbol{x}+\int_{\partial\Omega_w}(\boldsymbol{\sigma}_\eta\cdot\mathbf{n})\cdot\mathbf{u}_\tau ds+\int_\Omega\mu\nabla\phi\cdot\mathbf{u}d\boldsymbol{x}-\int_\Omega\lambda\delta_\varepsilon\mathscr{P}:\nabla\mathbf{u}d\boldsymbol{x}\right.\\ &\quad\left.+\int_{\partial\Omega_w}(\lambda\delta_\varepsilon\mathscr{P}\cdot\mathbf{n})\cdot\mathbf{u}_\tau ds\right\}\\ &= \frac{1}{Re}\left\{-\int_\Omega 2\eta|\boldsymbol{D}_\eta|^2d\boldsymbol{x}-\int_\Omega\lambda\delta_\varepsilon\mathscr{P}:\nabla\mathbf{u}d\boldsymbol{x}-l_s^{-1}\int_{\partial\Omega_w}|\mathbf{u}_\tau|^2ds\right.\\ &\quad\left.+\int_{\partial\Omega_w}L(\phi)\partial_\tau\phi\cdot\mathbf{u}_\tau ds+\int_\Omega\mu\nabla\phi\cdot\mathbf{u}d\boldsymbol{x}\ ,\right\} \quad (4.23)\end{aligned}$$

where the slip boundary condition in Eq. (4.18) is applied.

Taking the inner product of the third equation in Eq. (4.17) with $\frac{\mu}{Re}$ results in

$$\frac{1}{Re}\int_\Omega\frac{\partial\phi}{\partial t}\mu d\boldsymbol{x}+\frac{1}{Re}\int_\Omega\mathbf{u}\cdot\nabla\phi\mu d\boldsymbol{x}=-\frac{1}{Re}\mathscr{M}\int_\Omega|\mu|^2d\boldsymbol{x}\ . \quad (4.24)$$

Multiplying the fourth equation in Eq. (4.17) with $\frac{1}{Re}\frac{\partial\phi}{\partial t}$ and integration by part give rise to

$$\begin{aligned}\frac{1}{Re}\int_\Omega\mu\frac{\partial\phi}{\partial t}d\boldsymbol{x} &= \frac{1}{Re}\left\{\kappa_B\int_\Omega g\frac{\partial\phi}{\partial t}d\boldsymbol{x}+\frac{d}{dt}\left(\mathscr{M}_v\frac{(V(\phi)-V(\phi_0))^2}{2V(\phi_0)}\right)+\mathscr{M}_s\frac{S(\phi)-S(\phi_0)}{S(\phi_0)}\int_\Omega f\frac{\partial\phi}{\partial t}d\boldsymbol{x}\right\}\\ &= \frac{\kappa_B}{Re}\int_\Omega f\frac{\partial}{\partial t}\left(-\Delta\phi+\frac{1}{\varepsilon^2}(\phi^3-\phi)\right)d\boldsymbol{x}-\frac{\kappa_B}{Re}\int_{\partial\Omega_w}\partial_n f\frac{\partial\phi}{\partial t}ds\\ &\quad+\frac{d}{dt}\left(\mathscr{M}_v\frac{(V(\phi)-V(\phi_0))^2}{ReV(\phi_0)}\right)+\mathscr{M}_s\frac{d}{dt}\left(\frac{(S(\phi)-S(\phi_0))^2}{2ReS(\phi_0)}\right)\\ &\quad-\mathscr{M}_s\left(\frac{S(\phi)-S(\phi_0)}{ReS(\phi_0)}\right)\int_{\partial\Omega_w}\varepsilon\partial_n\phi\frac{\partial\phi}{\partial t}ds\\ &= \frac{d}{dt}\left(\kappa_B\int_\Omega\frac{|f|^2}{2Re\varepsilon}d\boldsymbol{x}\right)+\frac{d}{dt}\left(\mathscr{M}_v\frac{(V(\phi)-V(\phi_0))^2}{2ReV(\phi_0)}\right)\\ &\quad+\mathscr{M}_s\frac{d}{dt}\left(\frac{(S(\phi)-S(\phi_0))^2}{2ReS(\phi_0)}\right)-\int_{\partial\Omega_w}\frac{L(\phi)}{Re}\frac{\partial\phi}{\partial t}ds+\frac{\alpha_w}{Re}\frac{d}{dt}\int_{\partial\Omega_w}f_w ds\end{aligned}$$

$$= \frac{d}{dt}(\mathscr{E}_{cell}+\mathscr{E}_w) - \int_{\partial\Omega_w}\frac{L(\phi)}{Re}\frac{\partial\phi}{\partial t}ds\,, \tag{4.25}$$

where the definitions of $f(\phi)$, $g(\phi)$ and the boundary conditions of ϕ and f are utilized.

Multiplying the last equations with $\frac{\lambda}{Re}$ and integration by parts leads to

$$\frac{1}{Re}\int_\Omega(\lambda\delta_\varepsilon\mathscr{P}):\nabla\mathbf{u}d\boldsymbol{x} - \frac{1}{Re}\int_\Omega\xi\varepsilon^2\phi^2(\nabla\lambda)^2 = 0\,. \tag{4.26}$$

Finally, the energy dissipation law (4.22) is obtained by combining Eqs. (4.23), (4.24), (4.25) and (4.26). ■

4.4 Numerical Scheme and Discrete Energy law

4.4.1 Time-discrete primitive method

The numerical scheme for solving Eqs. (4.17)-(4.18) uses the mid-point method for temporal discretization. Let Δt denote the time step size, $()^{n+1}$ and $()^n$ denote the value of the variables at times $(n+1)\Delta t$ and $n\Delta t$, respectively. The semi-discrete in time equations are as follows: in Ω

$$\begin{cases}
\frac{\mathbf{u}^{n+1}-\mathbf{u}^n}{\Delta t}+(\mathbf{u}^{n+\frac12}\cdot\nabla)\mathbf{u}^{n+\frac12}+\frac{1}{Re}\nabla P^{n+\frac12}=\frac{1}{Re}\nabla\cdot(\eta^n(\nabla\mathbf{u}^{n+\frac12}+(\nabla\mathbf{u}^{n+\frac12})^T))\\
\qquad+\frac{1}{Re}\mu^{n+\frac12}\nabla\phi^{n+\frac12}+\frac{1}{Re}\nabla\cdot\left(\lambda^{n+\frac12}\mathscr{P}^n\delta_\varepsilon\right)\,,\\
\nabla\cdot\mathbf{u}^{n+\frac12}=0\,,\\
\frac{\phi^{n+1}-\phi^n}{\Delta t}+(\mathbf{u}^{n+\frac12}\cdot\nabla)\phi^{n+\frac12}=-\mathscr{M}\mu^{n+\frac12}\,,\\
\mu^{n+\frac12}=\kappa_B g(\phi^{n+1},\phi^n)+\mathscr{M}_v\frac{(V(\phi^{n+\frac12})-V(\phi_0))}{V(\phi_0)}\\
\qquad+\mathscr{M}_s\frac{(S(\phi^{n+\frac12})-S(\phi_0))}{S(G_0)}f(\phi^{n+1},\phi^n)\,,\\
f^{n+\frac12}=-\varepsilon\Delta\phi^{n+\frac12}+\frac{1}{\varepsilon}((\phi^{n+\frac12})^2-1)\phi^{n+\frac12}\,,\\
\xi\varepsilon^2\nabla\cdot((\phi^n)^2\nabla\lambda^{n+\frac12})+\delta_\varepsilon\mathscr{P}^n:\nabla\mathbf{u}^{n+\frac12}=0\,.
\end{cases} \tag{4.27}$$

The numerical boundary conditions can be written as:

$$\begin{cases}
\kappa\dot{\phi}^{n+\frac12}=-L^{n+\frac12}\,, & \text{on } \partial\Omega_w\,,\\
L^{n+\frac12}=\kappa_B\partial_n f^{n+\frac12}+\mathscr{M}_s\varepsilon\frac{S(\phi^{n+\frac12})-S_0}{S_0}\partial_n\phi^{n+\frac12}+\alpha_w\frac{f_w^{n+1}-f_w^n}{\phi^{n+1}-\phi^n}\,, & \text{on } \partial\Omega_w\,,\\
-l_s^{-1}u_{\tau_i}^{n+\frac12}=\boldsymbol{\tau_i}\cdot(\eta^n(\nabla\mathbf{u}^{n+\frac12}+(\nabla\mathbf{u}^{n+\frac12})^T)+\lambda^{n+\frac12}\delta_\varepsilon\mathscr{P}^n)\cdot\boldsymbol{n}\\
\qquad -L^{n+\frac12}\partial_{\tau_i}\phi^{n+\frac12}\,,\ \ i=1,2, & \text{on } \partial\Omega_w\,,\\
f^{n+\frac12}=0\,, & \text{on } \partial\Omega_w\,,\\
\partial_n\lambda^{n+\frac12}=0\,, & \text{on } \partial\Omega_w\,,
\end{cases} \tag{4.28}$$

where

$$f(\phi^{n+1},\phi^n) = -\varepsilon\Delta\phi^{n+\frac{1}{2}} + \frac{1}{4\varepsilon}((\phi^{n+1})^2+(\phi^n)^2-2)(\phi^{n+1}+\phi^n)\ , \tag{4.29}$$

$$g(\phi^{n+1},\phi^n) = \left(-\Delta f^{n+\frac{1}{2}} + \frac{1}{\varepsilon^2}\left((\phi^{n+1})^2+(\phi^n)^2+\phi^{n+1}\phi^n-1\right)f^{n+\frac{1}{2}}\right)\ , \tag{4.30}$$

$(\cdot)^{n+\frac{1}{2}} = \frac{(\cdot)^n+(\cdot)^{n+1}}{2}$ and $\mathscr{P}^n = I - \mathbf{n}_m^n \otimes \mathbf{n}_m^n$ with $\mathbf{n}_m^n = \frac{\nabla\phi^n}{|\nabla\phi^n|}$.

The above scheme obeys the following theorem of energy stability.

Theorem 4.4.1. *If $(\phi^n, \mathbf{u}^n, P^n)$ are smooth solutions of the above system* (4.27)-(4.28)*, then the following energy law is satisfied:*

$$\begin{aligned}\mathscr{E}_{total}^{n+1} - \mathscr{E}_{total}^{n} &= (\mathscr{E}_{kin}^{n+1}+\mathscr{E}_{cell}^{n+1}+\mathscr{E}_{w}^{n+1}) - (\mathscr{E}_{kin}^{n}+\mathscr{E}_{cell}^{n}+\mathscr{E}_{w}^{n}) \\ &= \frac{\triangle t}{Re}\left(-2\|(\eta^n)^{1/2}\mathbf{D}_\eta^{n+\frac{1}{2}}\|^2 - \mathscr{M}\|\mu^{n+\frac{1}{2}}\|^2 - \xi\|\ \varepsilon\phi^n\nabla\lambda^{n+\frac{1}{2}}\|^2\right. \\ &\quad \left. -\frac{1}{\kappa}\|L(\phi^{n+\frac{1}{2}})\|_w^2 - \|l_s^{-1/2}\mathbf{u}_\tau^{n+\frac{1}{2}}\|_w^2\right)\ ,\end{aligned} \tag{4.31}$$

where $\mathscr{E}_{total}^n = \mathscr{E}_{kin}^n + \mathscr{E}_{cell}^n + \mathscr{E}_w^n$ with $\mathscr{E}_{kin}^n = \frac{1}{2}\|\mathbf{u}^n\|^2$, $\mathscr{E}_{cell}^n = \frac{\kappa_B\|f^n\|^2}{2Re\varepsilon} + \mathscr{M}_v\frac{(V(\phi^n)-V(\phi_0))^2}{2ReV(\phi_0)} + \mathscr{M}_s\frac{(S(\phi^n)-S(\phi_0))^2}{2ReS(\phi_0)}$ and $\mathscr{E}_w^n = \frac{\alpha_w}{Re}\int_{\partial\Omega_w} f_w^n ds$.

The following two lemmas are needed for proving **Theorem 4.4.1**. Proof of these two lemmas can be found in the appendix.

Lemma 4.4.2. *Let*

$$f(\phi^{n+1},\phi^n) = -\varepsilon\Delta\phi^{n+\frac{1}{2}} + \frac{1}{4\varepsilon}((\phi^{n+1})^2+(\phi^n)^2-2)(\phi^{n+1}+\phi^n)\ . \tag{4.32}$$

Then $f(\phi^{n+1},\phi^n)$ satisfies

$$\int_\Omega f(\phi^{n+1},\phi^n)(\phi^{n+1}-\phi^n)d\boldsymbol{x} = S^{n+1}-S^n - \int_{\partial\Omega_w}\varepsilon\partial_n\phi^{n+\frac{1}{2}}(\phi^{n+1}-\phi^n)ds\ , \tag{4.33}$$

where $S^{n+1} = \int_\Omega G(\phi^{n+1})d\boldsymbol{x}, S^n = \int_\Omega G(\phi^n)d\boldsymbol{x}$.

Lemma 4.4.3. *Let $g(\phi^{n+1},\phi^n) = -\Delta f^{n+\frac{1}{2}} + \frac{1}{\varepsilon^2}((\phi^{n+1})^2+(\phi^n)^2+\phi^{n+1}\phi^n-1)f^{n+\frac{1}{2}}$. Then $g(\phi^{n+1},\phi^n)$ satisfies*

$$\begin{aligned}&\int_\Omega g(\phi^{n+1},\phi^n)(\phi^{n+1}-\phi^n)d\boldsymbol{x} \\ =\ &\int_\Omega\frac{1}{2\varepsilon}((f^{n+1})^2-(f^n)^2)d\boldsymbol{x} - \int_{\partial\Omega_w}\partial_n f^{n+\frac{1}{2}}(\phi^{n+1}-\phi^n)ds\ ,\end{aligned} \tag{4.34}$$

where $f^{n+1} = -\varepsilon\Delta\phi^{n+1} + \frac{1}{\varepsilon}((\phi^{n+1})^2-1)\phi^{n+1}, f^n = -\varepsilon\Delta\phi^n + \frac{1}{\varepsilon}((\phi^n)^2-1)\phi^n$.

Proof of Theorem 4.4.1: Multiplying the first equation in system (4.27) by $\Delta t\mathbf{u}^{n+\frac{1}{2}}$ gives

$$\begin{aligned}
&\int_\Omega \frac{1}{2}((\mathbf{u}^{n+1})^2-(\mathbf{u}^n)^2)d\boldsymbol{x}+\int_\Omega \Delta t\mathbf{u}^{n+\frac{1}{2}}\cdot((\mathbf{u}^{n+\frac{1}{2}}\nabla)\cdot\mathbf{u}^{n+\frac{1}{2}})d\boldsymbol{x}\\
&-\frac{\Delta t}{Re}\int_\Omega P^{n+\frac{1}{2}}\nabla\cdot\mathbf{u}^{n+\frac{1}{2}}d\boldsymbol{x}\\
=\;&-\frac{\Delta t}{Re}\int_\Omega \nabla\mathbf{u}^{n+\frac{1}{2}}:\eta^n(\nabla\mathbf{u}^{n+\frac{1}{2}}+(\nabla\mathbf{u}^{n+\frac{1}{2}})^T)d\boldsymbol{x}+\frac{\Delta t}{Re}\int_\Omega \mathbf{u}^{n+\frac{1}{2}}\cdot\nabla\phi^{n+1}\mu^{n+1}d\boldsymbol{x}\\
&-\frac{\Delta t}{Re}\int_\Omega \lambda\delta_\varepsilon\mathscr{P}^n:\nabla\mathbf{u}^{n+\frac{1}{2}}d\boldsymbol{x}+\frac{\Delta t}{Re}\int_{\partial\Omega_w}\lambda^{n+\frac{1}{2}}(\delta_\varepsilon\mathscr{P}^n\cdot\mathbf{n})\cdot\mathbf{u}_\tau^{n+\frac{1}{2}}ds\\
&+\frac{\Delta t}{Re}\int_{\partial\Omega_w}\mathbf{u}^{n+\frac{1}{2}}\cdot\eta^n((\nabla\mathbf{u}^{n+\frac{1}{2}}+(\nabla\mathbf{u}^{n+\frac{1}{2}})^T)\cdot\boldsymbol{n})ds\,. \qquad (4.35)
\end{aligned}$$

Multiplying the fourth equation in system (4.27) by $\frac{\phi^{n+1}-\phi^n}{Re}$ and integration by parts lead to

$$\begin{aligned}
&\frac{1}{Re}\int_\Omega \mu^{n+1/2}(\phi^{n+1}-\phi^n)d\boldsymbol{x}=\frac{\kappa_B}{Re}\int_\Omega\frac{1}{2\varepsilon}((f^{n+1})^2-(f^n)^2)d\boldsymbol{x}\\
&+\frac{\mathscr{M}_v}{Re}\frac{(V(\phi^{n+1})-V_0)^2-(V(\phi^n)-V_0)^2}{2V_0}+\frac{\mathscr{M}_s}{Re}\frac{(S(\phi^{n+1})-S_0)^2-(S(\phi^n)-S_0)^2}{2S_0}\\
&-\frac{\kappa_B}{Re}\int_{\partial\Omega_w}\partial_n f^{n+\frac{1}{2}}(\phi^{n+1}-\phi^n)ds-\frac{\mathscr{M}_s}{Re}\int_{\partial\Omega_w}\frac{S(\phi^{n+\frac{1}{2}})-S_0}{S_0}\varepsilon\partial_n\phi^{n+\frac{1}{2}}(\phi^{n+1}-\phi^n)ds\,. \qquad (4.36)
\end{aligned}$$

Multiplying the third equation in system (4.27) by $\frac{\mu^{n+1}\Delta t}{Re}$ and integration by parts yield

$$\begin{aligned}
&\frac{1}{Re}\int_\Omega \mu^{n+1}(\phi^{n+1}-\phi^n)d\boldsymbol{x}+\frac{\Delta t}{Re}\int_\Omega \mu^{n+1}(\mathbf{u}^{n+1/2}\cdot\nabla)\phi^{n+1}d\boldsymbol{x}\\
=\;&-\frac{\mathscr{M}\Delta t}{Re}\int_\Omega(\mu^{n+1})^2d\boldsymbol{x}\,. \qquad (4.37)
\end{aligned}$$

Multiplying the last equation in system (4.27) by $\frac{\lambda^{n+\frac{1}{2}}\Delta t}{Re}$ and integration by parts give

$$-\frac{\Delta t}{Re}\int_\Omega \xi\varepsilon^2(\phi^n)^2\left|\nabla\lambda^{n+\frac{1}{2}}\right|^2d\boldsymbol{x}+\frac{\Delta t}{Re}\int_\Omega(\lambda^{n+\frac{1}{2}}\delta_\varepsilon\mathscr{P}^n):\nabla\mathbf{u}^{n+\frac{1}{2}}d\boldsymbol{x}=0\,. \qquad (4.38)$$

The discretized energy dissipation law (4.31) is obtained by combining Eqs. (4.35)-(4.38) and organizing the terms according to the boundary conditions $L(\phi)$ as shown in (4.28). ■

Remark 4.4.1. *The system* (4.27) *is second-order accurate in time except for the last equation. It can be changed to be second-order accurate as well by using* $\phi^{n+1/2}$ *and* $\mathscr{P}^{n+1/2}$*. By doing this, theorem 4.4.1 still holds with the term* $\xi\|\varepsilon\phi^n\nabla\lambda^{n+\frac{1}{2}}\|^2$ *changed into* $\xi\|\varepsilon\phi^{n+\frac{1}{2}}\nabla\lambda^{n+\frac{1}{2}}\|^2$*. However, this change makes the Newton iteration discussed in next session very complicated. For simplicity of computer implementation, a first-order accurate treatment for the last equation is adopted here.*

The unique solvability of the scheme can be referred to Theorem 3.3.3. We don't show it here.

4.4.2 Fully-discrete C^0 finite element scheme

The spatial discretization using C^0 finite element is straight forward. Let Ω be the domain of interest with a Lipschitz-continuous boundary $\partial\Omega$. Let ${\mathbf{W}_b}^h \subset \mathbf{W}_b$ be a finite element space with respect to the triangulation of the domain Ω. The fully discrete scheme of the system is to find $({\phi_h}^{n+1}, {\mu_h}^{n+1}, {f_h}^{n+1},\ {\lambda_h}^{n+1}, {p_h}^{n+1}, {\mathbf{u}_h}^{n+1}) \in {\mathbf{W}_b}^h$, such that for any $(\psi_h, \chi_h, \zeta_h, \Theta_h, q_h, \mathbf{v}_h) \in \mathbf{W}_b^h$,

$$
\begin{cases}
\int_\Omega \left(\frac{\mathbf{u}_h^{n+1}-\mathbf{u}_h^n}{\Delta t} + (\mathbf{u}_h^{n+\frac{1}{2}} \cdot \nabla)\mathbf{u}_h^{n+\frac{1}{2}} + \frac{1}{Re}\nabla P_h^{n+\frac{1}{2}} \right) \cdot \mathbf{v}_h d\boldsymbol{x} \\
= -\int_\Omega \frac{1}{Re}(\eta_h^n(\nabla \mathbf{u}_h^{n+\frac{1}{2}} + (\nabla \mathbf{u}_h^{n+\frac{1}{2}})^T)) : \nabla \mathbf{v}_h d\boldsymbol{x} \\
\qquad + \int_\Omega \frac{1}{Re}\mu_h^{n+\frac{1}{2}} \nabla \phi_h^{n+\frac{1}{2}} \cdot \mathbf{v}_h d\boldsymbol{x} - \int_\Omega \frac{1}{Re}\lambda_h^{n+\frac{1}{2}} \mathscr{P}_h^n \delta_\varepsilon : \mathbf{v}_h d\boldsymbol{x} \\
\qquad + \int_{\partial\Omega_w} \frac{1}{Re}\mathbf{n} \cdot (\eta_h^n(\nabla \mathbf{u}_h^{n+\frac{1}{2}} + (\nabla \mathbf{u}_h^{n+\frac{1}{2}})^T) + \lambda_h^{n+\frac{1}{2}} \mathscr{P}_h^n \delta_\varepsilon) \cdot \mathbf{v}_h d\boldsymbol{x}\ , \\
\int_\Omega (\nabla \cdot \mathbf{u}_h^{n+\frac{1}{2}}) q_h d\boldsymbol{x} = 0\ , \\
\int_\Omega (\frac{\phi_h^{n+1}-\phi_h^n}{\Delta t} + (\mathbf{u}_h^{n+\frac{1}{2}} \cdot \nabla)\phi_h^{n+\frac{1}{2}}) \psi_h d\boldsymbol{x} = -\int_\Omega \mathscr{M} \mu_h^{n+\frac{1}{2}} \psi_h d\boldsymbol{x}\ , \\
\int_\Omega \mu_h^{n+\frac{1}{2}} \chi_h d\boldsymbol{x} = \int_\Omega \Bigg(\kappa_B \frac{1}{\varepsilon^2}((\phi_h^{n+1})^2 + (\phi_h^n)^2 + \phi_h^{n+1}\phi_h^n - 1) f_h^{n+\frac{1}{2}} \\
\qquad + \mathscr{M}_v \frac{(V(\phi_h^{n+\frac{1}{2}}) - V(\phi_0))}{V(\phi_0)} \\
\qquad + \mathscr{M}_s \frac{(S(\phi_h^{n+\frac{1}{2}}) - S(\phi_0))}{S(G_0)} (\frac{1}{4\varepsilon}((\phi_h^{n+1})^2 + (\phi_h^n)^2 - 2)(\phi_h^{n+1} + \phi_h^n)) \Bigg) \chi_h d\boldsymbol{x} \\
\qquad + \int_\Omega (\kappa_B \nabla f_h^{n+\frac{1}{2}} + \mathscr{M}_s \varepsilon \frac{(S(\phi_h^{n+\frac{1}{2}}) - S(\phi_0))}{S(G_0)} \nabla \phi_h^{n+\frac{1}{2}}) \cdot \nabla \chi_h d\boldsymbol{x} \\
\qquad - \int_{\partial\Omega_w} (\kappa_B \partial_{\mathbf{n}} f_h^{n+\frac{1}{2}} + \mathscr{M}_s \varepsilon \frac{(S(\phi_h^{n+\frac{1}{2}}) - S(\phi_0))}{S(G_0)} \partial_{\mathbf{n}} \phi_h^{n+\frac{1}{2}}) \chi_h d\boldsymbol{x}\ , \\
\int_\Omega f_h^{n+\frac{1}{2}} \zeta_h = \int_\Omega \varepsilon \nabla \phi_h^{n+\frac{1}{2}} \cdot \nabla \zeta_h + \int_\Omega \frac{1}{\varepsilon}((\phi_h^{n+\frac{1}{2}})^2 - 1)\phi_h^{n+\frac{1}{2}} \zeta_h d\boldsymbol{x} \\
\qquad - \int_{\partial\Omega_w} \varepsilon \partial_{\mathbf{n}} \phi_h^{n+\frac{1}{2}} \zeta_h d\boldsymbol{x}\ , \\
\int_\Omega \xi \varepsilon^2 ((\phi_h^n)^2 \nabla \lambda_h^{n+\frac{1}{2}}) \cdot \nabla \Theta_h dx = \int_\Omega \delta_\varepsilon \mathscr{P}_h^n : \nabla \mathbf{u}_h^{n+\frac{1}{2}} \Theta_h d\boldsymbol{x} \\
\qquad + \int_{\partial\Omega_w} \xi \varepsilon^2 ((\phi_h^n)^2 \partial_{\mathbf{n}} \lambda_h^{n+\frac{1}{2}}) \Theta_h d\boldsymbol{x}\ .
\end{cases}
\tag{4.39}
$$

Theorem 4.4.4. *If $({\phi_h}^{n+1}, {\mu_h}^{n+1}, {f_h}^{n+1}, {\lambda_h}^{n+1}, {p_h}^{n+1}, {\mathbf{u}_h}^{n+1}) \in {\mathbf{W}_b}^h$ are solutions of the above system, then the following energy law is satisfied:*

$$
\begin{aligned}
\mathscr{E}_{total,h}^{n+1} - \mathscr{E}_{total,h}^n \ = \ & \frac{\triangle t}{Re} \Bigg(-2\|(\eta_h^n)^{1/2} \mathbf{D}_\eta^{n+\frac{1}{2}}\|^2 - \mathscr{M}\|\mu_h^{n+\frac{1}{2}}\|^2 - \xi \| \ \varepsilon \phi_h^n \nabla \lambda_h^{n+\frac{1}{2}}\|^2 \\
& - \frac{1}{\kappa}\|L(\phi_h^{n+\frac{1}{2}})\|_w^2 - \|l_s^{-1/2} \mathbf{u}_{\tau,h}^{n+\frac{1}{2}}\|_w^2 \Bigg)\ ,
\end{aligned}
\tag{4.40}
$$

It is easy to prove this theorem by letting $\mathbf{v}_h = \Delta t \mathbf{u}_h^{n+1}, q_h = \frac{\Delta t p_h^{n+1}}{Re}, \psi_h = \frac{c_h^{n+1} - c_h^n}{Re}, \chi_h = \frac{\Delta t \mu_h^n + 1}{Re}, \Theta_h = \frac{\Delta t \lambda_h^{n+1}}{Re}$ and following the process of proving **Theorem 4.1**. Details of the proof is presented in the Appendix.

4.4.3 Linearization and unique solvability

Note that the energy stable scheme (4.39) is a coupled nonlinear system. Newton's method [53] is used to solve the scheme equations. First, the scheme (4.39) can be written into the following form:

$$\mathscr{F}_h^{n+1} = \mathscr{C} \ ,$$

by relocating all of the constant terms to the right-hand side (RHS) and the terms containing unknown variables to the left-hand side.

For the sake of simplification, we let $\mathbb{U}_h^{n+1,k} = (\phi_h{}^{n+1,k}, \mu_h{}^{n+1,k}, f_h{}^{n+1,k}, \lambda_h{}^{n+1,k}, \mathbf{u}_h{}^{n+1,k}, p_h{}^{n+1,k})$ be the solution at time $(n+1)\Delta t$ in the k^{th} iteration of Newton's method, and the variation between iterations be

$$(\delta\mathbb{U})_h^{n+1,k} = ((\delta\phi_h)^{n+1,k+1}, (\delta\mu_h)^{n+1,k+1}, (\delta f_h)^{n+1,k+1}, (\delta\lambda_h)^{n+1,k+1}, (\delta\mathbf{u}_h)^{n+1,k+1}, (\delta p_h)^{n+1,k+1}).$$

Here $(\delta\cdot)$ stands for the amount of change of the value, $(\delta\cdot)^{n+1,k} = (\cdot)^{n+1,k+1} - (\cdot)^{n+1,k}$. Newton's method can be formally written as:

$$\mathscr{F}_h^{n+1}(\mathbb{U}_h^{n+1,k}) + \nabla_{\mathbb{U}_h^{n+1,k}} \mathscr{F}_h^{n+1}(\mathbb{U}_h^{n+1,k}) \cdot (\delta\mathbb{U})_h^{n+1,k} = \mathscr{C}(\mathbb{U}_h^n) \ .$$

The solution is updated by $\mathbb{U}_h^{n+1,k+1} = \mathbb{U}_h^{n+1,k} + \delta\mathbb{U}_h^{n+1,k}$, where $\mathbb{U}_h^{n+1,0} = \mathbb{U}_h^n$.

Then the theorem for the solvability of the fully discrete scheme could be given.

Theorem 4.4.5. *If the time step Δt is small enough, then the equations of the scheme* (4.39) *is uniquely solvable.*

Proof: From the last three equations we find $\mu_h^{n+1} = \mu(\phi_h^{n+1})$, $f_h^{n+1} = f(\phi_h^{n+1})$, $\lambda_h^{n+1} = \lambda(\mathbf{u}_h^{n+1})$. With the first and the second equations, P_h^{n+1} can be expressed as $P_h^{n+1} = P(\mathbf{u}_h^{n+1}, \phi_h^{n+1})$. Then the first and the third equations can be solved separately. Applying Newton's method to the first three equations, we have their linearized form:

$$\begin{aligned} &\mathscr{F}_h^{n+1}(\mathbf{u}_h^{n+1,k}, \phi_h^{n+1,k}) + \nabla_{\mathbf{u}_h^{n+1,k}, \phi_h^{n+1,k}} \mathscr{F}_h^{n+1}(\mathbf{u}_h^{n+1,k}, \phi_h^{n+1,k}) \cdot (\mathbf{u}_h^{n+1,k+1} - \mathbf{u}_h^{n+1,k}, \phi_h^{n+1,k+1} - \phi_h^{n+1,k})^T \\ &= \mathscr{C}. \end{aligned} \tag{4.41}$$

Note that $\mathbf{u}_h^{n+1,k+1} = (u_h^{n+1,k}, v_h^{n+1,k+1})$. Multiplying Δt to (4.41) yields

$$\begin{pmatrix} I-\Delta tA_{11} & \Delta tA_{12} & \Delta tA_{13} \\ \Delta tA_{21} & I-\Delta tA_{22} & \Delta tA_{23} \\ \Delta tA_{31} & \Delta tA_{32} & I-\Delta tA_{33} \end{pmatrix} \begin{pmatrix} u_h^{n+1,k+1} \\ v_h^{n+1,k+1} \\ \phi_h^{n+1,k+1} \end{pmatrix} = \mathscr{C}' \tag{4.42}$$

where

$A_{11} = \frac{1}{4}(u_h^{n+1,k}\partial_{x,h} + \partial_{x,h}u_h^{n+1,k} + u_h^n\partial_{x,h} + \partial_{x,h}u_h^n + \partial_{y,h}v_h^{n+1,k}) - \frac{1}{2Re}(2\partial_{x,h}(\eta_h^n\partial_{x,h}) + \partial_{y,h}(\eta_h^n\partial_{y,h})) + \frac{1}{2Re}\frac{\partial_h(\partial_{x,h}P_h^{n+1,k})}{\partial_h u_h^{n+1,k}} - \frac{1}{4Re}\frac{\partial_h(\partial_{x,h}(\lambda_h^{n+1,k}(\partial_{x,h}\phi_h^n)^2)) + \partial_{y,h}(\lambda_h^{n+1,k}\partial_{x,h}\phi_h^n\partial_{y,h}\phi_h^n)}{\partial u_h^{n+1,k}}$,

$A_{12} = \frac{1}{4}u_h^{n+1,k}\partial_{y,h} - \frac{1}{2Re}\eta_h^n\partial_{x,h}\partial_{y,h} + \frac{1}{2Re}\frac{\partial_h(\partial_{x,h}P_h^{n+1,k})}{\partial_h v_h^{n+1,k}} - \frac{1}{4Re}\frac{\partial_h(\partial_{x,h}(\lambda_h^{n+1,k}(\partial_{x,h}\phi_h^n)^2)) + \partial_{y,h}(\lambda_h^{n+1,k}\partial_{x,h}\phi_h^n\partial_{y,h}\phi_h^n)}{\partial v_h^{n+1,k}}$,

$A_{13} = -\frac{1}{4Re}(\mu_h^{n+1,k}\partial_{x,h} + \frac{\partial\mu_h^{n+1,k}}{\partial\phi_h^{n+1,k}}\partial_{x,h}\phi_h^{n+1,k} + \mu_h^n\partial_{x,h} + \frac{\partial\mu_h^{n+1,k}}{\partial\phi_h^{n+1,k}}\partial_{x,h}\phi_h^n)$,

$A_{21} = \frac{1}{4}v_h^{n+1,k}\partial_{x,h} - \frac{1}{2Re}\eta_h^n\partial_{x,h}\partial_{y,h} + \frac{1}{2Re}\frac{\partial_h(\partial_{y,h}P_h^{n+1,k})}{\partial_h u_h^{n+1,k}} - \frac{1}{4Re}\frac{\partial_h(\partial_{y,h}(\lambda_h^{n+1,k}(\partial_{y,h}\phi_h^n)^2)) + \partial_{x,h}(\lambda_h^{n+1,k}\partial_{x,h}\phi_h^n\partial_{y,h}\phi_h^n)}{\partial u_h^{n+1,k}}$,

$A_{22} = \frac{1}{4}(v_h^{n+1,k}\partial_{y,h} + \partial_{y,h}v_h^{n+1,k} + v_h^n\partial_{y,h} + \partial_{y,h}v_h^n + \partial_{x,h}u_h^{n+1,k}) - \frac{1}{2Re}(\partial_{x,h}(\eta_h^n\partial_{x,h}) + 2\partial_{y,h}(\eta_h^n\partial_{y,h})) + \frac{1}{2Re}\frac{\partial_h(\partial_{y,h}P_h^{n+1,k})}{\partial_h v_h^{n+1,k}} - \frac{1}{4Re}\frac{\partial_h(\partial_{y,h}(\lambda_h^{n+1,k}(\partial_{y,h}\phi_h^n)^2)) + \partial_{x,h}(\lambda_h^{n+1,k}\partial_{x,h}\phi_h^n\partial_{y,h}\phi_h^n)}{\partial v_h^{n+1,k}}$,

$A_{23} = -\frac{1}{4Re}(\mu_h^{n+1,k}\partial_{y,h} + \frac{\partial\mu_h^{n+1,k}}{\partial\phi_h^{n+1,k}}\partial_{y,h}\phi_h^{n+1,k} + \mu_h^n\partial_{y,h} + \frac{\partial\mu_h^{n+1,k}}{\partial\phi_h^{n+1,k}}\partial_{y,h}\phi_h^n)$,

$A_{31} = \frac{1}{4}\partial_x(\phi_h^{n+1,k} + \phi_h^n)$,

$A_{32} = \frac{1}{4}\partial_y(\phi_h^{n+1,k} + \phi_h^n)$,

$A_{33} = \frac{1}{4}((u_h^{n+1,k} + u_h^n)\partial_{x,h} + (v_h^{n+1,k} + v_h^n)\partial_{y,h}) + \mathscr{M}\frac{\partial\mu_h^{n+1,k}}{\partial\phi_h^{n+1,k}}$.

Using Gaussian elimination, left side of the above matrix system can be transformed as follows:

$$\begin{pmatrix} I-\Delta tA_{11} & \Delta tA_{12} & \Delta tA_{13} \\ 0 & I-\Delta tA_{22}-(\Delta t)^2(I-\Delta tA_{11})^{-1}A_{21}A_{12} & \Delta tA_{23}-(\Delta t)^2(I-\Delta tA_{11})^{-1}A_{21}A_{13} \\ 0 & 0 & A'_{33} \end{pmatrix} \tag{4.43}$$

Where $A'_{33} = I-\Delta tA_{33}-(\Delta t)^2(I-\Delta tA_{22}-(\Delta t)^2(I-\Delta tA_{11})^{-1}A_{21}A_{12})^{-1}A_{32}A_{23}$. C, C' are constant matrices. When Δt is small enough, $I-\Delta tA_{ii}(i=1,2,3)$ is invertible. Thus the given matrix is invertible, we can obtain the unique solution of $(\mathbf{u}_h^{n+1,k+1}, \phi_h^{n+1,k+1})$ with given boundary condition, which means the equation (4.39) is uniquely solvable. ■

4.5 Simulation Results

Numerical simulations using the model introduced in the paper are presented in this section. The first example is used to illustrate the convergence and energy stability of the proposed numerical scheme. Then feasibility of the proposed model and the model simulation scheme to studying vesicle motion and shape transformation is assessed by cell tank treading and tumbling tests. The last simulation is devoted to studying effects of mechanical and geometric properties of a vesicle on its deformability when it passes through a narrow channel.

4.5.1 Convergence study

The initial condition of the convergence test is set to be a 2D tear shape vesicle in a closed cube with intercellular and extracellular fluid velocity being 0. The initial conditions are:

$$\phi_0(x) = \begin{cases} -\tanh[(15(y-0.185)(y-0.065)-x+0.125)/\sqrt{2}\varepsilon], & x < 0.125 \\ -\tanh[(\sqrt{(x-0.125)^2+(y-0.125)^2}-0.06)/\sqrt{2}\varepsilon], & x >= 0.125, \end{cases} \tag{4.44}$$
$$\mathbf{u}_0 = (0,0).$$

Remark 4.5.1. *During the convergence test, we mainly focus on the convergence rates of the velocity and the phase-field function. The local inextensibility is neglected, and only the global area and volume constraints are taken into consideration.*

Thanks to the bending force of the cell membrane, the shape of the vesicle gradually transforms into a perfect circle to minimize the total energy (see Figure 4.1). The parameter values used for this simulation are chosen as follows: $Re = 2\times10^{-4}$, $\mathscr{M} = 5\times10^{-5}$, $\kappa_B = 8\times10^{-1}$, $\varepsilon = 2.5\times10^{-2}$, $\mathscr{M}_v = 20$, $\mathscr{M}_s = 2$, $\xi = 1.6\times10^{5}$, $\kappa = 8\times10^{-10}$, $l_s = 5\times10^{-3}$.

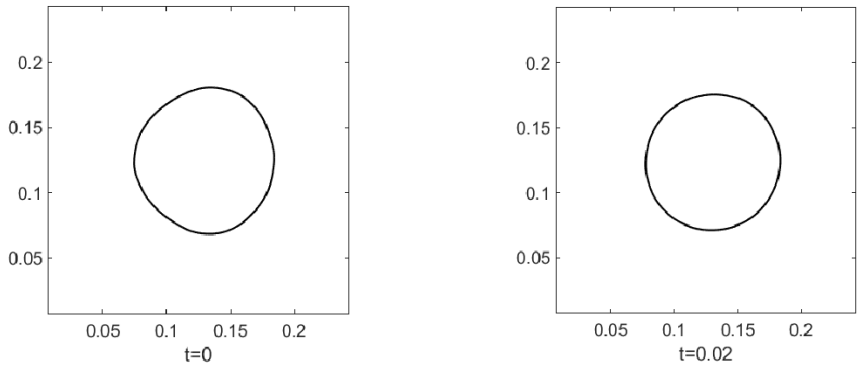

Figure 4.1: Relaxation of a tear shape vesicle.

In the simulations, the numerical solution computed with a mesh size $h = 1/240$ is treated as the reference solution or "the true solution". As shown in Table 4.1, our scheme is a second-order accurate in space.

Spacial mesh size h	P2 Element					
	Err(u_x)	Convergence Rate(u_x)	Err(u_y)	Convergence Rate(u_y)	Err(ϕ)	Convergence Rate(ϕ)
1/47	1.3e-1		1.5e-1		1.4e-2	
1/71	8.3e-2	1.15	7.6e-2	1.71	6.1e-3	1.97
1/107	3.8e-2	1.94	3.7e-2	1.83	2.3e-3	2.45
1/160	1.5e-2	2.35	1.3e-2	2.59	5.7e-4	3.42

Table 4.1: L^2 norm of the error and convergence rate for velocity $\mathbf{u} = (u_x, u_y)$, phase-field function ϕ, at time $t = 0.02$ with both intercellular and extracellular fluid viscosity being 1.

The time convergence rate of the scheme is obtained by comparing the numerical errors calculated using each pair of successively reduced time step sizes. The purpose of doing so is to eliminate the influence from the error of the reference solution which is also a numerical result. Larger Reynolds number Re and interface thickness ε, and a smoother initial profile of the interface are applied to ensure that the convergence rate is not affected by any sharp changes in the phase field label function $\phi(\boldsymbol{x})$. Results in Table 4.2 confirm that our scheme is a also second-order accurate in time.

time step Δt	P2 Element					
	Err(u_x)	Convergence Rate(u_x)	Err(u_y)	Convergence Rate(u_y)	Err(ϕ)	Convergence Rate(ϕ)
0.025	-		-		-	
0.0125	8.12e-6		8.13e-6		9.92e-6	
0.00625	2.90e-6	1.49	2.97e-6	1.45	2.42e-6	2.04
0.003125	1.03e-6	1.48	1.07e-6	1.48	5.98e-7	2.01
0.0015625	2.53e-7	2.03	2.60e-7	2.03	1.49e-7	2.01

Table 4.2: L^2 norm of the error and convergence rate for velocity $\mathbf{u} = (u_x, u_y)$, phase-field function ϕ, at time $t = 0.05$ with both intercellular and extracellular fluid viscosities being 1.

Finally, the energy law (**Theorem 4.4.1**) and conservation of mass and surface area of vesicles are tested by simulating the relaxation of a bent vesicle. The vesicle gradually evolves back to its equilibrium biconcave shape. Figure 4.2 shows the snapshots of the vesicle profile at different times $t = 0, 0.25, 0.5$ and 1.25. The parameter values used here are:

$Re = 2 \times 10^{-4}$, $\mathscr{M} = 2.5 \times 10^{-3}$, $\kappa_B = 2$, $\varepsilon = 7.5 \times 10^{-3}$, $\mathscr{M}_v = 20$, $\mathscr{M}_s = 2$, $\xi = 7.1 \times 10^4$, $\kappa = 2 \times 10^{-10}$, $l_s = 0.5$.

The initial conditions are:

$$\phi_0(x) = \begin{cases} -tanh[(5(y-0.7)(y-0.3)-x+0.5)/\sqrt{2}\varepsilon], & x < 0.5 \\ -tanh[(400(y-0.7)(y-0.3)(y-0.5)^2+x-0.5)/\sqrt{2}\varepsilon], & x >= 0.5, \end{cases} \quad (4.45)$$

$\mathbf{u}_0 = (0,0)$.

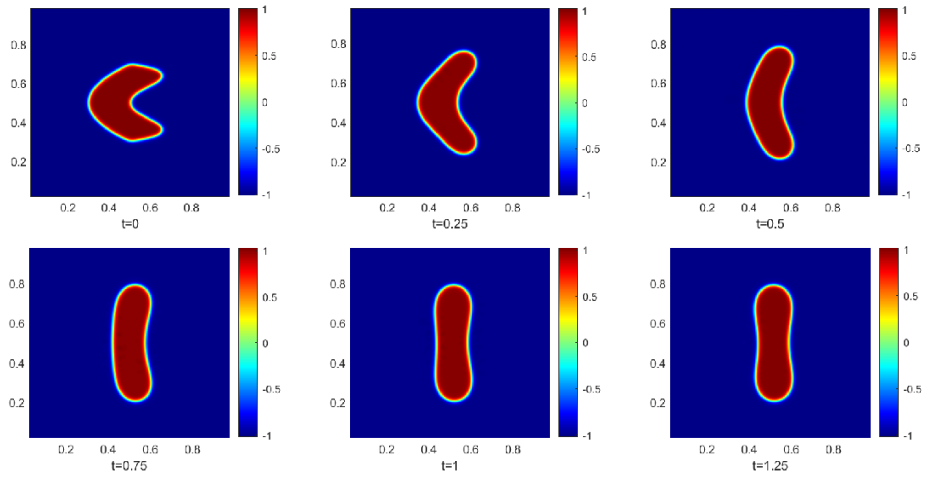

Figure 4.2: Relaxation of a bent vesicle. The fluid viscosities are 1 and 50 for intercellular and extracellular fluids, respecfively.

The changes of vesicle mass and surface area and the change of total discrete energy of this test case computed by the scheme (Eqs. (4.17)-(4.18)) are shown in Figure 4.3. It is evident that the vesicle mass and surface area are almost perfectly preserved, and the total energy decays over the course of time as expected.

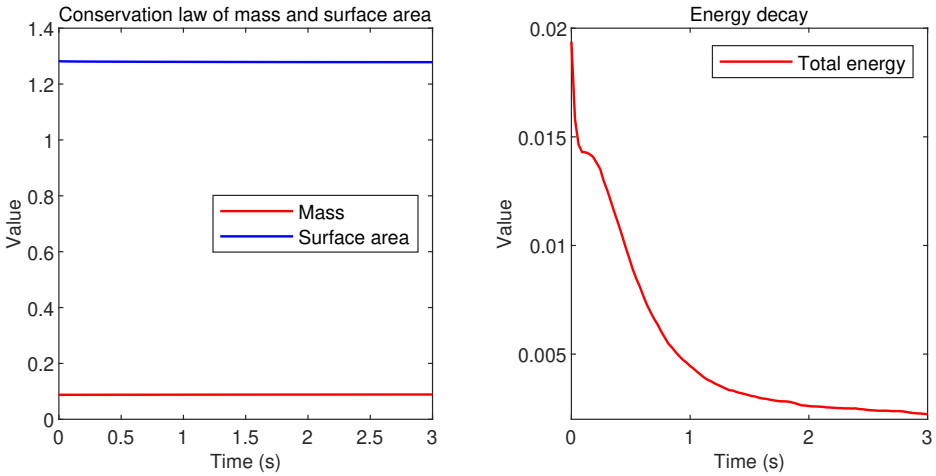

Figure 4.3: The test case of relaxation of a bent vesicle. Left: Change of mass and surface area vs. time; Right: Change of discrete energy vs. time.

4.5.2 Vesicle-wall interaction

This example is used to investigate the effect of the contact line model used for describing vesicle-wall interaction. As shown in the Figure 4.4, a vesicle is initially placed at a location with a point-wise vesicle-wall contact, and a shear flow from left to right is introduced to the system. The parameter values of this simulation are listed as follows:

$Re = 2 \times 10^{-4}, \mathscr{M} = 1.5 \times 10^{-3}, \kappa_B = 0.1, \varepsilon = 0.03, \mathscr{M}_v = 200, \mathscr{M}_s = 2 \times 10^5, \xi = 10^4, \kappa = 1 \times 10^{-10}, \alpha_w = 80, l_s = 0.5$. θ_s is set to be 85° (or 180°) for different interactions between the vesicle and the vessel wall.

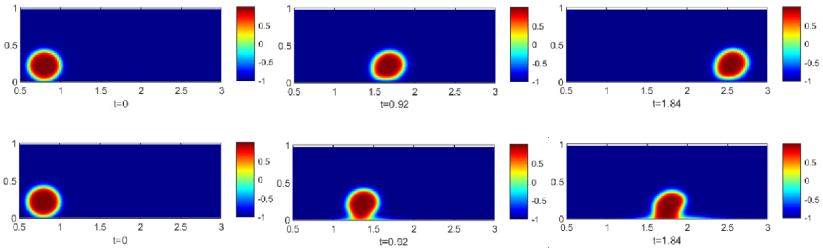

Figure 4.4: The top three pictures show the result of no wetting force modeled using a contact angle 180°. The bottom three pictures show the result of existing cell-wall wetting condition modeled using a contact angle 85°.

Remark 4.5.2. *As can be seen in Figure 4.4, when the contact angel is 180° high, the cell is carried away by the flow due to an absence of "attraction"between cell and the wall by a wetting force which is introduced by the contact line model. When the contact angle is significant lower, say 85°, the vesicle membrane is torn apart at the vesicle-wall contact location due to the existence of a wetting force. We point out that the simulation using 85° contact angle is not biologically relevant. This shows the limitation of our current model based only on hydrophobicity in considering interaction. The idea of modeling cell-wall adhesion by forming ligand-receptor bonds from [48] could be a good way to model the adhesion force by introducing a wall phase and its interacting potential with the vesicle phase. We will thus use a significantly higher contact angle, i.e. $\theta_s = 180^\circ$ in the rest of simulations presented in the paper.*

4.5.3 Tank treading and tumbling

The vesicle motion in a Couette flow changes with respect to the ratio of the viscosities η_{in} and η_{out} of intracellular and extracellular fluids [85, 10, 40, 60]. When this viscosity ratio is small, the vesicle is prone to move in the tank treading mode; while the tumbling mode is preferred when the viscosity ratio is large. The parameter values utilized for this vesicle motion simulation are set as follows:

$Re = 2\times10^{-4}$, $\delta_\varepsilon = |\nabla\phi^n|^2$, $\mathscr{M} = 10^{-3}$, $\kappa_B = 5\times10^{-3}$, $\varepsilon = 7.5\times10^{-3}$, $\mathscr{M}_v = 20$, $\mathscr{M}_s = 200$, $\xi = 1.78\times10^{7}$, $\kappa = 2\times10^{-12}$, $l_s = 0.2$.

The upper and bottom walls of the domain are set to move in opposite direction horizontally with velocities -20 and 20, respectively. The simulation domain is 2×1, and the initial shape of the vesicle is chosen to be an ellipse with eccentricity $\sqrt{3}$. The ratios of viscosities of the intracellular and extracellular fluids are set to be $1:1$ and $1:500$, respectively. Figures 4.5 show the interfaces of tank treading vesicle (low viscosity ratio case) and tumbling vesicle (high viscosity ratio case) and corresponding fluid velocity fields at different times, respectively. A point on the interface (black solid) is tracked to illustrate these two different types of motion. For the tank treading motion, the angle between the long axis of the vesicle and horizontal axis is fixed when the vesicle is at equilibrium, but the tracer point rotates in a counter clockwise direction along the membrane. For the tumbling motion, the vesicle keeps rotating and the tracer point does not move with respect to the membrane shape.

Remark 4.5.3. *Tracking of the marker point (the black solid dot) is done by the following steps:*

1. *Determine a marker point P that is located on the interface with coordinate (x,y);*
2. *Compute the velocity $\mathbf{u}(P) = (u_x(P), u_y(P))$ of the marker point by interpolation;*
3. *Update the marker point position at the next time point by $(x+u_x(P)\Delta t, y+u_y(P)\Delta t)$;*
4. *Go to step 2.*

This tracking gives the trajectory of the marker point.

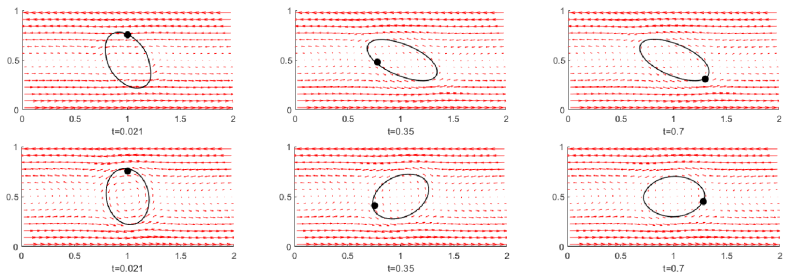

Figure 4.5: Top:Tank treading with viscosity ratio $1:1$. The orientation of the vesicle and the velocity field are kept stable when the system comes to equilibrium.; Bottom:Tumbling with viscosity ratio 1:500. The vesicle keeps rotating in the flow. Position of the tracer point (in black) is fixed with respect to the vesicle membrane

Next, simulation result of tumbling motion of a rigid ellipse is compared with the theoretical solution obtained using Jeffery's orbit theory [74]. Specifically, the angle between the long axis of the ellipse and the horizontal axis is compared. As shown in Figure 4.6, our simulation result is in close agreement with the analytical Jeffery orbit.

Remark 4.5.4. *The long axis of the rigid ellipse during the tumbling motion is determined as follows:*

1. *Determine the interface location of the ellipse by $\phi = 0$;*

2. *Find the point on the interface that is farthest away from the center of the vesicle in upper domain;*
3. *Match these two points and the line is considered as the long axis of the ellipse.*

Since the ellipse is located at the center of the domain at the initial time point, and the motion of the fluid is centrosymmetric according to the specified boundary condition, it is expected that the center of the ellipse is kept at the center of the domain Ω. Therefore the determination of the long axis of the ellipse based on its geometry character is acceptable.

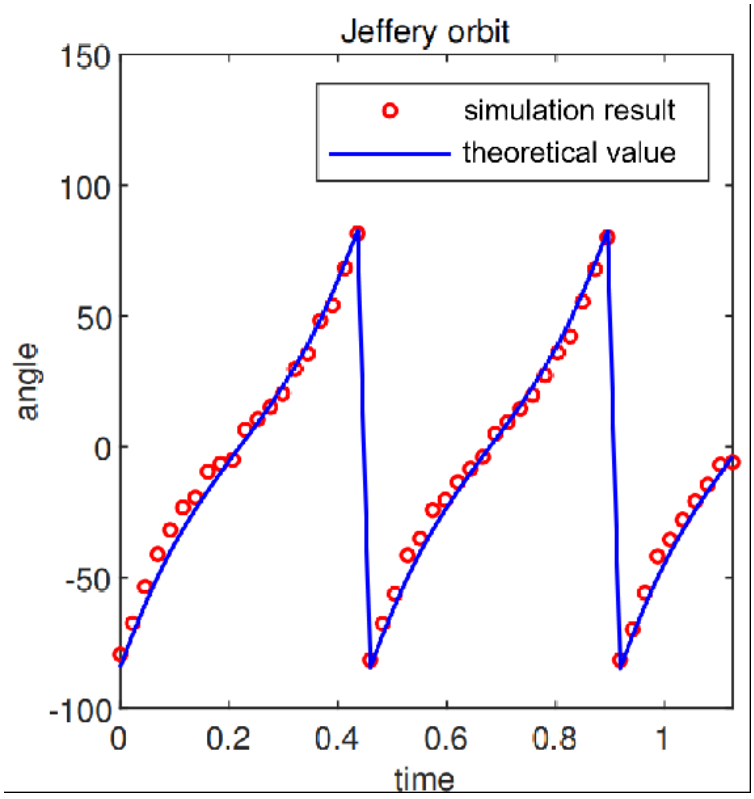

Figure 4.6: Comparison between theoretical and simulation results of the flipping ellipse. The blue line is the angle between the long axis of the ellipse and the horizontal axis predicted by the Jeffery orbit theory, and the red circles are the angle from the simulation.

4.5.4 Vesicle passing through a narrow fluid channel

Finally, the calibrated model is used to study the effects of mechanical properties of the membrane of the vesicle on its circulating through constricting micro channels [59]. The vesicle shape is described by an ellipse with eccentricity $\sqrt{3}$, and the width of the squeezing section of the narrow channel is 0.3 by default. A pressure drop boundary condition is applied at the inlet (left) and outlet (right) of the domain by setting the pressure on the inlet and outlet to be $P = 50$ and $P = -50$, respectively. Fluid viscosity ratio is set to be $1 : 10$ for extracellular and intracellular fluids, respectively. The other parameters are as follows:

$Re = 2 \times 10^{-4}$, $\delta_\varepsilon = 10 \times |\nabla \phi^n|^2$, $\mathscr{M} = 5 \times 10^{-4}$, $\kappa_B = 4 \times 10^{-2}$, $\varepsilon = 7.5 \times 10^{-3}$, $\mathscr{M}_v = 20$, $\mathscr{M}_s = 100$, $\xi = 7.1 \times 10^4$, $\kappa = 4 \times 10^{-11}$, $l_s = 5 \times 10^{-3}$.

The effect of the local inextensibility of vesicle membrane is assessed by comparing vesicle simulations with and without using the local inextensibility constraint $\mathscr{P} : \nabla \mathbf{u} = 0$ in the model. Snapshots of these simulations at different times are shown in Figure 4.7. They illustrate that a vesicle modeled without using the local inextensiblity can pass through the channel by introducing large extension and deformation of its body with a relatively small value of global inextensibility coefficient $\mathscr{M}_s$; while a vesicle modeled with the local inextensibility hardly exhibits large extension and deformation of its body and blocks the channel. This is also confirmed by Figure 4.8. It shows under otherwise same conditions, the total arc length of the membrane of the vesicle modeled without the local inextensibility increases significantly when it passes through the channel, and the vesicle with the local inextensibilty preserves its membrane arc length well during the course of the simulation.

Although the total arc length of a vesicle without the local inextensibility and with a very large $\mathscr{M}_s$ value could maintain almost unchanged as shown in 4.7 (c) and 4.8, the morphological changes of vesicles with and without the local inextensibility are drastically different. For the vesicles modeled without the local inextensibility, Figure 4.9(b,c) illustrates that the vesicle membranes are stretched (red) or compressed (blue) everywhere, even though the total arc length of the vesicle modeled using a large modulus $\mathscr{M}_s$ value could be preserved, and the vesicle forms the blockage. For the vesicle modeled with the local inextensibility, Figure 4.9(c) confirms that there is almost no local extension or compression of the membrane, which is consistent with experimental observations. All simulations described below use the local inextensibility.

Both experiments and clinic reports have shown that the cell bending modulus and surface-volume ratio play important roles in determining the deformability of vesicles, especially when they pass through narrow channels [147, 107, 125]. The latest results reveal that a moderate decrease in the surface-volume ratio has a more significant effect than varying the cell bending

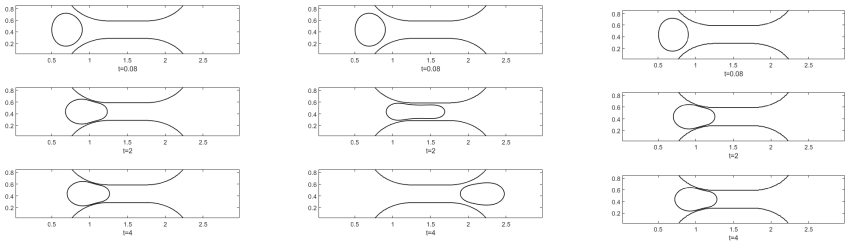

(a) (b) (c)

Figure 4.7: Snapshots of vesicles passing a narrowed channel with different surface area constraints at times $t = 0.08, 2$ and 4, respectively. (a) $\mathscr{M}_s = 100$ with the local inextensibility; (b) $\mathscr{M}_s = 100$ without the local inextensibility; (c) $\mathscr{M}_s = 20000$ without the local inextensibility. The curves on the top and bottom ceiling are the wall boundary of the narrowed channel.

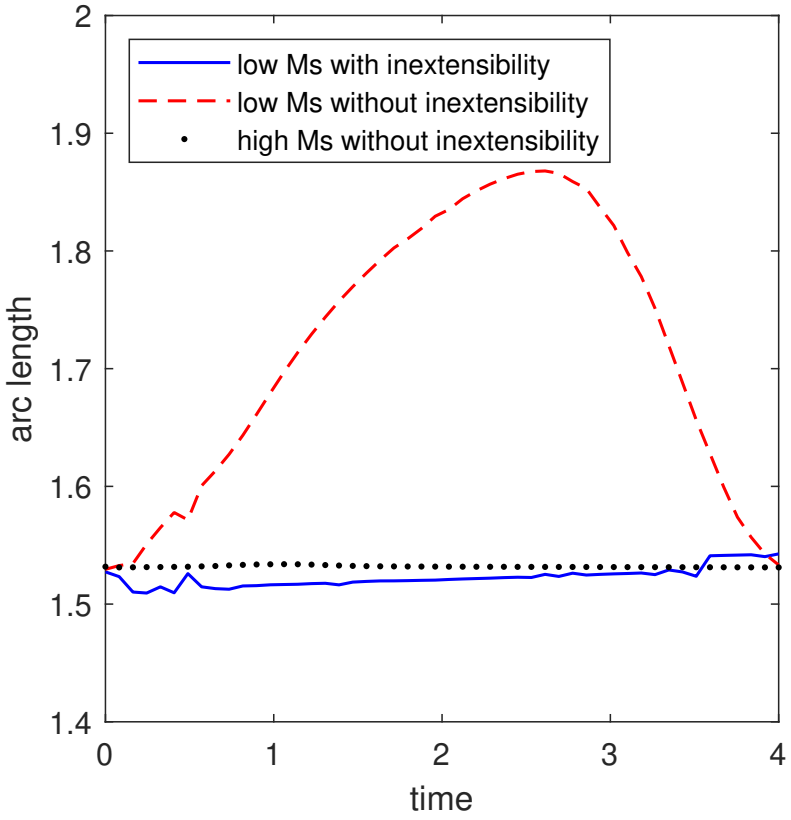

Figure 4.8: Total arc length of vesicle membrane with the local inextensibility (blue line), and the total arc lengths of vesicle membranes with low (100) (red dashed line) and high (20000) (black point) $\mathscr{M}_s$ and no local inextensibility, respectively, during vesicles passing through the constriction of the micro channel with otherwise same parameter values and settings.

stiffness. This surface-volume ratio effect is tested by increasing the ratio value slightly from $1.5 : 1$ to $2 : 1$. Results in Figures 4.10 and 4.11 confirm that the more rounded vesicles are much harder to pass through the narrow channel and can easily form the blockage. This is consistent with the experimental observations.

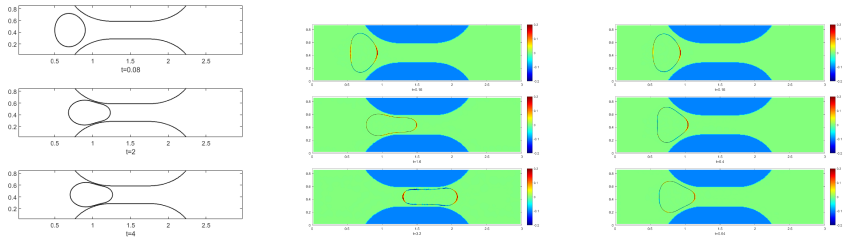

(a) (b) (c)

Figure 4.9: Effects of the local inextensibility $\mathscr{P} : \nabla \mathbf{u} = 0$. Snapshots of membrane forces of vesicles: (a) $\mathscr{M}_s = 100$ with the local inextensibility; (b) $\mathscr{M}_s = 100$ without the local inextensibility; and (c) $\mathscr{M}_s = 20000$ without the local inextensibility.

The effect of the bending modulus is assessed by increasing its value 10 times. The surface-volume ratio of the vesicle is $2 : 1$ in this test. Figure 4.11 illustrates that this more rigid vesicle can also pass the same size channel but exhibits very different shape transformation.

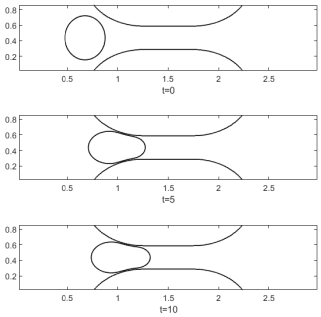

Figure 4.10: Side view of a vesicle with surface-volume ratio $1.5 : 1$ at different times.

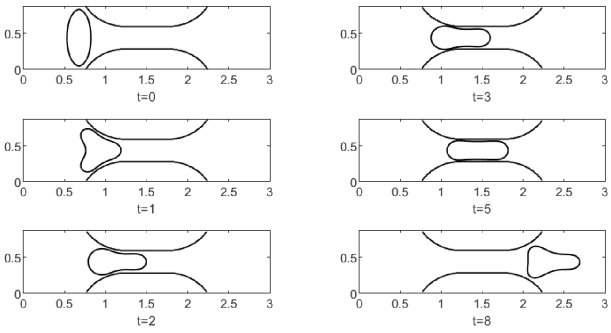

Figure 4.11: Side view of a vesicle with surface-volume ratio $2 : 1$ at different times.

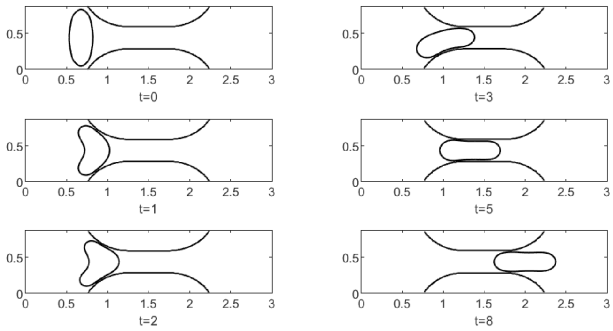

Figure 4.12: Side view of a vesicle with large bending modulus $\kappa_B = 4 \times 10^{-1}$ and surface-volume ratio $2 : 1$ at different times.

4.6 Conclusion

In this chapter, an energy variational method is used to derive a thermodynamically consistent phase-field model for simulating vesicle motion and deformation under flow conditions. Corresponding Allen-Cahn GNBC boundary conditions accounting for the vesicle-wall (or fluid-structure) interaction are also proposed by introducing the proper boundary dissipation and vesicle-wall interaction energy.

Then an efficient scheme using C^0 finite element spatial discretization and the mid-point temporal discretization is proposed to solve the obtained model equations. Thanks to the mid-point temporal discretization, the obtained numerical scheme is unconditionally energy stable. The numerical experiments confirm that this scheme is second-order accurate in both space and time. Simulations of the vesicle tank treading and tumbling motions reproduce experimental observations. And the flipping ellipse simulation agrees with the analytical solution well. Finally, the model is used to investigate how vesicles' mechanical properties affect the vesicles' capability to pass through narrow channels. It is shown that whether a vesicle can pass a narrow channel is largely determined by the surface-volume ratio of the vesicle, which is consistent with *in vitro* experiments.

The model can be used to study the impaired dynamics of red blood cells due to altered mechanical properties of red blood cell membranes in sickle cell disease [9] and in diabetes [102]. Combining with the restricted diffusion model [117], our model can be generalized to model the mass transfer through a semi-permeable membrane, for example oxygen delivering [153].

There are limitations in our model if we need to consider an adhesion based on the ligand-receptor binding. When the static contact angle is lower than 180°, the vesicle is torn apart due to the wetting effect. In [48], the authors proposed an adhesion model by introducing a new phase label for vascular wall, and an adhesion energy functional using labels of wall phase and cell. In the future, we will combine the adhesion model with the contact line model and

more realistic sub-models for cell-wall and cell-cell interactions to model the cells aggregation [162, 164], cells crawling and invasion problems [129, 22]. In the next chapter, a new idea of modelling wall adhesion is used to overcome the tear phenomenon together with the multiple cell interaction model.

Chapter 5

Multiple Vesicle Interaction Model with Allan-Cahn Type Interface

5.1 Introduction

In the previous chapters, phase field models with GNBC are given in moving contact line and vesicle motion. However, despite of good numerical performance, we find that the adhesion force between vesicle and wall is likely to lead to a tear of the cell at the wall. Thus indicates the GNBC used in the model is not consistent with the physics of vesicle mechanics. To avoid the non-physical phenomenon, some modifications need to be applied to the cell-wall modelling. Furthermore, a single vesicle model is not enough for hemodynamics study. A Multiple cell model considering the interaction with each other need to be established.

The main purpose of this chapter is to model vesicles interacting with each other and the domain boundaries in a flow, such as red blood cells passing a branched blood vessel. The first goal of this chapter thus is to derive a thermodynamically consistent phase-field model for vesicles' motion and shape transformation in a closed spatial domain by using an energy variational method [140, 52]. All the physics taken into consideration are introduced through definitions of energy functionals and dissipation functional, together with the kinematic assumptions of laws of conservation. In this model, all of the energy and dissipation terms are defined on bulk region of the domain including boundary effects energy.

A few works have been published about modeling of the interaction between cells[49, 118]. Lennard-Jones potential is applied to model the interaction in [118], an energy related to the inter-cell attraction is introduced using phase-field method in With phase-field theory in [49]. Those models all provide good simulation results compared with experiment in lab [105, 80]. In this paper a new potential with phase-field method would be derived based on the previous works. A Lennard-Jones type potential would be established with respect to the phase order. The boundary effect part in the new model are counted as a independent phase which is defined in the bulk. Then performing variation of these functionals yields an Cahn-Hilliard-Navier-Stokes (CHNS) system with Allen-Cahn general Navier boundary conditions (GNBC) [116]. This is in contrast to most previous works [27, 29, 19] in which boundary

effect was rarely derived during the course of model derivation. Dirichlet or Neumann type conditions were simply added to these models at the end to close the governing equations [3, 32, 31]. Moreover, in our model derivation, the incompressibility of the fluid and the local and global inextensibility of the vesicle membrane are taken into account by introducing two Lagrangian multipliers, hydrostatic pressure p and surface pressure λ [108] and penalty terms, respectively.

In the first section of the chapter, a model including interaction between cells are given. The formula corresponding potential is derived in the following part. Finally, results of numerical simulation are shown and compared with the data received by experiments.

5.2 Model Derivation

5.2.1 Multi-vesicle interaction System

Energy variational method [140] is adopted for model derivation to ensure the thermaldynamics consistence. It consists of two functionals for the total energy and dissipation of the system, and the kinematic equations based on physical laws of conservation. The specific forms of the flux and stress functions in the kinematic equations are obtained by taking the time derivative of the total energy functional and comparing with the defined dissipation functional. More details of this method can be found in [140, 141, 163].

For multicellular system, the motion of i^{th} vesicle is tracked by the phase field function ϕ_i. We start from the following laws of conservation for the mass and momentum and interface local inextensibility [142],

$$\begin{cases} \frac{\partial \phi_i}{\partial t} + \nabla \cdot (\mathbf{u}\phi_i) = \nabla \cdot q_{\phi_i} \ , \\ \rho(\frac{\partial \mathbf{u}}{\partial t} + (\mathbf{u}\cdot\nabla)\mathbf{u}) = \nabla \cdot \boldsymbol{\sigma}_\eta + \mathbf{F}_{\phi_1,\phi_2,...,\phi_N} \ , \\ \nabla \cdot \mathbf{u} = 0 \ , \\ \delta_i(\mathscr{P}_i : \nabla \mathbf{u}) + \ \xi\gamma^2 \nabla \cdot (\phi_i^2 \nabla \lambda_i) = 0 \ . \end{cases} \tag{5.1}$$

and the boundary conditions on the top and bottom of the domain, denoted by $\partial\Omega_w$:

$$\begin{cases} \mathbf{u}\cdot\mathbf{n} = 0 \ , \\ \mathbf{u}_\tau \cdot \boldsymbol{\tau}_k = f_{\tau_k} \ , \\ \frac{\partial \phi_i}{\partial t} + \mathbf{u}\cdot\nabla_\Gamma \phi_i = J_{\Gamma_i} \ , \\ q_{\phi_i}\cdot\mathbf{n} = 0 \ , \end{cases} \tag{5.2}$$

where $(.)_i, i = 1,2,3,...N$ refers to different cells. The first equation with undetermined flux q_{ϕ_i} is used to track the motion of vesicle, where Cahn-Hilliard equation is used to ensure the conservation of vesicle's volume during the motion. The second equation is Navier-Stokes equation of the velocity field $\mathbf{u}$ with viscous stress σ_η and body force induced by vesicle-

fluid interaction $\boldsymbol{F}_{\phi_1,\phi_2,\ldots,\phi_n}$. The third equation are incompressibility of fluids. And the fourth one is diffusive interface approximation for the local inextensibility of i^{th} cell membrane with relaxation [141, 3]. $\delta_i = \frac{1}{2}\gamma^2|\nabla\phi_i|^2$ is the surface delta function with the diffusive interface thickness γ. $\mathscr{P}_i$ is the projection operator defined to be $(I - \mathbf{n}_{i,m} \otimes \mathbf{n}_{i,m})$, and $\mathbf{n}_m = \frac{\nabla\phi_i}{|\nabla\phi_i|}$ is the unit outward normal vector of the interface when it is defined as an implicit surface by the level function. ξ is a parameter independent of γ, and λ is a function that measures the interface "pressure" induced by the inextensibility of the membrane.

On the boundary $\partial\Omega_w$, the Allen-Cahn type boundary condition is employed for ϕ_i. $\nabla_\Gamma = \nabla - \mathbf{n}(\mathbf{n}\cdot\nabla)$ is the surface gradient operator and $\mathbf{u}_\tau = \mathbf{u} - (\mathbf{u}\cdot\mathbf{n})\mathbf{n}$ is the fluid slip velocity with respect to the wall where $\tau_i, i = 1,2$ are the tangential directions and $\mathbf{n}$ is outward norm vector of the wall. f_{τ_i} is the slip velocity of the fluid on the wall along the τ_i direction. And J_Γ represents the Allan-Cahn type of relaxation on the wall by using the phase-field method.

The total energetic functional for the multicellular system is formed by the kinetic energy in the macroscale E_{kin}, cell membrane energy E_{cell}, cell-cell interaction energy E_{int} and cell-wall adhesion energy E_w in the microscale,

$$E_{total} = \underbrace{E_{kin}}_{Macroscale} + \underbrace{E_{cell} + E_{int} + E_w}_{Microscale} \tag{5.3}$$

$$= \int_\Omega \left(\frac{1}{2}\rho|\mathbf{u}|^2\right) d\boldsymbol{x} + \sum_{i=1}^{N}\int_\Omega \frac{\hat{\kappa}_B}{2\gamma}\left|\frac{f(\phi_i)}{\gamma}\right|^2 d\boldsymbol{x} + \sum_{i=1}^{N}\frac{M_s}{2}\frac{(S(\phi_i) - S(\phi_{i,0}))^2}{S(\phi_{i,0})}$$

$$+ \int_\Omega H d\boldsymbol{x} + \sum_{i=1}^{N}\int_\Omega f_w(\phi_i) ds. \tag{5.4}$$

Here ρ is the density of fluid which is constant in this work and $\mathbf{u}$ is velocity. $\hat{\kappa}_B$ is bending modulus of the membrane, and

$$f(\phi_i) = \frac{\delta G}{\delta\phi_i} = -\gamma^2\Delta\phi_i + (\phi_i^2 - 1)\phi_i\ , \tag{5.5}$$

with

$$G(\phi_i) = \frac{\gamma^2|\nabla\phi_i|^2}{2} + \frac{(1-\phi_i^2)^2}{4}. \tag{5.6}$$

The function $S(\phi_i) = \int_\Omega \frac{G(\phi_i)}{\gamma} dx$ is used to measure the surface area of the cell with constrain constant M_s.

The term H denotes the interaction energy density induced by the interaction of cells. There are many different previous works to define interaction potential H. See [50, 76, 167]. Here we begin with considering mechanical interaction between two cells identified by phase-field functions ϕ_1 and ϕ_2, respectively. Recall that $\phi_i = 1$ represents the intracellular space, and $\phi_i = -1$ represents the extracellular space of the i^{th} cell, respectively. Whether there exists mechanical interaction between the two cells can be determined by measuring the overlapping (i.e., occupying the same physical space) of the intracellular spaces of these two cells.

In this work, we propose the following Lennard-Jones type interaction energy density

$$H = Q_1(\phi_1+1)^2(\phi_2+1)^2 - Q_2(\phi_1^2-1)^2(\phi_2^2-1)^2 \ . \tag{5.7}$$

The first term in Eq. (5.7) accounts for the repulsion and achieves the maximum when two cells overlap at a spatial location $\boldsymbol{x}$, i.e., $\phi_1(\boldsymbol{x}) = \phi_2(\boldsymbol{x}) = 1$. The second term represents the adhesion and is nonzero only when the diffuse layers of the two cells overlap, i.e., at the overlapping location $\boldsymbol{x}$, $-1 < \phi_1(\boldsymbol{x}) < 1$ and $-1 < \phi_2(\boldsymbol{x}) < 1$. This is used to mimic the adhesive interaction mediated by the formation of adhesive bonds with cell adhesion molecules (CAM) on adjacent cell membranes, or via forming binding bonds between CAM and cell-extracellular matrix. In general, the formation and dissociation of the bonds are stochastic and depend on the concentrations of agonists [64, 24]. Here for simplicity, we set the Q_1 and Q_2 as constants in the work.

Figure 5.1 plots the energy landscape of the interaction potential at a space point due to presence of the phases ϕ_1 and ϕ_2. The energy is equal to 0 when two phases do not touch or overlap i.e., $\phi_1 = \phi_2 = -1$. When they start to overlap, the energy firstly decreases which means that the attraction force between these two phases dominates. Then the energy goes up which indicates the repulsive force dominates. This prevents the two phases from occupying the same physical space. So the interacting potential energy behaves conceptually similar to a 2D kind of Lennard-Jones potential. We remark that in [48] a potential of form $(\phi_1^2-1)^2(\phi_2^2-1)$ is used, where only attractive feature is included.

Eq. 5.7 could be understood in the following way as well. It may be formulated by the following two measurements of the relative position of cells.

$$d_1(\boldsymbol{x}) = (\phi_1(\boldsymbol{x})-1)(\phi_2(\boldsymbol{x})-1) \ , \ \ \boldsymbol{x} \in \Omega \ ,$$

and

$$d_2(\boldsymbol{x}) = (\phi_1(\boldsymbol{x})+1)(\phi_2(\boldsymbol{x})+1) \ , \ \ \boldsymbol{x} \in \Omega \ .$$

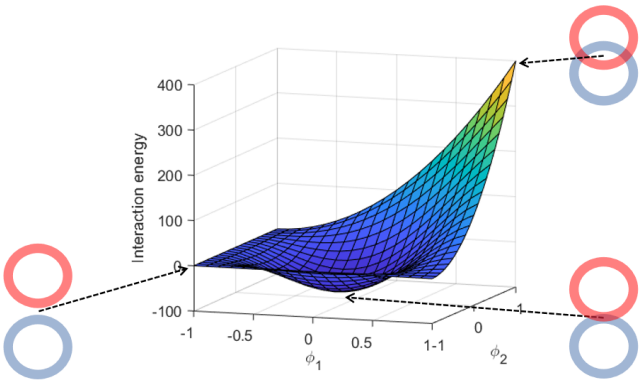

Figure 5.1: Interaction energy with respect to ϕ_1 and ϕ_2 at a space point. The energy status of different overlapping condition of the cell phase at the point are pointed out as well. ($Q_1 = 50$, $Q_2 = 400$.)

It is obvious that $d_1, d_2 \in [0,4]$. From physical point of view, we can regard d_1 as the "distance" in the space of phase-field functions since it reaches maximum when both $\phi_1(\boldsymbol{x})$ and $\phi_2(\boldsymbol{x})$ equal to -1, namely, there is no overlap between the two cells at $\boldsymbol{x}$. d_1 reaches minimum when diffused surfaces of two cells fully overlap, i.e., $\phi_1(\boldsymbol{x}) = \phi_2(\boldsymbol{x}) = 1$. Similarly, d_2 could be regarded as the extent of overlapping since it reaches maximum when diffused surfaces of cells fully overlap, and reaches minimum when there is no overlap. Then we may propose the interaction potential H to be a polynomial function of d_2 and d_1:

$$H = Q(d_2^{\alpha} + C)d_1^{\beta} = QC(\phi_1+1)^{\beta}(\phi_2+1)^{\beta} - Q(\phi_1^2-1)^{\alpha}(\phi_2^2-1)^{\alpha}(\phi_1+1)^{\beta-\alpha}(\phi_2+1)^{\beta-\alpha}, \quad (5.8)$$

where Q and C are constants that control the minimum of the interaction energy and result in attractive/repulsive Lennard-Jones kind of behaviour in 2D as shown in Figure 5.1. So Eq. (5.7) may be considered as a case of Eq. (5.8) with $\alpha = \beta = 2$, $QC = Q_1$, $Q = Q_2$.

More general, the interaction energy in the multiple phases case based on Eq. (5.7) goes:

$$H = \sum_{i=1}^{N}\sum_{i<j} H_{ij} = \sum_{i=1}^{N}\sum_{i<j}\left[Q_1(\phi_i+1)^2(\phi_j+1)^2 - Q_2(\phi_i^2-1)^2(\phi_j^2-1)^2\right]. \quad (5.9)$$

For the cell-wall adhesion energy, ϕ_w is defined along the wall with a thickness [48] as shown in Figure 5.3. We simply use the same interaction potential formulae and the cell-wall interaction energy is defined by setting $\phi_2 = \phi_w$ in Eq. (5.7),

$$f_w(\phi_i) = Q_{w_1}(\phi_i+1)^2(\phi_w+1)^2 - Q_{w_2}(\phi_i^2-1)^2(\phi_w^2-1)^2, \quad (5.10)$$

where Q_{w_1} is repulsive energy density and Q_{w_2} is adhesion energy density. Notice that the cell-wall energy E_w is defined in the bulk not on the boundary. However, f_w is non-zero only when the two phases overlap which could be regarded as the attraction force is only induced when the vesicle is contacting (or close enough to) the wall.

Then the corresponding chemical potential for each vesicle μ_i is defined as follows

$$\mu_i = \frac{\delta E_{cell_i}}{\delta \phi_i} = \frac{\hat{\kappa}_B}{\gamma^3} g(\phi_i) + \frac{\partial H}{\partial \phi_i} + \frac{M_s}{\gamma} \frac{S(\phi_i) - S(\phi_{i,0})}{S(\phi_{i,0})} f(\phi_i) + \frac{\partial f_w(\phi_i)}{\partial \phi_i} \ , \tag{5.11}$$

where $g(\phi_i) = -\gamma^2 \Delta f(\phi_i) + (3\phi_i^2 - 1) f(\phi_i)$.

The dissipation functional consists of the dissipation induced by fluid viscosity, friction near the wall, and interfacial mixing due to diffuse interface representation [141],:

$$\begin{aligned} \Delta &= \int_\Omega 2\eta |\boldsymbol{D}_\eta|^2 d\boldsymbol{x} + \sum_{i=1}^N \int_\Omega M_\phi^{-1} |q_{\phi_i}|^2 d\boldsymbol{x} + \int_{\partial\Omega_w} \beta_s |\mathbf{u}_{\boldsymbol{\tau}}|^2 ds \\ &\quad + \sum_{i=1}^N \left(\int_{\partial\Omega_w} \kappa_\Gamma |J_{\Gamma_i}|^2 ds + \int_{\partial\Omega_w} \xi |\gamma \phi_i \nabla \lambda_i|^2 ds \right) \ , \end{aligned} \tag{5.12}$$

where $\boldsymbol{D}_\eta = \frac{\nabla \mathbf{u} + (\nabla \mathbf{u})^T}{2}$, η is the viscosity of fluid mixture, β_s is wall fraction, M_ϕ and κ_Γ are the mobility of phase in the bulk and boundary. Especially, in general, the viscosity η could be a function of all phases ϕ_i

$$\eta = \eta(\phi_w, \phi_1, \cdots, \phi_n). \tag{5.13}$$

Then the time derivative of the total energy goes:

$$\begin{aligned} \frac{dE_{total}}{dt} &= \frac{d}{dt} E_{kin} + \frac{d}{dt} E_{cell} + \frac{d}{dt} E_w & (5.14) \\ &\equiv I_1 + I_2 + I_3 \ . & (5.15) \end{aligned}$$

For the first term, the conservation law of momentum and imcompressibility yield

$$\begin{aligned} I_1 &= \frac{d}{dt} \int_\Omega \frac{\rho |\mathbf{u}|^2}{2} d\boldsymbol{x} \\ &= \int_\Omega \frac{1}{2} \frac{\partial \rho}{\partial t} |\mathbf{u}|^2 d\boldsymbol{x} + \int_\Omega \rho \frac{\partial \mathbf{u}}{\partial t} \cdot \mathbf{u} d\boldsymbol{x} \\ &= \int_\Omega \frac{1}{2} \frac{\partial \rho}{\partial t} |\mathbf{u}|^2 d\boldsymbol{x} + \int_\Omega \rho \frac{d\mathbf{u}}{dt} \cdot \mathbf{u} d\boldsymbol{x} - \int_\Omega (\rho \mathbf{u} \cdot \nabla \mathbf{u}) \cdot \mathbf{u} d\boldsymbol{x} \\ &= \int_\Omega \frac{1}{2} \frac{\partial \rho}{\partial t} |\mathbf{u}|^2 d\boldsymbol{x} + \int_\Omega \rho \frac{d\mathbf{u}}{dt} \cdot \mathbf{u} d\boldsymbol{x} + \int_\Omega \nabla \cdot (\rho \mathbf{u}) \frac{|\mathbf{u}|^2}{2} d\boldsymbol{x} \\ &= \int_\Omega (\nabla \cdot \boldsymbol{\sigma}_\eta) \cdot \mathbf{u} d\boldsymbol{x} + \int_\Omega \mathbf{F} \cdot \mathbf{u} d\boldsymbol{x} + \sum_{i=1}^N \int_\Omega \lambda_i \delta_i \mathscr{P}_i : \nabla \mathbf{u} d\boldsymbol{x} + \sum_{i=1}^N \int_\Omega \xi \gamma^2 \lambda_i \nabla \cdot (\phi_i^2 \nabla \lambda_i) d\boldsymbol{x} - \int_\Omega pI : \nabla \mathbf{u} d\boldsymbol{x} \end{aligned}$$

$$
\begin{aligned}
&= -\int_\Omega ((\boldsymbol{\sigma}_\eta + pI) : \nabla \mathbf{u}) d\boldsymbol{x} + \int_\Omega \mathbf{F}\cdot\mathbf{u} dx - \sum_{i=1}^N \int_\Omega \nabla\cdot(\lambda_i \delta_i \mathscr{P}_i)\cdot \mathbf{u} d\boldsymbol{x} \\
&\quad - \sum_{i=1}^N \int_\Omega \xi\gamma^2 \phi_i^2 (\nabla\lambda_i)^2 d\boldsymbol{x} + \int_{\partial\Omega_w} ((\boldsymbol{\sigma}_\eta + \sum_{i=1}^N \lambda_i\delta_i\mathscr{P}_i)\cdot\mathbf{n})\cdot\mathbf{u}_\tau dS\ , \qquad (5.16)
\end{aligned}
$$

where the slip boundary condition is used.

The second term is calculated by using the conservation of each phase

$$
\begin{aligned}
I_2 &= \frac{d}{dt}\int_\Omega \frac{\hat{\kappa}_B}{2\gamma}\sum_{i=1}^N \left|\frac{f(\phi_i)}{\gamma}\right|^2 d\boldsymbol{x} + \frac{d}{dt}\int_\Omega H d\boldsymbol{x} + \sum_{i=1}^N \frac{d}{dt}\frac{M_s}{2}\frac{(S(\phi_i)-S(\phi_{i,0}))^2}{S(\phi_{i,0})} \\
&= \int_\Omega \frac{\hat{\kappa}_B}{\gamma}\sum_{i=1}^N \frac{f_i}{\gamma^2}\frac{\partial f_i}{\partial t} d\boldsymbol{x} + \int_\Omega \sum_{i=1}^N \frac{\partial H}{\partial\phi_i}\frac{\partial\phi_i}{\partial t} d\boldsymbol{x} + \sum_{i=1}^N \frac{d}{dt}\frac{M_s}{2}\frac{(S(\phi_i)-S(\phi_{i,0}))^2}{S(\phi_{i,0})} \\
&= \int_\Omega \frac{\hat{\kappa}_B}{\gamma}\sum_{i=1}^N \frac{f_i}{\gamma^2}\left(-\gamma^2\Delta\left(\frac{\partial\phi_i}{\partial t}\right) + (3\phi_i^2-1)\frac{\partial\phi_i}{\partial t}\right) d\boldsymbol{x} + \int_\Omega \sum_{i=1}^N \frac{\partial H}{\partial\phi_i}\frac{\partial\phi_i}{\partial t} d\boldsymbol{x} \\
&\quad + \sum_{i=1}^N \frac{d}{dt}\frac{M_s}{2}\frac{(S(\phi_i)-S(\phi_{i,0}))^2}{S(\phi_{i,0})} \\
&= \int_\Omega \frac{\hat{\kappa}_B}{\gamma^3}\sum_{i=1}^N \left(-\gamma^2\Delta f_i + (3\phi_i^2-1)f_i + \frac{\partial H}{\partial\phi_i} + \frac{M_s}{\gamma}\frac{S(\phi_i)-S(\phi_{i,0})}{S(\phi_{i,0})} f(\phi_i)\right)\frac{\partial\phi_i}{\partial t} d\boldsymbol{x} \\
&\quad - \int_{\partial\Omega_w} \frac{\hat{\kappa}_B}{\gamma}\sum_{i=1}^N f_i \frac{\partial}{\partial t}(\partial_n\phi_i) ds + \int_{\partial\Omega_w}\frac{\hat{\kappa}_B}{\gamma}\sum_{i=1}^N \partial_n f_i \frac{\partial\phi_i}{\partial t} ds + \sum_{i=1}^N \int_{\partial\Omega_w} M_s \frac{S(\phi_i)-S(\phi_{i,0})}{S(\phi_{i,0})}\gamma\partial_n\phi_i\frac{\partial\phi_i}{\partial t} ds \\
&= \sum_{i=1}^N \left(\int_\Omega \mu_i \frac{\partial\phi_i}{\partial t} d\boldsymbol{x} + \int_{\partial\Omega_w}\frac{\hat{\kappa}_B}{\gamma} f_i\frac{\partial}{\partial t}(\partial_n\phi_i) ds + \int_{\partial\Omega_w} M_s\frac{S(\phi_i)-S(\phi_{i,0})}{S(\phi_{i,0})}\gamma\partial_n\phi_i\frac{\partial\phi_i}{\partial t} ds\right) \\
&= \sum_{i=1}^N \left(\int_\Omega \mu_i\nabla\cdot q_{\phi_i} d\boldsymbol{x} - \int_\Omega \mu_i\mathbf{u}\cdot\nabla\phi_i d\boldsymbol{x} + \int_{\partial\Omega_w}\frac{\hat{\kappa}_B}{\gamma}\partial_n f_i\frac{\partial\phi_i}{\partial t} ds + \int_{\partial\Omega_w} M_s\frac{S(\phi_i)-S(\phi_{i,0})}{S(\phi_{i,0})}\gamma\partial_n\phi_i\frac{\partial\phi_i}{\partial t} ds\right) \\
&= \sum_{i=1}^N \left(-\int_\Omega q_{\phi_i}\cdot\nabla\mu_i d\boldsymbol{x} - \int_\Omega \mu_i\mathbf{u}\cdot\nabla\phi_i d\boldsymbol{x} + \int_{\partial\Omega_w}\frac{\hat{\kappa}_B}{\gamma}\partial_n f_i\frac{\partial\phi_i}{\partial t} ds\right. \\
&\quad \left. + \int_{\partial\Omega_w} M_s\frac{S(\phi_i)-S(\phi_{i,0})}{S(\phi_{i,0})}\gamma\partial_n\phi_i\frac{\partial\phi_i}{\partial t} ds\right)\ , \qquad (5.17)
\end{aligned}
$$

where the Allan-Cahn boundary condition for each phase is used.

For the last term, it yields

$$
I_3 = \sum_{i=1}^N \left(\int_{\partial\Omega}\frac{\partial f_w(\phi_i)}{\partial\phi_i}\frac{\partial\phi_i}{\partial t} ds\right)\ . \qquad (5.18)
$$

Combining above Eqs. (5.16), (5.17) and (5.18), we have:

$$
\frac{d}{dt}E_{total} = -\int_\Omega ((\boldsymbol{\sigma}_\eta + pI) : \nabla\mathbf{u}) d\boldsymbol{x} + \int_\Omega (\mathbf{F} - \sum_{i=1}^N \mu_i\nabla\phi_i - \sum_{i=1}^N \nabla\cdot(\lambda_i\delta_i\mathscr{P}_i))\cdot\mathbf{u} d\boldsymbol{x}
$$

$$
\begin{aligned}
& -\sum_{i=1}^{N}\int_{\Omega} q_{\phi_i}\cdot\nabla\mu_i d\boldsymbol{x}+\sum_{i=1}^{N}\int_{\Omega}\xi\gamma^2\phi_i^2(\nabla\lambda_i)^2 d\boldsymbol{x}+\int_{\partial\Omega_w}((\boldsymbol{\sigma}_\eta+\sum_{i=1}^{N}\lambda_i\delta_i\mathscr{P}_i)\cdot\mathbf{n})\cdot\mathbf{u}_\tau ds \\
& +\sum_{i=1}^{N}\int_{\partial\Omega_s}\hat{L}_i\frac{\partial\phi_i}{\partial t}ds \\
= & -\int_{\Omega}((\boldsymbol{\sigma}_\eta+pI):\nabla\mathbf{u})d\boldsymbol{x}+\int_{\Omega}(\mathbf{F}-\sum_{i=1}^{N}\mu_i\nabla\phi_i-\sum_{i=1}^{N}\nabla\cdot(\lambda_i\delta_i\mathscr{P}_i))\cdot\mathbf{u}d\boldsymbol{x} \\
& -\sum_{i=1}^{N}\int_{\Omega} q_{\phi_i}\cdot\nabla\mu_i d\boldsymbol{x}+\sum_{i=1}^{N}\int_{\Omega}\xi\gamma^2\phi_i^2(\nabla\lambda_i)^2 d\boldsymbol{x}+\int_{\partial\Omega_w}((\boldsymbol{\sigma}_\eta+\sum_{i=1}^{N}\lambda_i\delta_i\mathscr{P}_i)\cdot\mathbf{n})\cdot\mathbf{u}_\tau ds \\
& +\sum_{i=1}^{N}\int_{\partial\Omega_s}\hat{L}_i(-\mathbf{u}\cdot\nabla_\Gamma\phi_i+J_{\Gamma_i})ds \\
= & -\int_{\Omega}((\boldsymbol{\sigma}_\eta+pI):\nabla\mathbf{u})d\boldsymbol{x}+\int_{\Omega}(\mathbf{F}-\sum_{i=1}^{N}\mu_i\nabla\phi_i-\sum_{i=1}^{N}\nabla\cdot(\lambda_i\delta_i\mathscr{P}_i))\cdot\mathbf{u}d\boldsymbol{x} \\
& -\sum_{i=1}^{N}\int_{\Omega} q_{\phi_i}\cdot\nabla\mu_i d\boldsymbol{x}+\sum_{i=1}^{N}\int_{\Omega}\xi\gamma^2\phi_i^2(\nabla\lambda_i)^2 d\boldsymbol{x} \\
& +\int_{\partial\Omega_w}((\boldsymbol{\sigma}_\eta+\sum_{i=1}^{N}\lambda_i\delta_i\mathscr{P}_i)\cdot\mathbf{n}-\sum_{i=1}^{N}\hat{L}_i\nabla_\Gamma\phi_i)\cdot\mathbf{u}_\tau ds+\sum_{i=1}^{N}\int_{\partial\Omega_w}\hat{L}_i J_{\Gamma_i}ds\ , \qquad (5.19)
\end{aligned}
$$

where $\hat{L}_i=\dfrac{\hat{\kappa}_B}{\gamma}\partial_n f_i+M_s\dfrac{S(\phi_i)-S(\phi_{i,0})}{S(\phi_{i,0})}\gamma\partial_n\phi_i$.

For the close system, we have the energy dissipation law [161, 140, 96]

$$
\frac{dE}{dt}=-\Delta, \qquad (5.20)
$$

where means the changing rate of energy is induced by the dissipation. Comparing with predefined dissipation functional in Eq. (5.12) yields

$$
\begin{cases}
\boldsymbol{\sigma}_\eta=2\eta\boldsymbol{D}_\eta-pI\ , & \text{in } \Omega\ , \\
q_{\phi_j}=M_{\phi_j}\nabla\mu_j\ , & \text{in } \Omega\ , \\
\mathbf{F}=\sum_{i=1}^{N}(\mu_i\nabla\phi_i+\nabla\cdot(\lambda_i\delta_i\mathscr{P}_i))\ , & \text{in } \Omega\ , \\
J_{\Gamma_i}=-\kappa_{\Gamma_i}^{-1}\hat{L}_i\ , & \text{on } \partial\Omega_w\ , \\
u_{\tau_j}=\beta_s^{-1}(-(\mathbf{n}\cdot(\boldsymbol{\sigma}_\eta+\sum_{i=1}^{N}\lambda_i\delta_i\mathscr{P}_i)\cdot\boldsymbol{\tau}_j)+\sum_{i=1}^{N}\hat{L}_i\partial_{\tau_j}\phi_i)\ ,\ j=1,2, & \text{on } \partial\Omega_w\ .
\end{cases} \qquad (5.21)
$$

To this end, the proposed multi-cellular interaction model is composed of the following equations:

$$\begin{cases} \frac{\partial \phi_i}{\partial t} + \nabla \cdot (\mathbf{u}\phi_i) = M_{\phi_i} \Delta \mu_i \ , \\ \mu_i = \frac{\hat{\kappa}_B}{\gamma^3} g(\phi_i) + \frac{\partial H}{\partial \phi_i} + \frac{M_s}{\gamma} \frac{S(\phi_i) - S(\phi_{i,0})}{S(\phi_{i,0})} f(\phi_i) + \frac{\partial f_w(\phi_i)}{\partial \phi_i} \ , \\ g(\phi_i) = -\gamma^2 \Delta f_i + (3\phi^2 - 1) f(\phi_i), \\ f(\phi_i) = -\gamma^2 \Delta \phi_i + (\phi_i^2 - 1)\phi_i \ , \\ \rho(\frac{\partial \mathbf{u}}{\partial t} + (\mathbf{u} \cdot \nabla)\mathbf{u}) + \nabla p = \nabla \cdot (2\eta \boldsymbol{D}_\eta) + \sum_{j=1}^{i} (\mu_j \nabla \phi_j + \nabla \cdot (\lambda_j \delta_j \mathscr{P}_j)) \ , \\ \nabla \cdot \mathbf{u} = 0 \ , \\ \delta_i (\mathscr{P}_i : \nabla \mathbf{u}) + \xi \gamma^2 \nabla \cdot (\phi_i^2 \nabla \lambda_i) = 0 \ , \end{cases} \tag{5.22}$$

with the boundary conditions on $\partial \Omega_w$

$$\begin{cases} \mathbf{u} \cdot \mathbf{n} = 0 \ , \\ -\beta_s u_{\tau_j} = (\mathbf{n} \cdot (\boldsymbol{\sigma}_\eta + \sum_{i=1}^{N} \lambda_i \delta_i \mathscr{P}_i) \cdot \boldsymbol{\tau}_j) - \sum_{i=1}^{N} \hat{L}_i \partial_{\tau_j} \phi_i \ , \ j = 1,2, \\ f_i = 0 \ , \\ \kappa_{\Gamma_i} \left(\frac{\partial \phi_i}{\partial t} + \mathbf{u} \cdot \nabla_\Gamma \phi_i \right) = -\hat{L}_i \ , \\ \hat{L}_i = \frac{\hat{\kappa}_B}{\gamma} \partial_n f_i + M_s \frac{s(\phi_i) - S(\phi_{i,0})}{S(\phi_{i,0})} \gamma \partial_n \phi_i \ , \\ \partial_n \mu_i = 0 \ . \end{cases} \tag{5.23}$$

5.2.2 Dimensionless

The viscosity, length, velocity, time, bulk and boundary chemical potentials in the equations are scaled by their corresponding characteristic values η_0, L, U, $\frac{L}{U}$, $\frac{\eta_0 U}{L}$ and $\eta_0 U$, respectively. Write $Q_{w_1}, Q_{w_2}, Q_1, Q_2$ into $Q_0 q_{w_1}, Q_0 q_{w_2}. Q_0 q_1, Q_0 q_2$, where Q_0 is the character energy density. The governing equation of the system can be rewritten as

$$\begin{cases} Re(\frac{\partial \mathbf{u}}{\partial t} + (\mathbf{u} \cdot \nabla)\mathbf{u}) + \nabla P = \nabla \cdot (2\eta \boldsymbol{D}) + \sum_i \mu_i \nabla \phi_i + \sum_i \nabla \cdot (\lambda_i \delta_{\varepsilon_i} \mathscr{P}_i) \ , & \text{in } \Omega \ , \\ \nabla \cdot \mathbf{u} = 0 \ , & \text{in } \Omega \ , \\ \frac{\partial \phi_i}{\partial t} + \mathbf{u} \cdot \nabla \phi_i = -\mathscr{M} \Delta \mu_i \ , & \text{in } \Omega \ , \\ \mu_i = \kappa_B g(\phi_i) + \mathscr{M}_s \frac{(S(\phi_i) - S(\phi_{i,0}))}{S(\phi_{i,0})} f_i + \alpha \frac{\partial H}{\partial \phi_i} + \alpha \frac{\partial f_w(\phi_i)}{\partial \phi_i} \ , & \text{in } \Omega \ , \\ f_i = -\varepsilon \Delta \phi_i + \frac{(\phi_i^2 - 1)}{\varepsilon} \phi_i, \ g(\phi_i) = -\Delta f_i + \frac{1}{\varepsilon^2}(3\phi_i^2 - 1) f_i \ , & \text{in } \Omega \ , \\ \delta_{\varepsilon_i} (\mathscr{P}_i : \nabla \mathbf{u}) + \xi \varepsilon^2 \nabla \cdot (\phi_i^2 \nabla \lambda_i) = 0 \ , & \text{in } \Omega \ , \end{cases} \tag{5.24}$$

with the boundary conditions

$$\begin{cases} \kappa\dot{\phi}_i + L(\phi_i) = 0 \,, & \text{on } \partial\Omega_w \,, \\ L(\phi_i) = \kappa_B \partial_n f(\phi_i) + \varepsilon \mathscr{M}_s \frac{S(\phi_i) - S(\phi_{i,0})}{S(\phi_{i,0})} \partial_n \phi_i \,, & \text{on } \partial\Omega_w \,, \\ -l_s^{-1} u_{\tau_i} = \boldsymbol{\tau_i} \cdot (2\eta \mathbf{D}_\eta + \sum_i \lambda_i \delta_{\varepsilon_i} \mathscr{P}_i) \cdot \boldsymbol{n} - \sum_i L(\phi_i) \partial_{\tau_i} \phi_i \,,\ i = 1,2, & \text{on } \partial\Omega_w \,, \\ f_i = 0 \,, & \text{on } \partial\Omega_w \,, \\ \partial_n \mu_i = 0 \,, & \text{on } \partial\Omega_w \,, \end{cases} \tag{5.25}$$

where $S(\phi_i) = \int_\Omega \dfrac{\varepsilon}{2}|\nabla\phi_i|^2 + \dfrac{1}{4\varepsilon}(\phi_i^2 - 1)^2 d\boldsymbol{x}$ and $\delta_{\varepsilon_i} = \frac{1}{2}\varepsilon^2 |\nabla\phi_i|^2$.

The dimensionless constants appeared in Eqs. (5.24)-(5.25) are given by $\varepsilon = \frac{\gamma}{L}$, $Re = \frac{\rho_0 U L}{\eta_0}$, $\mathscr{M} = \frac{M_\phi \eta_0}{L^2}$, $\kappa_B = \frac{\hat{\kappa}_B}{L^2 \eta_0 U}$, $k = \frac{\hat{\kappa}_B}{\eta_0 L}$, $l_s = \frac{\eta_0}{\beta_s L}$, $\alpha = \frac{Q_0}{\eta_0 U}$, $\mathscr{M}_s = \frac{M_s}{\eta_0 U}$.

If we define the Sobolev spaces as follows [53, 140]

$$\boldsymbol{W}^{1,3} = (W^{1,3})^2 \,, \tag{5.26}$$

$$\boldsymbol{W}_N^{1,\frac{3}{2}} = (W^{1,\frac{3}{2}})^N \,, \tag{5.27}$$

$$\boldsymbol{W}_N^{1,3} = (W^{1,3})^N \,, \tag{5.28}$$

$$\boldsymbol{W}_N^{1,\frac{3}{2}}(\Omega) = \left\{ \Lambda = (\lambda_1, \lambda_2, ... \lambda_N)^T \right\} \,, \tag{5.29}$$

$$\boldsymbol{W}^{1,3}(\Omega) = \left\{ \mathbf{u} = (u_x, u_y)^T \in \boldsymbol{W}^{1,3} | \mathbf{u} \cdot \boldsymbol{n} = 0, \text{ on } \partial\Omega_w \right\} \,, \tag{5.30}$$

$$\boldsymbol{W}_\Phi^{1,3}(\Omega) = \left\{ \Phi = (\phi_1, \phi_2, ... \phi_N)^T \in \boldsymbol{W}_N^{1,3} | -1 \le \phi_i \le 1, i = 1,2,...N, \text{ in } \Omega \right\} \,, \tag{5.31}$$

$$\boldsymbol{W}_{\boldsymbol{U}}^{1,3}(\Omega) = \left\{ \boldsymbol{U} = (\mu_1, \mu_2, ... \mu_N)^T \in \boldsymbol{W}_N^{1,3} | \partial_n \mu_i = 0, i = 1,2,...N, \text{ on } \partial\Omega_w \right\} \,, \tag{5.32}$$

$$\boldsymbol{W}_F^{1,3}(\Omega) = \left\{ F = (f_1, f_2, ... f_N)^T \in \boldsymbol{W}_N^{1,3} | f_i = 0, i = 1,2,...N, \text{ on } \partial\Omega_w \right\} \,, \tag{5.33}$$

$$\boldsymbol{W}_b = \boldsymbol{W}_\Phi^{1,3}(\Omega) \times \boldsymbol{W}_F^{1,3}(\Omega) \times \boldsymbol{W}_{\boldsymbol{U}}^{1,3}(\Omega) \times \boldsymbol{W}_N^{1,\frac{3}{2}}(\Omega) \times W^{1,\frac{3}{2}}(\Omega) \times \boldsymbol{W}^{1,3}(\Omega) \,, \tag{5.34}$$

and let $\|\cdot\| = \left(\int_\Omega |\cdot|^2 d\boldsymbol{x}\right)^{\frac{1}{2}}$ and $\|\cdot\|_w = \left(\int_{\partial\Omega_w} |\cdot|^2 ds\right)^{\frac{1}{2}}$ denote the L^2 norm defined in the domain and on the domain boundary respectively, then the system (5.24)-(5.25) satisfies the following energy law.

Theorem 5.2.1. *If* $(\Phi,\ F,\ \boldsymbol{U},\ \lambda,\ P,\ \mathbf{u}) \in \boldsymbol{W}_b$ *are smooth solutions of the above system* (5.24)-(5.25)*, then the following energy law is satisfied:*

$$\begin{aligned} &\frac{d}{dt}\mathscr{E}_{total} = \frac{d}{dt}(\mathscr{E}_{kin} + \mathscr{E}_{cell} + \mathscr{E}_w) \\ = \ &\frac{1}{Re}\left(-2\|\eta^{1/2}\mathbf{D}_\eta\|^2 - \mathscr{M}\sum_i \|\nabla\mu_i\|^2 - \xi\sum_i \|\varepsilon\phi_i\nabla\lambda_i\|^2 - \kappa\sum_i \|\dot{\phi}_i\|_w^2 - \|l_s^{-1/2}\mathbf{u}_\tau\|_w^2 \right) \end{aligned} \tag{5.35}$$

where $\mathscr{E}_{total} = \mathscr{E}_{kin} + \mathscr{E}_{cell} + \mathscr{E}_w$, $\mathscr{E}_{kin} = \frac{1}{2}\int_\Omega |\mathbf{u}|^2 d\boldsymbol{x}$, $\mathscr{E}_{cell} = \frac{\kappa_B}{2Re\varepsilon}\sum_i \int_\Omega |f_i|^2 d\boldsymbol{x} + \mathscr{M}_s \sum_i \frac{(S(\phi_i) - S(\phi_{i,0}))^2}{2ReS(\phi_{i,0})} + \frac{\alpha}{Re}\int_\Omega H d\boldsymbol{x}$ *and* $\mathscr{E}_w = \frac{\alpha}{Re}\sum_i \int_\Omega f_w(\phi_i) d\boldsymbol{x}$.

Proof: Multiplying the first equation in Eq. (5.24) with $\mathbf{u}$ and integration by parts yield

$$\begin{aligned}
\frac{d}{dt}\mathscr{E}_{kin} &= \frac{1}{Re}\Bigg\{ -\int_\Omega 2\eta |\boldsymbol{D}_\eta|^2 d\boldsymbol{x} + \int_{\partial\Omega_w} (\boldsymbol{\sigma}_\eta \cdot \mathbf{n}) \cdot \mathbf{u}_\tau ds + \sum_i \int_\Omega \mu_i \nabla\phi_i \cdot \mathbf{u} d\boldsymbol{x} - \sum_i \int_\Omega \lambda_i \delta_{\varepsilon_i} \mathscr{P}_i : \nabla \mathbf{u} d\boldsymbol{x} \\
&\quad + \sum_i \int_{\partial\Omega_w} (\lambda_i \delta_{\varepsilon_i} \mathscr{P}_i \cdot \mathbf{n}) \cdot \mathbf{u}_\tau ds \Bigg\} \\
&= \frac{1}{Re}\Bigg\{ -\int_\Omega 2\eta |\boldsymbol{D}_\eta|^2 d\boldsymbol{x} - \sum_i \int_\Omega \lambda_i \delta_{\varepsilon_i} \mathscr{P}_i : \nabla \mathbf{u} d\boldsymbol{x} - l_s^{-1} \int_{\partial\Omega_w} |\mathbf{u}_\tau|^2 ds \\
&\quad + \sum_i \int_{\partial\Omega_w} L(\phi_i) \partial_\tau \phi \cdot \mathbf{u}_\tau ds + \sum_i \int_\Omega \mu_i \nabla\phi_i \cdot \mathbf{u} d\boldsymbol{x} \ , \Bigg\}
\end{aligned} \tag{5.36}$$

where the slip boundary condition in Eq. (5.25) is applied.

Taking the inner product of the third equation in Eq. (5.24) with $\frac{\mu_i}{Re}$ and summing up with respect to i result in

$$\frac{1}{Re}\sum_i \int_\Omega \frac{\partial \phi_i}{\partial t}\mu_i d\boldsymbol{x} + \frac{1}{Re}\sum_i \int_\Omega \mathbf{u} \cdot \nabla\phi_i \mu_i d\boldsymbol{x} = -\frac{1}{Re}\mathscr{M}\sum_i \int_\Omega |\nabla \mu_i|^2 d\boldsymbol{x} \ , \tag{5.37}$$

where $\partial_n \mu_i = 0$ is considered here.

Multiplying the fourth equation in Eq. (5.24) with $\frac{1}{Re}\frac{\partial \phi_i}{\partial t}$ and integration by parts give rise to

$$\begin{aligned}
&\frac{1}{Re}\sum_i \int_\Omega \mu \frac{\partial \phi_i}{\partial t} d\boldsymbol{x} \\
&= \frac{1}{Re}\sum_i \Bigg\{ \kappa_B \int_\Omega g_i \frac{\partial \phi_i}{\partial t} d\boldsymbol{x} + \mathscr{M}_s \frac{S(\phi_i) - S(\phi_{i,0})}{S(\phi_{i,0})} \int_\Omega f_i \frac{\partial \phi_i}{\partial t} d\boldsymbol{x} + \alpha \int_\Omega \frac{\partial H}{\partial \phi_i}\frac{\partial \phi_i}{\partial t} d\boldsymbol{x} + \alpha \int_\Omega \frac{f_w(\phi_i)}{\partial \phi_i}\frac{\partial \phi_i}{\partial t} d\boldsymbol{x} \Bigg\} \\
&= \frac{\kappa_B}{Re}\sum_i \int_\Omega f_i \frac{\partial}{\partial t}\left(-\Delta\phi_i + \frac{1}{\varepsilon^2}(\phi_i^3 - \phi_i) \right) d\boldsymbol{x} - \frac{\kappa_B}{Re}\sum_i \int_{\partial\Omega_w} \partial_n f_i \frac{\partial \phi_i}{\partial t} ds + \mathscr{M}_s \sum_i \frac{d}{dt}\left(\frac{(S(\phi_i) - S(\phi_{i,0}))^2}{2ReS(\phi_{i,0})} \right) \\
&\quad - \mathscr{M}_s \sum_i \left(\frac{S(\phi_i) - S(\phi_{i,0})}{ReS(\phi_{i,0})} \right) \int_{\partial\Omega_w} \varepsilon \partial_n \phi_i \frac{\partial \phi_i}{\partial t} ds + \frac{\alpha}{Re}\sum_i \int_\Omega \frac{\partial f_w(\phi_i)}{\partial \phi_i}\frac{\partial \phi_i}{\partial t} d\boldsymbol{x} + \frac{\alpha}{Re}\sum_i \int_\Omega \frac{\partial H}{\partial \phi_i}\frac{\partial \phi_i}{\partial t} d\boldsymbol{x} \\
&= \frac{d}{dt}\left(\kappa_B \sum_i \int_\Omega \frac{|f_i|^2}{2Re\varepsilon} d\boldsymbol{x} \right) + \mathscr{M}_s \frac{d}{dt}\left(\sum_i \frac{(S(\phi_i) - S(\phi_{i,0}))^2}{2ReS(\phi_{i,0})} \right) + \frac{\alpha}{Re}\frac{d}{dt}\sum_i \int_\Omega f_w(\phi_i) d\boldsymbol{x} + \frac{\alpha}{Re}\frac{d}{dt}\int_\Omega H d\boldsymbol{x} \\
&\quad - \sum_i \int_{\partial\Omega_w} \frac{L(\phi_i)}{Re}\frac{\partial \phi_i}{\partial t} ds \\
&= \frac{d}{dt}(\mathscr{E}_{cell} + \mathscr{E}_w) - \int_{\partial\Omega_w} \frac{L(\phi)}{Re}\frac{\partial \phi}{\partial t} ds \ ,
\end{aligned} \tag{5.38}$$

where the definitions of $f(\phi)$, $g(\phi)$ and the boundary conditions of ϕ and f are utilized.

Multiplying the last equations with $\frac{\lambda_i}{Re}$ and integration by parts and sum up by i leads to

$$\frac{1}{Re}\sum_i \int_\Omega (\lambda_i \delta_{\varepsilon_i} \mathscr{P}_i) : \nabla \mathbf{u} d\boldsymbol{x} - \frac{1}{Re}\sum_i \int_\Omega \xi \varepsilon^2 \phi_i^2 (\nabla \lambda_i)^2 d\boldsymbol{x} = 0 \,. \tag{5.39}$$

Finally, the energy dissipation law (5.35) is obtained by combining Eqs. (5.36), (5.37), (5.38) and (5.39) considering the boundary conditions in (5.25). ■

5.3 Numerical Scheme and Discrete Energy law

In this section, an energy stable temporal discretization scheme is first proposed for the multi-celluar system (5.24)-(5.25). Then C^0 finite element method is used for spacial discretization to obtain the fully discretization scheme.

5.3.1 Time-discrete primitive method

The mid-point method is used for temporal discretization of Eqs. (5.24)-(5.25). Let Δt denote the time step size, $()^{n+1}$ and $()^n$ denote the value of the variables at times $(n+1)\Delta t$ and $n\Delta t$, respectively. The semi-discrete in time equations are as follows: in Ω

$$\begin{cases} \frac{\mathbf{u}^{n+1}-\mathbf{u}^n}{\Delta t} + (\mathbf{u}^{n+\frac{1}{2}}\cdot\nabla)\mathbf{u}^{n+\frac{1}{2}} + \frac{1}{Re}\nabla P^{n+\frac{1}{2}} = \frac{1}{Re}\nabla\cdot(\eta^n(\nabla\mathbf{u}^{n+\frac{1}{2}} + (\nabla\mathbf{u}^{n+\frac{1}{2}})^T)) \\ \qquad + \frac{1}{Re}\sum_i \mu_i^{n+\frac{1}{2}}\nabla\phi_i^{n+\frac{1}{2}} + \sum_i \frac{1}{Re}\nabla\cdot\left(\lambda_i^{n+\frac{1}{2}}\mathscr{P}_i^n\delta_{\varepsilon_i}\right) \,, \\ \nabla\cdot\mathbf{u}^{n+\frac{1}{2}} = 0 \,, \\ \frac{\phi_i^{n+1}-\phi_i^n}{\Delta t} + (\mathbf{u}^{n+\frac{1}{2}}\cdot\nabla)\phi_i^{n+\frac{1}{2}} = -\mathscr{M}\Delta\mu_i^{n+\frac{1}{2}} \,, \\ \mu_i^{n+\frac{1}{2}} = \kappa_B g(\phi_i^{n+1},\phi_i^n) + \mathscr{M}_s\frac{(S(\phi_i^{n+\frac{1}{2}})-S(\phi_{0_i}))}{S(\phi_{0_i})}f(\phi_i^{n+1},\phi_i^n) \\ \qquad + \alpha\frac{H_i^{n+1}-H_i^n}{\phi_i^{n+1}-\phi_i^n} + \alpha\frac{f_w(\phi_i^{n+1})-f_w(\phi_i^n)}{\phi_i^{n+1}-\phi_i^n} \,, \\ f_i^{n+\frac{1}{2}} = -\varepsilon\Delta\phi_i^{n+\frac{1}{2}} + \frac{1}{\varepsilon}((\phi_i^{n+\frac{1}{2}})^2-1)\phi_i^{n+\frac{1}{2}} \,, \\ \delta_{\varepsilon_i}\mathscr{P}_i^n : \nabla\mathbf{u}^{n+\frac{1}{2}} + \xi\varepsilon^2\nabla\cdot((\phi_i^n)^2\nabla\lambda_i^{n+\frac{1}{2}}) = 0 \,, \end{cases} \tag{5.40}$$

with boundary conditions on $\partial\Omega_w$,

$$\begin{cases} \kappa\dot{\phi}_i^{n+\frac{1}{2}} = -L_i^{n+\frac{1}{2}} \,, \\ L_i^{n+\frac{1}{2}} = \kappa_B\partial_n f_i^{n+\frac{1}{2}} + \mathscr{M}_s\varepsilon\frac{S(\phi_i^{n+\frac{1}{2}})-S_{0_i}}{S_{0_i}}\partial_n\phi_i^{n+\frac{1}{2}} \,, \\ -l_s^{-1}u_{\tau_j}^{n+\frac{1}{2}} = \boldsymbol{\tau_j}\cdot(\eta^n(\nabla\mathbf{u}^{n+\frac{1}{2}} + (\nabla\mathbf{u}^{n+\frac{1}{2}})^T) + \sum_i\lambda_i^{n+\frac{1}{2}}\delta_{\varepsilon_i}\mathscr{P}_i^n)\cdot\boldsymbol{n} \\ \qquad\qquad - \sum_i L_i^{n+\frac{1}{2}}\partial_{\tau_j}\phi_i^{n+\frac{1}{2}} \,, \quad j=1,2, \\ f_i^{n+\frac{1}{2}} = 0 \,, \\ \partial_n\lambda_i^{n+\frac{1}{2}} = 0 \,, \end{cases} \tag{5.41}$$

with $(\cdot)^{n+\frac{1}{2}} = \frac{(\cdot)^n+(\cdot)^{n+1}}{2}$ and $\mathscr{P}_i^n = I - \mathbf{n}_m^n \otimes \mathbf{n}_m^n$ with $\mathbf{n}_m^n = \frac{\nabla\phi_i^n}{|\nabla\phi_i^n|}$ and

$$\begin{cases} f(\phi_i^{n+1},\phi_i^n) = -\varepsilon\Delta\phi_i^{n+\frac{1}{2}} + \frac{1}{4\varepsilon}((\phi_i^{n+1})^2+(\phi_i^n)^2-2)(\phi_i^{n+1}+\phi_i^n)\ , \\ g(\phi_i^{n+1},\phi_i^n) = \left(-\Delta f_i^{n+\frac{1}{2}} + \frac{1}{\varepsilon^2}\left((\phi_i^{n+1})^2+(\phi_i^n)^2+\phi_i^{n+1}\phi_i^n-1\right)f_i^{n+\frac{1}{2}}\right)\ , \\ H_i^n = \frac{q_1}{2}(\phi_i^n+1)^2\sum_{j\neq i}\left[(\phi_j^{n+\frac{1}{2}}+1)^2\right] - \frac{q_2}{4}((\phi_i^n)^2-1)^2\sum_{j\neq i}\left[((\phi_j^{n+\frac{1}{2}})^2-1)^2\right]\ , \\ H_i^{n+1} = \frac{q_1}{2}(\phi_i^{n+1}+1)^2\sum_{j\neq i}\left[(\phi_j^{n+\frac{1}{2}}+1)^2\right] - \frac{q_2}{4}((\phi_i^{n+1})^2-1)^2\sum_{j\neq i}\left[((\phi_j^{n+\frac{1}{2}})^2-1)^2\right]\ , \\ f_w(\phi^n) = q_{w_1}(\phi_i^n+1)^2(\phi_w+1)^2 - q_{w_2}((\phi_i^n)^2-1)((\phi_w)^2-1)\ . \end{cases} \tag{5.42}$$

Thus we have

$$\begin{aligned} \frac{H_i^{n+1}-H_i^n}{\phi_i^{n+1}-\phi_i^n} &= \frac{1}{\phi_i^{n+1}-\phi_i^n}\left(q_1(\phi_i^{n+1}+1)^2\sum_{j\neq i}\left[(\phi_j^{n+\frac{1}{2}}+1)^2\right] - q_2((\phi_i^{n+1})^2-1)^2\sum_{j\neq i}\left[((\phi_j^{n+\frac{1}{2}})^2-1)^2\right]\right. \\ &\quad \left. - q_1(\phi_i^n+1)^2\sum_{j\neq i}\left[(\phi_j^{n+\frac{1}{2}}+1)^2\right] + q_2((\phi_i^n)^2-1)^2\sum_{j\neq i}\left[(\phi_j^{n+\frac{1}{2}})^2-1\right]\right) \\ &= q_1(\phi_i^{n+1}+\phi_i^n+2)\sum_{j\neq i}\left[(\phi_j^{n+\frac{1}{2}}+1)^2\right] \\ &\quad -q_2(\phi_i^{n+1}+\phi_i^n)((\phi_i^{n+1})^2+(\phi_i^n)^2-2)\sum_{j\neq i}\left[((\phi_j^{n+\frac{1}{2}})^2-1)^2\right] \end{aligned} \tag{5.43}$$

Similarly,

$$\begin{aligned} \frac{f_w(\phi_i^{n+1})-f_w(\phi_i^n)}{\phi_i^{n+1}-\phi_i^n} &= q_{w_1}(\phi_i^{n+1}+\phi_i^n+2)(\phi_w+1)^2 \\ &\quad -q_{w_2}(\phi_i^{n+1}+\phi_i^n)((\phi_i^{n+1})^2+(\phi_i^n)^2-2)(\phi_w^2-1)^2 \end{aligned} \tag{5.44}$$

Later on, we keep the form $\frac{f_w(\phi_i^{n+1})-f_w(\phi_i^n)}{\phi_i^{n+1}-\phi_i^n}$ and $\frac{H(\phi_i^{n+1})-H(\phi_i^n)}{\phi_i^{n+1}-\phi_i^n}$for convenience in later derivation.

The above scheme obeys the following theorem of energy stability.

Theorem 5.3.1. *If* $(\phi_i^n,\mu_i^n,\mathbf{u}^n,P^n)$ *are smooth solutions of the above system* (5.40)-(5.41)*, then the following energy law is satisfied:*

$$\begin{aligned} \mathscr{E}_{total}^{n+1}-\mathscr{E}_{total}^n &= (\mathscr{E}_{kin}^{n+1}+\sum_i^N\left[\mathscr{E}_{cell_i}^{n+1}+\mathscr{E}_{i,int}^{n+1}+\mathscr{E}_{w_i}^{n+1}\right]) - (\mathscr{E}_{kin}^n+\sum_i^N\left[\mathscr{E}_{cell_i}^n+\mathscr{E}_{i,int}^n+\mathscr{E}_{w_i}^n\right]) \\ &= \frac{\triangle t}{Re}\left(-2\|(\eta^n)^{1/2}\mathbf{D}_\eta^{n+\frac{1}{2}}\|^2 - \mathscr{M}\sum_i^N\|\nabla\mu_i^{n+\frac{1}{2}}\|^2 - \xi\sum_i^N\|\ \varepsilon\phi_i^n\nabla\lambda_i^{n+\frac{1}{2}}\|^2\right. \\ &\quad \left. -\frac{1}{\kappa}\|\sum_i^N L(\phi_i^{n+\frac{1}{2}})\|_w^2 - \|l_s^{-1/2}\mathbf{u}_\tau^{n+\frac{1}{2}}\|_w^2\right)\ , \end{aligned} \tag{5.45}$$

where $\mathscr{E}^n_{total} = \mathscr{E}^n_{kin} + \sum_i^N \left[\mathscr{E}^n_{cell_i} + \mathscr{E}^n_{i,int} + \mathscr{E}^n_{w_i}\right]$ *with* $\mathscr{E}^n_{kin} = \frac{1}{2}\|\mathbf{u}^n\|^2$, $\mathscr{E}^n_{cell_i} = \frac{\kappa_B\|f_i^n\|^2}{2Re\varepsilon} + \mathscr{M}_s\frac{(S(\phi_i^n)-S(\phi_{i,0}))^2}{2ReS(\phi_{i,0})} + \frac{\alpha}{Re}H_i^n$ *and* $\mathscr{E}^n_{i,w} = \frac{\alpha}{Re}\int_\Omega f^n_{i,w}d\boldsymbol{x}$.

The following two lemmas are needed for proving **Theorem 5.3.1**. Proof of these two lemmas can be found in [141].

Lemma 5.3.2. *Let*

$$f(\phi^{n+1},\phi^n) = -\varepsilon\Delta\phi^{n+\frac{1}{2}} + \frac{1}{4\varepsilon}((\phi^{n+1})^2 + (\phi^n)^2 - 2)(\phi^{n+1}+\phi^n)\ . \tag{5.46}$$

Then $f(\phi^{n+1},\phi^n)$ *satisfies*

$$\int_\Omega f(\phi^{n+1},\phi^n)(\phi^{n+1}-\phi^n)d\boldsymbol{x} = S^{n+1} - S^n - \int_{\partial\Omega_w}\varepsilon\partial_n\phi^{n+\frac{1}{2}}(\phi^{n+1}-\phi^n)ds\ , \tag{5.47}$$

where $S^{n+1} = \int_\Omega G(\phi^{n+1})d\boldsymbol{x}, S^n = \int_\Omega G(\phi^n)d\boldsymbol{x}$.

Lemma 5.3.3. *Let* $g(\phi^{n+1},\phi^n) = -\Delta f^{n+\frac{1}{2}} + \frac{1}{\varepsilon^2}((\phi^{n+1})^2 + (\phi^n)^2 + \phi^{n+1}\phi^n - 1)f^{n+\frac{1}{2}}$. *Then* $g(\phi^{n+1},\phi^n)$ *satisfies*

$$\begin{aligned}&\int_\Omega g(\phi^{n+1},\phi^n)(\phi^{n+1}-\phi^n)d\boldsymbol{x}\\ =\ &\int_\Omega\frac{1}{2\varepsilon}((f^{n+1})^2-(f^n)^2)d\boldsymbol{x} - \int_{\partial\Omega_w}\partial_n f^{n+\frac{1}{2}}(\phi^{n+1}-\phi^n)ds\ ,\end{aligned} \tag{5.48}$$

where $f^{n+1} = -\varepsilon\Delta\phi^{n+1} + \frac{1}{\varepsilon}((\phi^{n+1})^2-1)\phi^{n+1}, f^n = -\varepsilon\Delta\phi^n + \frac{1}{\varepsilon}((\phi^n)^2-1)\phi^n$.

Proof of Theorem 5.3.1: Multiplying the first equation in system (5.40) by $\Delta t\mathbf{u}^{n+\frac{1}{2}}$ gives

$$\begin{aligned}&\int_\Omega\frac{1}{2}((\mathbf{u}^{n+1})^2-(\mathbf{u}^n)^2)d\boldsymbol{x} + \int_\Omega\Delta t\mathbf{u}^{n+\frac{1}{2}}\cdot((\mathbf{u}^{n+\frac{1}{2}}\nabla)\cdot\mathbf{u}^{n+\frac{1}{2}})d\boldsymbol{x}\\ &-\frac{\Delta t}{Re}\int_\Omega P^{n+\frac{1}{2}}\nabla\cdot\mathbf{u}^{n+\frac{1}{2}}d\boldsymbol{x}\\ =\ &-\frac{\Delta t}{Re}\int_\Omega\nabla\mathbf{u}^{n+\frac{1}{2}}:\eta^n(\nabla\mathbf{u}^{n+\frac{1}{2}} + (\nabla\mathbf{u}^{n+\frac{1}{2}})^T)d\boldsymbol{x} + \frac{\Delta t}{Re}\sum_i\int_\Omega\mathbf{u}^{n+\frac{1}{2}}\cdot\nabla\phi_i^{n+1}\mu_i^{n+1}d\boldsymbol{x}\\ &-\frac{\Delta t}{Re}\sum_i\int_\Omega\lambda_i\delta_{\varepsilon_i}\mathscr{P}_i^n:\nabla\mathbf{u}^{n+\frac{1}{2}}d\boldsymbol{x} + \frac{\Delta t}{Re}\sum_i\int_{\partial\Omega_w}\lambda_i^{n+\frac{1}{2}}(\delta_{\varepsilon_i}\mathscr{P}_i^n\cdot\mathbf{n})\cdot\mathbf{u}_\tau^{n+\frac{1}{2}}ds\\ &+\frac{\Delta t}{Re}\int_{\partial\Omega_w}\mathbf{u}^{n+\frac{1}{2}}\cdot\eta^n((\nabla\mathbf{u}^{n+\frac{1}{2}} + (\nabla\mathbf{u}^{n+\frac{1}{2}})^T)\cdot\boldsymbol{n})ds\ .\end{aligned} \tag{5.49}$$

Multiplying the fourth equation in system (5.40) by $\frac{\phi_i^{n+1}-\phi_i^n}{Re}$ and integration by parts lead to

$$\begin{aligned}&\frac{1}{Re}\sum_i\int_\Omega\mu_i^{n+1/2}(\phi_i^{n+1}-\phi_i^n)d\boldsymbol{x}\\ =\ &\frac{\kappa_B}{Re}\sum_i\int_\Omega\frac{1}{2\varepsilon}((f_i^{n+1})^2-(f_i^n)^2)d\boldsymbol{x}\end{aligned}$$

$$
\begin{aligned}
&+\frac{\mathscr{M}_s}{Re}\frac{(S(\phi_i^{n+1})-S_{i,0})^2-(S(\phi_i^n)-S_{i,0})^2}{2S_{i,0}}\\
&+\frac{\alpha}{Re}\sum_i\int_\Omega(H_i^{n+1}-H_i^n)d\boldsymbol{x}+\frac{\alpha}{Re}\sum_i\int_\Omega(f_w(\phi_i^{n+1})-f_w(\phi_i^n))d\boldsymbol{x}\\
&-\frac{\kappa_B}{Re}\sum_i\int_{\partial\Omega_w}\partial_n f_i^{n+\frac{1}{2}}(\phi_i^{n+1}-\phi_i^n)ds\\
&-\frac{\mathscr{M}_s}{Re}\sum_i\int_{\partial\Omega_w}\frac{S(\phi_i^{n+\frac{1}{2}})-S_{i,0}}{S_{i,0}}\varepsilon\partial_n\phi_i^{n+\frac{1}{2}}(\phi_i^{n+1}-\phi_i^n)ds\,. \qquad (5.50)
\end{aligned}
$$

Multiplying the third equation in system (5.40) by $\frac{\mu_i^{n+\frac{1}{2}}\Delta t}{Re}$ yield

$$
\begin{aligned}
&\frac{1}{Re}\sum_i\int_\Omega\mu_i^{n+\frac{1}{2}}(\phi_i^{n+1}-\phi_i^n)d\boldsymbol{x}+\frac{\Delta t}{Re}\sum_i\int_\Omega\mu_i^{n+\frac{1}{2}}(\mathbf{u}^{n+\frac{1}{2}}\cdot\nabla)\phi_i^{n+\frac{1}{2}}d\boldsymbol{x}\\
=\;&-\frac{\mathscr{M}\Delta t}{Re}\sum_i\int_\Omega(\nabla\mu_i^{n+\frac{1}{2}})^2d\boldsymbol{x}\,. \qquad (5.51)
\end{aligned}
$$

Multiplying the last equation in system (5.40) by $\frac{\lambda^{n+\frac{1}{2}}\Delta t}{Re}$ and integration by parts then sum by i give

$$
\frac{\Delta t}{Re}\sum_i\int_\Omega(\lambda_i^{n+\frac{1}{2}}\delta_{\varepsilon_i}\mathscr{P}_i^n):\nabla\mathbf{u}^{n+\frac{1}{2}}d\boldsymbol{x}-\frac{\Delta t}{Re}\sum_i\int_\Omega\xi\varepsilon^2(\phi_i^n)^2\left|\nabla\lambda_i^{n+\frac{1}{2}}\right|^2d\boldsymbol{x}=0\,. \qquad (5.52)
$$

The discretized energy dissipation law (5.45) is obtained by combining Eqs. (5.49)-(5.52) and organizing the terms according to the boundary conditions $L(\phi_i)$ as shown in (5.41). ■

5.3.2 Fully Discrete C^0 Finite Element Scheme

The spatial discretization using C^0 finite element is straight forward. Let Ω be the domain of interest with a Lipschitz-continuous boundary $\partial\Omega$. Let $\mathbf{W}_b{}^h\subset\mathbf{W}_b$ be a finite element space with respect to the triangulation of the domain Ω. The fully discrete scheme of the system is to find

$$
\left(\{\Phi_h\}^{n+1},\{\boldsymbol{U}\}_h^{n+1},\{F_h\}^{n+1},\{\Lambda_h\}^{n+1},\{p_h\}^{n+1},\{\mathbf{u}_h\}^{n+1}\right)\in\mathbf{W}_b^h,
$$

such that for any $(\psi_{1,h},...,\psi_{N,h},\chi_{1,h},...,\chi_{N,h},\zeta_{1,h},...,\zeta_{N,h},\Theta_{1,h},...,\Theta_{N,h},q_h,\mathbf{v}_h)\in\mathbf{W}_b^h$, the following scheme holds.

$$
\begin{cases}
\int_\Omega\left(\frac{\mathbf{u}_h^{n+1}-\mathbf{u}_h^n}{\Delta t}+(\mathbf{u}_h^{n+\frac12}\cdot\nabla)\mathbf{u}_h^{n+\frac12}+\frac{1}{Re}\nabla P_h^{n+\frac12}\right)\cdot\mathbf{v}_h d\boldsymbol{x}\\
=-\int_\Omega\frac{1}{Re}(\eta_h^n(\nabla\mathbf{u}_h^{n+\frac12}+(\nabla\mathbf{u}_h^{n+\frac12})^T)):\nabla\mathbf{v}_h d\boldsymbol{x}\\
\quad+\sum_i\int_\Omega\frac{1}{Re}\mu_{i,h}^{n+\frac12}\nabla\phi_h^{n+\frac12}\cdot\mathbf{v}_h d\boldsymbol{x}-\sum_i\int_\Omega\frac{1}{Re}\lambda_{i,h}^{n+\frac12}\mathscr{P}_{i,h}^n\delta_{i,h,\varepsilon}:\mathbf{v}_h d\boldsymbol{x}\\
\quad+\int_{\partial\Omega_w}\frac{1}{Re}\mathbf{n}\cdot(\eta_h^n(\nabla\mathbf{u}_h^{n+\frac12}+(\nabla\mathbf{u}_h^{n+\frac12})^T)+\sum_i\lambda_{i,h}^{n+\frac12}\mathscr{P}_{i,h}^n\delta_{i,\varepsilon})\cdot\mathbf{v}_h d\boldsymbol{x}\ ,\\
\int_\Omega(\nabla\cdot\mathbf{u}_h^{n+\frac12})q_h d\boldsymbol{x}=0\ ,\\
\int_\Omega(\frac{\phi_{i,h}^{n+1}-\phi_{i,h}^n}{\Delta t}+(\mathbf{u}_h^{n+\frac12}\cdot\nabla)\phi_{i,h}^{n+\frac12})\psi_{i,h}d\boldsymbol{x}=-\int_\Omega\mathscr{M}\nabla\mu_{i,h}^{n+\frac12}\nabla\psi_{i,h}d\boldsymbol{x}\ ,\\
\int_\Omega\mu_{i,h}^{n+\frac12}\chi_{i,h}d\boldsymbol{x}=\int_\Omega\Bigg(\kappa_B\frac{1}{\varepsilon^2}((\phi_{i,h}^{n+1})^2+(\phi_{i,h}^n)^2+\phi_{i,h}^{n+1}\phi_{i,h}^n-1)f_{i,h}^{n+\frac12}\\
\quad+\mathscr{M}_s\frac{(S(\phi_{i,h}^{n+\frac12})-S(\phi_{i,h,0}))}{S(\phi_{i,h,0})}(\frac{1}{4\varepsilon}((\phi_{i,h}^{n+1})^2+(\phi_{i,h}^n)^2-2)(\phi_{i,h}^{n+1}+\phi_{i,h}^n))\Bigg)\chi_{i,h}d\boldsymbol{x}\\
\quad+\int_\Omega(\kappa_B\nabla f_{i,h}^{n+\frac12}+\mathscr{M}_s\varepsilon\frac{(S(\phi_{i,h}^{n+\frac12})-S(\phi_{i,h,0}))}{S(\phi_{i,h,0})}\nabla\phi_{i,h}^{n+\frac12})\cdot\nabla\chi_{i,h}d\boldsymbol{x}\\
\quad+\int_\Omega\alpha\frac{f_w(\phi_{i,h}^{n+1})-f_w(\phi_{i,h}^n)}{\phi_{i,h}^{n+1}-\phi_{i,h}^n}\chi_{i,h}d\boldsymbol{x}+\int_\Omega\alpha\frac{(H_{i,h}^{n+1}-H_{i,h}^n)}{\phi_{i,h}^{n+1}-\phi_{i,h}^n}\chi_{i,h}d\boldsymbol{x}\\
\quad-\int_{\partial\Omega_w}(\kappa_B\partial_{\mathbf{n}}f_{i,h}^{n+\frac12}+\mathscr{M}_s\varepsilon\frac{(S(\phi_{i,h}^{n+\frac12})-S(\phi_{i,h,0}))}{S(\phi_{i,h})}\partial_{\mathbf{n}}\phi_{i,h}^{n+\frac12})\chi_{i,h}ds\ ,\\
\int_\Omega f_{i,h}^{n+\frac12}\zeta_{i,h}=\int_\Omega\varepsilon\nabla\phi_{i,h}^{n+\frac12}\cdot\nabla\zeta_{i,h}+\int_\Omega\frac{1}{\varepsilon}((\phi_{i,h}^{n+\frac12})^2-1)\phi_{i,h}^{n+\frac12}\zeta_{i,h}d\boldsymbol{x}\\
\quad-\int_{\partial\Omega_w}\varepsilon\partial_{\mathbf{n}}\phi_{i,h}^{n+\frac12}\zeta_{i,h}d\boldsymbol{x}\ ,\\
\int_\Omega\delta_{i,h,\varepsilon}\mathscr{P}_{i,h}^n:\nabla\mathbf{u}_{i,h}^{n+\frac12}\Theta_{i,h}d\boldsymbol{x}-\int_\Omega\xi\varepsilon^2((\phi_{i,h}^n)^2\nabla\lambda_{i,h}^{n+\frac12})\cdot\nabla\Theta_{i,h}d\boldsymbol{x}\\
\quad+\int_{\partial\Omega_w}\xi\varepsilon^2((\phi_{i,h}^n)^2\partial_{\mathbf{n}}\lambda_{i,h}^{n+\frac12})\Theta_{i,h}d\boldsymbol{x}=0\ .
\end{cases}
\tag{5.53}
$$

Newton method is applied to linearize the equations. The proof of the unique solvability can be referred to [141].

5.4 Numerical Results

5.4.1 Bench mark: nonlinear elastic and viscoelastic deformation

Experiments in lab have tested the non-linear elasticity and deformation of red blood cell [105]. Optical tweezers are used to provide stretching force to the cells. Detail about the experiment can be found in [105]. In this part, we set up a numerical simulation of the experiment. New phases ϕ_{tw_1},ϕ_{tw_2} are introduced to represent optical tweezers. The corresponding energy is defined as:

$$
H_{tw_i}=Q_{tw1}(\phi_1+1)^2(\phi_{tw_i}+1)^2-Q_{tw2}(\phi_1^2-1)^2(\phi_{tw_i}^2-1)^2, i=1,2 \tag{5.54}
$$

where Q_{tw} is a coefficient that controls the attraction the optical tweezers provide. The value of other parameters are chosen to fit the experimental data: $Re = 2 \times 10^{-4}, \mathscr{M} = 0.25, \kappa_B = 2 \times 10^{-3}, k = 2 \times 10^{-12}, l_s = 5 \times 10^{-3}, \mathscr{M}_s = 2.$

The force of applied on the cell is calculated by the following equation:

$$\mathbf{F} = \int_{\Omega} \frac{\partial H_{tw_i}}{\partial \phi} \nabla \phi d\boldsymbol{x} \tag{5.55}$$

The curve of axial and transverse diameter versus stretching force is shown in 5.2 together with the experimental data from [105]. From the figures we can see that the numerical simu-

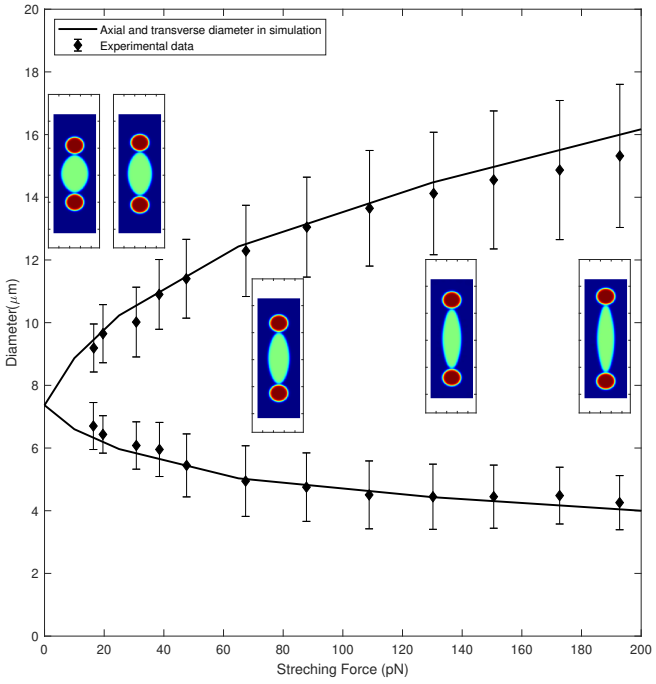

Figure 5.2: Nonlinear elastic deformation of red blood cell. The curve shows the change of the diameter versus stretching force. The diamond is the experiment data published in [105]. In the experiment schematic diagram, the centered phase is set to be the cell and the circulate area on the two side stands for the light tweezers. The force applied on the membrane is kept a constant when the tweezers moving. The equilibrium is reached when the membrane no longer extends under the certain stretch force.

lation fits the experimental data very well. However, the error still exist since the simulation is in 2-D domain and the initial shape of the red blood cell a circle instead of a biconcave curve.

5.4.2 Wall attraction

This example is used to investigate the effect of the vesicle-wall interaction, for example platelets adhesion to vessel wall under blood flow conditions [157]. As shown in Figure 5.3, a vesicle is initially placed at a location with a point-wise contact with the wall phase. Then the deformation of the vesicle with and without local inextensibility is shown in Figure 5.4 The parameter values of this simulation are listed as follows: $Re = 2\times10^{-4}, \mathscr{M} = 5\times10^{-4}, \kappa_B = 2\times10^{-2}, \varepsilon = 2\times10^{-3}, \mathscr{M}_s = 10^2, k = 4\times10^{-11}, l_s = 5\times10^{-6}, \alpha = 1000, q_{w_1} = 2, q_{w_2} = 1.$

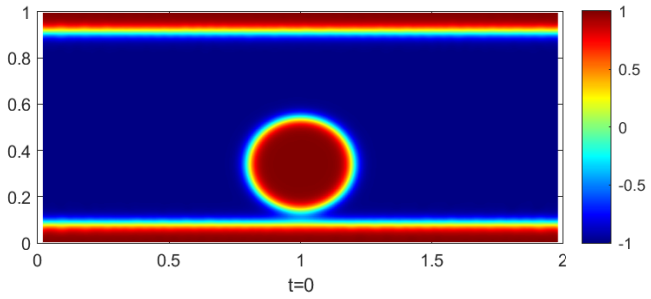

Figure 5.3: The initial state of the case.

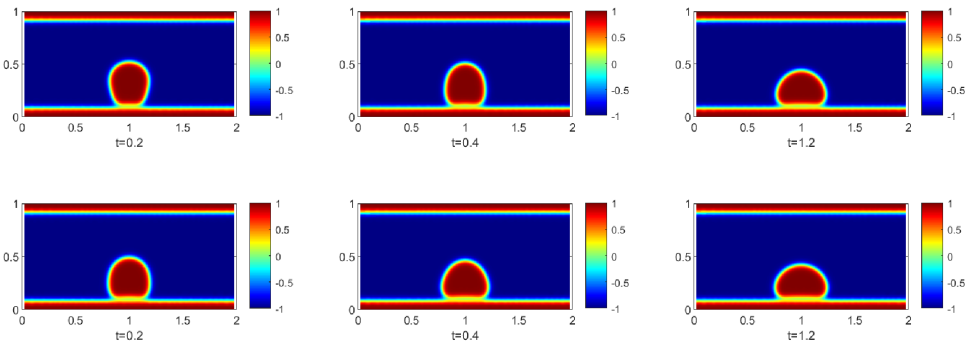

Figure 5.4: The top three pictures shows the deformation of the vesicle with local inextensibility. The bottom three pictures shows the deformation of the vesicle without local inextensibility.

As can be seen, dispite the equilibrium states are similar, the motion of the vesicle is highly different when local inextensibility is applied. Figure 5.5 shows the map of the value of surface divergence $\mathscr{P} : \nabla\mathbf{u}$ of each case.

The total energy change with time of different cases are also shown in Figure 5.6.

The effect of the strength of the adhesion force is also tested. As shown in Figure 5.7, different adhesion force is applied by setting $\alpha = 400, 1000, 2500$ which represents weak, moderate and strong adhesion. It is easily to observe that the stronger the force is, the larger the defromatin would be.

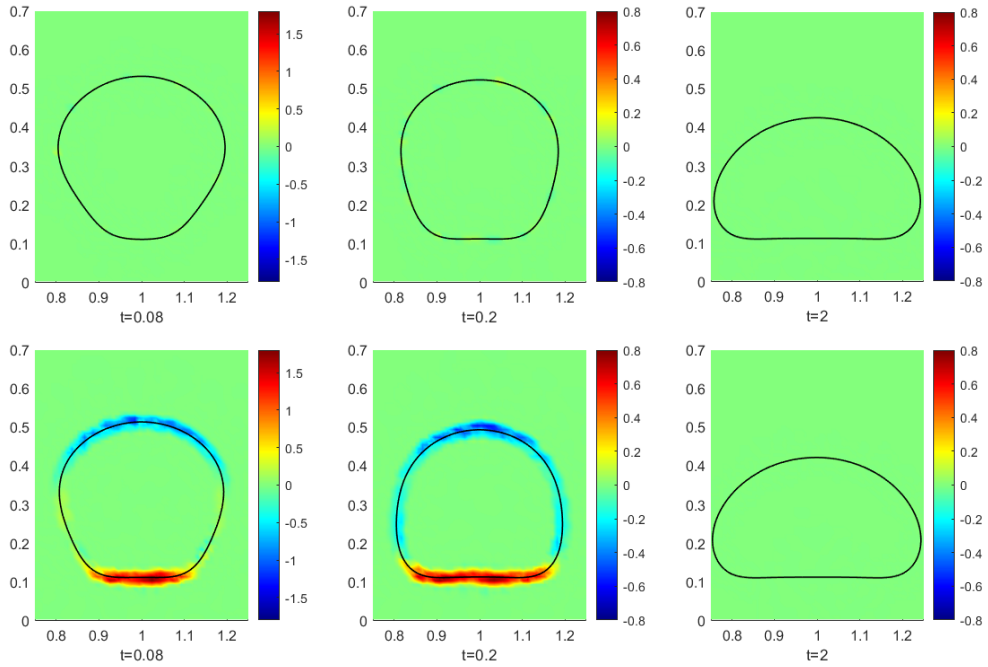

Figure 5.5: The top two pictures shows the value of surface divergence with local inextensibility. The bottom pictures shows the surface divergence of the vesicle without local inextensibility.

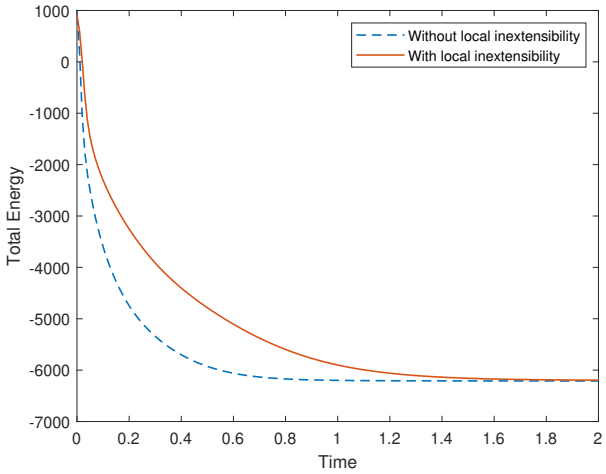

Figure 5.6: Total energy of the two system versus time.

Finally, a dynamic test is also performed by applying a shear flow goes form left hand side to the right of the field, as shown in Figure 5.8. Two cases of strong and weak adhesion is simulated by setting $\alpha_{strong} = 1500$ and $\alpha_{weak} = 150$. It is obvious that the weakly adhesive cell deforms less and is more likely to be flashed away.

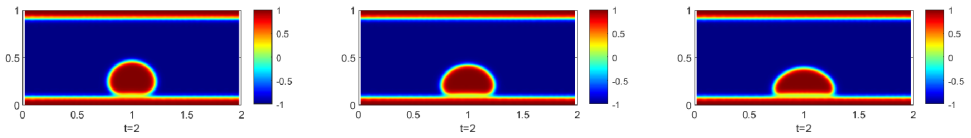

Figure 5.7: Equilibrium of the cells at different strength of the adhesion force. (Left: $\alpha = 400$; Mid: $\alpha = 1000$; Right: $\alpha = 2500$.)

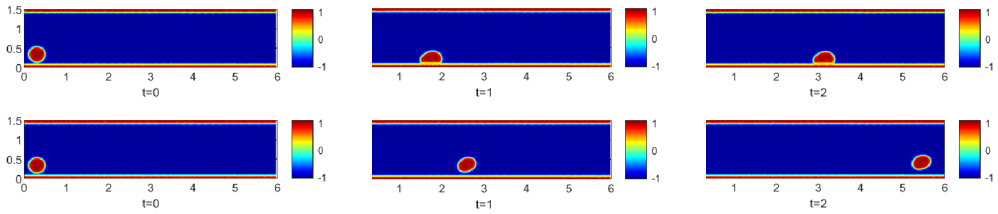

Figure 5.8: The top three picture shows the motion of the cell in strong adhesion case. The bottom three pictures shows the cell motion in weak adhesion case.

The corresponded surface area and volume versus time is also shown in Figure 5.9

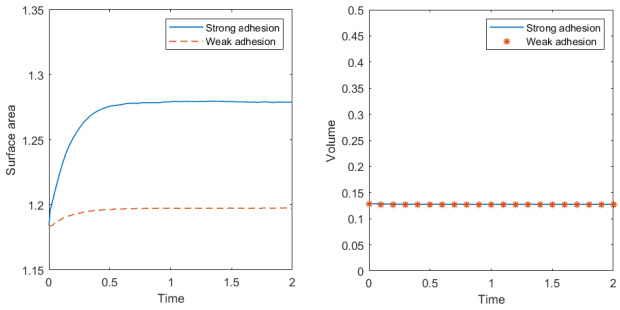

Figure 5.9: The curves show how the surface and volume change with time.

5.4.3 Aggregating and offset

Aggregation of red blood cell is a phenomenon observed in experiment [80]. In this part, we set up a simulation with four red blood cells contacted with each other at a small point. The parameters are shown below. $Re = 2 \times 10^{-5}, \mathscr{M} = 5 \times 10^{-4}, \kappa_B = 4 \times 10^{-2}, k = 4 \times 10^{-12}, l_s = 5 \times 10^{-3}, \mathscr{M}_s = 10^3, \alpha = 3 \times 10^3, q_1 = 1, q_2 = 0.5$ The evolution of the system with time is shown in 5.10.

From the result we can see that they are creeping together with time under the attractive force which is consistent with the experimental result shown in [80].

Also, the deformation of the cells at equilibrium is related to the value of the attractive force. 5.11 shows the status of moderately and strongly aggregate. The parameters are shown below. $Re = 2 \times 10^{-4}, \mathscr{M} = 5 \times 10^{-4}, \kappa_B = 2 \times 10^{-2}, k = 2 \times 10^{-11}, l_s = 5 \times 10^{-3}, \mathscr{M}_s = 10.$

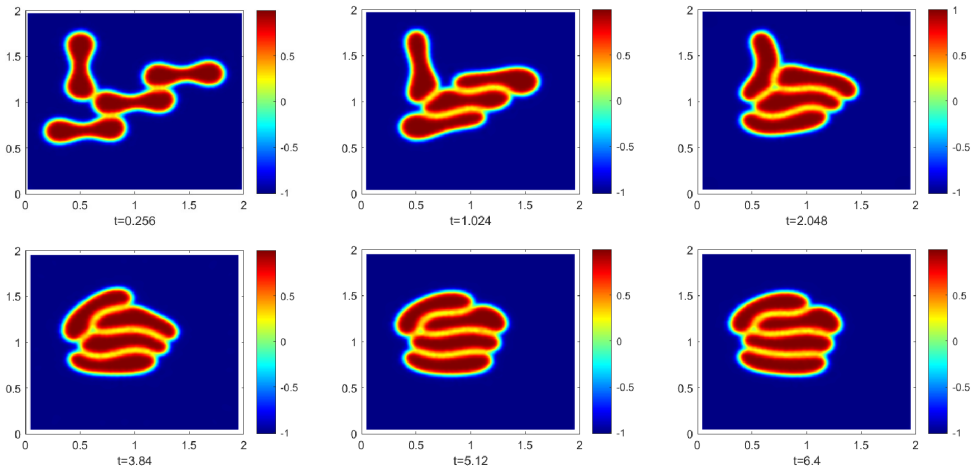

Figure 5.10: Aggregating of four red blood cells.

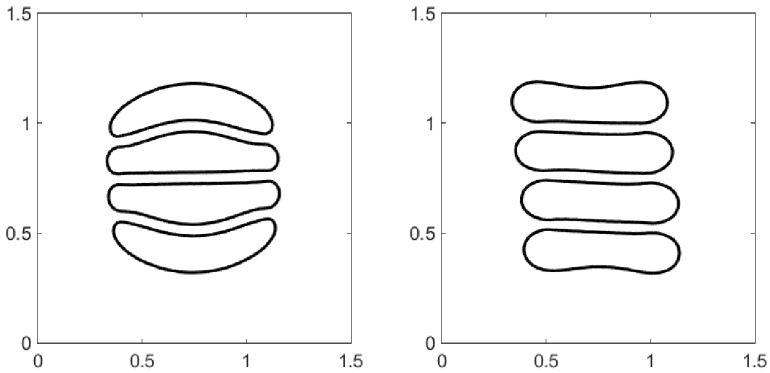

Figure 5.11: Left: Strong aggregate $\alpha = 15 \times 10^3, q_1 = 1, q_2 = 1$. Right: moderate aggregate $\alpha = 100, q_1 = 1, q_2 = 1$.

From the figure we can see that under strong aggregation force, obvious terminal hemispherical caps is shown and the offset between each adjacent cell is smaller as well. This result fits the experimental phenomenon observed well[80]. In the following test we set the cells on a Couette flow with shear rate equal to 20^{-s}. The motion of the cells are shown in figure 5.12. This result is consistent with the sharp interface model reported in [173].

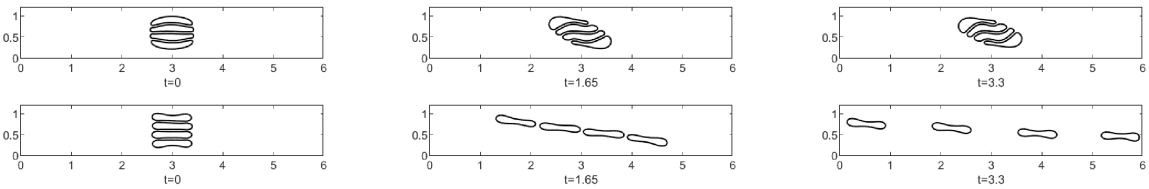

Figure 5.12: The top three figures shows the motion of the cells with strong aggregation. The bottom three figures shows the motion under moderate aggregation.

5.4.4 Red blood cell motion at bifurcation

In this part, we simulate the red blood cells' motion in branched vessel. 4 cells are initially set in the Y shaped branch. The width of the main channel and the bottom branch of the vessel is set to be 1×10^{-7} meter and the top branch is 0.7×10^{-7} meter, which is close to the size of red blood cell. A pressure drop is applied to the channel inducing a shear flow in the vessel with the velocity around $5 \times 10^{-4} m/s$, which is close to the blood flow in capillaries. Other parameters are shown below: $Re = 2 \times 10^{-4}, \mathscr{M} = 5 \times 10^{-4}, \kappa_B = 4 \times 10^{-2}, k = 4 \times 10^{-11}, l_s = 2 = 5 \times 10^{-6}, \mathscr{M}_s = 20$. The motion of the cells and the velocity field of the flow are shown in Figure 5.14, 5.15, 5.13. We firstly test the motion of the cell group with moderate aggregation force when they pass a Y-shaped channel with the same width of the both branches. The cells divide equally at the bifurcation. Then one of the channel is widen and we observe a non-equal deviation. Finally, a strong aggregation force is applied to the cells and we could observe that all of the cells goes into the wider channel.

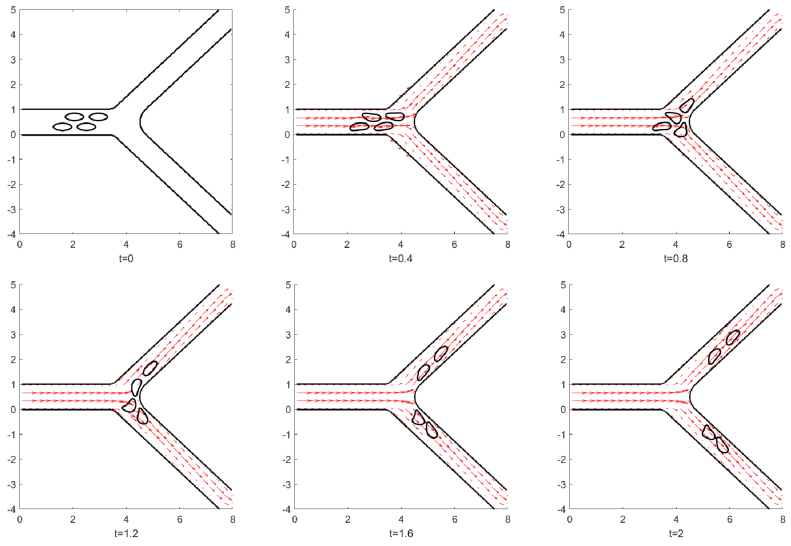

Figure 5.13: Cells are set in a cluster initially under a moderate aggregating force with $\alpha = 25, q_1 = 1, q_2 = 1$.The main channel width is 1 and the branches width is 0.7 cells divide equally. The velocity field is shown as well.

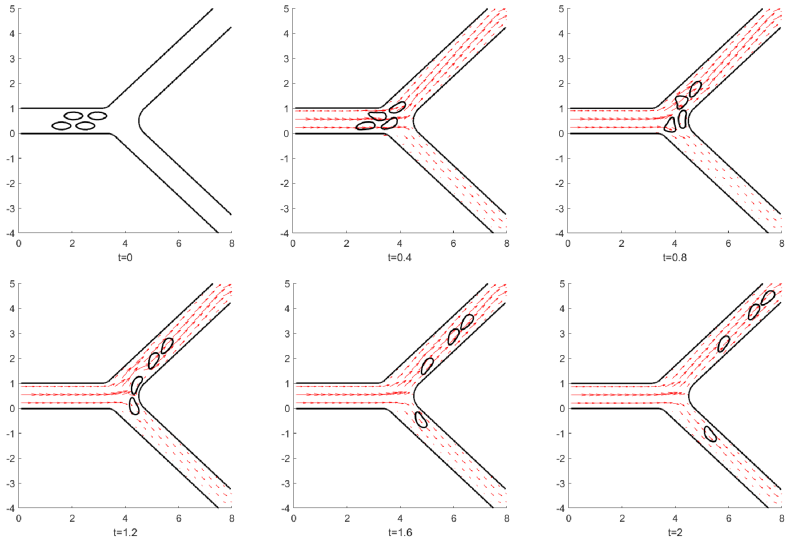

Figure 5.14: Cells are set in a cluster initially under a moderate aggregating force with $\alpha = 25, q_1 = 1, q_2 = 1$. The top branch is set to be 1 with the other stays 0.7. One of the cells is going into the branched vessel. The velocity field is shown as well.

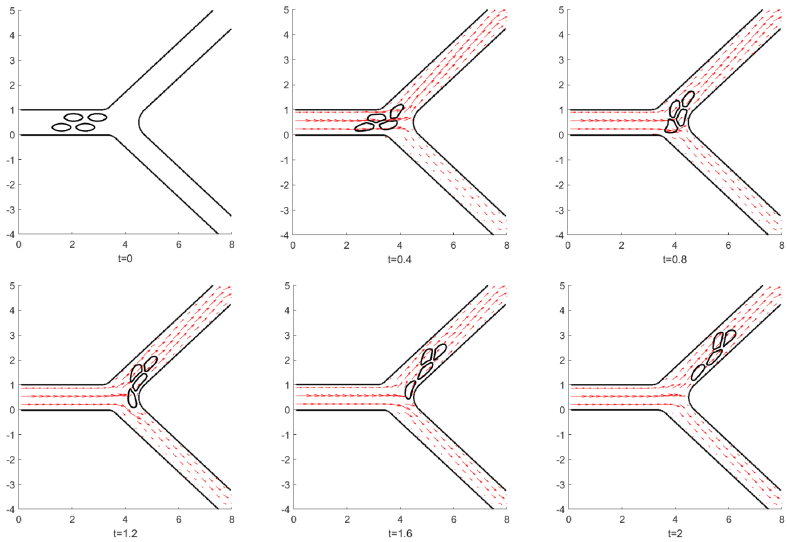

Figure 5.15: Cells are set in a cluster initially under a strong aggregating force with $\alpha = 1.5 \times 10^3, 1_1 = 1, Q_2 = 1$. The set up is the same as Figure 5.14. None of the cells is going into the branched vessel. The velocity field is shown as well.

The simulation result explains the experimental result in [80], which a great number of red blood cells are observed to be absent in the branched vessel under strong aggregate case compared with moderate aggregate.

5.5 Conclusion

Based on last chapter, a more powerful model is established in this chapter which is able to simulate the interaction between vesicles and overcome the shortage of vesicle-wall interaction.

Same as before, energy variational method is used to derive a thermodynamically consistent phase-field model.Chan-Hilliard type interface is applied instead of Allen-Cahn type interface. Interaction energy of different vesicle phase is included to describe the vesicle-vesicle interaction. GNBC boundary conditions are modified with contact angle term removed. Instead, a wall phase is introduced in the domain together with the corresponding energy that describes the vesicle-wall adhesion.

Then C^0 finite element spatial discretization and the mid-point temporal discretization is still used to derive the unconditionally energy stable discrete scheme. Simulations of the vesicle nonlinear deformation reproduce experimental observations. The red blood cell aggregation test is also highly consistent with published experiment. And the simulation of the red blood cell motion in branched vessel well explains the phenomenon recorded in the lab.

The model can be used in the study of hemodynamics especially in terms of the problems need to consider the interaction between cells and vessel wall like growth of the blood clot and platelet agglutination.

Chapter 6

Conclusion and Future Works

In this thesis, we first establish a phase field model of moving contact line coupled with general Navier boundary condition. A quasi-incompressible Chan-Hilliard type interface is used in order to describe large density difference of different phases. The interface is described using a diffusion equation. Combined with Navier-Stokes equation, the governing equations of the system is established. Energy variational method is used to derive the equations based on some assumptions of the system energy. Thus the energy decaying law can be proof easily. Then a C^0 finite element scheme is given together with the discrete energy law. Finally, numerical simulations are applied and the results shows model performs well in large density difference condition.

Based on the study of moving contact line, we model biological membrane using a diffuse interface. An Allan-Chan type interface model using phase field method is established and coupled with GNBC. Same as previous, energy variational method is still used in the derivation. A C^0 fintie element scheme with second order convergence rate using Crank-Nicloson method is given together with the energy law. In the numerical test, the new model works well in showing the motion and large deformation of the vesicle. The results fits the experimental data on red blood cells well. However, the model has a limitation in dealing with wall adhesion. When the vesicle contacts the wall, the adhesion force is likely to tear the cell apart, which is not consistent with the mechanics. Furthermore, for a better application in hemodynamics, a model which is able to simulate a number of cells is needed, the interaction between cells also requires consideration.

To solve the problem found in the single vesicle model, modification and implement is applied. A Chan-Hilliard-Navier-Stokes system with a modified GNBC is then given in the thesis. In the new model derivation, we treat the wall as a new phase which is defined in the domain, thus the wall adhesion could is treated as a type of energy in the energy variational approach. Furthermore, we added interaction energy of between cells into the derivation. By doing such a modification, we finally establish a multiple vesicle model with the interaction between each other and the adhesion with the wall. continuous and discrete energy law is given as before.

Numerical simulation is carried out using finite element method. From the results we find that the model can well perform in adhesion test and other kinds blood flow simulation which indicates the model proper to be used in hemodynamics research like blood clot growth and red blood cell distribution pattern in blood flow.

In future works, we plan to expand the model into 3-dimensional thus more complicated cases can be studied which is more close to real condition. In multiple vesicle model, the wall is treated as a independent phase, which brings the idea that the visco-elastic model can be introduced in the system to describe the dynamcs of the vessel wall. Then a more complex model would be established to perform much more simulations and research in the blood flow related problem.

Bibliography

[1] Helmut Abels, Harald Garcke and Günther Grün. “Thermodynamically consistent diffuse interface models for incompressible two-phase flows with different densities”. In: *arXiv preprint arXiv:1011.0528* (2010).

[2] Helmut Abels, Harald Garcke and Günther Grün. “Thermodynamically consistent, frame indifferent diffuse interface models for incompressible two-phase flows with different densities”. In: *Mathematical Models and Methods in Applied Sciences* 22.03 (2012), p. 1150013.

[3] Sebastian Aland et al. “Diffuse interface models of locally inextensible vesicles in a viscous fluid”. In: *Journal of computational physics* 277 (2014), pp. 32–47.

[4] Yunus Alapan, Jane A Little and Umut A Gurkan. “Heterogeneous red blood cell adhesion and deformability in sickle cell disease”. In: *Scientific reports* 4.1 (2014), pp. 1–8.

[5] Chérif Amrouche and Ahmed Rejaiba. “Lp-theory for Stokes and Navier–Stokes equations with Navier boundary condition”. In: *Journal of Differential Equations* 256.4 (2014), pp. 1515–1547.

[6] Daniel M Anderson, Geoffrey B McFadden and Adam A Wheeler. “Diffuse-interface methods in fluid mechanics”. In: *Annual review of fluid mechanics* 30.1 (1998), pp. 139–165.

[7] Joseph E Aslan et al. “Platelet shape change and spreading”. In: *Platelets and Megakaryocytes*. Springer, 2012, pp. 91–100.

[8] Kai Bao et al. “A finite element method for the numerical solution of the coupled Cahn–Hilliard and Navier–Stokes system for moving contact line problems”. In: *Journal of Computational Physics* 231.24 (2012), pp. 8083–8099.

[9] Gilda A Barabino, Manu O Platt and Dhananjay K Kaul. “Sickle cell biomechanics”. In: *Annual review of biomedical engineering* 12 (2010), pp. 345–367.

[10] Himanish Basu et al. “Tank treading of optically trapped red blood cells in shear flow”. In: *Biophysical journal* 101.7 (2011), pp. 1604–1612.

[11] Julien Beaucourt et al. “Steady to unsteady dynamics of a vesicle in a flow”. In: *Physical Review E* 69.1 (2004), p. 011906.

[12] Andrea Bonito, Ricardo H Nochetto and M Sebastian Pauletti. “Parametric FEM for geometric biomembranes”. In: *Journal of Computational Physics* 229.9 (2010), pp. 3171–3188.

[13] Daniel Bonn et al. “Wetting and spreading”. In: *Reviews of modern physics* 81.2 (2009), p. 739.

[14] Franck Boyer. “Nonhomogeneous Cahn–Hilliard fluids”. In: *Annales de l’Institut Henri Poincaré C* 18.2 (2001), pp. 225–259.

[15] Jan Breitenbach, Ilia V Roisman and Cameron Tropea. “From drop impact physics to spray cooling models: a critical review”. In: *Experiments in Fluids* 59.3 (2018), pp. 1–21.

[16] Franco Brezzi and Juhani Pitkäranta. “On the stabilization of finite element approximations of the Stokes equations”. In: *Efficient solutions of elliptic systems*. Springer, 1984, pp. 11–19.

[17] Victor I Burenkov. *Sobolev spaces on domains*. Vol. 137. Springer, 1998.

[18] G Caimi and R Lo Presti. “Techniques to evaluate erythrocyte deformability in diabetes mellitus”. In: *Acta diabetologica* 41.3 (2004), pp. 99–103.

[19] Rui Chen et al. “Decoupled energy stable schemes for phase-field vesicle membrane model”. In: *Journal of Computational Physics* 302 (2015), pp. 509–523.

[20] TJ Chung. “Finite element analysis in fluid dynamics”. In: *NASA STI/Recon Technical Report A* 78 (1978), p. 44102.

[21] Philippe G Ciarlet. *Introduction to linear shell theory*. Vol. 98. Elsevier Masson, 1998.

[22] Yamicia Connor et al. “A mathematical model of tumor-endothelial interactions in a 3D co-culture”. In: *Scientific Reports* 9.1 (2019), pp. 1–14.

[23] Stephen H Davis et al. “On the motion of a fluid-fluid interface along a solid surface”. In: *Journal of Fluid Mechanics* 65.1 (1974), pp. 71–95.

[24] Yixiang Deng et al. “Quantifying fibrinogen-dependent aggregation of red blood cells in type 2 diabetes mellitus”. In: *Biophysical journal* 119.5 (2020), pp. 900–912.

[25] Hang Ding, Peter DM Spelt and Chang Shu. “Diffuse interface model for incompressible two-phase flows with large density ratios”. In: *Journal of Computational Physics* 226.2 (2007), pp. 2078–2095.

[26] Suchuan Dong and Jie Shen. “A time-stepping scheme involving constant coefficient matrices for phase-field simulations of two-phase incompressible flows with large density ratios”. In: *Journal of Computational Physics* 231.17 (2012), pp. 5788–5804.

[27] Qiang Du, Chun Liu and Xiaoqiang Wang. “A phase field approach in the numerical study of the elastic bending energy for vesicle membranes”. In: *Journal of Computational Physics* 198.2 (2004), pp. 450–468.

[28] Qiang Du, Chun Liu and Xiaoqiang Wang. “Retrieving topological information for phase field models”. In: *SIAM Journal on Applied Mathematics* 65.6 (2005), pp. 1913–1932.

[29] Qiang Du and Jian Zhang. “Adaptive finite element method for a phase field bending elasticity model of vesicle membrane deformations”. In: *SIAM Journal on Scientific Computing* 30.3 (2008), pp. 1634–1657.

[30] Qiang Du et al. “A phase field formulation of the Willmore problem”. In: *Nonlinearity* 18.3 (2005), p. 1249.

[31] Qiang Du et al. “Modeling the spontaneous curvature effects in static cell membrane deformations by a phase field formulation”. In: *Communications on Pure & Applied Analysis* 4.3 (2005), p. 537.

[32] Qiang Du et al. “Energetic variational approaches in modeling vesicle and fluid interactions”. In: *Physica D: Nonlinear Phenomena* 238.9-10 (2009), pp. 923–930.

[33] EB Dussan. “On the spreading of liquids on solid surfaces: static and dynamic contact lines”. In: *Annual Review of Fluid Mechanics* 11.1 (1979), pp. 371–400.

[34] M ten Eikelder et al. “Unified analysis of Navier-Stokes Cahn-Hilliard models with non-matching densities”. In: *arXiv preprint arXiv:2110.11912* (2021).

[35] Bob Eisenberg, Yunkyong Hyon and Chun Liu. “Energy variational analysis of ions in water and channels: Field theory for primitive models of complex ionic fluids”. In: *The Journal of Chemical Physics* 133.10 (2010), p. 104104.

[36] David J Eyre. “Unconditionally gradient stable time marching the Cahn-Hilliard equation”. In: *MRS Online Proceedings Library (OPL)* 529 (1998).

[37] Dmitry A Fedosov, Hiroshi Noguchi and Gerhard Gompper. “Multiscale modeling of blood flow: from single cells to blood rheology”. In: *Biomechanics and modeling in mechanobiology* 13.2 (2014), pp. 239–258.

[38] James J Feng et al. “An energetic variational formulation with phase field methods for interfacial dynamics of complex fluids: advantages and challenges”. In: *Modeling of soft matter*. Springer, 2005, pp. 1–26.

[39] Tuba Firincioglu, Erdal Ozkan and Chet Ozgen. “Thermodynamics of multiphase flow in unconventional liquids-rich reservoirs”. In: *SPE Annual Technical Conference and Exhibition*. OnePetro. 2012.

[40] Thomas M Fischer. “Shape memory of human red blood cells”. In: *Biophysical journal* 86.5 (2004), pp. 3304–3313.

[41] Daniel Flormann et al. “The buckling instability of aggregating red blood cells”. In: *Scientific reports* 7.1 (2017), pp. 1–10.

[42] Aaron L Fogelson and Keith B Neeves. “Fluid mechanics of blood clot formation”. In: *Annual review of fluid mechanics* 47 (2015), pp. 377–403.

[43] Yanbiao Gan et al. “Discrete Boltzmann modeling of multiphase flows: Hydrodynamic and thermodynamic non-equilibrium effects”. In: *Soft Matter* 11.26 (2015), pp. 5336–5345.

[44] Min Gao and Xiao-Ping Wang. “A gradient stable scheme for a phase field model for the moving contact line problem”. In: *Journal of Computational Physics* 231.4 (2012), pp. 1372–1386.

[45] Min Gao and Xiao-Ping Wang. “An efficient scheme for a phase field model for the moving contact line problem with variable density and viscosity”. In: *Journal of Computational Physics* 272 (2014), pp. 704–718.

[46] Alf Gerisch and Mark AJ Chaplain. “Mathematical modelling of cancer cell invasion of tissue: local and non-local models and the effect of adhesion”. In: *Journal of Theoretical Biology* 250.4 (2008), pp. 684–704.

[47] Mi-Ho Giga, Arkadz Kirshtein and Chun Liu. “Variational modeling and complex fluids”. In: *Handbook of mathematical analysis in mechanics of viscous fluids* (2017), pp. 1–41.

[48] Rui Gu, Xiaoqiang Wang and M Gunzburger. “Simulating vesicle–substrate adhesion using two phase field functions”. In: *Journal of Computational Physics* 275 (2014), pp. 626–641.

[49] Rui Gu, Xiaoqiang Wang and Max Gunzburger. “A two phase field model for tracking vesicle–vesicle adhesion”. In: *Journal of mathematical biology* 73.5 (2016), pp. 1293–1319.

[50] Rui Gu, Xiaoqiang Wang and Max Gunzburger. “A two phase field model for tracking vesicle–vesicle adhesion”. In: *Journal of mathematical biology* 73.5 (2016), pp. 1293–1319.

[51] Francisco Guillén-González and Giordano Tierra. “Unconditionally energy stable numerical schemes for phase-field vesicle membrane model”. In: *Journal of computational physics* 354 (2018), pp. 67–85.

[52] Zhenlin Guo and Ping Lin. “A thermodynamically consistent phase-field model for two-phase flows with thermocapillary effects”. In: *Journal of Fluid Mechanics* 766 (2015), pp. 226–271.

[53] Zhenlin Guo, Ping Lin and John S Lowengrub. “A numerical method for the quasi-incompressible Cahn–Hilliard–Navier–Stokes equations for variable density flows with a discrete energy law”. In: *Journal of Computational Physics* 276 (2014), pp. 486–507.

[54] Zhenlin Guo et al. “Mass conservative and energy stable finite difference methods for the quasi-incompressible Navier–Stokes–Cahn–Hilliard system: Primitive variable and projection-type schemes”. In: *Computer Methods in Applied Mechanics and Engineering* 326 (2017), pp. 144–174.

[55] Zhenlin Guo et al. “A diffuse domain method for two-phase flows with large density ratio in complex geometries”. In: *Journal of Fluid Mechanics* 907 (2021).

[56] Morton E Gurtin, Eliot Fried and Lallit Anand. *The mechanics and thermodynamics of continua*. Cambridge University Press, 2010.

[57] Morton E Gurtin, Debra Polignone and Jorge Vinals. “Two-phase binary fluids and immiscible fluids described by an order parameter”. In: *Mathematical Models and Methods in Applied Sciences* 6.06 (1996), pp. 815–831.

[58] Nicolas G Hadjiconstantinou. “Hybrid atomistic–continuum formulations and the moving contact-line problem”. In: *Journal of Computational physics* 154.2 (1999), pp. 245–265.

[59] Yunlong Han et al. “Flow-induced translocation of vesicles through a narrow pore”. In: *Soft matter* 15.16 (2019), pp. 3307–3314.

[60] Wenrui Hao et al. “A fictitious domain method with a hybrid cell model for simulating motion of cells in fluid flow”. In: *Journal of Computational Physics* 280 (2015), pp. 345–362.

[61] Ping He and Ahmed F Ghoniem. “A sharp interface method for coupling multiphase flow, heat transfer and multicomponent mass transfer with interphase diffusion”. In: *Journal of Computational Physics* 332 (2017), pp. 316–332.

[62] Xiaoyi He and Gary D Doolen. “Thermodynamic foundations of kinetic theory and lattice Boltzmann models for multiphase flows”. In: *Journal of Statistical Physics* 107.1 (2002), pp. 309–328.

[63] Frédéric Hecht. “New development in FreeFem++”. In: *Journal of numerical mathematics* 20.3-4 (2012), pp. 251–266.

[64] Peter Höök et al. “Strong binding of platelet integrin αIIbβ3 to fibrin clots: Potential target to destabilize thrombi”. In: *Scientific reports* 7.1 (2017), pp. 1–8.

[65] Thomas Y Hou, John S Lowengrub and Michael J Shelley. “Boundary integral methods for multicomponent fluids and multiphase materials”. In: *Journal of Computational Physics* 169.2 (2001), pp. 302–362.

[66] Dan Hu, Pingwen Zhang and E Weinan. “Continuum theory of a moving membrane”. In: *Physical Review E* 75.4 (2007), p. 041605.

[67] Wei-Fan Hu et al. “Vesicle electrohydrodynamic simulations by coupling immersed boundary and immersed interface method”. In: *Journal of Computational Physics* 317 (2016), pp. 66–81.

[68] Zhengzheng Hu et al. “Stable and efficient finite-difference nonlinear-multigrid schemes for the phase field crystal equation”. In: *Journal of Computational Physics* 228.15 (2009), pp. 5323–5339.

[69] Jinsong Hua, Ping Lin and Jan F Stene. “Numerical simulation of gas bubbles rising in viscous liquids at high Reynolds number”. In: *Moving interface problems and applications in fluid dynamics, contemporary mathematics* 466 (2008), pp. 17–34.

[70] Jinsong Hua et al. “Energy law preserving C0 finite element schemes for phase field models in two-phase flow computations”. In: *Journal of Computational Physics* 230.19 (2011), pp. 7115–7131.

[71] Jizu Huang and Xiao-Ping Wang. “A lattice Boltzmann model for multiphase flows with moving contact line and variable density”. In: *Journal of Computational Physics* 353 (2018), pp. 26–45.

[72] Yunkyong Hyon, Chun Liu et al. “Energetic variational approach in complex fluids: maximum dissipation principle”. In: *Discrete & Continuous Dynamical Systems* 26.4 (2010), p. 1291.

[73] David Jacqmin. “Calculation of two-phase Navier–Stokes flows using phase-field modeling”. In: *Journal of computational physics* 155.1 (1999), pp. 96–127.

[74] George Barker Jeffery. “The motion of ellipsoidal particles immersed in a viscous fluid”. In: *Proceedings of the Royal Society of London. Series A, Containing papers of a mathematical and physical character* 102.715 (1922), pp. 161–179.

[75] James T Jenkins. “The equations of mechanical equilibrium of a model membrane”. In: *SIAM Journal on Applied Mathematics* 32.4 (1977), pp. 755–764.

[76] J Jiang, K Garikipati and S Rudraraju. “A diffuse interface framework for modeling the evolution of multi-cell aggregates as a soft packing problem driven by the growth and division of cells”. In: *Bulletin of mathematical biology* 81.8 (2019), pp. 3282–3300.

[77] Yongyue Jiang et al. “Numerical simulation for moving contact line with continuous finite element schemes”. In: *Communications in Computational Physics* 18.1 (2015), pp. 180–202.

[78] Jonghwun Jung, Ahmed Hassanein and Robert W Lyczkowski. “Hemodynamic computation using multiphase flow dynamics in a right coronary artery”. In: *Annals of biomedical engineering* 34.3 (2006), pp. 393–407.

[79] Yongsam Kim and Ming-Chih Lai. “Simulating the dynamics of inextensible vesicles by the penalty immersed boundary method”. In: *Journal of Computational Physics* 229.12 (2010), pp. 4840–4853.

[80] Thomas Kirschkamp et al. “Effects of Fibrinogen and α2-Macroglobulin and Their Apheretic Elimination on General Blood Rheology and Rheological Characteristics of Red Blood Cell Aggregates”. In: *Therapeutic Apheresis and Dialysis* 12.5 (2008), pp. 360–367.

[81] Ebrahim M Kolahdouz and David Salac. “A numerical model for the trans-membrane voltage of vesicles”. In: *Applied Mathematics Letters* 39 (2015), pp. 7–12.

[82] Joel Koplik, Jayanth R Banavar and Jorge F Willemsen. “Molecular dynamics of Poiseuille flow and moving contact lines”. In: *Physical review letters* 60.13 (1988), p. 1282.

[83] Joel Koplik, Jayanth R Banavar and Jorge F Willemsen. “Molecular dynamics of fluid flow at solid surfaces”. In: *Physics of Fluids A: Fluid Dynamics* 1.5 (1989), pp. 781–794.

[84] Satish Kumar. “Liquid transfer in printing processes: Liquid bridges with moving contact lines”. In: *Annual Review of Fluid Mechanics* 47 (2015), pp. 67–94.

[85] Aymen Laadhari, Pierre Saramito and Chaouqi Misbah. “Vesicle tumbling inhibited by inertia”. In: *Physics of Fluids* 24.3 (2012), p. 031901.

[86] Ming-Chih Lai, Yu-Hau Tseng, Huaxiong Huang et al. “Numerical simulation of moving contact lines with surfactant by immersed boundary method”. In: *Communications in Computational Physics* 8.4 (2010), p. 735.

[87] Kisung Lee et al. “Optical tweezers study of red blood cell aggregation and disaggregation in plasma and protein solutions”. In: *Journal of biomedical optics* 21.3 (2016), p. 035001.

[88] Na Li, Ping Lin and Gao Fuzheng. “The SAV finite element method for the Cahn-Hilliard equation with dynamic boundary conditions”. In: *Computational and Applied Mathematics, Submitted* (2021).

[89] Zhen Li et al. “A dissipative particle dynamics method for arbitrarily complex geometries”. In: *Journal of Computational Physics* 355 (2018), pp. 534–547.

[90] Ping Lin. “A sequential regularization method for time-dependent incompressible Navier–Stokes equations”. In: *SIAM journal on numerical analysis* 34.3 (1997), pp. 1051–1071.

[91] Ping Lin, Xianqiao Chen and Ming Tze Ong. “Finite element methods based on a new formulation for the non-stationary incompressible Navier–Stokes equations”. In: *International journal for numerical methods in fluids* 46.12 (2004), pp. 1169–1180.

[92] Ping Lin and Chun Liu. “Simulations of singularity dynamics in liquid crystal flows: a C0 finite element approach”. In: *Journal of Computational Physics* 215.1 (2006), pp. 348–362.

[93] Chun Liu and Jie Shen. “A phase field model for the mixture of two incompressible fluids and its approximation by a Fourier-spectral method”. In: *Physica D: Nonlinear Phenomena* 179.3-4 (2003), pp. 211–228.

[94] Chun Liu, Jie Shen and Xiaofeng Yang. “Decoupled energy stable schemes for a phase-field model of two-phase incompressible flows with variable density”. In: *Journal of Scientific Computing* 62.2 (2015), pp. 601–622.

[95] Chun Liu and Yiwei Wang. “A variational Lagrangian scheme for a phase-field model: A discrete energetic variational approach”. In: *SIAM Journal on Scientific Computing* 42.6 (2020), B1541–B1569.

[96] Chun Liu and Hao Wu. “An energetic variational approach for the Cahn–Hilliard equation with dynamic boundary condition: model derivation and mathematical analysis”. In: *Archive for Rational Mechanics and Analysis* 233.1 (2019), pp. 167–247.

[97] Xiaoling Liu, Fangying Song and Chuanju Xu. “An efficient spectral method for the inextensible immersed interface in incompressible flows”. In: *Commun. Comput. Phys.* 25.4 (2019), pp. 1071–1096.

[98] Yaling Liu and Wing Kam Liu. “Rheology of red blood cell aggregation by computer simulation”. In: *Journal of Computational Physics* 220.1 (2006), pp. 139–154.

[99] John Lowengrub and Lev Truskinovsky. “Quasi–incompressible Cahn–Hilliard fluids and topological transitions”. In: *Proceedings of the Royal Society of London. Series A: Mathematical, Physical and Engineering Sciences* 454.1978 (1998), pp. 2617–2654.

[100] John S Lowengrub, Andreas Rätz and Axel Voigt. “Phase-field modeling of the dynamics of multicomponent vesicles: Spinodal decomposition, coarsening, budding, and fission”. In: *Physical Review E* 79.3 (2009), p. 031926.

[101] Li Luo, Xiao-Ping Wang and Xiao-Chuan Cai. “An efficient finite element method for simulation of droplet spreading on a topologically rough surface”. In: *Journal of Computational Physics* 349 (2017), pp. 233–252.

[102] Roy Malka, David M Nathan and John M Higgins. “Mechanistic modeling of hemoglobin glycation and red blood cell kinetics enables personalized diabetes monitoring”. In: *Science translational medicine* 8.359 (2016), 359ra130–359ra130.

[103] Wieland Marth, Sebastian Aland and Axel Voigt. “Margination of white blood cells: a computational approach by a hydrodynamic phase field model”. In: *Journal of Fluid Mechanics* 790 (2016), pp. 389–406.

[104] Nader Masmoudi and Frédéric Rousset. “Uniform regularity for the Navier–Stokes equation with Navier boundary condition”. In: *Archive for Rational Mechanics and Analysis* 203.2 (2012), pp. 529–575.

[105] JP Mills et al. “Nonlinear elastic and viscoelastic deformation of the human red blood cell with optical tweezers”. In: *Molecular & Cellular Biomechanics* 1.3 (2004), p. 169.

[106] Rajat Mittal and Gianluca Iaccarino. “Immersed boundary methods”. In: *Annu. Rev. Fluid Mech.* 37 (2005), pp. 239–261.

[107] Arman Namvar et al. “Surface area-to-volume ratio, not cellular viscoelasticity, is the major determinant of red blood cell traversal through small channels”. In: *Cellular microbiology* 23.1 (2021), e13270.

[108] Kian Chuan Ong and Ming-Chih Lai. “An immersed boundary projection method for simulating the inextensible vesicle dynamics”. In: *Journal of Computational Physics* 408 (2020), p. 109277.

[109] Stanley Osher and Ronald P Fedkiw. “Level set methods: an overview and some recent results”. In: *Journal of Computational physics* 169.2 (2001), pp. 463–502.

[110] Igor V Pivkin and George Em Karniadakis. “Accurate coarse-grained modeling of red blood cells”. In: *Physical review letters* 101.11 (2008), p. 118105.

[111] Igor V Pivkin, Peter D Richardson and George Em Karniadakis. “Effect of red blood cells on platelet aggregation”. In: *IEEE Engineering in Medicine and Biology Magazine* 28.2 (2009), pp. 32–37.

[112] Johannes MB Pöschl et al. “Endotoxin binding to erythrocyte membrane and erythrocyte deformability in human sepsis and in vitro”. In: *Critical care medicine* 31.3 (2003), pp. 924–928.

[113] C Pozrikidis. “Effect of inertia on the Marangoni instability of two-layer channel flow, Part I: numerical simulations”. In: *Journal of engineering mathematics* 50.2 (2004), pp. 311–327.

[114] Karsten Pruess and Julio Garcia. “Multiphase flow dynamics during CO2 disposal into saline aquifers”. In: *Environmental Geology* 42.2 (2002), pp. 282–295.

[115] Tiezheng Qian, Xiao-Ping Wang and Ping Sheng. “Molecular scale contact line hydrodynamics of immiscible flows”. In: *Physical Review E* 68.1 (2003), p. 016306.

[116] Tiezheng Qian, Xiao-Ping Wang and Ping Sheng. “A variational approach to moving contact line hydrodynamics”. In: *Journal of Fluid Mechanics* 564 (2006), pp. 333–360.

[117] Yuzhe Qin et al. “A phase field model for mass transport with semi-permeable interfaces”. In: *arXiv preprint arXiv:2103.06430* (2021).

[118] Bryan Quaife, Shravan Veerapaneni and Y-N Young. “Hydrodynamics and rheology of a vesicle doublet suspension”. In: *Physical Review Fluids* 4.10 (2019), p. 103601.

[119] P Raghu, Amirtham Rajagopal and JN Reddy. “Thermodynamically consistent variational approach for modeling brittle fracture in thick plates by a hybrid phase field model”. In: *Journal of Applied Mechanics* 87.2 (2020).

[120] Rolf Rannacher. “On the Numerical Solution of the Incompressible Navier-Stokes Equations”. In: *ZAMM-Journal of Applied Mathematics and Mechanics/Zeitschrift für Angewandte Mathematik und Mechanik* 73.9 (1993), pp. 203–216.

[121] Junuthula Narasimha Reddy. *Introduction to the finite element method*. McGraw-Hill Education, 2019.

[122] Weiqing Ren and Weinan E. “Boundary conditions for the moving contact line problem”. In: *Physics of fluids* 19.2 (2007), p. 022101.

[123] Weiqing Ren, Dan Hu and Weinan E. “Continuum models for the contact line problem”. In: *Physics of fluids* 22.10 (2010), p. 102103.

[124] Weiqing Ren and E Weinan. “Heterogeneous multiscale method for the modeling of complex fluids and micro-fluidics”. In: *Journal of Computational Physics* 204.1 (2005), pp. 1–26.

[125] Céline Renoux et al. “Impact of surface-area-to-volume ratio, internal viscosity and membrane viscoelasticity on red blood cell deformability measured in isotonic condition”. In: *Scientific reports* 9.1 (2019), pp. 1–7.

[126] P Rodriguez et al. “A variational approach to the phase field modeling of brittle and ductile fracture”. In: *International Journal of Mechanical Sciences* 144 (2018), pp. 502–517.

[127] David Salac and Michael Miksis. “A level set projection model of lipid vesicles in general flows”. In: *Journal of Computational Physics* 230.22 (2011), pp. 8192–8215.

[128] Abner J Salgado. “A diffuse interface fractional time-stepping technique for incompressible two-phase flows with moving contact lines”. In: *ESAIM: Mathematical Modelling and Numerical Analysis* 47.3 (2013), pp. 743–769.

[129] Nicholas J Savill and Paulien Hogeweg. “Modelling morphogenesis: from single cells to crawling slugs”. In: *Journal of theoretical biology* 184.3 (1997), pp. 229–235.

[130] Ruben Scardovelli and Stéphane Zaleski. “Direct numerical simulation of free-surface and interfacial flow”. In: *Annual review of fluid mechanics* 31.1 (1999), pp. 567–603.

[131] Yunchang Seol et al. “An immersed boundary method for simulating vesicle dynamics in three dimensions”. In: *Journal of Computational Physics* 322 (2016), pp. 125–141.

[132] Jie Shen. “On pressure stabilization method and projection method for unsteady Navier-Stokes equations”. In: *Advances in Computer Methods for Partial Differential Equations*. Citeseer. 1992.

[133] Jie Shen and Jie Xu. “Convergence and error analysis for the scalar auxiliary variable (SAV) schemes to gradient flows”. In: *SIAM Journal on Numerical Analysis* 56.5 (2018), pp. 2895–2912.

[134] Jie Shen, Jie Xu and Jiang Yang. “The scalar auxiliary variable (SAV) approach for gradient flows”. In: *Journal of Computational Physics* 353 (2018), pp. 407–416.

[135] Jie Shen and Xiaofeng Yang. “A phase-field model and its numerical approximation for two-phase incompressible flows with different densities and viscosities”. In: *SIAM Journal on Scientific Computing* 32.3 (2010), pp. 1159–1179.

[136] Jie Shen and Xiaofeng Yang. “Energy stable schemes for Cahn-Hilliard phase-field model of two-phase incompressible flows”. In: *Chinese Annals of Mathematics, Series B* 31.5 (2010), pp. 743–758.

[137] Jie Shen and Xiaofeng Yang. “Decoupled, energy stable schemes for phase-field models of two-phase incompressible flows”. In: *SIAM Journal on Numerical Analysis* 53.1 (2015), pp. 279–296.

[138] Jie Shen, Xiaofeng Yang and Qi Wang. “Mass and volume conservation in phase field models for binary fluids”. In: *Communications in Computational Physics* 13.4 (2013), pp. 1045–1065.

[139] Jie Shen, Xiaofeng Yang and Haijun Yu. “Efficient energy stable numerical schemes for a phase field moving contact line model”. In: *Journal of Computational Physics* 284 (2015), pp. 617–630.

[140] Lingyue Shen et al. “An energy stable C0 finite element scheme for a quasi-incompressible phase-field model of moving contact line with variable density”. In: *Journal of Computational Physics* 405 (2020), p. 109179.

[141] Lingyue Shen et al. “An Energy Stable Cˆ0 Finite Element Scheme for A Phase-Field Model of Vesicle Motion and Deformation”. In: *SIAM Journal on Scientific Computing* 44.1 (2022), B122–B145.

[142] Lingyue Shen et al. “Thermodynamically Consistent Diffuse Interface Model for Cell Adhesion and Aggregation”. In: *arXiv preprint arXiv:2205.07190* (2022).

[143] Eun-Kyung Shin et al. “Platelet shape changes and cytoskeleton dynamics as novel therapeutic targets for anti-thrombotic drugs”. In: *Biomolecules & therapeutics* 25.3 (2017), p. 223.

[144] Farid Smaı. “A thermodynamic formulation for multiphase compositional flows in porous media”. In: (2020).

[145] Edward R Smith et al. “Moving contact lines: Linking molecular dynamics and continuum-scale modeling”. In: *Langmuir* 34.42 (2018), pp. 12501–12518.

[146] Jacco H Snoeijer and Bruno Andreotti. “Moving contact lines: scales, regimes, and dynamical transitions”. In: *Annual review of fluid mechanics* 45 (2013), pp. 269–292.

[147] Shu Takagi et al. “The deformation of a vesicle in a linear shear flow”. In: (2009).

[148] Naoki Takeishi et al. “Deformation of a red blood cell in a narrow rectangular microchannel”. In: *Micromachines* 10.3 (2019), p. 199.

[149] SJ Tavener and KA Cliffe. “Two-fluid Marangoni–Bénard convection with a deformable interface”. In: *Journal of Computational Physics* 182.1 (2002), pp. 277–300.

[150] Massimiliano Tirone. “Petrological geodynamics of mantle melting II. AlphaMELTS+ Multiphase flow: Dynamic fractional melting”. In: *Frontiers in Earth Science* 6 (2018), p. 18.

[151] Massimiliano Tirone and Jan Sessing. “Petrological geodynamics of mantle melting I. AlphaMELTS+ multiphase flow: Dynamic equilibrium melting, method and results”. In: *Frontiers in Earth Science* 5 (2017), p. 81.

[152] Chih-kuan Tung et al. “A contact line pinning based microfluidic platform for modelling physiological flows”. In: *Lab on a Chip* 13.19 (2013), pp. 3876–3885.

[153] Xiaolong Wang et al. “An immersed boundary method for mass transfer through porous biomembranes under large deformations”. In: *Journal of Computational Physics* 413 (2020), p. 109444.

[154] Steven M Wise, Cheng Wang and John S Lowengrub. “An energy-stable and convergent finite-difference scheme for the phase field crystal equation”. In: *SIAM Journal on Numerical Analysis* 47.3 (2009), pp. 2269–2288.

[155] Hao Wu and Xiang Xu. “Strong solutions, global regularity, and stability of a hydrodynamic system modeling vesicle and fluid interactions”. In: *SIAM Journal on Mathematical Analysis* 45.1 (2013), pp. 181–214.

[156] Tenghu Wu and James J Feng. “Simulation of malaria-infected red blood cells in microfluidic channels: Passage and blockage”. In: *Biomicrofluidics* 7.4 (2013), p. 044115.

[157] Ziheng Wu et al. “Three-dimensional multi-scale model of deformable platelets adhesion to vessel wall in blood flow”. In: *Philosophical Transactions of the Royal Society A: Mathematical, Physical and Engineering Sciences* 372.2021 (2014), p. 20130380.

[158] Jian-Jun Xu and Weiqing Ren. “A level-set method for two-phase flows with moving contact line and insoluble surfactant”. In: *Journal of Computational Physics* 263 (2014), pp. 71–90.

[159] Jian-Jun Xu et al. “A level-set method for interfacial flows with surfactant”. In: *Journal of Computational Physics* 212.2 (2006), pp. 590–616.

[160] Shixin Xu, Mark Alber and Zhiliang Xu. “Three-phase model of visco-elastic incompressible fluid flow and its computational implementation”. In: *Communications in computational physics* 25.2 (2019), p. 586.

[161] Shixin Xu, Ping Sheng and Chun Liu. “An energetic variational approach for ion transport”. In: *Communications in Mathematical Sciences* 12.4 (2014), pp. 779–789.

[162] Shixin Xu et al. “Model predictions of deformation, embolization and permeability of partially obstructive blood clots under variable shear flow”. In: *Journal of the Royal Society Interface* 14.136 (2017), p. 20170441.

[163] Shixin Xu et al. “Osmosis through a semi-permeable membrane: a consistent approach to interactions”. In: *arXiv preprint arXiv:1806.00646* (2018).

[164] Zhiliang Xu et al. “A multiscale model of thrombus development”. In: *Journal of the Royal Society Interface* 5.24 (2008), pp. 705–722.

[165] Zhiliang Xu et al. “Study of blood flow impact on growth of thrombi using a multiscale model”. In: *Soft Matter* 5.4 (2009), pp. 769–779.

[166] Xiaofeng Yang. “Linear, first and second-order, unconditionally energy stable numerical schemes for the phase field model of homopolymer blends”. In: *Journal of Computational Physics* 327 (2016), pp. 294–316.

[167] Xiaofeng Yang, Vladimir Mironov and Qi Wang. “Modeling fusion of cellular aggregates in biofabrication using phase field theories”. In: *Journal of theoretical biology* 303 (2012), pp. 110–118.

[168] Xiaofeng Yang and Haijun Yu. “Efficient second order unconditionally stable schemes for a phase field moving contact line model using an invariant energy quadratization approach”. In: *SIAM Journal on Scientific Computing* 40.3 (2018), B889–B914.

[169] Xiaofeng Yang, Jia Zhao and Qi Wang. “Numerical approximations for the molecular beam epitaxial growth model based on the invariant energy quadratization method”. In: *Journal of Computational Physics* 333 (2017), pp. 104–127.

[170] Xiaofeng Yang et al. “Numerical approximations for a three-component Cahn–Hilliard phase-field model based on the invariant energy quadratization method”. In: *Mathematical Models and Methods in Applied Sciences* 27.11 (2017), pp. 1993–2030.

[171] Haijun Yu and Xiaofeng Yang. “Numerical approximations for a phase-field moving contact line model with variable densities and viscosities”. In: *Journal of Computational Physics* 334 (2017), pp. 665–686.

[172] Pengtao Yue et al. “A diffuse-interface method for simulating two-phase flows of complex fluids”. In: *Journal of Fluid Mechanics* 515 (2004), pp. 293–317.

[173] Junfeng Zhang, Paul C Johnson and Aleksander S Popel. “Red blood cell aggregation and dissociation in shear flows simulated by lattice Boltzmann method”. In: *Journal of biomechanics* 41.1 (2008), pp. 47–55.

[174] Qian Zhang, Tie-Zheng Qian and Xiao-Ping Wang. “Phase field simulation of a droplet impacting a solid surface”. In: *Physics of Fluids* 28.2 (2016), p. 022103.

[175] Zhen Zhang, Shixin Xu and Weiqing Ren. “Derivation of a continuum model and the energy law for moving contact lines with insoluble surfactants”. In: *Physics of Fluids* 26.6 (2014), p. 062103.

[176] Hua Zhou and Robert H Davis. “Axisymmetric thermocapillary migration of two deformable viscous drops”. In: *Journal of colloid and interface science* 181.1 (1996), pp. 60–72.

[177] Primoz Ziherl. “Aggregates of two-dimensional vesicles: Rouleaux, sheets, and convergent extension”. In: *Physical review letters* 99.12 (2007), p. 128102.

[178] Primoz Ziherl and Saša Svetina. “Flat and sigmoidally curved contact zones in vesicle–vesicle adhesion”. In: *Proceedings of the National Academy of Sciences* 104.3 (2007), pp. 761–765.

Appendix A

A.1 Appendix of Chapter 3

A.1.1 Energy Variation Details

For the first term I_1 in (3.16), using the last two equations in Eq.(3.8) yields

$$\begin{aligned}
I_1 &= \frac{d}{dt}\int_\Omega \frac{\rho|\mathbf{u}|^2}{2}d\boldsymbol{x} \\
&= \int_\Omega \frac{1}{2}\frac{\partial \rho}{\partial t}|\mathbf{u}|^2 d\boldsymbol{x} + \int_\Omega \rho \frac{\partial \mathbf{u}}{\partial t}\cdot \mathbf{u} d\boldsymbol{x} \\
&= \int_\Omega \frac{1}{2}\frac{\partial \rho}{\partial t}|\mathbf{u}|^2 d\boldsymbol{x} + \int_\Omega \rho \frac{D\mathbf{u}}{Dt}\cdot \mathbf{u} d\boldsymbol{x} - \int_\Omega (\rho\mathbf{u}\cdot\nabla\mathbf{u})\cdot\mathbf{u} d\boldsymbol{x} \\
&= \int_\Omega \frac{1}{2}\frac{\partial \rho}{\partial t}|\mathbf{u}|^2 d\boldsymbol{x} + \int_\Omega \rho \frac{D\mathbf{u}}{Dt}\cdot \mathbf{u} d\boldsymbol{x} + \int_\Omega \nabla\cdot(\rho\mathbf{u})\frac{|\mathbf{u}|^2}{2} d\boldsymbol{x} \\
&= \int_\Omega (\nabla\cdot(\boldsymbol{\sigma}_\eta + \boldsymbol{\sigma}_c))\cdot\mathbf{u} d\boldsymbol{x} + \int_\Omega p\left(\frac{1}{\rho^2}\frac{d\rho}{dc}\nabla\cdot\boldsymbol{j}_c - \nabla\cdot\mathbf{u}\right) d\boldsymbol{x} \\
&= \int_\Omega (\nabla\cdot(\boldsymbol{\sigma}_\eta + \boldsymbol{\sigma}_c))\cdot\mathbf{u} d\boldsymbol{x} + \int_\Omega p(-\alpha\nabla\cdot\boldsymbol{j}_c - \nabla\cdot\mathbf{u}) d\boldsymbol{x} \\
&= -\int_\Omega (\boldsymbol{\sigma}_\eta : \nabla\mathbf{u} + \boldsymbol{\sigma}_c : \nabla\mathbf{u}) d\boldsymbol{x} + \int_\Omega \nabla(\alpha p)\cdot\boldsymbol{j}_c d\boldsymbol{x} - \int_\Omega p\nabla\cdot\mathbf{u} d\boldsymbol{x} \\
&\quad + \int_{\partial\Omega_w} ((\boldsymbol{\sigma}_\eta + \boldsymbol{\sigma}_c)\cdot\mathbf{n})\cdot\mathbf{u}_\tau dS. \qquad \text{(A.1)}
\end{aligned}$$

where we have introduced a Lagrangian multiplier p with respect to the constraint (3.11) and have used the boundary condition $\mathbf{u}\cdot\mathbf{n} = 0$ and $\boldsymbol{j}_c\cdot\mathbf{n} = 0$.

For the second term I_2 in (3.16), using the first equation in Eq.(3.8) and last two boundary conditions in Eq. (3.12) yields

$$\begin{aligned}
I_2 &= \frac{d}{dt}\int_\Omega \rho\lambda_c\left(G(c) + \frac{\gamma^2}{2}|\nabla c|^2\right) d\boldsymbol{x} \\
&= \int_\Omega \rho\lambda_c \frac{D}{Dt}\left(G + \frac{\gamma^2}{2}|\nabla c|^2\right) d\boldsymbol{x} \\
&= \int_\Omega \rho\lambda_c \frac{dG}{dc}\frac{Dc}{Dt} d\boldsymbol{x} + \int_\Omega \rho\lambda_c\gamma^2\left(\nabla c\cdot\frac{D}{Dt}(\nabla c)\right) d\boldsymbol{x}
\end{aligned}$$

$$
\begin{aligned}
&= \int_\Omega \rho\lambda_c \frac{dG}{dc}\frac{Dc}{Dt}d\boldsymbol{x} + \int_\Omega \rho\lambda_c\gamma^2\left(\nabla c\cdot\left(\frac{\partial}{\partial t}(\nabla c)+(\mathbf{u}\cdot\nabla)(\nabla c)\right)\right)d\boldsymbol{x}\\
&= \int_\Omega \rho\lambda_c \frac{dG}{dc}\frac{Dc}{Dt}d\boldsymbol{x} + \int_\Omega \rho\lambda_c\gamma^2\left(\nabla c\cdot\left(\nabla\frac{\partial c}{\partial t}\right)\right)d\boldsymbol{x} + \int_\Omega \rho\lambda_c\gamma^2(\partial_i c u_j\partial^2_{ji}c)d\boldsymbol{x}\\
&= \int_\Omega \rho\lambda_c \frac{dG}{dc}\frac{Dc}{Dt}d\boldsymbol{x} + \int_\Omega \rho\lambda_c\gamma^2\left(\nabla c\cdot\left(\nabla\frac{\partial c}{\partial t}\right)\right)d\boldsymbol{x}\\
&\quad + \int_\Omega \rho\lambda_c\gamma^2(\partial_i c\partial_i(u_j\partial_j c)-\partial_i c\partial_j c\partial_i u_j)d\boldsymbol{x}\\
&= \int_\Omega \rho\lambda_c \frac{dG}{dc}\frac{Dc}{Dt}d\boldsymbol{x} + \int_\Omega \rho\lambda_c\gamma^2\nabla c\cdot\nabla\left(\frac{Dc}{Dt}\right)d\boldsymbol{x} - \int_\Omega \rho\lambda_c\gamma^2(\nabla c\otimes\nabla c):\nabla\mathbf{u}d\boldsymbol{x}\\
&= \int_\Omega \rho\lambda_c \frac{dG}{dc}\frac{Dc}{Dt}d\boldsymbol{x} - \int_\Omega \nabla\cdot\left(\rho\lambda_c\gamma^2\nabla c\right)\left(\frac{Dc}{Dt}\right)d\boldsymbol{x} - \int_\Omega \rho\lambda_c\gamma^2(\nabla c\otimes\nabla c):\nabla\mathbf{u}d\boldsymbol{x}\\
&\quad + \int_{\partial\Omega_w}\rho\lambda_c\gamma^2\partial_n c\frac{D_\Gamma c}{Dt}dS\\
&= \int_\Omega \rho\mu\frac{Dc}{Dt}d\boldsymbol{x} - \int_\Omega \lambda_c\gamma^2(\rho\nabla c\otimes\nabla c):\nabla\mathbf{u}d\boldsymbol{x} + \int_{\partial\Omega_w}\rho\lambda_c\gamma^2\partial_n c\frac{D_\Gamma c}{Dt}dS\\
&= -\int_\Omega \mu\nabla\cdot\boldsymbol{j}_c d\boldsymbol{x} - \int_\Omega \lambda_c\gamma^2(\rho\nabla c\otimes\nabla c):\nabla\mathbf{u}d\boldsymbol{x} + \int_{\partial\Omega_w}\rho\lambda_c\gamma^2\partial_n c\frac{D_\Gamma c}{Dt}dS\\
&= \int_\Omega \nabla\mu\cdot\boldsymbol{j}_c d\boldsymbol{x} - \int_\Omega \lambda_c\gamma^2(\rho\nabla c\otimes\nabla c):\nabla\mathbf{u}d\boldsymbol{x} + \int_{\partial\Omega_w}\rho\lambda_c\gamma^2\partial_n c\frac{D_\Gamma c}{Dt}dS
\end{aligned}
\tag{A.2}
$$

where $\mu = \lambda_c\left(\frac{dG}{dc} - \frac{1}{\rho}\gamma^2\nabla\cdot(\rho\nabla c)\right)$. Here the boundary condition $\mathbf{u}\cdot\mathbf{n}$ is used.

A.1.2 Proof of Lemma 3.2.1

Proof:

$$
\begin{aligned}
&\frac{d}{dt}\int_\Omega(\rho(\boldsymbol{x},t)f(\boldsymbol{x},t))\,d\boldsymbol{x}\\
&= \int_\Omega \frac{\partial\rho}{\partial t}f + \rho\frac{\partial f}{\partial t}d\boldsymbol{x}\\
&= -\int_\Omega \nabla\cdot(\mathbf{u}\rho)f d\boldsymbol{x} + \int_\Omega \rho\frac{\partial f}{\partial t}d\boldsymbol{x}\\
&= \int_\Omega \rho(\frac{\partial f}{\partial t}+\mathbf{u}\cdot\nabla f)d\boldsymbol{x}\\
&= \int_\Omega \rho\frac{Df}{Dt}d\boldsymbol{x}.
\end{aligned}
\tag{A.3}
$$

A.1.3 Tensor Calculation

$$
\begin{aligned}
& (\nabla \mathbf{u} + (\nabla \mathbf{u})^T) : \nabla \mathbf{u} - \frac{2}{3}(\nabla \cdot \mathbf{u})^2 \\
= & \sum_{i,j=1,2,3} (\partial_i u_j + \partial_j u_i)\partial_j u_i - \frac{2}{3}\sum_{i=1,2,3}(\partial_i u_i)^2 \\
= & \sum_{i=1,2,3} 2(\partial_i u_i)^2 + \sum_{i<j} 2(\partial_i u_j \partial_j u_i) + \sum_{i\neq j}(\partial_i u_j)^2 - \frac{2}{3}\sum_{i=1,2,3}(\partial_i u_i)^2 - \frac{2}{3}\sum_{i<j} 2(\partial_i u_i \partial_j u_j) \\
= & \sum_{i<j}(\partial_i u_j + \partial_j u_i)^2 + \frac{4}{3}(\sum_{i=1,2,3}(\partial_i u_i)^2 - \sum_{i<j}(\partial_i u_i \partial_j u_j)) \\
= & \sum_{i<j}(\partial_i u_j + \partial_j u_i)^2 + \frac{2}{3}\sum_{i<j}(\partial_i u_i - \partial_j u_j)^2
\end{aligned} \tag{A.4}
$$

A.2 Appendix of Chapter 4

A.2.1 Derivation of Total Energy

By taking the time derivative of the total energy functional, it is obtained that

$$\frac{dE_{total}}{dt} = \frac{d}{dt}E_{kin} + \frac{d}{dt}E_{cell} + \frac{d}{dt}E_w \tag{A.5}$$
$$\equiv I_1 + I_2 + I_3 \, . \tag{A.6}$$

This leads to

$$\begin{aligned}
I_1 &= \frac{d}{dt}\int_\Omega \frac{\rho|\mathbf{u}|^2}{2}d\boldsymbol{x} \\
&= \int_\Omega \frac{1}{2}\frac{\partial \rho}{\partial t}|\mathbf{u}|^2 d\boldsymbol{x} + \int_\Omega \rho \frac{\partial \mathbf{u}}{\partial t}\cdot \mathbf{u} d\boldsymbol{x} \\
&= \int_\Omega \frac{1}{2}\frac{\partial \rho}{\partial t}|\mathbf{u}|^2 d\boldsymbol{x} + \int_\Omega \rho \frac{d\mathbf{u}}{dt}\cdot \mathbf{u} d\boldsymbol{x} - \int_\Omega (\rho \mathbf{u}\cdot\nabla \mathbf{u})\cdot \mathbf{u} d\boldsymbol{x} \\
&= \int_\Omega \frac{1}{2}\frac{\partial \rho}{\partial t}|\mathbf{u}|^2 d\boldsymbol{x} + \int_\Omega \rho \frac{d\mathbf{u}}{dt}\cdot \mathbf{u} d\boldsymbol{x} + \int_\Omega \nabla\cdot(\rho\mathbf{u})\frac{|\mathbf{u}|^2}{2} d\boldsymbol{x} \\
&= \int_\Omega (\nabla\cdot\boldsymbol{\sigma}_\eta)\cdot\mathbf{u} d\boldsymbol{x} + \int_\Omega \mathbf{F}_\phi\cdot\mathbf{u} d\boldsymbol{x} + \int_\Omega \lambda\delta_\gamma \mathscr{P} : \nabla\mathbf{u} d\boldsymbol{x} + \int_\Omega \xi\gamma^2\lambda\nabla\cdot(\phi^2\nabla\lambda) d\boldsymbol{x} - \int_\Omega pI : \nabla\mathbf{u} d\boldsymbol{x} \\
&= -\int_\Omega ((\boldsymbol{\sigma}_\eta + pI) : \nabla\mathbf{u}) d\boldsymbol{x} + \int_\Omega \mathbf{F}_\phi\cdot\mathbf{u} dx - \int_\Omega \nabla\cdot(\lambda\delta_\gamma\mathscr{P})\cdot\mathbf{u} d\boldsymbol{x} \\
&\quad -\int_\Omega \xi\gamma^2\phi^2(\nabla\lambda)^2 d\boldsymbol{x} + \int_{\partial\Omega_w} ((\boldsymbol{\sigma}_\eta + \lambda\delta_\gamma\mathscr{P})\cdot\mathbf{n})\cdot\mathbf{u}_\tau dS \, ,
\end{aligned} \tag{A.7}$$

where p and λ are introduced as Lagrange multipliers accounting for fluid incompressiblity and local inextensibility of the cell membrane, respectively. The velocity boundary conditions and integration by parts are utilized in the above derivation from step 4 to step 6.

Using the first equation in conservation assumption, and the definitions of $g(\phi)$ and $f(\phi)$ gives rise to

$$\begin{aligned}
I_2 &= \frac{d}{dt}\int_\Omega \frac{\hat{\kappa}_B}{2\gamma}\left|\frac{f(\phi)}{\gamma}\right|^2 d\boldsymbol{x} + \frac{d}{dt}\left(\frac{M_v}{2}\frac{(V(\phi)-V(\phi_0))^2}{V(\phi_0)} + \frac{M_s}{2}\frac{(S(\phi)-S(\phi_0))^2}{S(\phi_0)}\right) \\
&= \int_\Omega \frac{\hat{\kappa}_B}{\gamma}\frac{f}{\gamma^2}\frac{\partial f}{\partial t} d\boldsymbol{x} + M_v\int_\Omega \frac{V(\phi)-V(\phi_0)}{V(\phi_0)}\frac{\partial \phi}{\partial t} d\boldsymbol{x} + M_s\int_\Omega \frac{S(\phi)-S(\phi_0)}{S(\phi_0)}\frac{\partial S(\phi)}{\partial t} d\boldsymbol{x} \\
&= \int_\Omega \frac{\hat{\kappa}_B}{\gamma}\frac{f}{\gamma^2}\left(-\gamma^2\Delta\left(\frac{\partial\phi}{\partial t}\right) + (3\phi^2-1)\frac{\partial\phi}{\partial t}\right) d\boldsymbol{x} \\
&\quad + M_v\int_\Omega \frac{V(\phi)-V(\phi_0)}{V(\phi_0)}\frac{\partial\phi}{\partial t} d\boldsymbol{x} \\
&\quad + M_s\int_\Omega \frac{S(\phi)-S(\phi_0)}{S(\phi_0)}\frac{1}{\gamma}\left(\gamma^2\nabla\phi\cdot\nabla\frac{\partial\phi}{\partial t} + (\phi^2-1)\phi\frac{\partial\phi}{\partial t}\right) d\boldsymbol{x}
\end{aligned}$$

$$
\begin{aligned}
&= \int_\Omega \frac{\hat{\kappa}_B}{\gamma^3}\left(-\gamma^2\Delta f + (3\phi^2-1)f\right)\frac{\partial\phi}{\partial t}d\boldsymbol{x} \\
&\quad + M_v\int_\Omega \frac{V(\phi)-V(\phi_0)}{V(\phi_0)}\frac{\partial\phi}{\partial t}d\boldsymbol{x} \\
&\quad + M_s\int_\Omega \frac{S(\phi)-S(\phi_0)}{S(\phi_0)}\frac{1}{\gamma}\left(-\gamma^2\Delta\phi + (\phi^2-1)\phi\right)\frac{\partial\phi}{\partial t}d\boldsymbol{x} \\
&\quad - \int_{\partial\Omega_w}\frac{\hat{\kappa}_B}{\gamma}f\frac{\partial}{\partial t}(\partial_n\phi)ds + \int_{\partial\Omega_w}\frac{\hat{\kappa}_B}{\gamma}\partial_n f\frac{\partial\phi}{\partial t}ds + M_s\int_{\partial\Omega_w}\frac{S(\phi)-S(\phi_0)}{S(\phi_0)}\gamma\partial_n\phi\frac{\partial\phi}{\partial t}ds \\
&= \int_\Omega \mu\frac{\partial\phi}{\partial t}d\boldsymbol{x} - \int_{\partial\Omega_w}\frac{\hat{\kappa}_B}{\gamma}f\frac{\partial}{\partial t}(\partial_n\phi)ds \\
&\quad + \int_{\partial\Omega_w}\frac{\hat{\kappa}_B}{\gamma}\partial_n f\frac{\partial\phi}{\partial t}ds + M_s\int_{\partial\Omega_w}\frac{S(\phi)-S(\phi_0)}{S(\phi_0)}\gamma\partial_n\phi\frac{\partial\phi}{\partial t}ds \\
&= \int_\Omega \mu q_\phi d\boldsymbol{x} - \int_\Omega \mu\mathbf{u}\cdot\nabla\phi d\boldsymbol{x} + \int_{\partial\Omega_w}\frac{\hat{\kappa}_B}{\gamma}\partial_n f\frac{\partial\phi}{\partial t}ds + M_s\int_{\partial\Omega_w}\frac{S(\phi)-S(\phi_0)}{S(\phi_0)}\gamma\partial_n\phi\frac{\partial\phi}{\partial t}ds\,.
\end{aligned}
\tag{A.8}
$$

Here the second and third equations in the boundary conditions and integration by parts are used in step 4 in the above derivation.

For I_3 in Eq. (A.5), it is easy to see that

$$
I_3 = \int_{\partial\Omega_w}\frac{\partial f_w}{\partial\phi}\frac{\partial\phi}{\partial t}ds\,. \tag{A.9}
$$

A.2.2 Proof of Lemma 3.4.2

$$
\begin{aligned}
&\int_\Omega f(\phi^{n+1},\phi^n)(\phi^{n+1}-\phi^n)d\boldsymbol{x} \\
&= \int_\Omega\left(\varepsilon\Delta\phi^{n+\frac{1}{2}}(\phi^{n+1}-\phi^n) + \frac{1}{4\varepsilon}((\phi^{n+1})^2+(\phi^n)^2-2)(\phi^{n+1}+\phi^n)(\phi^{n+1}-\phi^n)\right)d\boldsymbol{x} \\
&= \int_\Omega \varepsilon\nabla\phi^{n+\frac{1}{2}}\cdot\nabla(\phi^{n+1}-\phi^n)d\boldsymbol{x} - \int_{\partial\Omega_W}\varepsilon\partial_n\phi^{n+\frac{1}{2}}(\phi^{n+1}-\phi^n)ds \\
&\quad + \int_\Omega\frac{1}{4\varepsilon}((\phi^{n+1})^4 - 2(\phi^{n+1})^2 - (\phi^n)^4 + 2(\phi^n)^2)d\boldsymbol{x} \\
&= \int_\Omega\left[\frac{\varepsilon}{2}((\nabla\phi^{n+1})^2-(\nabla\phi^n)^2) + \frac{1}{4\varepsilon}(((\phi^{n+1})^2-1)^2 - ((\phi^n)^2-1)^2)\right]d\boldsymbol{x} \\
&\quad - \int_{\partial\Omega_W}\varepsilon\partial_n\phi^{n+\frac{1}{2}}(\phi^{n+1}-\phi^n)ds \\
&= \int_\Omega\left(\frac{\varepsilon}{2}(\nabla\phi^{n+1})^2 + \frac{1}{4\varepsilon}(\phi^{n+1}-1)^2\right)d\boldsymbol{x} - \int_\Omega\left(\frac{\varepsilon}{2}(\nabla\phi^n)^2 + \frac{1}{4\varepsilon}(\phi^n-1)^2\right)d\boldsymbol{x} \\
&\quad - \int_{\partial\Omega_w}\varepsilon\partial_n\phi^{n+\frac{1}{2}}(\phi^{n+1}-\phi^n)ds \\
&= S^{n+1} - S^n - \int_{\partial\Omega_w}\varepsilon\partial_n\phi^{n+\frac{1}{2}}(\phi^{n+1}-\phi^n)ds\,.
\end{aligned}
$$

A.2.3 Proof of Lemma 3.4.3

By the definition of g, we have

$$\begin{aligned}
&\int_\Omega g(\phi^{n+1},\phi^n)(\phi^{n+1}-\phi^n)d\boldsymbol{x}\\
=\;&\int_\Omega \nabla f^{n+\frac{1}{2}}\nabla(\phi^{n+1}-\phi^n)d\boldsymbol{x}-\int_{\partial\Omega_w}\partial_n f^{n+\frac{1}{2}}(\phi^{n+1}-\phi^n)ds\\
&+\int_\Omega \frac{1}{\varepsilon^2}f^{n+\frac{1}{2}}((\phi^{n+1})^2+(\phi^n)^2+\phi^{n+1}\phi^n-1)(\phi^{n+1}-\phi^n)d\boldsymbol{x}\\
=\;&\int_\Omega \nabla f^{n+\frac{1}{2}}\nabla(\phi^{n+1}-\phi^n)d\boldsymbol{x}-\int_{\partial\Omega_w}\partial_n f^{n+\frac{1}{2}}(\phi^{n+1}-\phi^n)ds\\
&+\int_\Omega \frac{1}{\varepsilon^2}f^{n+\frac{1}{2}}(((\phi^{n+1})^2-1)\phi^{n+1}-((\phi^n)^2-1)\phi^n)d\boldsymbol{x}. \qquad \text{(A.10)}
\end{aligned}$$

Similarly, the definition of f^{n+1} and f^n yields

$$\int_\Omega f^{n+\frac{1}{2}}f^{n+1}d\boldsymbol{x}=\varepsilon\int_\Omega\nabla f^{n+\frac{1}{2}}\nabla\phi^{n+1}d\boldsymbol{x}+\frac{1}{\varepsilon}\int_\Omega f^{n+\frac{1}{2}}((\phi^{n+1})^2-1)\phi^{n+1}d\boldsymbol{x} \qquad \text{(A.11)}$$

$$\int_\Omega f^{n+\frac{1}{2}}f^{n}d\boldsymbol{x}=\varepsilon\int_\Omega\nabla f^{n+\frac{1}{2}}\nabla\phi^{n}d\boldsymbol{x}+\frac{1}{\varepsilon}\int_\Omega f^{n+\frac{1}{2}}((\phi^{n})^2-1)\phi^{n}d\boldsymbol{x}. \qquad \text{(A.12)}$$

Then we have

$$\begin{aligned}
&\int_\Omega\frac{1}{2\varepsilon}((f^{n+1})^2-(f^n)^2)d\boldsymbol{x} \qquad \text{(A.13)}\\
=\;&\frac{1}{\varepsilon}\int_\Omega f^{n+\frac{1}{2}}(f^{n+1}-f^n)d\boldsymbol{x}\\
=\;&\int_\Omega\nabla f^{n+\frac{1}{2}}\nabla(\phi^{n+1}-\phi^n)d\boldsymbol{x}+\int_\Omega\frac{1}{\varepsilon^2}f^{n+\frac{1}{2}}(((\phi^{n+1})^2-1)\phi^{n+1}-((\phi^n)^2-1)\phi^n)d\boldsymbol{x}.
\end{aligned}$$

Comparing Eq. (A.10) with (A.14) yields Lemma 3.4.3.

A.2.4 Proof of Theorem 3.4.5

Let V_h in (3.4.13) equal to $\Delta t\mathbf{u}_h^{n+\frac{1}{2}}$ and do integration by parts gives

$$\begin{aligned}
&RHS\\
=\;&\int_\Omega\frac{1}{2}((\mathbf{u}_h^{n+1})^2-(\mathbf{u}_h^n)^2)d\boldsymbol{x}+\int_\Omega\Delta t\mathbf{u}_h^{n+\frac{1}{2}}\cdot\nabla(\frac{1}{2}|\mathbf{u}_h^{n+\frac{1}{2}}|^2)d\boldsymbol{x}\\
&-\frac{\Delta t}{Re}\int_\Omega P_h^{n+\frac{1}{2}}\nabla\cdot\mathbf{u}_h^{n+\frac{1}{2}}d\boldsymbol{x}+\frac{\Delta t}{Re}\int_{\Omega_w}P_h^{n+\frac{1}{2}}\mathbf{u}_h^{n+\frac{1}{2}}\cdot\mathbf{n}ds\\
=\;&\int_\Omega\frac{1}{2}((\mathbf{u}_h^{n+1})^2-(\mathbf{u}_h^n)^2)d\boldsymbol{x}-\int_\Omega\Delta t\nabla\cdot\mathbf{u}_h^{n+\frac{1}{2}}(\frac{1}{2}|\mathbf{u}_h^{n+\frac{1}{2}}|^2)d\boldsymbol{x}+\int_{\Omega_w}\Delta t\mathbf{u}_h^{n+\frac{1}{2}}\cdot\mathbf{n}(\frac{1}{2}|\mathbf{u}_h^{n+\frac{1}{2}}|^2)ds\\
&-\frac{\Delta t}{Re}\int_\Omega P^{n+\frac{1}{2}}\nabla\cdot\mathbf{u}_h^{n+\frac{1}{2}}d\boldsymbol{x}+\frac{\Delta t}{Re}\int_{\Omega_w}P_h^{n+\frac{1}{2}}\mathbf{u}_h^{n+\frac{1}{2}}\cdot\mathbf{n}ds
\end{aligned}$$

$$
\begin{aligned}
& LHS \\
= \quad & -\frac{\Delta t}{Re}\int_\Omega \nabla \mathbf{u}_h^{n+\frac{1}{2}} : \eta_h^n(\nabla \mathbf{u}_h^{n+\frac{1}{2}} + (\nabla \mathbf{u}_h^{n+\frac{1}{2}})^T)d\boldsymbol{x} + \frac{\Delta t}{Re}\int_\Omega \mathbf{u}^{n+\frac{1}{2}} \cdot \nabla \phi_h^{n+\frac{1}{2}} \mu_h^{n+\frac{1}{2}} d\boldsymbol{x} \\
& -\frac{\Delta t}{Re}\int_\Omega \lambda_h^{n+\frac{1}{2}} \delta_\varepsilon \mathscr{P}_h^n : \nabla \mathbf{u}_h^{n+\frac{1}{2}} d\boldsymbol{x} + \frac{\Delta t}{Re}\int_{\partial\Omega_w} \lambda_h^{n+\frac{1}{2}} (\delta_\varepsilon \mathscr{P}_h^n \cdot \mathbf{n}) \cdot \mathbf{u}_{h,\tau}^{n+\frac{1}{2}} ds \\
& +\frac{\Delta t}{Re}\int_{\partial\Omega_w} \mathbf{u}_h^{n+\frac{1}{2}} \cdot \eta_h^n((\nabla \mathbf{u}_h^{n+\frac{1}{2}} + (\nabla \mathbf{u}_h^{n+\frac{1}{2}})^T) \cdot \boldsymbol{n}) ds \, . \qquad \text{(A.14)}
\end{aligned}
$$

With the boundary condition $\mathbf{u}_h^{n+\frac{1}{2}} \cdot \mathbf{n} = 0$ and the constrain$\nabla \cdot \mathbf{u}_h^{n+\frac{1}{2}} = 0$, we have

$$
RHS \qquad = \int_\Omega \frac{1}{2}((\mathbf{u}_h^{n+1})^2 - (\mathbf{u}_h^n)^2) d\boldsymbol{x} \qquad \text{(A.15)}
$$

thus we have

$$
\begin{aligned}
& \int_\Omega \frac{1}{2}((\mathbf{u}_h^{n+1})^2 - (\mathbf{u}_h^n)^2) d\boldsymbol{x} \\
& = -\frac{\Delta t}{Re}\int_\Omega \nabla \mathbf{u}_h^{n+\frac{1}{2}} : \eta_h^n(\nabla \mathbf{u}_h^{n+\frac{1}{2}} + (\nabla \mathbf{u}_h^{n+\frac{1}{2}})^T)d\boldsymbol{x} + \frac{\Delta t}{Re}\int_\Omega \mathbf{u}^{n+\frac{1}{2}} \cdot \nabla \phi_h^{n+\frac{1}{2}} \mu_h^{n+\frac{1}{2}} d\boldsymbol{x} \\
& -\frac{\Delta t}{Re}\int_\Omega \lambda_h^{n+\frac{1}{2}} \delta_\varepsilon \mathscr{P}_h^n : \nabla \mathbf{u}_h^{n+\frac{1}{2}} d\boldsymbol{x} + \frac{\Delta t}{Re}\int_{\partial\Omega_w} \lambda_h^{n+\frac{1}{2}} (\delta_\varepsilon \mathscr{P}_h^n \cdot \mathbf{n}) \cdot \mathbf{u}_{h,\tau}^{n+\frac{1}{2}} ds \\
& +\frac{\Delta t}{Re}\int_{\partial\Omega_w} \mathbf{u}_h^{n+\frac{1}{2}} \cdot \eta_h^n((\nabla \mathbf{u}_h^{n+\frac{1}{2}} + (\nabla \mathbf{u}_h^{n+\frac{1}{2}})^T) \cdot \boldsymbol{n}) ds \, . \qquad \text{(A.16)}
\end{aligned}
$$

Let ψ_h in system (3.4.13) equal to $\frac{\mu^{n+\frac{1}{2}}\Delta t}{Re}$ and do integration yield

$$
\begin{aligned}
& \frac{1}{Re}\int_\Omega \mu_h^{n+\frac{1}{2}}(\phi_h^{n+1} - \phi_h^n) d\boldsymbol{x} + \frac{\Delta t}{Re}\int_\Omega \mu_h^{n+\frac{1}{2}}(\mathbf{u}_h^{n+\frac{1}{2}} \cdot \nabla)\phi_h^{n+\frac{1}{2}} d\boldsymbol{x} \\
= \quad & -\frac{\mathscr{M}\Delta t}{Re}\int_\Omega (\mu_h^{n+\frac{1}{2}})^2 d\boldsymbol{x} \, . \qquad \text{(A.17)}
\end{aligned}
$$

Let χ_h in system (4.13) equal to $\frac{\phi_h^{n+1}-\phi_h^n}{Re}$ and integration by parts lead to

$$
LHS = \frac{1}{Re}\int_\Omega \mu_h^{n+\frac{1}{2}}(\phi_h^{n+1} - \phi_h^n) d\boldsymbol{x} \qquad \text{(A.18)}
$$

with Lemma 3.4.2 and Lemma 3.4.3 (which is also valid in fully discrete condition) we have the following result on the right hand side:

$$
\begin{aligned}
& \frac{\kappa_B}{2Re}\int_\Omega g(\phi_h^{n+1}, \phi_h^n)(\phi_h^{n+1} - \phi_h^n) d\boldsymbol{x} \\
& = \frac{\kappa_B}{2Re\varepsilon}\int_\Omega (f_h^{n+1})^2 - (f_h^n)^2 d\boldsymbol{x} - \frac{\kappa_B}{Re}\int_{\Omega_w} \partial_n f_h^{n+\frac{1}{2}}(\phi_h^{n+1} - \phi_h^n) ds
\end{aligned}
$$

$$
\begin{aligned}
&\frac{\mathscr{M}_s}{Re}\frac{S(\phi_h^{n+\frac{1}{2}})-S(\phi_{h,0})}{S(\phi_{h,0})}\int_\Omega f(\phi_h^{n+1},\phi_h^n)(\phi_h^{n+1}-\phi_h^n)d\boldsymbol{x}\\
&=\frac{\mathscr{M}_s}{Re}\frac{S(\phi_h^{n+1})+S(\phi_h^n)-2S(\phi_{h,0})}{2S(\phi_{h,0})}(S(\phi_h^{n+1})-S(\phi_h^n))\\
&-\frac{\mathscr{M}_s}{Re}\frac{S(\phi_h^{n+1})+S(\phi_h^n)-2S(\phi_{h,0})}{2S(\phi_{h,0})}\int_{\Omega_w}\varepsilon\partial_n\phi_h^{n+\frac{1}{2}}(\phi_h^{n+1}-\phi_h^n)ds\\
&=\frac{\mathscr{M}_s}{Re}\frac{S(\phi_h^{n+1})^2-S(\phi_h^n)^2-2S(\phi_{h,0})S(\phi_h^{n+1})+2S(\phi_{h,0})S(\phi_h^n)+S(\phi_{h,0})^2-S(\phi_{h,0})^2}{2S(\phi_{h,0})}\\
&-\frac{\mathscr{M}_s}{Re}\frac{S(\phi_h^{n+1})+S(\phi_h^n)-2S(\phi_{h,0})}{2S(\phi_{h,0})}\int_{\Omega_w}\varepsilon\partial_n\phi_h^{n+\frac{1}{2}}(\phi_h^{n+1}-\phi_h^n)ds\\
&=\frac{\mathscr{M}_s}{Re}\frac{(S(\phi_h^{n+1})-S(\phi_{h,0}))^2-(S(\phi_h^n)-S(\phi_{h,0}))^2}{2S(\phi_{h,0})}\\
&-\frac{\mathscr{M}_s}{Re}\frac{S(\phi_h^{n+1})+S(\phi_h^n)-2S(\phi_{h,0})}{2S(\phi_{h,0})}\int_{\Omega_w}\varepsilon\partial_n\phi_h^{n+\frac{1}{2}}(\phi_h^{n+1}-\phi_h^n)ds.
\end{aligned}
$$

By simple calculation we also have

$$
\begin{aligned}
&\frac{\mathscr{M}_v}{Re}\frac{V(\phi_h^{n+\frac{1}{2}})-V(\phi_{h,0})}{V_{h,0}}\int_\Omega(\phi_h^{n+1}-\phi_h^n)d\boldsymbol{x}\\
&=\frac{\mathscr{M}_v}{Re}\frac{V(\phi_h^{n+1})+V(\phi_h^n)-2V(\phi_{h,0})}{2V(\phi_{h,0})}(V(\phi_h^{n+1})-V(\phi_h^n))\\
&=\frac{\mathscr{M}_v}{Re}\frac{V(\phi_h^{n+1})^2-V(\phi_h^n)^-2V(\phi_{h,0})V(\phi_h^{n+1})+2V(\phi_{h,0})V(\phi_h^n)+V(\phi_{h,0})^2-V(\phi_{h,0})^2}{2V(\phi_{h,0})}\\
&=\frac{\mathscr{M}_v}{Re}\frac{(V(\phi_h^{n+1})-V(\phi_{h,0}))^2-(V(\phi_h^n)-V(\phi_{h,0}))^2}{2V(\phi_{h,0})}.
\end{aligned}
$$

Thus we have the equation

$$
\begin{aligned}
&\frac{1}{Re}\int_\Omega\mu^{n+\frac{1}{2}}(\phi_h^{n+1}-\phi_h^n)d\boldsymbol{x}\\
&=-\frac{\kappa_B}{2Re\varepsilon}\int_\Omega(f_h^{n+1})^2-(f_h^n)^2d\boldsymbol{x}+\frac{\kappa_B}{Re}\int_{\Omega_w}\partial_n f_h^{n+\frac{1}{2}}(\phi_h^{n+1}-\phi_h^n)ds\\
&+\frac{\mathscr{M}_s}{Re}\frac{(S(\phi_h^{n+1})-S(\phi_{h,0}))^2-(S(\phi_h^n)-S(\phi_{h,0}))^2}{2S(\phi_{h,0})}\\
&-\frac{\mathscr{M}_s}{Re}\frac{S(\phi_h^{n+1})+S(\phi_h^n)-2S(\phi_{h,0})}{2S(\phi_{h,0})}\int_{\Omega_w}\varepsilon\partial_n\phi_h^{n+\frac{1}{2}}(\phi_h^{n+1}-\phi_h^n)ds\\
&+\frac{\mathscr{M}_v}{Re}\frac{(V(\phi_h^{n+1})-V(\phi_{h,0}))^2-(V(\phi_h^n)-V(\phi_{h,0}))^2}{2V(\phi_{h,0})}
\end{aligned}
\tag{A.19}
$$

Where $\phi_{h,0}$ is the initial condition of phase order. $V(\phi_h^n)=\int_\Omega\phi_h^n d\boldsymbol{x}, S(\phi_h^n)=\int_\Omega\frac{\varepsilon}{2}|\nabla\phi_h^n|^2+\frac{1}{4\varepsilon}((\phi_h^n)^2-1)^2d\boldsymbol{x}$. $V(\phi_h^{n+\frac{1}{2}})=\frac{1}{2}(V(\phi_h^n+1)+V(phi_h^n)), S(\phi_h^{n+\frac{1}{2}})=\frac{1}{2}(S(\phi_h^n+1)+S(\phi_h^n))$ are considered as constants in the integration.

Let Θ_h in system (3.4.13) equal to $\frac{\lambda_h^{n+\frac{1}{2}}\Delta t}{Re}$ and integration by parts give

$$-\frac{\Delta t}{Re}\int_\Omega \xi\varepsilon^2(\phi_h^n)^2\left|\nabla\lambda_h^{n+\frac{1}{2}}\right|^2 d\boldsymbol{x}+\frac{\Delta t}{Re}\int_{\Omega_w}\xi\varepsilon^2(\phi_h^n)^2\lambda_h^{n+\frac{1}{2}}\partial_n\lambda_h^{n+\frac{1}{2}}ds+\frac{\Delta t}{Re}\int_\Omega(\lambda_h^{n+\frac{1}{2}}\delta_\varepsilon\mathscr{P}_h^n):\nabla\mathbf{u}_h^{n+\frac{1}{2}}d\boldsymbol{x}=0\,.$$

With the boundary condition $\partial_n\lambda_h^{n+\frac{1}{2}}=0$, we have

$$-\frac{\Delta t}{Re}\int_\Omega \xi\varepsilon^2(\phi_h^n)^2\left|\nabla\lambda_h^{n+\frac{1}{2}}\right|^2 d\boldsymbol{x}+\frac{\Delta t}{Re}\int_\Omega(\lambda_h^{n+\frac{1}{2}}\delta_\varepsilon\mathscr{P}_h^n):\nabla\mathbf{u}_h^{n+\frac{1}{2}}d\boldsymbol{x}=0\,. \tag{A.20}$$

(A.16)-(A.17)+(A.19)-(A.20) and relocate some terms we have

$$\begin{aligned}
&\frac{1}{2}(||\mathbf{u}_h^{n+1}||^2-||\mathbf{u}_h^n||^2)+\frac{\kappa_B}{2Re\varepsilon}(||f_h^{n+1}||^2-||f_h^n||^2)\\
&+\frac{\mathscr{M}_s}{Re}\frac{(S(\phi_h^{n+1})-S(\phi_{h,0}))^2-(S(\phi_h^n)-S(\phi_{h,0}))^2}{2S(\phi_{h,0})}+\frac{\mathscr{M}_v}{Re}\frac{(V(\phi_h^{n+1})-V(\phi_{h,0}))^2-(V(\phi_h^n)-V(\phi_{h,0}))^2}{2V(\phi_{h,0})}\\
&=-\frac{2\Delta t}{Re}||(\eta_h^n)^{\frac{1}{2}}D_{h,\eta}^{n+\frac{1}{2}}||^2-\frac{\mathscr{M}\Delta t}{Re}||\mu_h^{n+\frac{1}{2}}||^2-\frac{\Delta t}{Re}\xi||\varepsilon(\phi_h^n)\nabla\lambda_h^{n+\frac{1}{2}}||^2\\
&+\frac{\Delta t}{Re}\int_{\partial\Omega_w}\mathbf{u}_h^{n+\frac{1}{2}}\cdot\eta_h^n((\nabla\mathbf{u}_h^{n+\frac{1}{2}}+(\nabla\mathbf{u}_h^{n+\frac{1}{2}})^T)\cdot\boldsymbol{n})ds+\frac{\Delta t}{Re}\int_{\partial\Omega_w}\lambda_h^{n+\frac{1}{2}}(\delta_\varepsilon\mathscr{P}_h^n\cdot\mathbf{n})\cdot\mathbf{u}_{h,\tau}^{n+\frac{1}{2}}ds\\
&+\frac{\mathscr{M}_s}{Re}\frac{S(\phi_h^{n+1})+S(\phi_h^n)-2S(\phi_{h,0})}{2S(\phi_{h,0})}\int_{\Omega_w}\varepsilon\partial_n\phi_h^{n+\frac{1}{2}}(\phi_h^{n+1}-\phi_h^n)ds+\frac{\kappa_B}{Re}\int_{\Omega_w}\partial_n f_h^{n+\frac{1}{2}}(\phi_h^{n+1}-\phi_h^n)ds
\end{aligned}$$

With boundary conditions: on $\partial\Omega_w$

$$\kappa\dot{\phi}_h^{n+\frac{1}{2}}=-L_h^{n+\frac{1}{2}}\,, \tag{A.21}$$

$$L_h^{n+\frac{1}{2}}=\kappa_B\partial_n f_h^{n+\frac{1}{2}}+\mathscr{M}_s\varepsilon\frac{S(\phi_h^{n+\frac{1}{2}})-S_{h,0}}{S_{h,0}}\partial_n\phi_h^{n+\frac{1}{2}}+\alpha_w\frac{f_{h,w}^{n+1}-f_{h,w}^n}{\phi_h^{n+1}-\phi_h^n}\,, \tag{A.22}$$

$$\begin{aligned}
-l_s^{-1}u_{h,\tau_i}^{n+\frac{1}{2}}&=\boldsymbol{\tau_i}\cdot(\eta_h^n(\nabla\mathbf{u}_h^{n+\frac{1}{2}}+(\nabla\mathbf{u}_h^{n+\frac{1}{2}})^T)+\lambda_h^{n+\frac{1}{2}}\delta_\varepsilon\mathscr{P}_h^n)\cdot\boldsymbol{n}\\
&\quad-L_h^{n+\frac{1}{2}}\partial_{\tau_i}\phi_h^{n+\frac{1}{2}}\,,\quad i=1,2,
\end{aligned} \tag{A.23}$$

We have the following derivations on those integration on the boundary.

$$\begin{aligned}
&\frac{\Delta t}{Re}\int_{\partial\Omega_w}\mathbf{u}_h^{n+\frac{1}{2}}\cdot\eta_h^n((\nabla\mathbf{u}_h^{n+\frac{1}{2}}+(\nabla\mathbf{u}_h^{n+\frac{1}{2}})^T)\cdot\boldsymbol{n})ds+\frac{\Delta t}{Re}\int_{\partial\Omega_w}\lambda_h^{n+\frac{1}{2}}(\delta_\varepsilon\mathscr{P}_h^n\cdot\mathbf{n})\cdot\mathbf{u}_{h,\tau}^{n+\frac{1}{2}}ds\\
&+\frac{\mathscr{M}_s}{Re}\frac{S(\phi_h^{n+1})+S(\phi_h^n)-2S(\phi_{h,0})}{2S(\phi_{h,0})}\int_{\Omega_w}\varepsilon\partial_n\phi_h^{n+\frac{1}{2}}(\phi_h^{n+1}-\phi_h^n)ds+\frac{\kappa_B}{Re}\int_{\Omega_w}\partial_n f_h^{n+\frac{1}{2}}(\phi_h^{n+1}-\phi_h^n)ds\\
&=\frac{\Delta t}{Re}\int_{\Omega_w}|\mathbf{u}_{h,\tau}^{n+\frac{1}{2}}|(-l_s^{-1}|\mathbf{u}_{h,\tau}^{n+\frac{1}{2}}|+L_h^{n+\frac{1}{2}}\partial_\tau\phi_h^{n+\frac{1}{2}})ds+\frac{1}{Re}\int_{\Omega_w}\left(L_h^{n+\frac{1}{2}}(\phi_h^{n+1}-\phi^n)-\alpha_w(f_{h,w}^{n+1}-f_{h,w}^n)\right)ds\\
&=-l_s^{-1}\frac{\Delta t}{Re}\int_{\Omega_w}|\mathbf{u}_{h,\tau}^{n+\frac{1}{2}}|^2ds+\frac{\Delta t}{Re}\int_{\Omega_w}L_h^{n+\frac{1}{2}}(\mathbf{u}_{h,\tau}^{n+\frac{1}{2}}\partial_\tau\phi_h^{n+\frac{1}{2}}+\frac{\phi_h^{n+1}-\phi^n}{\Delta t})ds-\frac{\alpha_w}{Re}(||f_{h,w}^{n+1}||w-||f_{h,w}^n||_w)
\end{aligned}$$

$$= \frac{\Delta t}{Re}(|| - l_s^{-\frac{1}{2}}\mathbf{u}_{h,\tau}^{n+\frac{1}{2}}||w^2 - \frac{1}{\kappa}||L_h^{n+\frac{1}{2}}||w^2) - \frac{\alpha_w}{Re}(||f_{h,w}^{n+1}||w - ||f_{h,w}^{n}||w)$$

By the definition of $\mathscr{E}_{h,kin}^{n}, \mathscr{E}_{h,cell}^{n}, \mathscr{E}_{h,w}^{n}$ and $\mathscr{E}_{h,kin}^{n+1}, \mathscr{E}_{h,cell}^{n+1}, \mathscr{E}_{h,w}^{n+1}$, we can finally get the energy law

$$\begin{aligned}
\mathscr{E}_{h,total}^{n+1} - \mathscr{E}_{h,total}^{n} &= (\mathscr{E}_{h,kin}^{n+1} + \mathscr{E}_{h,cell}^{n+1} + \mathscr{E}_{h,w}^{n+1}) - (\mathscr{E}_{h,kin}^{n} + \mathscr{E}_{h,cell}^{n} + \mathscr{E}_{h,w}^{n}) \\
&= \frac{\triangle t}{Re}\Bigg(-2\|(\eta_h^n)^{1/2}\mathbf{D}_{h,\eta}^{n+\frac{1}{2}}\|^2 - \mathscr{M}\|\mu_h^{n+\frac{1}{2}}\|^2 - \xi\|\ \varepsilon\phi_h^n\nabla\lambda_h^{n+\frac{1}{2}}\|^2 \\
&\quad -\frac{1}{\kappa}\|L(\phi_h^{n+\frac{1}{2}})\|_w^2 - \|l_s^{-1/2}\mathbf{u}_{h,\tau}^{n+\frac{1}{2}}\|_w^2\Bigg)\ ,
\end{aligned} \tag{A.24}$$